UNIVERSIDADE FEDERAL DO RIO GRANDE DO SUL
ESCOLA DE ENGENHARIA
DEPARTAMENTO DE ENGENHARIA QUÍMICA
PROGRAMA DE PÓS-GRADUAÇÃO EM ENGENHARIA QUÍMICA

ESTIMAÇÃO DE PARÂMETROS EM TEMPO REAL ATRAVÉS DE FILTRO DE KALMAN COM JANELA ROBUSTA SUAVIZANTE E ESTIMADORES DE ESTADOS NÃO LINEARES

TESE DE DOUTORADO

Andressa Apio

Porto Alegre
2020

UNIVERSIDADE FEDERAL DO RIO GRANDE DO SUL
ESCOLA DE ENGENHARIA
DEPARTAMENTO DE ENGENHARIA QUÍMICA
PROGRAMA DE PÓS-GRADUAÇÃO EM ENGENHARIA QUÍMICA

ESTIMAÇÃO DE PARÂMETROS EM TEMPO REAL ATRAVÉS DE FILTRO DE KALMAN COM JANELA ROBUSTA SUAVIZANTE E ESTIMADORES DE ESTADOS NÃO LINEARES

Andressa Apio

Tese de Doutorado (D.Sc.) apresentada como requisito parcial para obteção do título de Doutor em Engenharia

Área de concentração: Pesquisa e Desenvolvimento de Processos

Linha de Pesquisa: Projeto, Simulação, Modelagem, Controle e Otimização de Processo

Orientadores:
Prof. Dr. Jorge Otávio Trierweiler
Prof. Dr. Marcelo Farenzena

Porto Alegre
2020

UNIVERSIDADE FEDERAL DO RIO GRANDE DO SUL
ESCOLA DE ENGENHARIA
DEPARTAMENTO DE ENGENHARIA QUÍMICA
PROGRAMA DE PÓS-GRADUAÇÃO EM ENGENHARIA QUÍMICA

A Comissão Examinadora, abaixo assinada, aprova a Tese sobre "Estimação de parâmetros em tempo real através de filtro de Kalman com janela robusta suavizante e estimadores de estados não lineares", elaborada por Andressa Apio, como requisito parcial para obtenção do Grau de Doutor em Engenharia.

Comissão Examinadora:

Prof. Dr. Argimiro Resende Secchi (COPPE/UFRJ)

Prof. Dr. Rodrigo Iván Goytia Mejía (UNISINOS)

Prof. Dr. Marcelo Escobar Aragão (FURG)

Resumo

Os estimadores de estado, ou observadores, são técnicas que reconstroem os estados de um modelo dinâmico a partir das medidas de entrada e saída do sistema. Eles podem ser baseados na teoria probabilística (proposto por Kalman), que considera ruídos no modelo ou na teoria determinística (introduzida por Luenberger) sem a presença de ruídos. Embora, na sua gênese, o controle "moderno" tenha motivado o surgimento dessas técnicas em 1960, os estimadores de estado são hoje em dia aplicados também em reconciliação de dados, analisadores virtuais, estimação de parâmetros, gêmeos digitais e detecção de falhas. Por isso, esta tese aborda um estudo sobre filtros de Kalman e suas aplicações focado, principalmente, no uso de janela robusta suavizante. As principais contribuições do trabalho são: (1) revisão bibliográfica histórica dos estimadores de estado, abordando suas principais interligações e características, incluindo uma motivação prática de suas utilizações; (2) avaliação de cinco metodologias de filtro de Kalman (estendido - EKF, estendido com restrições - CEKF, formulação curta do estendido com restrições – CEKF2, estendido com restrições e suavizado - CEKFS, sem rastro - UKF, e de cubatura – CKF implementadas a dados industriais, mostrando a sua capacidade de aplicação em casos reais, sendo eles, na produção de petróleo offshore e em uma rede de trocadores de calor; (3) proposta de técnica de estimação de bias em casos em que o estimador não linear retorna resultados insatisfatórios; (4) avaliação de três métodos de estimadores de estado com horizonte móvel para estimação simultânea de estados e parâmetros (estimação do horizonte móvel - MHE, com horizonte retrocedido - RNK, e robusto com horizonte retrocedido - RRNK); e (5) apresentação de formulação robusta e simples para problema de otimização do RNK e RRNK utilizando programação quadrática. De modo geral os filtros de Kalman não-lineares (UKF e CKF) retornam melhores resultados para os dados industriais quando o modelo está bem ajustado. No entanto, eles possuem elevado custo computacional e desempenho insatisfatório para modelos mal ajustados, enquanto os filtros estendidos não apresentam essas desvantagens. Por isso, utilizando técnica simples da estimação de bias como uma variável através de técnica de estado aumentado, o filtro de Kalman sem rastro e de cubatura se mostraram mais acurados, mesmo em um cenário de ajuste inadequado do modelo. Para a estimação simultânea de estados e parâmetros, o RRNK exibiu as suas vantagens na redução de erros de modelagem, retornando parâmetros mais suavizados. Nesse sentido, a reformulação dos problemas de otimização do RNK e RRNK em uma formulação de programação quadrática simples e robusta obteve um custo computacional nove vezes menor que o MHE.

Palavras-chave: Estimadores de estado, observadores, filtro de Kalman, estimação de parâmetros.

Abstract

State estimators, or observers, are techniques that reconstruct the states of a dynamical model from the input and output measures of the system. They can be based on the probabilistic theory (proposed by Kalman), which considers noise in the model, or on the deterministic theory (introduced by Luenberger) without the presence of noise. Although in its genesis, "modern" control motivated the emergence of these techniques in 1960, state estimators are nowadays also applied in data reconciliation, virtual analyzers, parameter estimation, digital twins, and fault detection. For this reason, this thesis addresses a study on Kalman filters and their applications, focused mainly on the use of a robust softening window. The main contributions of the work are: (1) historical bibliographic review of state estimators, addressing their main interconnections and characteristics, including a practical motivation for their uses; (2) evaluation of five Kalman filter methodologies (extended – EKF, constrained extended – CEKF, short formulation of the constrained extended – CEKF2, constrained extended and smoother – CEKFS, unscented – UKF, cubature – CKF) implemented to industrial data, showing their ability to be applied in real cases, namely in offshore oil production and in a heat exchanger network; (3) proposal of bias estimation technique in cases where the nonlinear estimator returns unsatisfactory results; (4) evaluation of three methods of state estimators with moving window for simultaneous state and parameter estimation (moving horizon horizon – MHE, receding nonlinear Kalman filter – RNK, and robust receding nonlinear Kalman filter – RRNK), and (5) presentation of robust and simple formulation for RNK and RRNK optimization problem using quadratic programming. In general, non-linear Kalman filters (UKF and CKF) return better results for industrial data when the model is well adjusted. However, they have high computational costs and poor performance for poorly adjusted models, while extended filters do not present these disadvantages. Therefore, using a simple bias estimation technique as a variable using an increased state technique, the unscented and cubature Kalman filter proved to be more accurate, even in a scenario of inadequate model adjustment. For the simultaneous state and parameter estimation, the RRNK showed its advantages in reducing modeling errors, returning more smoothed parameters. In this sense, the RNK and RRNK optimization problems' reformulation in a robust and straightforwards quadratic programming formulation obtained a computational cost nine times smaller than the MHE.

Keywords: State estimators, observers, Kalman filter, parameter estimation.

“Cold comfort for change?”

Pink Floyd

“Does the flap of a butterfly’s wings in Brazil set off a tornado in Texas?”

Edward Lorenz

AGRADECIMENTOS

Aos meus pais, José Carlos e Zelfa, e ao meu irmão, Anderson, por serem meus principais exemplos, por acreditarem em mim e sempre me apoiarem nas minhas decisões.

Aos meus orientadores, prof. Jorge e prof. Farenzena, pela paciência e confiança, e por terem me ensinado tanto, pessoal e profissionalmente.

Ao meu namorado, amigo, colega e sócio, Jônathan, por estar sempre ao meu lado. Obrigada pelo carinho, companheirismo e pelas inúmeras coisas que fazemos juntos: das conversas filosóficas às indiadas esportivas.

Aos meus sogros, Maria e Sérgio, por terem me recebido e acolhido tão bem.

Às minhas melhores amigas, Carol Weber e Taís, por me aceitarem e entenderem. Obrigada por serem minha motivação e exemplo para superar momentos difíceis.

Às minhas amigas Engenheiras Andressa, Julia, Karen, Martina e Tanisa pelo companheirismo desde a faculdade. Vocês são meus orgulhos.

Aos amigos do DEQUI, Cris, Carol Agustini, Carol Machado, João e Aline, pela amizade, conselhos e conversas construtivas.

Ao Bruno, pelos diálogos progressivos.

Às minhas professoras do ensino médio, Silvia e Tatá, por terem acreditado em mim tão cedo, e por terem sido minhas primeiras inspirações profissionais e pessoais.

À Luna, minha companheira de todos os momentos.

À UFRGS, à Escola de Engenharia e ao DEQUI pela excelente infraestrutura.

Aos colegas do GIMSCOP.

À banca, prof. Argimiro, prof. Escobar e prof. Mejía, pelas contribuições e sugestões.

Aos Engenheiros Herbert e Maurício Posser, pelas valiosas trocas de experiência e pelo incentivo.

E a todos que tenham contribuído, direta ou indiretamente, para minha evolução pessoal e profissional durante esses muitos anos de academia (“*...and then one day you find ten years have got behind you”*).

SUMÁRIO

Capítulo 1 – Introdução 1
1.1 Motivação 1
1.2 Motivação para utilização de estimadores de estado com janela robusta suavizante 3
1.3 Objetivos 4
1.4 Contribuições 4
1.5 Estrutura 4
1.6 Produção científica e demais atividade 5
1.6.1 Capítulos deste trabalho: 5
1.6.2 Trabalhos completos publicados em anais de congresso 6
Capítulo 2 – Revisão Bibliográfica 7
2.1 Breve revisão histórica 7
2.2 Equacionamento do filtro de Kalman 14
2.2.1 Equacionamento do filtro de Kalman resumido 14
2.2.2 Dedução da matriz de covariância a posteriori 15
2.2.3 Dedução do ganho de Kalman 15
2.2.4 Simplificação da fórmula da covariância do erro a posterori 16
2.3 Demais equacionamentos dos estimadores de estado 17
Capítulo 3 – Comparison of Kalman-filter based approaches for permanent downhole gauge estimation in offshore oil production 19
3.1 Introduction 19
3.2 Comparison of Kalman filter-based approaches in different applications 21
3.3 Methodology 22
3.3.1 Kalman filter approaches 22
3.3.1.1. Discrete Extended Kalman Filter 23
3.3.1.2. Constrained Extended Kalman Filter 24
3.3.1.3. Constrained Extended Kalman Filter and Smoother 24
3.3.1.4. Unscented Kalman Filter 25
3.3.1.5. Cubature Kalman Filter 27
3.3.2 Performance evaluation criteria 28
3.4 Case studies 28
3.4.1 Plant model 28
3.4.2 Simulated data 32
3.4.3 Real data 33
3.4.4 Simulation settings 34
3.5 Results and discussion 36
3.5.1 Simulated data 36
3.5.2 Real data 47
3.6 Conclusions 51
3.7 Acknowledgement 52
Capítulo 4 – Fouling and operational monitoring of heat exchanger network by a state estimator technique 53
4.1 Introduction 53

4.2 Review of heat exchanger network synthesis and Kalman filter applications 55
4.3 Case study 55
4.3.1 Plant description 55
4.3.2 Heat exchanger network configuration 56
4.3.3 Heat exchanger model 57
4.3.4 Process data 60
4.4 Methodology 61
4.4.1 Kalman filter approach 62
3.3.1.1. Constrained Kalman filter and smoother 62
4.4.2 Simulation settings 63
4.5 Results and discussion 65
4.5.1 Model simulation results 65
4.5.2 Kalman filter results 67
4.6 Conclusions 73
4.7 Acknowledgments 74

Capítulo 5 – Bias estimation: a simple solution for the main drawback of the nonlinear state estimators 75

5.1 Introduction 75
5.2 Kalman filters, case study model and data 77
5.2.1 Kalman filters 77
5.2.1.1. Unscented Kalman Filter 77
5.2.1.2. Cubature Kalman filter 78
5.2.2 Case study 79
5.2.2.1. Plant Model 80
5.2.2.2. Experimental data 83
5.3 Methodology 84
5.3.1 Bias estimation 84
5.3.2 Observability analysis 85
5.3.3 Simulation settings 86
5.4 Results and discussion 87
5.5 Conclusions 91
5.6 Acknowledgments 92

Capítulo 6 – Robust extended Kalman filter estimation with moving window through a quadratic programming formulation 93

6.1 Introduction 94
6.2 Literature review 96
6.3 Methodology 96
6.3.1 Moving Horizon Estimation 98
6.3.2 Constrained Extended Kalman Filter 99
6.3.3 Constrained Extended Kalman Filter– rewritten in the short formulation 102
6.3.4 Extended Kalman Filter with Moving Window Estimation 103
6.3.5 Robust Extended Kalman Filter with Moving Window Estimation 106
6.3.6 Constrained Extended Kalman Filter and Smoother 110
6.4 Case study 110
6.4.1 Plant model 110
6.4.2 Simulation Settings 117
6.4.3 Simultaneous State and Parameter Estimation 118
6.4.4 Performance Evaluation Criteria 118
6.5 Results and Discussion 118
6.6 Summary of Contributions 125
6.7 Conclusions 126
6.8 Acknowledgments 127

6.9 Appendix A 127
A.1. QP derivation for the constrained extended Kalman filter – short implementation 127
A.2. QP derivation for the robust extended extended Kalman filter 129
Capítulo 7 – Considerações finais 131
7.1 Conclusões..... 131
7.2 Sugestões para trabalhos futuros 132
Referências 133

LISTA DE FIGURAS

Figura 1.1: Esquema da planta de quatro tanques esféricos (adaptado de Santos (2016)). 2
Figura 1.2: Relação entre as contribuições e estimadores de estados aplicados nos principais capítulos desta tese. 5
Figura 2.1: Esquema de interligação entre os estimadores de estado. 8
Figura 2.2: Diagrama de blocos de cálculo para o filtro de Kalman. 9
Figura 2.3: Esquema das técnicas de estimadores de estado determinísticas e estocásticas, onde as linha tracejada vermelha representa a conexão entre os estimadores. 10
Figura 2.4: Cronologia dos estimadores de estado, onde os pontos com as cores mais escuras representam estimadores não-lineares, e as cores mais claras os estimadores lineares/estendidos. 12
Figure 3.1: Data simulated in OLGA for a real oil production system used in scenarios A and B. 33
Figure 3.2: Data simulated in OLGA for a real oil production system with perturbations in the choke valve opening used in scenarios C and D. 33
Figure 3.3: Real industrial data from an oil production system used in scenarios E and F. 34
Figure 3.4: Comparison of the experimental data (rigorous model simulation in OLGA and industrial) and the simplified model simulation results for a) scenarios A and B, b) E and F, and c) C and D. 36
Figure 3.5: Scenario A: $ppdg$ estimation using prt and ptt measurements by a) DEKF, b) CEKF, c) CEKF&S, d) UKF, and e) CKF. 37
Figure 3.6: Scenario B: $ppdg$ estimation using ptt measurement by a) DEKF, b) CEKF, c) CEKF&S, d) UKF, and e) CKF. 39
Figure 3.7: Residual box plot for $ppdg$ for a) Scenario A and b) Scenario B. 39
Figure 3.8: Residual violin plot for $ppdg$ for a) Scenario A and b) Scenario B. 40
Figure 3.9: Derivative of the $ppdg$ estimated by the DEKF and the CKF for a) Scenario A and b) Scenario B. 40
Figure 3.10: Scenario C: $ppdg$estimation using prt and ptt measurements by a) DEKF, b) CEKF, c) CEKF&S, d) UKF, and e) CKF. 42
Figure 3.11: Scenario D: $ppdg$ estimation ptt measurements by a) DEKF, b) CEKF, c) CEKF&S, d) UKF, and e) CKF. 44
Figure 3.12: Residual box plot of the $ppdg$ for a) Scenario C and b) Scenario D. 45
Figure 3.13: Residual violin plot of the $ppdg$ for a) Scenario C and b) Scenario D. 46
Figure 3.14: Derivative of the $ppdg$ estimated by the CEKFS and the CKF for a) Scenario C, and by the DEKF and the CKF for b) Scenario D. 46
Figure 3.15: Scenario E: $ppdg$ estimation using prt and ptt measurements of a real production system with a) DEKF, b) CEKF, c) UKF, and d) CKF. 47
Figure 3.16: Scenario F: $ppdg$ estimation using ptt measurements of a real production system by a) DEKF, b) CEKF, c) UKF, and d) CKF. 48
Figure 3.17: Residual box plot of the $ppdg$ for a) Scenario E and b) Scenario F. 49
Figure 3.18: Residual violin plot of the $ppdg$ for a) Scenario E and b) Scenario F. 49

Figure 3.19: Derivative of the $ppdg$ estimated by the DEKF and the CKF for a) Scenario E and b) Scenario F. 50
Figure 4.1: The heating system of the crude oil distillation unit. 56
Figure 4.2: Heat exchanger network configuration of PHT of a distillation unit. 57
Figure 4.3: Mass flow input measurements for the heat exchanger network. 65
Figure 4.4: Simulation results of the PHT system, where *meas* refers to measurements and *sim* to simulation data. 67
Figure 4.5: Kalman filter application results of the PHT system. 69
Figure 4.7: Kalman filter application results of the PHT system – temperature exchange. 73
Figure 5.1: Data simulated in OLGA for a real oil production system with perturbations in the choke valve opening. 83
Figure 5.2: Comparison of the OLGA dataset and the FOWM simulation results. 84
Figure 5.3: Decision flowchart for the use of bias variables for the UKF and CKF estimation 85
Figure 5.4: $ppdg$ estimation by a) DEKF, b) UKF, and c) CKF without bias estimation..... 88
Figure 5.5: $ppdg$ estimation by a) UKF with bias estimation, and e) CKF with bias estimation. 89
Figure 5.6: . $ppdg$ estimation by a) UKF and e) CKF with bias estimation in both prt and ptt. 90
Figura 5.7: Fragment zoom of $ppdg$ estimation with bias estimation in a) both prt, and b) both prt and ptt. 91
Figure 6.1: Illustration of a moving window sequence scheme. 98
Figure 6.2: Calculation scheme of the extended Kalman filter with moving window estimation. 105
Figure 6.4: The spherical-quadruple-tank process. 111
Figure 6.5: Inputs variables $x1$, $x2$, $F1$ and $F2$ of the spherical-quadruple-tank plant. 113
Figure 6.6: Outputs $h1$, $h2$, $h3$ and $h4$ of the spherical-quadruple-tank plant. 115
Figure 6.7: Results for the seven scenarios of the spherical-quadruple-tank case study. 122
Figure 6.8: Window size versus the $R1$ MSE for Scenario C. 125

LISTA DE TABELAS

Tabela 2.1: Nomenclatura dos estimadores de estado. 13
Tabela 2.2: Relação entre os estimadores de estado e seções onde são detalhados. 17
Table 3.1: Parameters and variables of the Fast Offshore Well Model (FOWM). 31
Table 3.2: Filter parameters for all scenarios. 34
Table 3.3: Data used in the Kalman filter for each scenario. 34
Table 3.4: FOWM adjust parameters for all the scenarios. 35
Table 3.5: Mean squared error for the model simulation considering all the scenarios. .. 36
Table 3.6: Computational time and MSE for scenario A. 38
Table 3.7: Computational time and MSE for scenario B. 39
Table 3.8: Computational time and MSE for scenario C. 43
Table 3.9: Computational time and MSE for scenario D. 45
Table 3.10: Computational time and MSE for scenario E. 48
Table 3.11: Computational time and MSE for scenario F. 48
Table 4.1: Description of the model variables. 57
Table 4.2: Variables connections for the heat exchanger network model. 60
Table 4.3: Physical properties of the heat exchanger network. 61
Table 4.4: Physical properties of the heat exchanger fluids. 61
Table 4.5: Filter parameters for the heat exchanger network. 64
Table 4.6: Data used in the Kalman filter for heat exchanger network. 64
Table 4.7: Initial conditions for the heat exchanger network. 64
Table 5.1: Parameters and variables of the Fast Offshore Well Model (FOWM). 81
Table 5.2: Data used in the Kalman filter for the FOWM model. 86
Table 5.3: Initial conditions for FOWM model. 86
Table 5.4: Mean squared error for the prt, ptt and $ppdg$ variables. 89
Table 5.5: Mean squared error for the prt, ptt and $ppdg$ variables. 90
Table 6.1: Description of the spherical-quadruple-tank process. 111
Table 6.2: Scenarios of the spherical-quadruple-tank plant. 112
Table 6.3: Filter parameters for spherical/cylindrical-quadruple-tank model. 117
Table 6.4: Initial conditions for the states of the spherical/cylindrical-quadruple-tank model. 117
Table 6.5: Mean squared error for scenario A of the spherical-quadruple-tank case study using the CEKF-OPT and CEKF-QP methodologies. 118
Table 6.6: Mean squared error for the eight scenarios of the spherical/cylindrical-quadruple-tank case study. 123

Capítulo 1 – **Introdução**

Os estimadores de estado estimam os estados de um modelo dinâmico através das medidas das entradas e saídas disponíveis, podendo ser utilizados em reconciliação de dados, analisadores virtuais, controle avançado, estimação de parâmetros, gêmeos digitais e detecção de falhas. Este capítulo aborda as motivações, objetivos, contribuições e estrutura do trabalho, finalizando com a apresentação da produção científica desenvolvida durante o projeto.

1.1 Motivação

Apesar das técnicas de estimadores de estado terem surgido em meados dos anos 1960 com mais força devido ao controle moderno, existem muitas outras aplicações úteis para essas metodologias, tais como reconciliação de dados, analisadores virtuais, estimação de parâmetros, gêmeos digitais e detecção de falhas. Por isso, o objetivo dessa seção é demonstrar a relevância dessas técnicas em exemplos simples de aplicação no estudo de caso clássico dos quatro tanques esféricos proposto inicialmente por Escobar e Trierweiler (2013), conforme Figura 1.1.

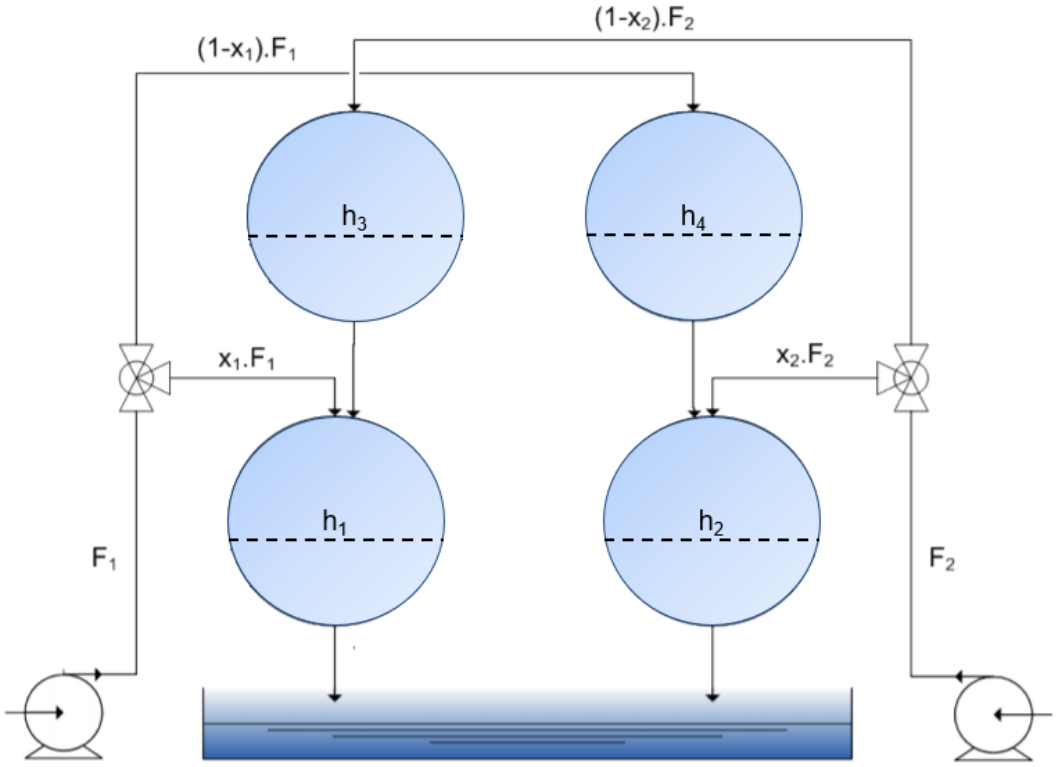


Figura 1.1: Esquema da planta de quatro tanques esféricos (adaptado de Santos (2016)).

Esse sistema possui como variáveis de estado os níveis dos quatro tanques (h_1, h_2, h_3 e h_4), como variáveis de entrada as vazões de alimentação (F_1 e F_2) e a abertura das válvulas de distribuição direta aos tanques 1 e 2 (x_1 e x_2). D_i representa o diâmetro do tanque i e R_i representa o coeficiente de descarga do tanque i. A modelagem fenomenológica dessa unidade advém do balanço de massa em cada tanque, conforme as seguintes equações:

$$\frac{dh_1}{dt} = \frac{x_1 F_1 + R_3\sqrt{h_3} - R_1\sqrt{h_1}}{\pi h_1 (D_1 - h_1)} \tag{1.1}$$

$$\frac{dh_2}{dt} = \frac{x_2 F_2 + R_4\sqrt{h_4} - R_2\sqrt{h_2}}{\pi h_2 (D_2 - h_2)} \tag{1.2}$$

$$\frac{dh_3}{dt} = \frac{(1-x_2) F_2 - R_3\sqrt{h_3}}{\pi h_3 (D_3 - h_3)} \tag{1.3}$$

$$\frac{dh_4}{dt} = \frac{(1-x_1) F_1 - R_4\sqrt{h_4}}{\pi h_4 (D_4 - h_4)} \tag{1.4}$$

Esse estudo de caso pode ser aplicado em:

- **Reconciliação de dados**: neste caso, se as medições de todos os estados estiverem disponíveis, é possível obter os dados filtrados de h_1, h_2, h_3 e h_4 pelo estimador de estados através da reconciliação dos valores da predição do modelo e das medidas experimentais.

- **Analisadores virtuais**: supondo que apenas as medições de h_1 e h_2 estejam disponíveis e que h_3 *e* h_4 sejam as variáveis desejadas, poderia ser feita a medição manual desses níveis, o que resultaria em poucos pontos e atrasos

entre os tempos de amostragem. Com o analisador virtual, seria possível inferir as variáveis h_3 *e* h_4 através de estimadores de estado, que fornecem informações online sobre as variáveis não-medidas.

- **Retroalimentação em controladores preditivos multivariáveis** : considerando o caso do analisador virtual, onde os estados h_3 *e* h_4 seriam as variáveis desejadas em termos de controle, a estimação dessa variável possibilitaria o controle retroalimentado das variáveis de estado desse sistema, permitindo a operação robusta do sistema de controle em várias taxas amostrais da medida. Mesmo nos casos em que as variáveis de interesse sejam as medidas, os estimadores de estado consistem em uma alternativa para se fazer a retroalimentação em controladores preditivos multivariáveis.

- **Estimação de parâmetros**: quando o valor de algum dos coeficientes de descarga R_i dos tanques não é conhecido, é possível estimá-lo simultaneamente com os estados do modelo utilizando estimadores de estado. Isso possibilita a estimação dos parâmetros desconhecidos ou incertos do modelo para aumentar a sua fidelidade.

- **Gêmeos digitais**: usando um modelo simples do sistema de quatro tanques como cópia digital do sistema físico real, é possível melhorar seus resultados através da reconciliação do modelo e dos dados reais da planta. Isso permite realizar vários testes na cópia digital, tais otimizar pontos de operação, reduzir custos de energia e testar a capacidade de adaptação do processo, prever falhas, entre outros.

- **Detecção de falhas**: através da estimação online da altura do tanque h_4 com estimador de estados, por exemplo, é possível detectar possíveis mudanças significativas nessa variável, que indicariam a presença de falhas.

No entanto, é necessário analisar critérios de observabilidade do sistema a fim de garantir que é possível obter valores atuais de alguns estados através de outras variáveis medidas. Isso acontece porque é necessário estabelecer o número mínimo de medições que, combinadas com o modelo matemático, possam garantir a sua observabilidade (SALAU, 2009). Uma forma simples de fazer avaliar esse critério, é utilizar o procedimento de cálculo proposto por Popov-Belevitch-Hautus (1969).

1.2 Motivação para utilização de estimadores de estado com janela robusta suavizante

A utilização de janelas móveis em filtros de Kalman foi proposta por Jazwinski (1968), uma vez que o filtro de Kalman estendido apresentava desempenhos ruins ou divergia devido a erros de modelagem e computacionais. A ideia dessa técnica é, na estimação do vetor de estados, utilizar um número finito de amostras passadas medidas, onde a amostra mais antiga é descartada quando uma nova amostra se torna disponível. Por isso, a janela deslizante reduz os efeitos de amostras antigas na filtragem e melhora a precisão da estimativa (HUANG *et al.*, 2019).

Além disso, estimadores de estado com janelas móveis são alternativas interessantes para aplicação em estudos de caso industriais com a presença de ruídos e valores espúrios. Para a suavização dos estados estimados, por exemplo, é necessária uma janela de dados,

já que para aplicação dessa técnica são utilizados valores futuros das amostras. Além disso, a adição de robustez a esse problema reduz o efeito dos outliers, cujas vantagens são destacadas ainda mais na utilização de janelas deslizantes.

1.3 Objetivos

O presente trabalho tem como objetivo geral o estudo e o desenvolvimento de filtros de Kalman com janela robusta suavizante e suas aplicações. Os objetivos específicos são:

1. Revisar a literatura sobre métodos de estimadores de estado;
2. Avaliar métodos de filtros de Kalman a dados provenientes da indústria;
3. Avaliar métodos de estimadores de estado com janela móvel para estimação simultânea de estados e parâmetros;
4. Propor técnica para melhoria dos resultados de estimador não-linear quando modelo não está bem ajustado;
5. Apresentar forma robusta e simples para problema de otimização de otimização de estimadores de estado com janela móvel utilizando programação quadrática.

1.4 Contribuições

Têm-se como contribuições do trabalho:

- CONT1: Revisão de métodos de estimadores de estado;
- CONT2: Avaliação de técnicas de filtro de Kalman a dados industriais;
- CONT3: Proposta de técnica de estimação de bias para casos em que o estimador não linear retorna resultados insatisfatórios;
- CONT4: Mostrar a relevância da utilização de estimadores de estados com janelas móveis para a estimação simultânea de estados e parâmetros;
- CONT5: Apresentação de formulação robusta e simples para problema de otimização de estimadores de estado com janela móvel utilizando programação quadrática.

1.5 Estrutura

O presente trabalho é estruturado em 7 capítulos, sendo que neste é apresentada uma motivação que aborda a implementação prática dos estimadores de estado, os objetivos, contribuições e estrutura do trabalho, além da produção científica desenvolvida durante o projeto.

O Capítulo 2 apresenta uma breve revisão bibliográfica sobre os métodos de estimação de estado em seu aspecto histórico, suas interligações, principais características e equacionamento.

No Capítulo 3, cinco metodologias de filtros de Kalman são aplicadas a um estudo de caso de produção de petróleo *offshore*. O capítulo aponta a comparação entre a aplicação desses estimadores de estado em dados simulados e reais.

No Capítulo 4 é realizada uma aplicação de filtro de Kalman para estimação simultânea de estados e parâmetros em uma rede de trocadores de calor industrial. O desenvolvimento desse artigo é motivado pela consideração de “pior cenário possível” com um modelo simplificado do sistema e poucos dados de planta.

No Capítulo 5 é apresentada uma metodologia para remoção do "bias" presente na estimação de modelos mal ajustados em filtros de Kalman não-lineares. A técnica proposta é baseada na estimação do bias como uma parâmetro utilizando metodologia de estados aumentados.

O Capítulo 6 apresenta uma comparação entre estimadores de estado com janela móvel para estimação simultânea de estados e parâmetros no estudo de caso que é a motivação desse trabalho, os quatro tanques esféricos. O objetivo, também, é corrobar a relevância do uso de filtro de Kalman com horizontes móveis para a estimação simultânea de estados e parâmetros em tempo real. Além disso, é proposta uma forma simples e robusta para reescrever os filtros de Kalman com horizonte retrocedido utilizando programação quadrática.

O trabalho finaliza com as conclusões e sugestões para trabalhos futuros.

Um resumo gráfico da relação entre os estimadores de estado utilizados nos principais capítulos desta tese é mostrado na Figura 1.2.

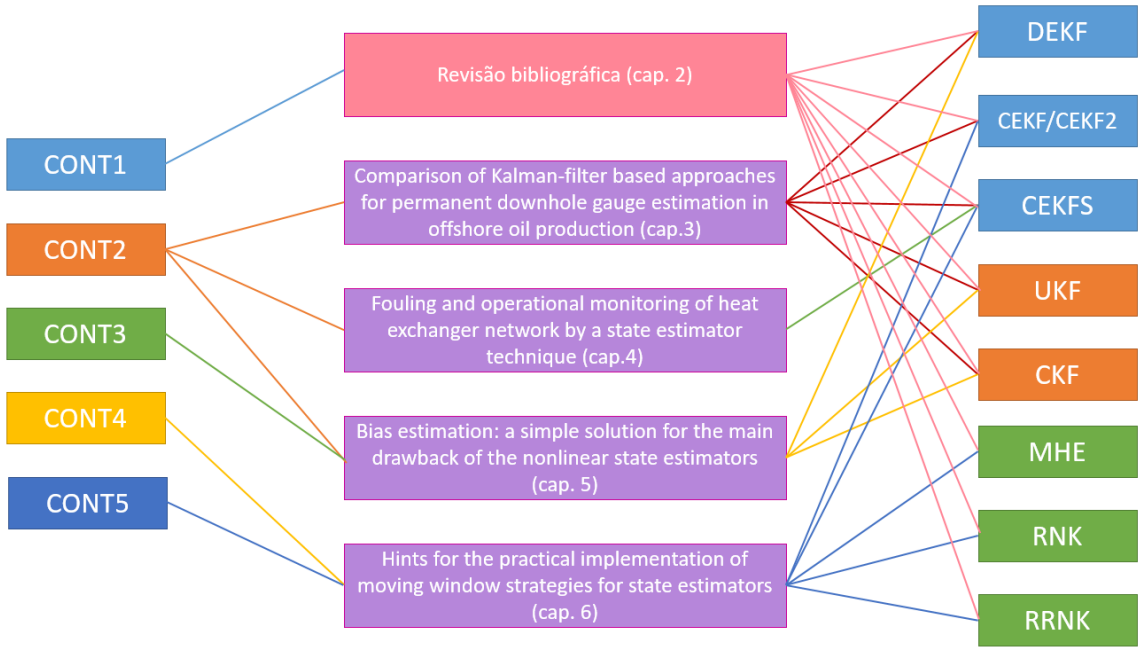


Figura 1.2: Relação entre as contribuições e estimadores de estados aplicados nos principais capítulos desta tese.

1.6 Produção científica e demais atividade

O desenvolvimento deste trabalho originou a produção científica listada a seguir e as demais atividades citadas.

1.6.1 Capítulos deste trabalho:

CAP3: APIO, A., FARENZENA, M., DAMBROS, J. W. V., and TRIERWEILER, J. O.; Capítulo 3 – Comparison of Kalman-filter based approaches for permanent downhole gauge estimation in offshore oil production, publicado na *Journal of Petroleum Science and Engineering.*

CAP4: APIO, A., MARTINELLI, G. B., TRIERWEILER, L. F., FARENZENA, M., and TRIERWEILER, J. O.; Capítulo 4 – Fouling and operational monitoring of heat exchanger network by a state estimator technique, submetido para publicação na *Industrial & Engineering Chemistry Research.*

CAP5: APIO, A., FARENZENA, M., and TRIERWEILER, J. O.; Capítulo 5 – Bias estimation: a simple solution for the main drawback of the nonlinear state estimators, será submetido em revista a ser definida.

CAP6: APIO, A., TRIERWEILER, J. O., and FARENZENA, M.; Capítulo 6 – Hints for the practical implementation of moving window strategies for state estimators, será submetido em revista a ser definida.

1.6.2 Trabalhos completos publicados em anais de congresso

CONG1: APIO, A.; DAMBROS, J. W. V.; DIEHL, F. C.; FARENZENA, M., e TRIERWEILER, J O.; PDG Pressure Estimation in Offshore Oil Well: Extended Kalman Filter vs. Artificial Neural Networks. IFAC-PAPERSONLINE, FAC-PAPERSONLINE, v. 52, p. 508-513, n. 2019.

CONG2: APIO, A.; DIEHL, F. C.; SANTOS, J. E. W, FARENZENA, M., e TRIERWEILER, J.; O. Comparação entre filtros de Kalman para estimação da PDG na produção de petróleo offshore. Este trabalho foi apresentado no XXII Congresso Brasileiro de Automática, 2018, em João Pessoa.

Capítulo 2 – **Revisão Bibliográfica**

Neste capítulo é apresentada uma breve revisão bibliográfica dos principais estimadores de estado e observadores lineares, não lineares, estendidos e com janela móvel. São apresentadas suas principais características, cronologia e ligações entre si. O capítulo finaliza com a formulação do estimador de estados mais relevante neste trabalho: o filtro de Kalman.

2.1 Breve revisão histórica

Enquanto as plantas modernas se tornavam mais e mais complexas devido à quantidade de entradas e saídas, a teoria de controle clássica com uma única entrada e uma única saída (SISO) foi se tornando ineficaz para sistemas com várias entradas e várias saídas (MIMO). Em 1960, devido ao advento de computadores digitais, foi possível a análise de sistemas complexos no domínio do tempo usando variáveis de estado, denominada teoria de controle moderna. Essa metodologia foi desenvolvida para lidar com o aumento da complexidade das plantas modernas e os rigorosos requisitos de precisão e custo em aplicações militares, espaciais e industriais (OGATA, 2009). Por isso, nessa época, o controle moderno serviu como motivação para o desenvolvimento das metodologias de estimação de estados.

Desde o começo da revisão bibliográfica, é importante deixar claro os conceitos de observador de estados e estimador de estados. Segundo Ogata (2009), o observador de estados estima as variáveis de estado baseado na medida de suas saídas e variáveis manipuladas. O estimador de estados possui essa mesma definição, embora o conceito "observador" seja mais usado nas aplicações de controle. Friedland (2010) considera um observador assintótico como estimador de estados, e também explica que o filtro de Kalman é um importante caso especial do observador de Luenberger. Surpreendentemente, o conceito de observador para sistemas dinâmicos foi introduzido anos após ao filtro de Kalman (KALMAN, 1960) por Luenberger (LUENBERGER, 1964). De modo geral, apesar de a definição de "observador" ser um conceito mais geral, o seu uso parece estar mais relacionado à abordagem determinística de Luenberger. Enquanto o filtro de Kalman é um caso especial do observador que considera variáveis estocásticas, i.e., o ruído presente nas entradas e saídas do processo. Neste texto optou-se pela definição de estimador de estados ao invés de observador como conceito generalizado de

estimação de estados. Na Figura 2.1 é mostrado um esquema de como diferentes estimadores de estado se interligam, onde a nomenclatura é apresentada na Tabela 2.1

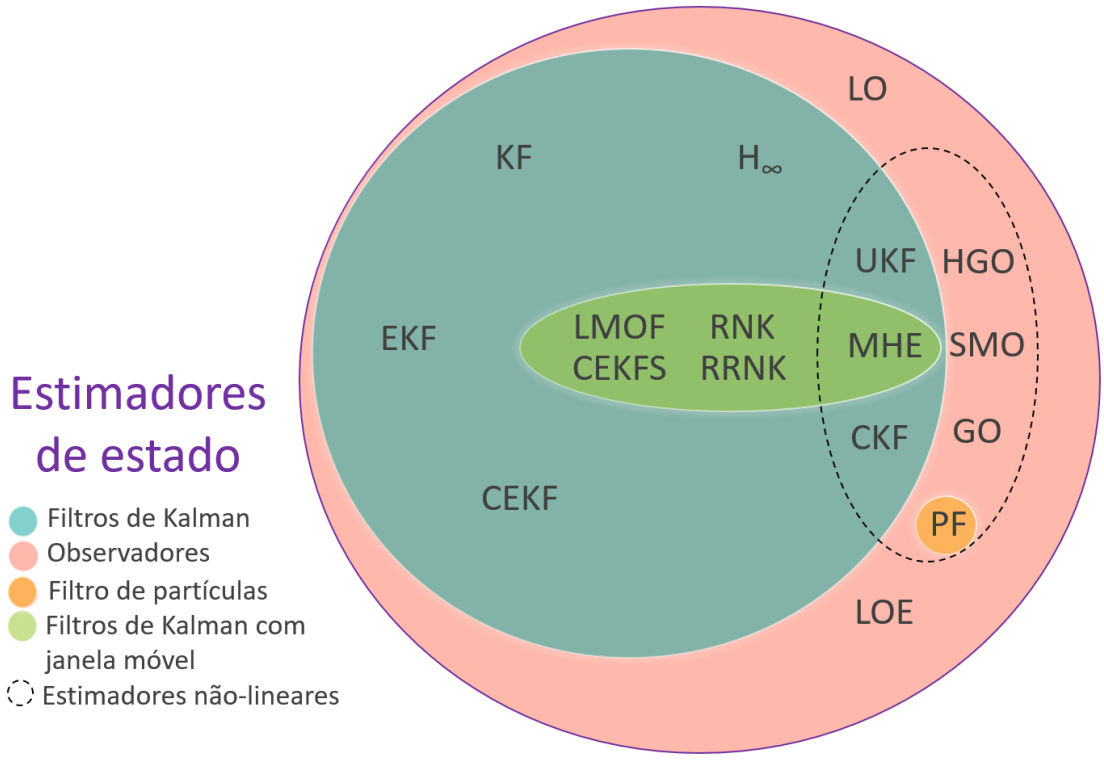


Figura 2.1: Esquema de interligação entre os estimadores de estado.

As contribuições para os estimadores de estado iniciaram muito antes da teoria de controle moderno com Thomas Bayes (1701-1761), o qual introduziu a regra Bayesiana para inferência estatística que fornece a fórmula básica para métodos de estimação Bayesiana. O estudo pioneiro que fornece um estado ótimo a partir de dados ruidosos foi proposto por Carl Friedrich Gauss (1777-1855). Ele inventou o método de estimação mínimos quadrados em 1795 e usou para estimação de problemas não-lineares. Mais tarde, Andrei Markov (1856-1922) introduziu as teorias de processo de Markov e cadeia de Markov, baseadas em métodos de probabilidade e estatísticos. Markov provou que a distribuição de probabilidade dos estados pode ser calculada usando a distribuição atual que contém efeitos de todos os eventos passados do sistema.

Norbert Wiener (1894-1962) introduziu o filtro de Wiener em 1949 para aplicações de processamento de sinais. Esse filtro reduz o ruído presente em um sinal em comparação com a estimação de um sinal desejado sem ruído. Kolmogorov (1903-1987), juntamente a Wiener, fez a fundação das teorias de estimação que foram usadas mais tarde para desenvolver a teoria de predição, filtragem e suavização. As pesquisas em estimadores ótimos ficariam então conhecidas como o filtro Wiener-Kolmogorov, um predecessor do filtro de Kalman (AFSHARI; GADSDEN; HABIBI, 2017).

Em 1960, com o advento do controle moderno, Rudolf Kalman, baseado nos trabalhos de seus antecessores, introduziu uma nova abordagem para filtragem não-linear e predição de problemas. O filtro de Kalman (KF) foi aplicado pela NASA no sistema de navegação da missão Apollo (BOGDANSKI; BEST, 2017) e rapidamente se tornou popular como o método

mais prático para estimação de estados. Rudolf Kalman baseou a construção desse estimador de estados na teoria de probabilidade e considera distúrbios estocásticos, onde as variáveis são aleatórias (e.g., ruído de medida e processo são considerados). Esse filtro usa um modelo dinâmico linear e medidas sequenciais do sistema para fornecer estados estimados ótimos na presença de ruído Gaussiano. Embora o filtro de Kalman seja uma representação alternativa do filtro de Wiener, a contribuição de Kalman foi vincular o problema de estimação de estados aos modelos de espaço de estado, além do conceito de observabilidade (LEVINE, 2009). O KF combina as novas informações introduzidas pelas medições com informações antigas incorporadas no estado anterior com a matriz de ganho de Kalman, o qual equilibra a incerteza nas medições com a incerteza no modelo dinâmico (ALFRIEND *et al.*, 2010). Portanto, a propagação do erro na matriz de covariância *P*, a qual estima as incertezas da predição dos estados, é o que fornece acuracidade ao filtro de Kalman (SIMON, 2006). O diagrama de blocos de cálculo para o filtro de Kalman pode ser visualizado na Figura 2.2.

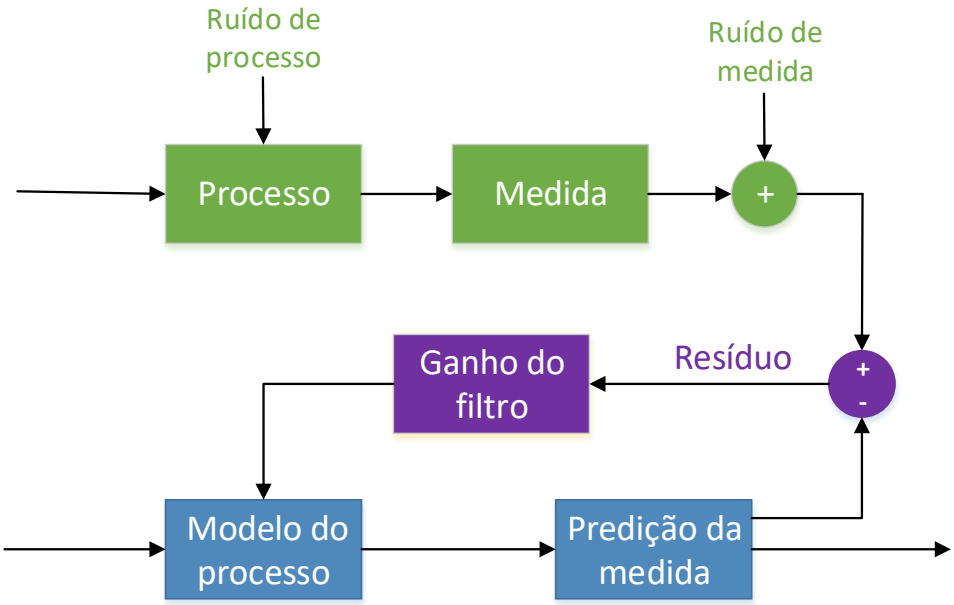


Figura 2.2: Diagrama de blocos de cálculo para o filtro de Kalman.

Paralelamente em 1964, LUENBERGER (1964) introduziu conceitos básicos de observadores de estado ("*Luenberger Observer*" - LO). Essa metodologia reconstrói o vetor de estados a partir de observações das entradas e saídas do sistema, no qual o sistema linear diminui sua complexidade à medida que o número de saídas disponíveis aumenta. O observador considera o modelo determinístico, no qual as variáveis são bem conhecidas, i.e., nenhuma delas é aleatória (GAO *et al.*, 2013). Nesse caso não se tem a presença de ruídos de modelo e processo, que são considerados pelo filtro de Kalman. Para os observadores, a matriz de ganho é computada *offline* para garantir estabilidade assintótica da estimação do erro (QI; TAHA; WANG, 2018). O observador Luenberger genérico apareceu quatro anos após o filtro de Kalman, sendo um caso especial do LO – um observador otimizado para a presença de ruídos nas saídas e entradas do processo (FRIEDLAND, 2010). Hoje, muitos observadores são simplesmente modificações e versões estendidas do observador clássico proposto por Luenberger e o filtro de Kalman (MOHD ALI *et al.*, 2015).

O observador de Luenberger estendido ("*Extended Luenberger Observer*" - ELO) foi proposto em 1987 (ZEITZ, 1987), sendo uma versão não-linear do LO. Os observadores de modo deslizante ("*Sliding Mode Observer*" - SMO) (WALCOTT; CORLESS; ŻAK, 1987) também surgiram em 1987 para sistemas altamente não-lineares e incertos, com a capacidade de gerar um movimento deslizante sobre o erro entre a saída medida da planta e a saída do observador. Essa metodologia produz um conjunto de estimativas de estado que são precisamente proporcionais à saída real da planta. O observador geométrico ("*Geometric Observer*" - GO) (BESTLE; ZEITZ, 1983) foi proposto em 1983, o qual pode ser projetado por uma atribuição de autovalor com base na equação diferencial linearizada do erro do observador. A atribuição de autovalor refere-se às coordenadas da forma canônica de observador do sistema não-linear. Essa metodologia pode ser aplicada a sistemas altamente não-lineares e com incertezas. Os observadores de alto ganho ("*High Order Observer*" - HGO) surgiram em 1991 (BORNARD; HAMMOURI, 1991) para sistemas não-lineares, onde as linearizações podem ser tratadas através de uma abordagem de alto ganho. Um esquema das técnicas de estimação de estados determinísticas e estocásticas é exibido na Figura 2.3.

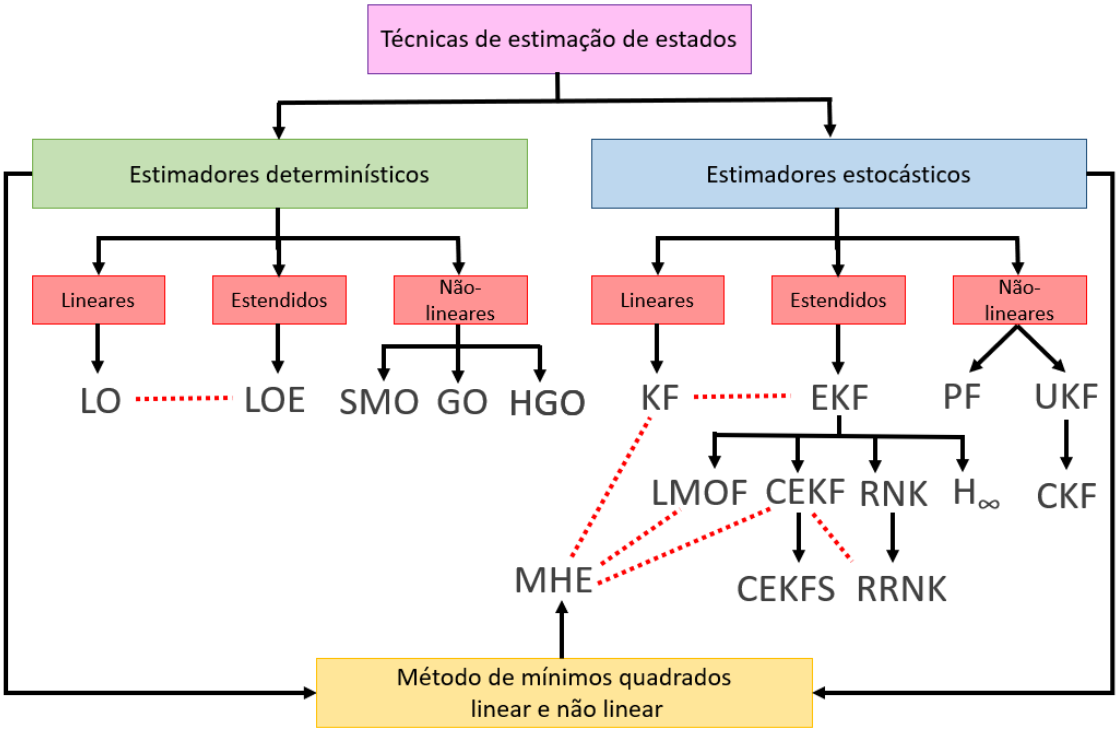


Figura 2.3: Esquema das técnicas de estimadores de estado determinísticas e estocásticas, onde as linha tracejada vermelha representa a conexão entre os estimadores.

Como a versão do KF é originalmente linear, a versão para modelos não-lineares lineariza todas as transformações não-lineares em transformações lineares através do cálculo da Jacobiana (JAZWINSKI, A. H., 1970). Esse filtro, denominado filtro de Kalman estendido ("*Extended Kalman Filter*" - EKF), é o algoritmo mais amplamente utilizado para estimação de estados em sistemas não-lineares. No entanto, o EKF pode ser difícil de ajustar e frequentemente fornece estados não confiáveis se as não-linearidades do sistema são severas. Isso acontece porque o EKF depende da linearização para propagar a média e a covariância do estado. Nesse quesito, o filtro de Kalman sem rastro ("*Unscented Kalman Filter*" - UKF), proposto em 1997, não requer linearizações para nenhuma de suas funções

não lineares: a distribuição dos estados é especificada usando pontos de amostra cuidadosamente selecionados. Esses pontos buscam capturar a verdadeira média e a covariância da variáveis, e, quando propagados através do verdadeiro sistema não-linear, eles também capturam a média posterior e a covariância com precisão de segunda ordem (expansão em série de Taylor) para qualquer não-linearidade (WAN; VAN DER MERWE, 2002).

Em 2009, Arasaratnam e Haykin (2009) propuseram o filtro de Kalman de cubatura ("*Cubature Kalman Filter*" - CKF), que possui melhorias em relação ao UKF. O CKF possui uma regra de cubatura esférica-radial de terceira ordem que fornece o conjunto de pontos de cubatura que são escalados linearmente com a dimensão do vetor do estado. Esses pontos têm pesos iguais para calcular a média e covariância das variáveis de estado que, depois de uma transformação não-linear, melhoram a qualidade da aproximação ótima não-linear, acuracidade do filtro e estabilidade numérica. Embora o UKF e o CKF possam fornecer melhorias significativas na acuracidade em relação ao EKF, eles ainda são estimadores não-lineares aproximados. O EKF estima a média de um sistema não-linear com acuracidade de primeira ordem, enquanto o UKF e o CKF fornecem uma estimativa com acuracidade de ordem maior. Isso apenas adia a divergência inevitável que acontecerá quando o sistema ou medidas não-lineares se tornarem muito não-lineares (SIMON, 2006).

Nesse quesito, o filtro de partículas ("*Particle Filter*" - PF) é um estimador de estados "completamente" não-linear com distribuição de ruídos não-gaussiana. O PF usa um conjunto randômico de partículas ponderadas que aproximam as características não-lineares ou distribuições do estado anterior com um uma função densidade de probabilidade (PDF) (AFSHARI; GADSDEN; HABIBI, 2017). Basicamente, ele é uma metodologia estatística que usa força bruta para estimação que frequentemente apresenta bom desempenho para problemas que são difíceis de serem resolvidos pelo filtro de Kalman convencional. O preço a ser pago por isso é o seu elevado esforço computacional. O PF teve seu início em 1949 com o trabalho de METROPOLIS; ULAM (1949), mas desde 1980 que a capacidade computacional foi suficiente para sua implementação (SIMON, 2006). A linha do tempo dos estimadores de estado é mostrada na Figura 2.4.

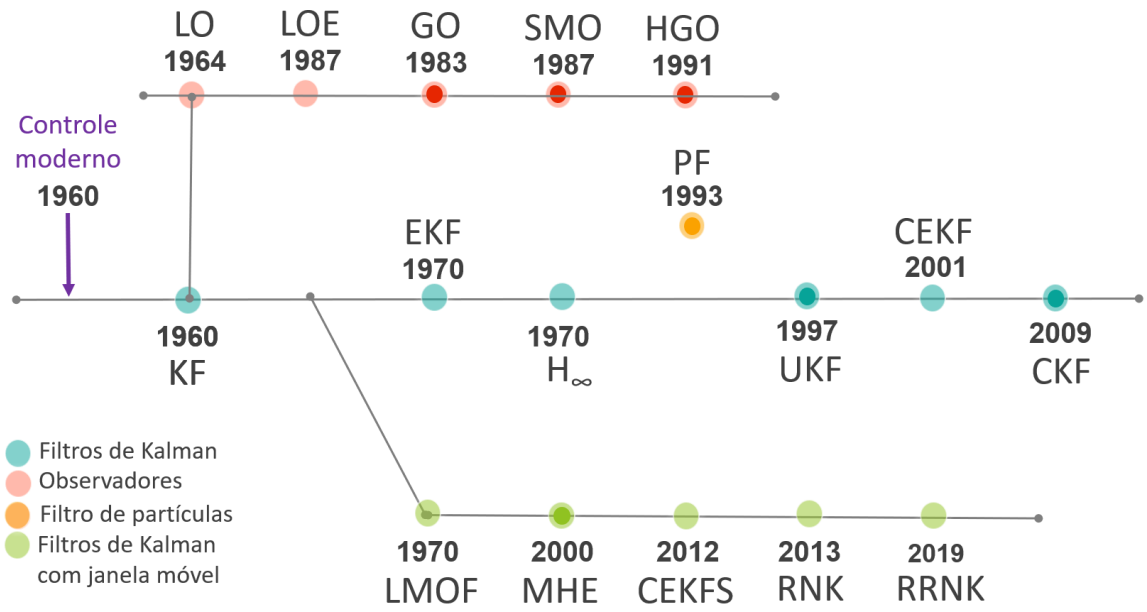


Figura 2.4: Cronologia dos estimadores de estado, onde os pontos com as cores mais escuras representam estimadores não-lineares, e as cores mais claras os estimadores lineares/estendidos.

Em 1970, surgiu o filtro H_∞, cuja proposta é ignorar a necessidade de um modelo perfeito ou conhecimento completo das estatísticas de entrada. Diferente do filtro de Kalman que tem como objetivo fornecer a estimativa quadrática média mínima, o filtro ótimo H_∞ tenta minimizar o efeito dos piores distúrbios possíveis na estimação dos erros e, portanto, é mais robusto em relação às incertezas do modelo (LI; JIA, 2010). De modo geral, comparando o filtro de Kalman com o filtro H_∞, esse último é simplesmente uma versão robusta do filtro de Kalman. As desvantagens do filtro H_∞ em relação ao filtro de Kalman são que sua performance é mais sensível aos parâmetros de projeto, e que a teoria desse filtro é mais abstrata e complicada. O filtro H_∞ é mais adequado para quando suas principais considerações são o pior desempenho da estimativa, sistemas em que o modelo muda de forma imprevisível e sistemas nos quais o modelo não é bem conhecido (SIMON, 2006). Além disso, o filtro H_∞ apresenta as mesmas dificuldades em sua linearização do que o EKF, tais como a suavização, erros de linearização e dificuldades no cálculo da matriz Jacobiana.

Devido à fraca performance e as divergências do filtro de Kalman estendido relacionadas a erros de modelagem, Jazwinski (1970) propôs o filtro otimizado de memória limitada. A ideia desse filtro com horizonte móvel é estimar o vetor de estados baseado em um número finito de amostras de medidas do passado, de modo que as medidas mais antigas sejam descartadas enquanto novas medidas ficam disponíveis. Limitando a memória do filtro, o estimado é computado baseado nos dados do passado recente, o qual pode representar uma aproximação satisfatória da realidade.

Nos anos 1990 (RAO, C. V; RAWLINGS; LEE, 2001), o avanço computacional possibilitou a popularização do estimador de horizonte móvel ("*Moving Horizon Estimation*" - MHE), que é uma metodologia baseada em otimização que advém do filtro otimizado de memória limitada com a adição de restrições. Para casos lineares sem restrições com ruído gaussiano, o MHE se reduz exatamente ao filtro de Kalman. No entanto, em casos não-lineares para um valor razoavelmente grande de tamanho de horizonte, o MHE não se

igualа ao EKF. Muitos exemplos de simulação mostram que o ajuste do MHE usando um modelo completamente não-linear nas equações de estado fornece um nível de robustez que não é alcançado com o EKF (HASELTINE; RAWLINGS, 2005; RAWLINGS; BAKSHI, 2006). Em 2001, Gesthuisen *et al.* (2001) propuseram o filtro de Kalman estendido com restrições, que advém do MHE com comprimento de horizonte igual a zero. Em 2012 surgiu o filtro de Kalman estendido com restrições e suavizado (CEKFS) (SALAU; TRIERWEILER; SECCHI, 2012b), o qual utiliza o suavizador Rauch-Tugh-Striebel (RTS) (HAYKIN, 2001; RAUCH; STRIEBEL; TUNG, 1965) para suavizar os estados e a sua matriz de covariância no comprimento da janela. Os novos valores suavizados dessas variáveis são utilizados como valores iniciais para a nova simulação do CEKF.

Rengaswamy *et al*. (2013, 2011) apresentaram em 2013 uma nova abordagem de horizonte móvel denominado filtro de Kalman não-linear de horizonte deslizante ("*Receding Horizon Non-Linear Kalman Filter*" - RNK) que, ao invés do MHE, segue a estrutura de predição e correção do filtro de Kalman. Essa metodologia apresenta vantagens computacionais uma vez que evita integrações repetidas no loop de otimização que são necessários no MHE. Uma versão robusta dessa metodologia foi apresentada por Rangegowda *et al.* (2019) com o objetivo de minimizar os efeitos grosseiros na estimação dos estados. O filtro de Kalman não linear de horizonte deslizante robusto ("*Robust Receding Horizon Non-Linear Kalman Filter*" - RRNK) foi desenvolvido integrando a função de Huber com o RNK a fim de incorporar robustez ao filtro. Essa metodologia proposta foi capaz de gerar desempenhos de estimação comparáveis ao estimador de horizonte móvel (MHE) robusto, a um custo computacional inferior.

Tabela 2.1: Nomenclatura dos estimadores de estado.

Sigla	Nome em inglês	Nome em português	Linear/ Estendido/ Não-linear	Horizonte
KF	*Kalman filter*	Filtro de Kalman	Linear	Não
EKF	*Extended Kalman filter*	Filtro de Kalman estendido	Estendido	Não
CEKF	*Constrained extended Kalman filter*	Filtro de Kalman estendido com restrições	Estendido	Não
CEKFS	*Constrained extended Kalman filter and smoother*	Filtro de Kalman estendido com restrições e suavizado	Estendido	Sim
UKF	*Unscented Kalman filter*	Filtro de Kalman sem rastro	Não-linear	Não
CKF	*Cubature Kalman filter*	Filtro de Kalman de cubatura	Não-linear	Não
LMOF	*Limited memory optimal filter*	Filtro otimizado de memória limitada	Estendido	Sim
MHE	*Moving horizon estimation*	Estimador de horizonte móvel	Não-linear	Sim
RNK	*Receding horizon non-linear Kalman filter*	Filtro de Kalman não-linear de horizonte retrocedido	Estendido	Sim
RRNK	*Robust receding horizon non-linear Kalman filter*	Filtro de Kalman não linear de horizonte retrocedido robusto	Estendido	Sim
H_∞	*H_∞ filter*	Filtro H_∞	Estendido	Não
PF	*Particle filter*	Filtro de partículas	Não-linear	Não
LO	*Luenberger observer*	Observador de Luenberger	Linear	Não

Sigla	Nome em inglês	Nome em português	Linear/ Estendido/ Não-linear	Horizonte
ELO	*Extended Luenberger observer*	Observador de Luenberger estendido	Estendido	Não
SMO	*Sliding mode observer*	Observador de modo deslizante	Não-linear	Não
GO	*Geometric observer*	Observador geométrico	Não-linear	Não
HGO	*High gain observer*	Observador de alto ganho	Não-linear	Não

Apesar desta revisão ter mostrado uma visão geral dos estimadores de estado, o foco deste trabalho são os filtros de Kalman. Dessa forma, a partir de agora, neste texto, o conceito de estimadores de estado considerará apenas os filtros de Kalman.

2.2 Equacionamento do filtro de Kalman

2.2.1 Equacionamento do filtro de Kalman resumido

Dado o sistema de equações não-lineares de um modelo dinâmico, os estados estimados e as saídas estimados *a priori* são:

$$\hat{x}_{k|k-1} = f(x, u, t) + \omega \tag{2.1}$$

$$y_k = h(x_k, t_k) + v_k \tag{2.2}$$

O sistema é, então, linearizado:

$$F(t) = \left(\frac{\partial f}{\partial x}\right)_{x,u,t} \tag{2.3}$$

$$\phi_{k-1} = e^{F(t_k - t_{k-1})} \tag{2.4}$$

$$H = \left(\frac{\partial h}{\partial x}\right)_{x,u,t} \tag{2.5}$$

A covariância dos estados estimados *a priori* é dada por:

$$P_{k|k-1} = \phi_{k-1} P_{k-1|k-1} \phi_{k-1}^T + Q_k \tag{2.6}$$

O ganho de Kalman é calculado

$$K_k = P_{k|k-1} H_k^T S_k^{-1} \tag{2.7}$$

onde a covariância de inovação é dada por

$$S_k = H_k P_{k|k-1} H_k^T + R_k \tag{2.8}$$

no qual os estados *a posteriori* são atualizados

$$\hat{x}_{k|k} = \hat{x}_{k|k-1} + K_k\left[y_k - h\left(\hat{x}_{k|k-1}, t_k\right)\right] \tag{2.9}$$

e a covariância *a posteriori* dos novos estados é:

$$P_{k|k} = [I_n - K_k H_k] P_{k|k-1} \tag{2.10}$$

onde *k* representa o passo considerado em tempo discreto, *x* é o vetor de estados, *f* é a função do modelo, *ω* é o vetor de ruído de processo, *y* é o vetor das saídas, *h* é a função que relaciona os estados às saídas, *v* é o vetor de ruído de medida, *F* é a Jacobina de *f* em relação aos estados, *φ* é a matriz de transição de um estado para outro, *H* é a Jacobiana de *h* em relação à saídas, *P* é a matriz de covariância dos estados, *Q* é a matriz de covariância do ruído de processo, *R* é a covariância do ruído de medida, e *K* é o ganho de Kalman.

2.2.2 Dedução da matriz de covariância a posteriori

Considerando que a covariância $P_{k|k}$ é dada por:

$$P_{k|k} = cov(x_k - \hat{x}_{k|k}) \tag{2.11}$$

substituindo a variável $\hat{x}_{k|k}$ pela equação 2.9:

$$P_{k|k} = cov\left(x_k - \left(\hat{x}_{k|k-1} + K_k\left(y_k - h\left(\hat{x}_{k|k-1}, t_k\right)\right)\right)\right) \tag{2.12}$$

e as variáveis y_k e $h\left(\hat{x}_{k|k-1}, t_k\right)$

$$P_{k|k} = cov\left(x_k - \left(\hat{x}_{k|k-1} + K_k(H_k x_k + v_k - H_k)\right)\right) \tag{2.13}$$

isolando x_k e $\hat{x}_{k|k-1}$

$$P_{k|k} = cov\left((I - K_k H_k)\left(x_k - \hat{x}_{k|k-1}\right) - K_k v_k\right) \tag{2.14}$$

como o erro da medida v_k é independente dos outros termos:

$$P_{k|k} = cov\left((I - K_k H_k)\left(x_k - \hat{x}_{k|k-1}\right)\right) + cov(K_k v_k) \tag{2.15}$$

Considerando a propriedade básica das matrizes de covariância:

$$var(AX + a) = A \cdot var(X) \cdot A^T \tag{2.16}$$

obtém-se:

$$P_{k|k} = (I - K_k H_k) cov\left(x_k - \hat{x}_{k|k-1}\right)(I - K_k H_k)^T + K_k cov(v_k) K_k^T \tag{2.17}$$

o qual, usando as definições de $P_{k|k-1}$ e R_k, se torna:

$$P_{k|k} = (I - K_k H_k) P_{k|k-1} (I - K_k H_k)^T + K_k R_k K_k^T \tag{2.18}$$

Essa fórmula é válida para qualquer valor de K_k, que pode ser simplificado conforme mostrado na próxima seção.

2.2.3 Dedução do ganho de Kalman

Considerando que o filtro de Kalman é um estimador de erro quadrático médio mínimo, o erro na estimação do estado *a posteriori* é:

$$x_k - \hat{x}_{k|k} \tag{2.19}$$

O objetivo é minimizar o valor esperado do quadrado da magnitude desse vetor $E\left[\left\|x_k - \hat{x}_{k|k}\right\|^2\right]$. Isso é equivalente a minimizar o traço de uma estimação *a posteriori* da matriz de covariância $P_{k|k}$, que é equivalente à soma dos elementos de sua diagonal principal dessa matriz quadrada. Expandindo os termos da equação 2.18 e isolando-os, obtêm-se:

$$P_{k|k} = P_{k|k-1} - K_k H_k P_{k|k-1} - P_{k|k-1} H_k^T K_k^T + K_k (H_k P_{k|k-1} H_k^T + R_k) K_k^T \tag{2.20}$$

$$P_{k|k} = P_{k|k-1} - K_k H_k P_{k|k-1} - P_{k|k-1} H_k^T K_k^T + K_k S_k K_k^T \tag{2.21}$$

O traço é minimizado quando a derivada da matriz em relação ao ganho é zero. Considerando as regras de matrizes de gradiente e a simetria das matrizes envolvidas, tem-se:

$$\frac{\partial\, tr(P_{k|k})}{\partial\, K_k} = -2\left(H_k P_{k|k-1}\right)^T + 2K_k S_k \tag{2.22}$$

resolvendo para o ganho de Kalman K_k:

$$K_k S_k = \left(H_k P_{k|k-1}\right)^T = P_{k|k-1} H_k^T \tag{2.23}$$

$$K_k = P_{k|k-1} H_k^T S_k^{-1} \tag{2.24}$$

O ganho de Kalman é aquele que leva a estimativas de erro quadrático médio mínimo, sendo a fórmula 2.24 denominada ganho de Kalman ótimo.

2.2.4 Simplificação da fórmula da covariância do erro a posterori

A fórmula utilizada para calcular a covariância do erro *a posteriori* pode ser simplificada quando o ganho de Kalman se iguala ao valor ótimo derivado acima. Multiplicando ambos os lados da fórmula do ganho de Kalman (equação 2.24) por $S_k K_k^T$

$$K_k S_k K_k^T = P_{k|k-1} H_k^T K_k^T \tag{2.25}$$

substituindo a equação 2.25 na covariância do erro a posteriori (equação 2.21):

$$P_{k|k} = P_{k|k-1} - K_k H_k P_{k|k-1} - P_{k|k-1} H_k^T K_k^T + P_{k|k-1} H_k^T K_k^T \tag{2.26}$$

cancelando os últimos dois termos e rearranjando a equação:

$$P_{k|k} = [I_n - K_k H_k] P_{k|k-1} \tag{2.27}$$

2.3 Demais equacionamentos dos estimadores de estado

Os equacionamentos dos respectivos estimadores de estado estão detalhados nas seguintes seções, conforme Tabela 2.2.

Tabela 2.2: Relação entre os estimadores de estado e seções onde são detalhados.

Estimador de estado	Seção
DEKF	3.3.1.1
CEKF	3.3.1.2 e 6.3.2
CEKF implementação curta	6.3.3
CEKFS	3.3.1.3
UKF	3.3.1.4
CKF	3.3.1.5
MHE	6.3.1
RNK	6.3.4
RRNK	6.3.5

Capítulo 3 – Comparison of Kalman-filter based approaches for permanent downhole gauge estimation in offshore oil production

O presente capítulo é a reprodução do manuscrito que foi publicado na *Journal of Petroleum Science and Engineering*

ABSTRACT: The permanent downhole gauge (PDG) pressure is the most critical variable to describe the dynamics of an offshore oil well. Unfortunately, this measurement is often unavailable due to premature sensor failure and the considerable price for its replacement. An alternative to dealing with the lack of PDG pressure measurement is its estimation. For this, Kalman filters are standard tools, with which two distinct state estimators (extended and unscented Kalman filters) were proposed in the literature. These approaches have disadvantages related to the requirement for system linearization and the high computational cost, bringing the necessity for new techniques. In this work, five different Kalman filter-based approaches are tested and compared for the PDG pressure estimation. Through simulated and industrial data, the advantages and disadvantages of each filter are pointed. The results broadly show that the cubature Kalman filter returns the best estimation in the industrial case study, in which the model was correctly adjusted. Meanwhile, the extended filters have the best performance in the simulated scenarios, considering that the model was not correctly adjusted. Also, the estimation using a single measurement that is highly correlated to the PDG pressure is enough for its estimation.

3.1 Introduction

Oil and natural gas are needful resources that, once combined, provide over half of the world energy supply. Since 2012, global offshore production has contributed to the dry gas industry with about 110 billion cubic feet per day (Bcf/d), which accounts for about one-third of the total global production (FENG, 2017). With a similar ratio, offshore oil production reaches nearly 30% of the overall production (27 million barrels of oil in 2015) (MANNING, 2016).

In offshore oil production, when the reservoir pressure is insufficient to sustain the oil flow up to the surface at demanded rates, the natural flow must be aided by an artificial lift through gas injection. However, oil production with gas lift can generate limit cycles depending on the process operational conditions. This phenomenon is called slugging and introduces oscillatory behavior into the process (DI MEGLIO, F; KAASA; PETIT, 2009; HU, 2004; JAHANSHAHI; SKOGESTAD; HANSEN, 2012; JANSEN *et al.*, 1999; SINEGRE; PETIT; MENEGATTI, 2006; TORRE *et al.*, 1987). Slugging is defined by Di Meglio *et al.* (2012) as an intermittent flow regime characterized by inhomogeneous distribution of the gas and liquid phases.

The permanent downhole gauge (PDG) is a device, which contains pressure and temperature sensors, usually placed subsea and close to the perforation in deepwater wells (HÜFFNER; TRIERWEILER; FARENZENA, 2019; YUAN, 2018). The pressure from the PDG (p_{pdg}) is the most critical variable to describe the dynamics of an offshore oil well (ANTONELO; CAMPONOGARA; FOSS, 2017; NYGAARD; NAEDAL; MYLVAGANAM, 2006) and to monitor the oil and gas production (ALGEROY *et al.*, 2010). The p_{pdg} is also important due to its frequent use as a controlled variable in oil productions operating in both anti-slugging (CAMPOS *et al.*, 2015) and slugging regions (GEREVINI; FARENZENA; TRIERWEILER, 2018). Since this permanent monitoring system is complex and installed in hazardous and remote areas, the cost to retrieve or repair it, as well as reinstalling its failed parts, is overly high (ALGEROY *et al.*, 2010).

As a replacement is unfeasible, techniques for p_{pdg} estimation have been arising. Some of these works rely on NARMAX (nonlinear autoregressive moving average models with exogenous inputs) and neural network models (AGUIRRE *et al.*, 2017; ANTONELO; CAMPONOGARA; FOSS, 2017; BARBOSA *et al.*, 2015; SPESIVTSEV *et al.*, 2018; TEIXEIRA *et al.*, 2014), or on the use of Kalman filters (i.e., extended Kalman filter (GRYZLOV; SCHIFERLI; MUDDE, 2013) and unscented Kalman filter (AGUIRRE *et al.*, 2017; REZENDE; TEIXEIRA; MENDES, 2015)).

Black box approaches, such as NARMAX and neural networks, require p_{pdg} data for the fit/training of a model that are later used for the estimation of unknown p_{pdg} values given that new input values are available. These approaches have a substantial disadvantage for the application in p_{pdg} estimations. Oil wells have very distinct operation conditions with two different behaviors: oscillatory and non-oscillatory. In order to generate a representative black-box model, data from different operational conditions are required. However, this is unfeasible to be obtained, mainly because dealing with the oscillatory regime is avoided.

Kalman filters are gray box approaches that combine a phenomenological model of the process and a set of known measurements to estimate unknown variables, ensuring estimation within a wide range of operating conditions. This guarantees the estimation within a large range of process operating conditions. Apio *et al.* (2019) compared the PDG pressure estimation using neural networks with extended Kalman filters, in which the results confirmed that neural network models could only estimate the p_{pdg} for the region where it was trained, so that outside this region the neural network produces poor results. On the other hand, the extended Kalman filter returned satisfactory estimations in all cases.

In the literature, the use of two Kalman filter approaches for the p_{pdg} estimation has been considered: extended Kalman filter (EKF) and unscented Kalman filter (UKF). Both filters have disadvantages, i.e., the EKF estimator linearizes the nonlinear dynamic system, and the UKF suffers from higher computational cost.

Here, we systematically compare the use of the following five Kalman filter-based approaches for the p_{pdg} estimation:

- discrete extended Kalman filter (DEKF) (JAZWINSKI, A. H., 1970),
- constrained extended Kalman filter (CEKF) (GESTHUISEN; KLATT; ENGELL, 2001),
- constrained extended Kalman filter and smoothing (CEKF&S) (SALAU; TRIERWEILER; SECCHI, 2012b),
- unscented Kalman filter (UKF) (JULIER, S. J.; UHLMANN, 2004), and
- cubature Kalman filter (CKF) (ARASARATNAM; HAYKIN, 2009).

The analysis and comparisons are handled by using three datasets. The first and second data sets contain simulated data generated in OLGA (OiL and GAs dynamic multiphase flow simulator), and the third contains measurements from a real offshore oil well. The performance of the filters is measured through the mean squared error (MSE), and the error distribution is visualized in both box and violin plots.

Following the introduction, this works continues in Section 3.2 with the comparison of Kalman filter-based approaches in different applications. Section 3.3 details the methodology, i.e. the Kalman filter-based approaches are explained and formulated, and the evaluation criteria are specified. In Section 3.4, the case studies and the applied model are presented. Section 3.5 shows the results for both OLGA and real datasets. The conclusions of the work are presented in Section 3.6.

3.2 Comparison of Kalman filter-based approaches in different applications

Kalman filters for state estimation have many distinct applications. This section presents recent researches in the area.

D'Alfonso *et al.* (2015) applied the EKF and the UKF to estimate the position and orientation of a mobile robot using real data. In this case, both filters performed reasonably well in reconstructing the position of the robot. Even though the approximation properties of the UKF are far superior to those of the EKF, the nonlinearities in the model were probably not bad enough to highlight the substantial difference.

Yang *et al.* (2017) compared the UKF with the EKF in applications of vehicle navigation, demonstrating that the UKF had the benefit of avoiding the Jacobian matrix calculation. In contrast, the EKF was more computationally efficient and more stable. Uilhoorn (2017) also compared the EKF with the UKF to estimate the gas flow dynamics in the pipeline. In this case, the difference in accuracy between the EKF and the UKF was not significant. The EKF performed even better in terms of accuracy. Considering the computation time of the UKF, the use of the EKF seemed the most suitable choice.

Astroza *et al.* (2019) performed a comparison of Kalman-based filters to estimate unknown model parameters of the nonlinear finite element model of a three-dimensional reinforced concrete frame building. They also ensured that the UKF outperformed the EKF slightly, preventing significant and abrupt changes in the estimation of the model parameters.

In a very recent work, Garcia *et al.* (2019) compared state estimators (EKF, UKF, and CKF) for sequential spacecraft attitude estimation with real data. The authors concluded that the filters are very competitive when compared to one another: the processing time of the EKF was faster than the others, but at the cost of possible divergence problems in the estimation process due to the linearization in the equations that describe the dynamic system.

In offshore oil wells, the PDG estimation is crucial, mainly in terms of control, since several anti-slugging control strategies are based on PDG control (CAMPOS *et al.*, 2015; DIEHL, Fabio C *et al.*, 2018; GEREVINI; FARENZENA; TRIERWEILER, 2018). In oil well systems, this is the first time that the CKF is applied as a soft sensor to estimate the PDG pressure. In this area, Teixeira *et al.* (2014) proposed a data-driven soft sensor to estimate online the PDG based on available measurements using two steps. Firstly, a discrete-time black-box and gray-box NARX (nonlinear autoregressive with exogenous with inputs) models were independently identified offline using historical data. In the sequence, recursive predictions of these models were combined with current measured data using a bank of unscented Kalman filters. The authors ensured that this UKF filter bank added robustness regarding outliers in measured data and time-varying dynamics. Although not discussed in the mentioned paper, the computational time of using the UKF as a state estimator is considerably high.

3.3 Methodology

This section presents a brief review of the five Kalman filter-based approaches and the performance measurement criteria applied to this work. The methodologies presented below, such as the Kalman filter and the model (Section 3.1), were entirely coded in Python 2.7 with the aid of JModelica (ÅKESSON *et al.*, 2010). The tests were run in a PC with an Intel® Core™ i7-3632QM CPU @ 2.20GHz 2.20 GHz processor and with 8 GB RAM.

3.3.1 Kalman filter approaches

The Kalman filter (KF) (KALMAN, 1960) is an approach for minimum mean-square error filtering that uses state-space methods. It was developed by the dynamic analysis branch of the National Aeronautics and Space Administration (NASA) for the real-time navigation system of the Apollo spacecraft mission (BOGDANSKI; BEST, 2017). The methodology requires a dynamic model of the system, input measurements, and other available measurements either to predict unknown variables or to filter known ones. This data may present noise and other discrepancies (e.g., from the sensors) that are corrected by the filter.

The Kalman filter equations provide a recursive estimate of the states and their covariance error. The quality of this estimation depends on the system parameters and the noise statistics given as inputs to the estimator. In this context, the Kalman filter blends new information introduced by the measurements with old information embodied in the

prior state with the Kalman gain matrix, which balances uncertainty in the measurements with the uncertainty in the dynamic model (ALFRIEND *et al.*, 2010). Thus, the error propagation in the covariance matrix *P*, which estimates the uncertainties from the state prediction, is what brings accuracy to the Kalman filter (SIMON, 2006).

In this section, five different Kalman filter-based approaches are described: discrete extended Kalman filter, constrained extended Kalman filter, constrained extended Kalman filter and smoother, unscented Kalman filter, and cubature Kalman filter.

3.3.1.1. Discrete Extended Kalman Filter

The most common application of the KF to nonlinear systems is the extended Kalman filter (EKF) (JAZWINSKI, A. H., 1970). The EKF simply linearizes all nonlinear transformations and substitutes the Jacobian matrices for linear transformations in the KF equations by expanding it into a Taylor series. According to Julier and Uhlmann (2004), although the EKF maintains the elegant and computationally efficient recursive update form of the KF, it suffers a number of serious limitations, such as: a) linearized transformations are only reliable if the error propagation can be properly approximated by a linear function. If this condition does not hold, the linearized approximation can be extremely poor; b) for the linearization, the Jacobian matrix is necessary, which is not always available. Some systems contain discontinuities, in which the parameters change abruptly, and other singularities that may hinder the evaluation of the system derivatives; c) calculating the Jacobian matrices can be very difficult due to its dense algebra. Thus, since approximations must be made in the linearization, the EKF is a suboptimal filter in the sense that its stability and performance are not guaranteed (ALFRIEND *et al.*, 2010).

In this work, the EKF in discrete-time is used, i.e., it considers measurements in discrete time about the current estimate, which is detailed in Simon (2006). The system of non-linear equations is given as follows:

$$\dot{x} = f(x, u, t) + \omega(t) \tag{3.1}$$

$$y_k = h(x_k, t_k) + v_k \tag{3.2}$$

The system is then linearized:

$$F(t) = \left(\frac{\partial f}{\partial x}\right)_{x,u,t} \tag{3.3}$$

$$\phi_{k-1} = e^{F(t_k - t_{k-1})} \tag{3.4}$$

$$H = \left(\frac{\partial h}{\partial x}\right)_{x,u,t} \tag{3.5}$$

The states covariance is:

$$P_{k|k-1} = \phi_{k-1} P_{k-1|k-1} \phi_{k-1}^T + Q_{k-1} \tag{3.6}$$

Given the correction step

$$K_k = P_{k|k-1} H_k^T \left[H_k P_{k|k-1} H_k^T + R_k\right]^{-1} \tag{3.7}$$

the states are updated as:

$$\hat{x}_{k|k} = \hat{x}_{k|k-1} + K_k\left[y_k - h\left(\hat{x}_{k|k-1}, t_k\right)\right] \tag{3.8}$$

and the covariance of the new states is:

$$P_{k|k} = [I_n - K_k H_k]P_{k|k-1} \tag{3.9}$$

where *k* represents the step considered in discrete time, *x* is the vector of states, *f* is a model function, *ω* is the process noise vector, *y* is the output vector, *h* is a function that relates the states to the outputs, *v* is the measurement noise vector, *F* is the Jacobian of *f* in relation to the states, *φ* is the transition matrix from one state to another, *H* is the Jacobian of *h* in relation to the outputs, *P* is the covariance matrix of the states, *Q* is the process noise covariance matrix, *R* is the measurement noise covariance, and *K* is the Kalman gain.

3.3.1.2. Constrained Extended Kalman Filter

The constrained extended Kalman filter (GESTHUISEN; KLATT; ENGELL, 2001) comes from the moving horizon estimation (MHE), which is an optimization approach to estimate measured and unmeasured states of dynamical systems considering a moving window when the horizon length is equal to zero. This simplifies the complexity of solving the MHE dynamic nonlinear optimization problem (FRANKE *et al.*, 2001), resulting exactly in the formulation of the CEKF, as follows:

$$\min_{\omega_{k-1|k}, v_{k|k}} J = \omega_{k-1|k}^T \left(P_{k-1|k-1}\right)^{-1} \omega_{k-1|k} + v_{k|k}^T (R_k)^{-1} v_{k|k} \tag{3.10}$$

with the following constraints:

$$H_k \omega_{k-1|k} + v_{k|k} = y_k - h\left(\hat{x}_{k|k}\right) \tag{3.11}$$

$$x_{min} - \hat{x}_{k|k} \leq \omega_{k-1|k} \leq x_{max} - \hat{x}_{k|k} \tag{3.12}$$

$$y_{min} - h\left(\hat{x}_{k|k}\right) \leq H_k \omega_{k|k-1} + v_{k|k} \leq y_{max} - h\left(\hat{x}_{k|k}\right) \tag{3.13}$$

in which the prediction matrix is given via the Riccati matrix in discrete time:

$$P_{k|k} = \phi_{k-1} P_{k-1|k-1} \phi_{k-1}^T - \left(\phi_{k-1} P_{k-1|k-1} H_k^T\right)\left(H_k P_{k-1|k-1} H_k^T + R_k\right)^{-1}\left(H_k P_{k-1|k-1} \phi_{k-1}^T\right) + Q_{k-1} \tag{3.14}$$

and the final correction by

$$\hat{x}_{k|k} = \hat{x}_{k|k-1} + \omega_{k-1|k} \tag{3.15}$$

$$y_k = \hat{y}_{k|k} + v_{k|k} \tag{3.16}$$

3.3.1.3. Constrained Extended Kalman Filter and Smoother

The constrained extended Kalman filter and smoother (SALAU; TRIERWEILER; SECCHI, 2012b) includes the EKF smoother counterpart in the CEKF. Its main difference is that the recursion in the filter moves forward and the smoother backward (HAYKIN, 2001). This smoothing is significant once the CEKF and DEKF fail to converge swiftly to the actual states when the system is subject to poor guesses at the initial state (RAUCH; STRIEBEL; TUNG,

1965). In this context, smoothing means providing an estimate of the system state at some time step, given that all the measurements, including the ones encountered after that particular time step, are available. In short, the smoother gives a smoothed estimate of the system history for all the measurements obtained so far.

Firstly, from the CEKF evaluation results, the following variables are set:

$$\hat{x}^S_{N|k} = \hat{x}_{k|k} \text{ and } P^S_{N|k} = P_{k|k} \tag{3.17}$$

Considering $i = N-1, N-2, \dots, 0$, the Rauch-Tugh-Striebel (RTS) smoother, which is detailed in Rauch *et al.* (1965) and Haykin (2001), is evaluated as:

$$\hat{x}_{k+1|k} = \hat{x}_{k|k} + \int_k^{k+1} f(x,u,t)\, dt \tag{3.18}$$

$$P_{k+1|k} = \phi_k P_{k|k} \phi_k^T + Q_k \tag{3.19}$$

$$C_k = P_{k|k} \phi_k^T P_{k+1|k}^{-1} \tag{3.20}$$

$$\hat{x}^S_{k|k} = \hat{x}_{k|k} + C_k(\hat{x}^S_{k+1|k} - \hat{x}_{k+1|k}) \tag{3.21}$$

$$P^S_{k|k} = P_{k|k} + C_k(P^S_{k+1|k} - P_{k+1|k})C_k^T \tag{3.22}$$

where *N* is the horizon size, and C_k is the RTS smoother of the Kalman gain. In this work, the horizon size is *N* = 4. The new smoothed values (P_0^S and $\hat{x}_0^S$) are the initial guess for the CEKF algorithm, which is re-evaluated until the current step:

$$P_k = P_0^S \quad \text{and} \quad \hat{x}_{k|k} = \hat{x}_0^S \tag{3.23}$$

3.3.1.4. Unscented Kalman Filter

Although the EKF has been widely used for many years, experience has shown that it is only reliable for systems that are not strongly nonlinear within the time scale of the update intervals (JULIER, S.; UHLMANN; DURRANT-WHYTE, 2000). The development of the EKF propagation and the update equations require ignoring some terms that may not be small for many nonlinear systems. The inherent linearization in the process typically can produce significant biases in the estimation results (JULIER, S. J.; UHLMANN, 2004).

Different from the extended Kalman filters, the unscented Kalman filter does not require the linearization of any nonlinear functions: the distribution of the states is specified using a minimum set of carefully selected sample points. These points capture entirely the true mean and the covariance of the Gaussian variable, and, when propagated through the true nonlinear system, they also capture the posterior mean and covariance with a second-order precision (expansion of Taylor series) for any non-linearity (WAN; VAN DER MERWE, 2002).

Firstly, the sigma points (χ) are evaluated:

$$\mu = \sqrt{ns + \lambda} \tag{3.24}$$

$$\lambda = \alpha^2(ns + \kappa) - ns \tag{3.25}$$

$$\chi_{i,k|k-1} = \begin{bmatrix} \hat{x}_{k-1} \\ \hat{x}_{k-1} + \mu\sqrt{P_{k-1}} \\ \hat{x}_{k-1} - \mu\sqrt{P_{k-1}} \end{bmatrix} \tag{3.26}$$

$$\hat{\chi}_{i,k|k-1} = f\left(\chi_{i,k|k-1}, u_{i,k|k-1}, \Delta t\right) \tag{3.27}$$

$$\hat{x}_{k|k-1} = \sum_{i=0}^{2ns} W_i^{(m)} \hat{\chi}_{i,k|k-1} \tag{3.28}$$

and the weights:

$$W_0^{(m)} = \frac{\lambda}{ns+\lambda} \tag{3.29}$$

$$W_0^{(c)} = \frac{\lambda}{ns+\lambda} + 1 - \alpha^2 + \beta \tag{3.30}$$

$$W_i^{(m)} = W_i^{(c)} = \frac{1}{2(ns+\lambda)}, \quad i = 1, \dots, 2ns \tag{3.31}$$

The covariance matrices are evaluated using the unscented transform:

$$P_{k|k-1} = \sum_{i=0}^{2ns} W_i^{(c)} \left(\hat{\chi}_{i,k|k-1} - \hat{x}_{k|k-1}\right) \left(\hat{\chi}_{i,k|k-1} - \hat{x}_{k|k-1}\right)^T + Q_{k-1} \tag{3.32}$$

$$\gamma_{i,k|k-1} = h\left(\hat{\chi}_{i,k|k-1}, u_{i,k|k-1}, \Delta t\right) \tag{3.33}$$

$$\hat{y}_{k|k-1} = \sum_{i=0}^{2ns} W_i^{(m)} \gamma_{i,k|k-1} \tag{3.34}$$

$$P_{y_k y_k} = \sum_{i=0}^{2ns} W_i^{(c)} \left(\gamma_{i,k|k-1} - \hat{y}_{k|k-1}\right)\left(\gamma_{i,k|k-1} - \hat{y}_{k|k-1}\right)^T + R_k \tag{3.35}$$

$$P_{x_k y_k} = \sum_{i=0}^{2ns} W_i^{(c)} \left(\hat{\chi}_{i,k|k-1} - \hat{x}_{k|k-1}\right)\left(\gamma_{i,k|k-1} - \hat{y}_{k|k-1}\right)^T \tag{3.36}$$

where the Kalman filter gain can be calculated

$$K_k = P_{x_k y_k} P_{y_k y_k}^{-1} \tag{3.37}$$

and the states and covariance of the filter are updated

$$\hat{x}_k = \hat{x}_{k|k-1} + K_k\left(y_k - \hat{y}_{k|k-1}\right) \tag{3.38}$$

$$P_k = P_{k|k-1} - K_k P_{y_k y_k} K_k^T \tag{3.39}$$

where *ns* is the number of states, α is the distribution of points around the mean ($0 \leq \alpha \leq 1$), β incorporates prior knowledge of the mean distribution (for Gaussian variables, $\beta = 2$) and κ is a secondary scaling parameter (usually set as 0 or 3-ns), χ and γ are the state and measurements sigma points, and $W_i^{(m)}$ and $W_i^{(c)}$ are the mean and covariance weights.

3.3.1.5. Cubature Kalman Filter

Similarly to the UKF technique, which does not linearize the system, Arasaratnam and Haykin (2009) developed a spherical-radial cubature rule to compute multivariate moment integrals encountered in the nonlinear Kalman filter. Specifically, a third-degree spherical-radial cubature rule is derived to provide a set of cubature points that scale linearly with the state-vector dimension. The cubature Kalman filter uses a set of cubature points with equal weights to calculate the mean and the covariance of state variables that, after a nonlinear transformation, improve the performance of the nonlinear optimal approximation, filtering accuracy, and numerical stability.

In contrast to the UKF, the CKF has a different set of deterministic weighting points. For the sigma-point set (UKF), the stem at the center is highly significant since it carries more weight, whereas the cubature-point set does not have a stem at the center and presents equally distributed weights. Also, Arasaratnam and Haykin (2009) mention some limitations of the sigma-point set built into the UKF, which are not present in the cubature-point built in the CKF, such as numerical inaccuracy, unavailability of a square root solution, and filter instability. The CKF also chooses fewer sample/simulation points to evaluate the method, i.e., 2n rather than 2n+1 as in the UKF where n is the number of states, thus being somewhat less costly in computations.

The following equations define the CKF algorithm. Firstly, generate the cubature points $\chi\ (i = 1,2, \dots ,2n)$:

$$\chi_{i,k|,k-1} = \sqrt{P_{k-1}}\xi^i + \hat{x}_{k-1} \tag{3.40}$$

where the unit cubature points are defined as $\xi^i = \sqrt{ns}$.

In the sequence, the cubature points are propagated:

$$\hat{\chi}_{i,k|k-1} = f\left(\chi_{i,k|,k-1}, u_{i,k|k-1}, \Delta t\right) \tag{3.41}$$

The propagated state and covariance matrix for instant k are estimated:

$$\hat{x}_{k|k-1} = \frac{1}{2ns}\sum_{i=0}^{2ns}\hat{\chi}_{i,k|k-1} \tag{3.42}$$

$$P_{k|k-1} = \frac{1}{2ns}\sum_{i=0}^{2ns}\hat{\chi}_{i,k|k-1}\hat{\chi}_{i,k|k-1}{}^T - \hat{x}_{k|k-1}\hat{x}_{k|k-1}{}^T + Q_{k-1} \tag{3.43}$$

$$\gamma_{i,k|k-1} = h\left(\hat{\chi}_{i,k|k-1}, u_{i,k|k-1}, \Delta t\right) \tag{3.44}$$

then, the measurement, the innovation, and the covariance and cross-covariance matrixes are predicted:

$$\hat{y}_{k|k-1} = \frac{1}{2ns}\sum_{i=0}^{2ns}\gamma_{i,k|k-1} \tag{3.45}$$

$$P_{y_k y_k} = \frac{1}{2ns}\sum_{i=0}^{2ns}\gamma_{i,k|k-1}\gamma_{i,k|k-1}{}^T - \hat{y}_{k|k-1}\hat{y}_{k|k-1}{}^T + R_k \tag{3.46}$$

$$P_{x_k y_k} = \frac{1}{2ns} \sum_{i=0}^{2ns} \hat{\chi}_{i,k|k-1} \gamma_{i,k|k-1}{}^T - \hat{x}_{k|k-1} \hat{y}_{k|k-1}{}^T \tag{3.47}$$

where the Kalman filter gain can be calculated by

$$K_k = P_{x_k y_k} P_{y_k y_k}^{-1} \tag{3.48}$$

and the states and covariance of the filter are updated as

$$\hat{x}_k = \hat{x}_{k|k-1} + K_k \left(y_k - \hat{y}_{k|k-1} \right) \tag{3.49}$$

$$P_k = P_{k|k-1} - K_k P_{y_k y_k} K_k^T \tag{3.50}$$

3.3.2 Performance evaluation criteria

The computational time required for the estimation by the Kalman filter-based approaches and the MSE between the expected and estimated data are the criteria for the performance evaluation, in which the MSE is given by:

$$MSE = \frac{1}{n} \sum_{i=1}^{n} (Y_i - \hat{Y}_i)^2 \tag{3.51}$$

where Y is the expected vector, $\hat{Y}$is the estimated vector, and n is the length of Y.

For better visualization of the results, box plots are presented. The box plot is a visual comparison tool that shows statistical information of the error between the expected and estimated data: a central tendency line represents the median, the quartiles (bottom and top line of box) show the data dispersion and data distribution, and the red circles are the outliers (atypical values).

The violin plot is more informative than the box plot, showing the error's full distribution using a density plot. Due to the lack of outlier visualization, the box plot complements the violin plot.

3.4 Case studies

The case studies aim the comparison of the Kalman filter-based approaches for estimating the PDG pressure of an offshore oil production system in a deepwater scenario. The used phenomenological model includes the mass balance of the riser, flowline, production column, gas lift annular, and reservoir. Both the process description and the detailed equations of the fast offshore well model (FOWM) are presented in the next subsection (Diehl *et al.* (2017)).

3.4.1 Plant model

As mentioned in the introduction, the choice of a representative model of the process is indispensable for the excellent performance of a Kalman filter. Among the simplified phenomenological models of the slugging behavior, the model proposed by Eikrem *et al*. (2004) assumed a pure mass balance to describe the dynamics of the gas lift well. Aamo *et al*. (2005) considered a two-phase flow mass balance in the tubing by treating oil and water as a single phase. Kaasa *et al.* (2007) proposed a simple empirical model describing the downhole's pressure's qualitative behavior during severe slugging. Jahanshahi *et al*. (2012)

developed a dynamic model for the casing-heading instability in gas-lifted oil wells. Di Meglio *et al*. (2012) assumed a mass balance in the flowline risers modeled with a virtual valve, which is an irregularity identified as the gas injection valve for gas-lifted wells. Diehl *et al.* (2017) designed the Fast Offshore Well Model (FOWM), an offshore production system in a deepwater scenario, including the riser, the flowline, the production column, the gas lift annular, and the reservoir.

The semi-empirical model proposed by Diehl *et al*. (2017) is the one used in this work. This is the most appropriate model for real applications since it considers the slugs generated by the casing heading and terrain/riser concomitantly, as well as the possibility of reproducing the limit cycles.

The fast offshore well model (FOWM) is based only on mass conservation equations:

$$\frac{dm_{ga}}{dt} = w_{gc} - w_{iv} \tag{3.52}$$

$$\frac{dm_{gt}}{dt} = w_r \alpha_{gw} + w_{iv} - w_{whg} \tag{3.53}$$

$$\frac{dm_{lt}}{dt} = w_r(1 - \alpha_{gw}) - w_{whl} \tag{3.54}$$

$$\frac{dm_{gb}}{dt} = (1 - \epsilon) w_{whg} - w_g \tag{3.55}$$

$$\frac{dm_{gr}}{dt} = \epsilon w_{whg} + w_g - w_{gout} \tag{3.56}$$

$$\frac{dm_{lr}}{dt} = w_{whl} - w_{lout} \tag{3.57}$$

The fluid flows used in the model are obtained by the following equations

$$w_{iv} = K_a \sqrt{\rho_{ai} \frac{(p_{ai} - p_{tb}) + \sqrt{(p_{ai} - p_{tb})^2 + \varepsilon}}{2}} \tag{3.58}$$

$$w_r = K_r \left(1 - 0.2 \left(\frac{P_{bh}}{P_r}\right) - 0.8 \left(\frac{P_{bh}}{P_r}\right)^2\right) \tag{3.59}$$

$$w_{whg} = \alpha_{gt} K_w \sqrt{\rho_l \frac{(p_{tt} - p_{rb}) + \sqrt{(p_{tt} - p_{rb})^2 + \varepsilon}}{2}} \tag{3.60}$$

$$w_{whl} = (1 - \alpha_{gt}) K_w \sqrt{\rho_l \frac{(p_{tt} - p_{rb}) + \sqrt{(p_{tt} - p_{rb})^2 + \varepsilon}}{2}} \tag{3.61}$$

$$w_g = C_g \frac{(p_{eb} - p_{rb}) + \sqrt{(p_{eb} - p_{rb})^2 + \varepsilon}}{2} \tag{3.62}$$

$$w_{gout} = \alpha_g C_{out} z \sqrt{\rho_l \frac{(p_{rt} - p_s) + \sqrt{(p_{rt} - p_s)^2 + \varepsilon}}{2}} \tag{3.63}$$

$$w_{lout} = \alpha_l C_{out} z \sqrt{\rho_l \frac{(p_{rt} - p_s) + \sqrt{(p_{rt} - p_s)^2 + \varepsilon}}{2}} \tag{3.64}$$

and the equations related to the model pressures are presented below:

$$\rho_{ai} = \frac{Mp_{ai}}{RT} \tag{3.65}$$

$$\alpha_{gt} = \frac{m_{gt}}{m_{gt}+m_{lt}} \tag{3.66}$$

$$\alpha_{gr} = \frac{m_{gr}}{m_{gr}+m_{lr}} \tag{3.67}$$

$$\alpha_{lr} = 1 - \alpha_{gr} \tag{3.68}$$

$$p_{ai} = \left(\frac{RT}{V_a M} + g\frac{L_a}{V_a}\right) m_{ga} \tag{3.69}$$

$$p_{tb} = p_{tt} + \rho_{mt} g H_{vgl} \tag{3.70}$$

$$p_{bh} = p_{pdg} + \rho_{mres} g (H_t - H_{pdg}) \tag{3.71}$$

$$p_{pdg} = p_{tb} + \rho_{mres} g (H_{pdg} - H_{vgl}) \tag{3.72}$$

$$p_{tt} = \frac{\rho_{gt} RT}{M} \tag{3.73}$$

$$p_{rb} = p_{rt} + \frac{g sin\theta}{A} (m_{lr} + m_{lstill}) \tag{3.74}$$

$$p_{eb} = \frac{RT}{M V_{eb}} m_{gb} \tag{3.75}$$

$$p_{rt} = \frac{RT}{M\left(V_r - \frac{m_{lr}+m_{lstill}}{\rho_l}\right)} m_{gr} \tag{3.76}$$

Some other equations regarding the physical properties of the model are also presented:

$$\rho_{mt} = \frac{m_{gt}+m_{lt}}{V_t} \tag{3.77}$$

$$\rho_{gt} = \frac{m_{gt}}{V_{gt}} \tag{3.78}$$

$$V_{gt} = V_t - \frac{m_{lt}}{\rho_l} \tag{3.79}$$

$$V_a = \frac{L_a \pi D_a^2}{4} \tag{3.80}$$

$$V_t = \frac{L_t \pi D_t^2}{4} \tag{3.81}$$

The set of parameters, their nomenclature and respective values are presented in Table 2.1. At these process conditions, the system presents oscillatory behavior, i.e., a limit cycle.

Table 3.1: Parameters and variables of the Fast Offshore Well Model (FOWM).

Parameter	Nomenclature	Value	Unit
α_{gw}	gas fraction of mass at the reservoir pressure and temperature conditions	0.026	-
D_a	diameter of the annular section	0.1016	m
D_t	diameter of the tubing section	0.1242	m
H_{pdg}	vertical length between the Christmas Tree and the PDG transmitter	1392.2	m
H_t	vertical length between the Christmas Tree and the bottom hole	1593.1	m
H_{vgl}	vertical length between the Christmas Tree and the gas lift valve	927.4	m
L_a	annular length	937.4	m
L_t	tubing length	1622	m
M	gas molecular weight	18	kg/kmol
p_r	pressure surrounding the production column bottom hole	3.52e7	Pa
p_s	pressure surrounding the production column gravitational separator	1013250	Pa
ρ_l	liquid density	965.5	kg/m3
ρ_{mres}	mixture density at the reservoir	902.5	kg/m3
T	average temperature in the production system	298	K
θ	average riser inclination	π/1.54	rad
R	universal gas constant	8314	J/kg.K
g	gravity acceleration	9.81	m2/s
m_{lstill}	minimum mass of liquid in the subsea pipeline	adjust parameter	kg
C_g	virtual valve constant	adjust parameter	m-1
C_{out}	choke valve constant	adjust parameter	m-1
V_{eb}	bubble volume	adjust parameter	m3
ϵ	gas fraction of mass that bypasses the bubble in the subsea pipeline	adjust parameter	-
K_w	flow coefficient between the annular and the tubing	adjust parameter	m-1
K_a	flow coefficient between the annular and the tubing	adjust parameter	m-1
V_r	riser volume	adjust parameter	m3
K_r	flow coefficient between the annular and the tubing	adjust parameter	m-1
w_{gc}	gas lift mass flow entering the annular	1.5205	kg/s
z	choke valve opening fraction	input variable	-
w_{gc}	gas lift flow	input variable	kg/s
V_a	annular volume	calculated	m3
V_{gt}	gas volume in the tubing	calculated	m3
V_t	tubing volume	calculated	m3
ρ_{mt}	mixture density in the tubing	calculated	kg/m3
ρ_{gt}	gas density in the tubing	calculated	kg/m3
α_{gt}	gas mass fraction in the tubing	calculated	-

Parameter	Nomenclature	Value	Unit
α_{gr}	liquid mass fractions in the subsea pipeline	calculated	-
α_{lr}	liquid mass fractions in the subsea pipeline	calculated	-
w_r	reservoir to the bottom hole flow	calculated	kg/s
w_{whg}	gas mass that flows at the Christmas Tree	calculated	kg/s
w_{whl}	liquid mass that flows at the Christmas Tree	calculated	kg/s
w_g	flow at the virtual valve	calculated	kg/s
w_{gout}	gas flow through the topside choke valve	calculated	kg/s
w_{lout}	liquid flow through the topside choke valve.	calculated	kg/s
p_{ai}	pressure in the annular gas injection point to the tubing	calculated	Pa
p_{tb}	pressure in the gas injection point on the tubing side	calculated	Pa
p_{bh}	pressure in the bottom hole	calculated	Pa
p_{rb}	pressure at the flowline before the bubble position	calculated	Pa
p_{eb}	bubble pressure	calculated	Pa
p_{pdg}	pressure at the PDG position	estimated	Pa
p_{tt}	pressure at the top of the tubing	filtered	Pa
p_{rt}	pressure at the top of the riser	filtered	Pa
m_{ga}	gas mass in the annular	estimated	kg
m_{gt}	gas mass in the production column or tubing	estimated	kg
m_{lt}	liquid mass in the tubing	estimated	kg
m_{gb}	gas mass in the bubble at the subsea production line	estimated	kg
m_{gr}	gas mass in the set flowline/riser	estimated	kg
m_{lr}	liquid mass in the set flowline/riser	estimated	kg

For more details about the Fast Offshore Well Model, see Diehl *et al*. (2017).

3.4.2 Simulated data

The simulated data used in this work was generated through the simulation of a real offshore oil production plant via a gas lift in OLGA (OiL and GAs – dynamic multiphase flow simulator). Two different data sets were generated. The first, shown in Figure 3.1, has a constant valve choke opening in open-loop mode. This data set also contains the p_{rt}, p_{tt}, p_{pdg}, z, and w_{gc} (a constant value of 1.5205 kg/s) measurements. The data have oscillatory behavior, the sampling time is equal to 60 seconds, and a total of 1437 measured points.

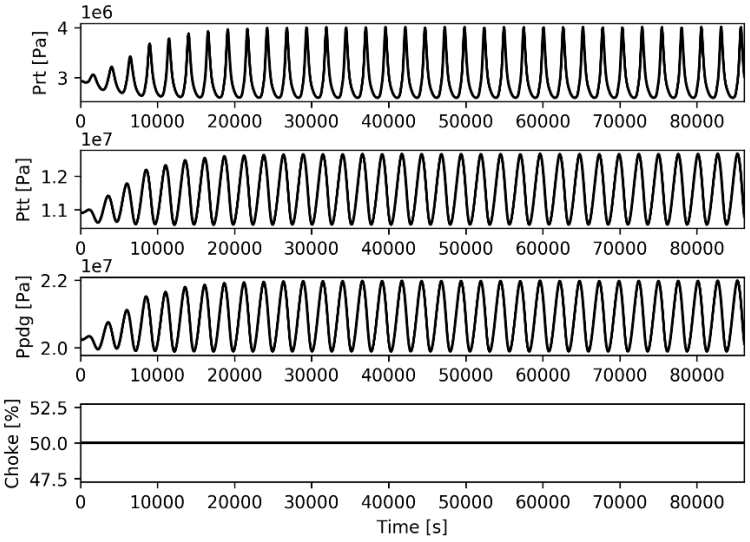


Figure 3.1: Data simulated in OLGA for a real oil production system used in scenarios A and B.

The second data set, shown in Figure 3.2, has perturbations in the choke valve opening in open-loop mode and also contains the p_{rt}, p_{tt}, p_{pdg}, z, and w_{gc} (a constant value of 1.5205 kg/s). The selected data have oscillatory behavior, the sampling time is equal to 60 seconds, and a total of 3411 measured points.

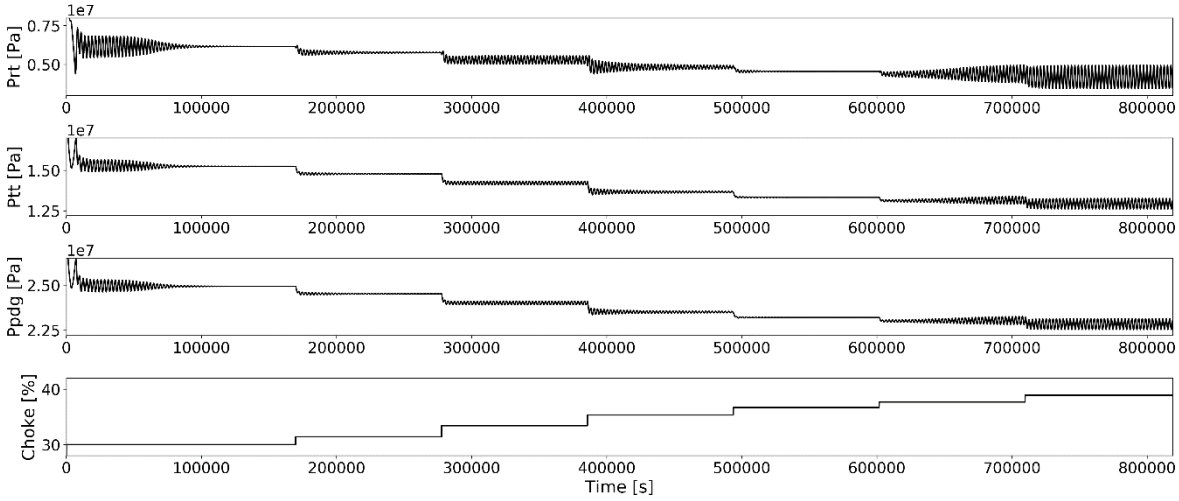


Figure 3.2: Data simulated in OLGA for a real oil production system with perturbations in the choke valve opening used in scenarios C and D.

3.4.3 Real data

The real data were extracted from a real offshore oil production via a gas lift plant from Petrobras (provided by Diehl *et al.*, 2018). This data set also contains the p_{rt}, p_{tt}, p_{pdg}, z, and w_{gc} measurements, as showed in Figure 3.3. The selected data have oscillatory behavior, the sampling time is equal to 300 seconds, and a total of 250 measured points.

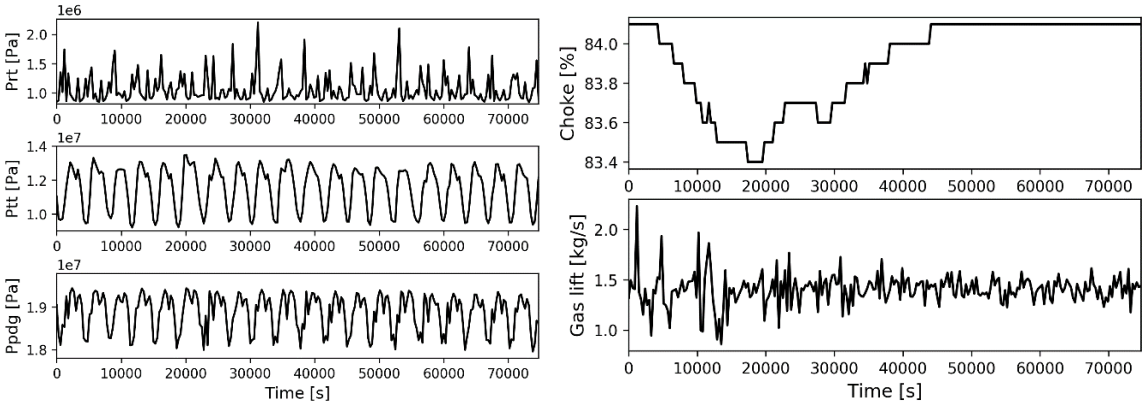


Figure 3.3: Real industrial data from an oil production system used in scenarios E and F.

All the measurements used as inputs for the estimations by the Kalman filters (i.e., p_{rt}, p_{tt}, z, and w_{gc}) are available and accurate in practical applications. The advantage of using the p_{rt} and p_{tt} (or only the p_{rt}) as inputs to estimate the p_{pdg} is that their gauges are easy to replace in case of fault and they are reliable, considering the process noise.

3.4.4 Simulation settings

In this work, the Kalman filters used the FOWM as the dynamic model of the system, the input measurements z and w_{gc}, and the available output measurements p_{rt} and p_{tt} to estimate the states (m_{ga}, m_{gt}, m_{lt}, m_{gb}. m_{gr}, m_{lr}). Then, from the state estimation, the variable p_{pdg} is calculated.

The filters parameters for all scenarios are shown in Table 3.2, in which the values of P_0 and Q_0 were chosen according to the state order of magnitude, and R_0 based on the measurement order of magnitude.

Table 3.2: Filter parameters for all scenarios.

	DEKF, CEKF, and CEKF			UKF and CKF			UKF parameters		
Scenario	P_0	R_0	Q_0	P_0	R_0	Q_0	α	β	κ
A and B	$I_3 10^2$	$I_6 10^6$	$I_3 10^2$	$I_3 10^2$	$I_6 10^6$	$I_3 10^2$	1	2	0
C and D	$I_3 10^2$	$I_6 10^6$	$I_3 10^2$	$I_3 10^2$	$I_6 10^{10}$	$I_3 10^2$	1	2	0
E and F	$I_3 10^2$	$I_6 10^6$	$I_3 10^2$	$I_3 10^2$	$I_6 10^{12}$	$I_3 10^2$	1	2	0

The Kalman filter available input and output measurements used for each scenario are shown in Table 3.3. Scenarios using only the p_{rt} measurement were not included, since the estimation returned bad results.

Table 3.3: Data used in the Kalman filter for each scenario.

Scenario	Input	Output	Data
A	z	p_{rt} and p_{tt}	Simulated with constant z
B	z	p_{tt}	Simulated with constant z
C	z	p_{rt} and p_{tt}	Simulated with perturbations in z
D	z	p_{tt}	Simulated with perturbations in z
E	z and w_{gc}	p_{rt} and p_{tt}	Industrial

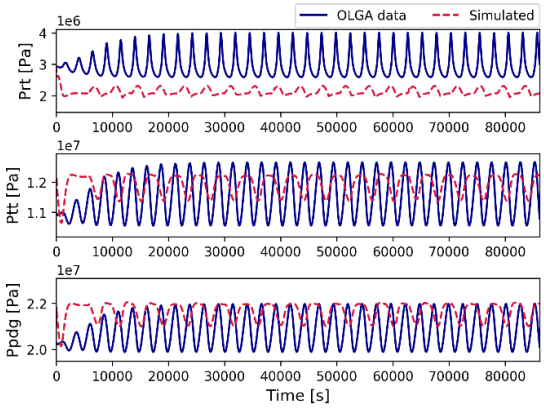
Scenario	Input	Output	Data
F	z and w_{gc}	p_{tt}	Industrial

The FOWM has different adjust parameters for the OLGA experimental data (A, B, C, and D) and the industrial data (E and F), as shown in Table 3.4.

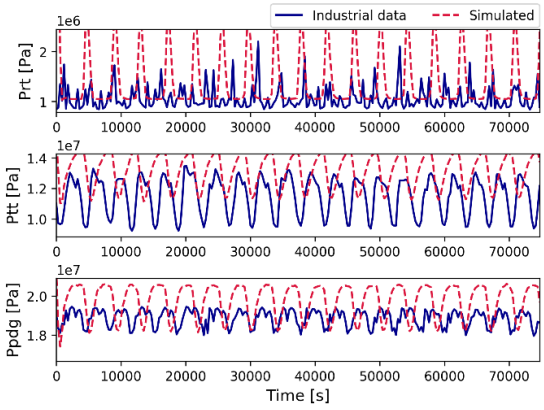
Table 3.4: FOWM adjust parameters for all the scenarios.

Scenarios	A, B, C, and D	E and F
m_{lstill}	$1.058.10^{3}$	62.22
C_g	$3.39.10^{-4}$	$1.137.10^{-3}$
C_{out}	0.0031	$2.039.10^{-3}$
V_{eb}	93.9382	60.98
ϵ	0.9183	0.1545
K_w	0.0031	$6.876.10^{-4}$
K_a	$1.38.10^{-4}$	$2.293.10^{-3}$
V_r	118.87	126.9
K_r	96.291	227.1

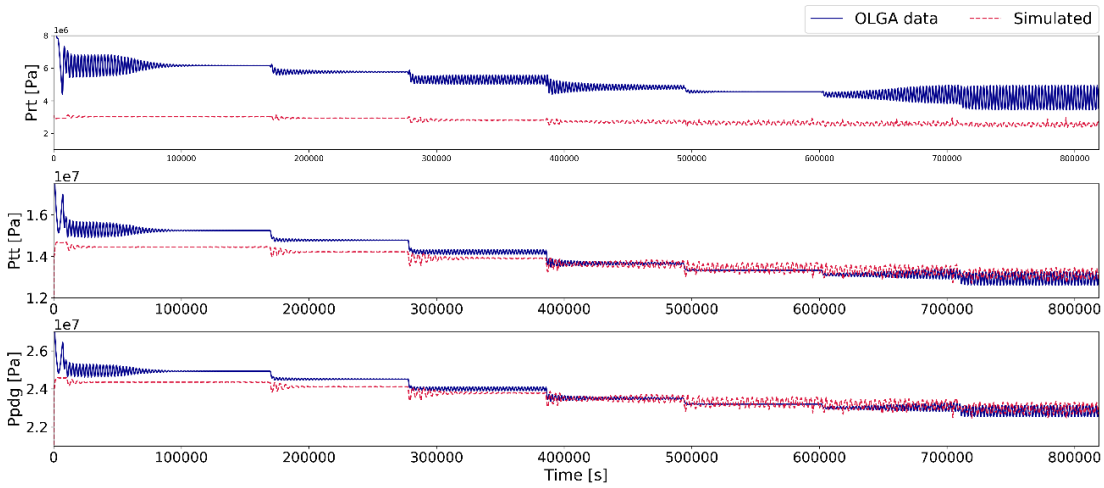
The comparison of the experimental data (simulated in OLGA and industrial) with the model simulation results, considering the adjust parameters for each scenario, is presented in Figure 3.4.



a) scenarios A and B



b) scenarios E and F



c) scenarios C and D

Figure 3.4: Comparison of the experimental data (rigorous model simulation in OLGA and industrial) and the simplified model simulation results for a) scenarios A and B, b) E and F, and c) C and D.

The mean squared error between the results of the model simulation and the experimental data is shown in Table 3.5.

Table 3.5: Mean squared error for the model simulation considering all the scenarios.

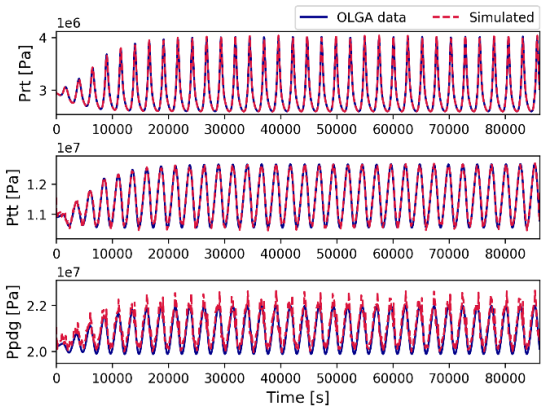
Scenario	A and B	C and D	E and F
Error	6.0e4	1.7e5	9.0e4

3.5 Results and discussion

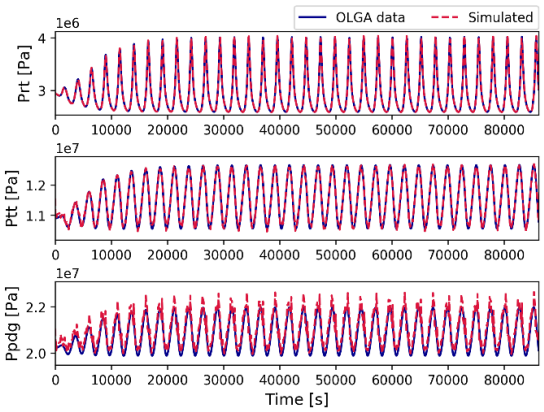
In this section, the five Kalman filter-based methodologies reviewed in Section 3.1 are applied to all scenarios specified in the last section. Firstly, the results for the simulated data sets are presented followed by the results for the real industrial data set. Besides showing the results for the p_{pdg} estimation, p_{rt} and p_{tt} measurements are also presented, since it is not reasonable to estimate properly the desired variable while hindering the filtration of other measurements.

3.5.1 Simulated data

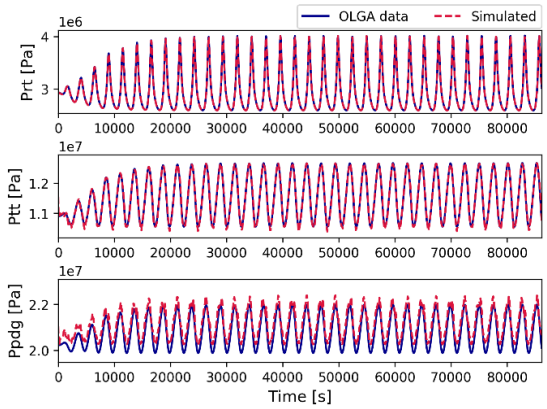
In this section, the estimation for scenarios A, B, C, and D are presented. The results for scenario A are shown in Figure 3.5.



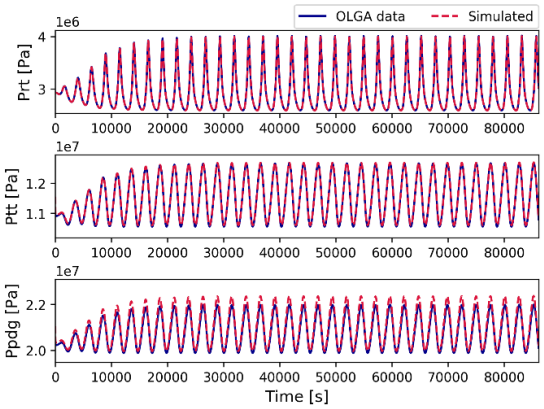
a) DEKF



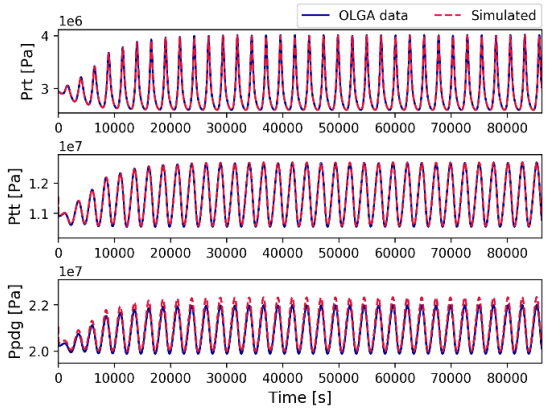
b) CEKF



c) CEKF&S



d) UKF



e) CKF

Figure 3.5: Scenario A: p_{pdg} estimation using p_{rt} and p_{tt} measurements by a) DEKF, b) CEKF, c) CEKF&S, d) UKF, and e) CKF.

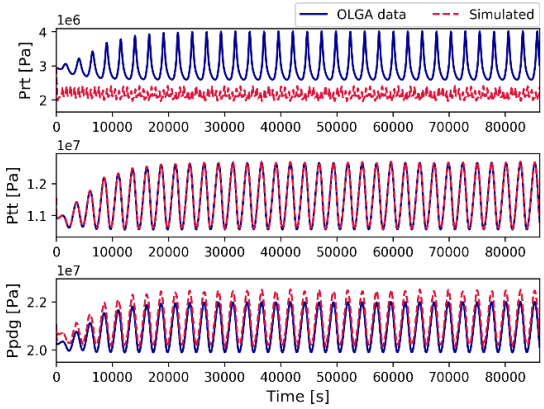
In scenario A, the CKF method returned the smallest MSE. However, it presented the second largest computational time, as seen in Table 3.6.

Table 3.6: Computational time and MSE for scenario A.

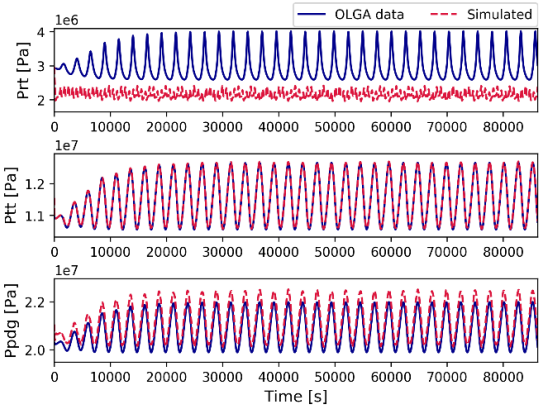
Filter	DEKF	CEKF	CEKFS	UKF	CKF	Ref. Value
Time (s)	1.00*	2.37*	12.28*	22.12*	20.84*	112.37
MSE (Pa)	2.03*	2.05*	2.93*	1.02*	1.00*	1985.94

* multiplied by the reference value.

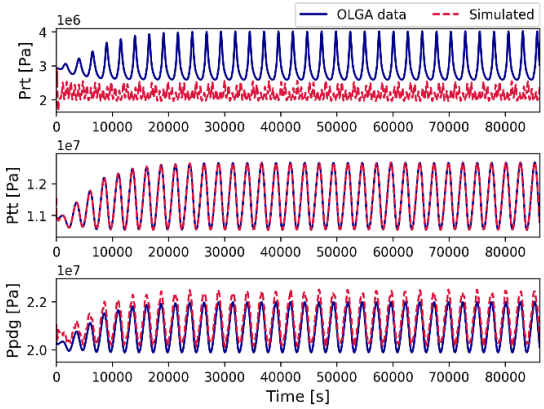
In Figure 3.6, the results are shown for the five Kalman filters approaches in scenario B.



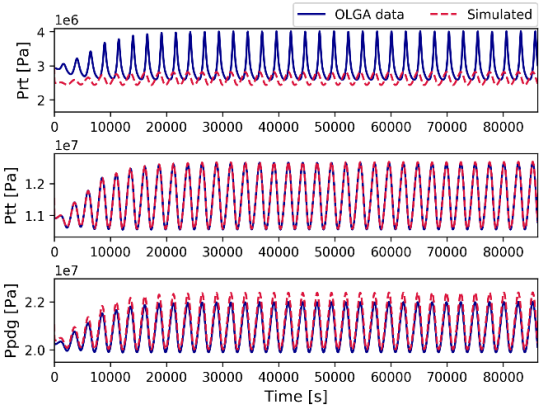
a) DEKF



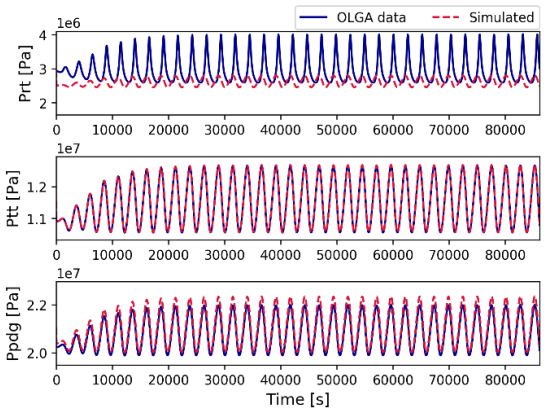
b) CEKF



c) CEKF&S



d) UKF



e) CKF

Figure 3.6: Scenario B: p_{pdg} estimation using p_{tt} measurement by a) DEKF, b) CEKF, c) CEKF&S, d) UKF, and e) CKF.

In scenario B, the CKF method also returned the smallest MSE value when compared with the others. Once again, the computational time for this method is the second largest one, as seen in Table 3.7.

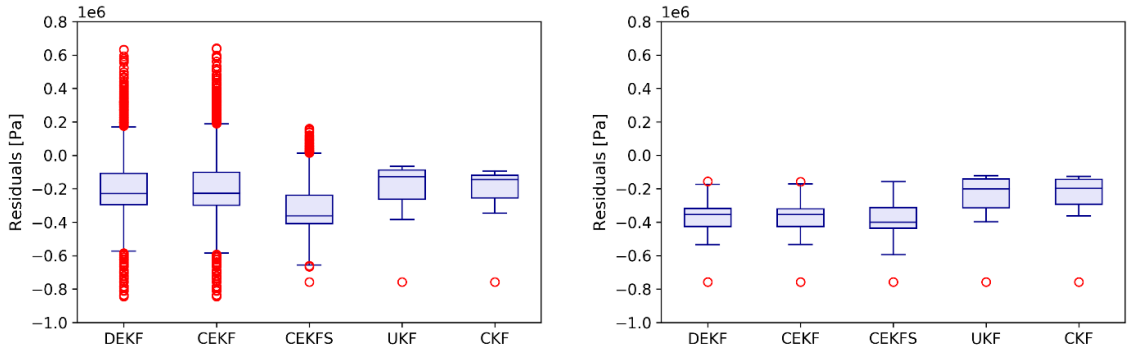
Table 3.7: Computational time and MSE for scenario B.

Filter	DEKF	CEKF	CEKFS	UKF	CKF	Ref. Value
Time (s)	1.00*	2.96*	14.95*	39.31*	26.66*	111.09
Error (Pa)	2.52*	2.53*	2.74*	1.11*	1.00*	2656.55

* multiplied by the reference value.

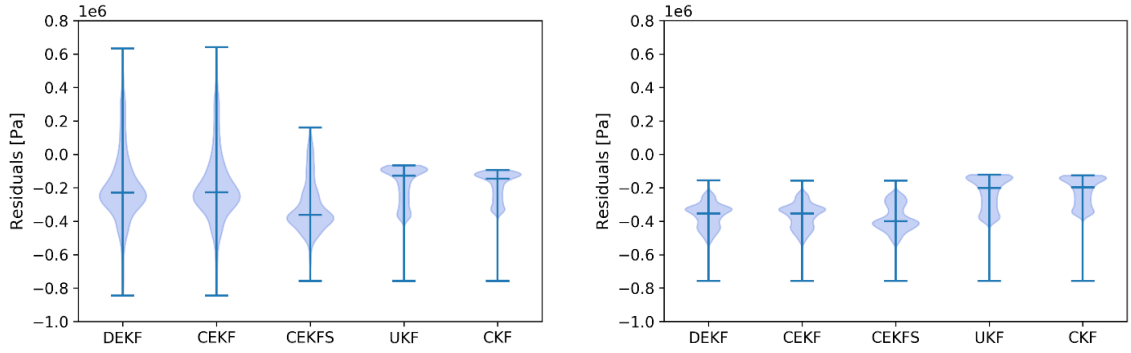
For scenarios A and B, the PDG pressure estimation follows a similar frequency to that of the experimental data. Considering its amplitude, the extended filters present higher error (amplitude) than the filters with no linearization. This indicates that information is lost in the linearization, thus hindering the desired variable estimation.

The box and violin plots of the p_{pdg} residuals for Scenarios A and B are presented in Figure 3.7 and Figure 3.8, respectively.



a) b)

Figure 3.7: Residual box plot for p_{pdg} for a) Scenario A and b) Scenario B.



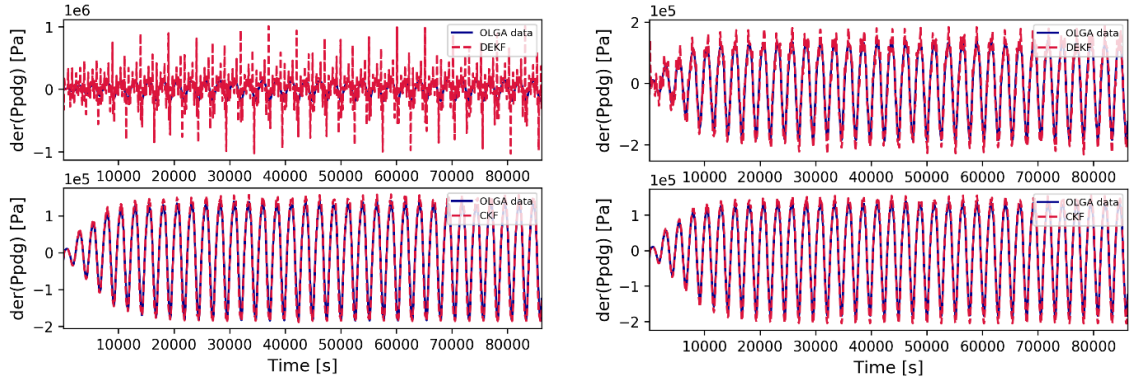
a) b)

Figure 3.8: Residual violin plot for p_{pdg} for a) Scenario A and b) Scenario B.

By analyzing the box and violin plots from scenario A, the CKF, and UKF, respectively, show the best performance between the chosen methodologies, i.e., they exhibit a smaller vertical distribution and the median is closer to zero. The CKF and UKF methods present fewer outliers than the remaining ones.

For scenario B, all the methods show similar results to those of scenario A, but with less discrepancy and outliers. The methods with no linearization (CKF and UKF) present, however, better overall results than the extended methods (DEKF, CEKF, and CEKFS), as seen in both box and violin plots. The mean error of the p_{pdg} estimated by CKF for scenario A is $1.85.10^5$ Pa (0.89%) and $2.20.10^5$ Pa (1.05%) for scenario B, both of which are considered small in terms of practical purposes.

Figure 3.9 shows the derivative of p_{pdg} estimated by the DEKF and the CKF to compare the errors, capture the behavior of this variable, and disregard its bias.



a) b)

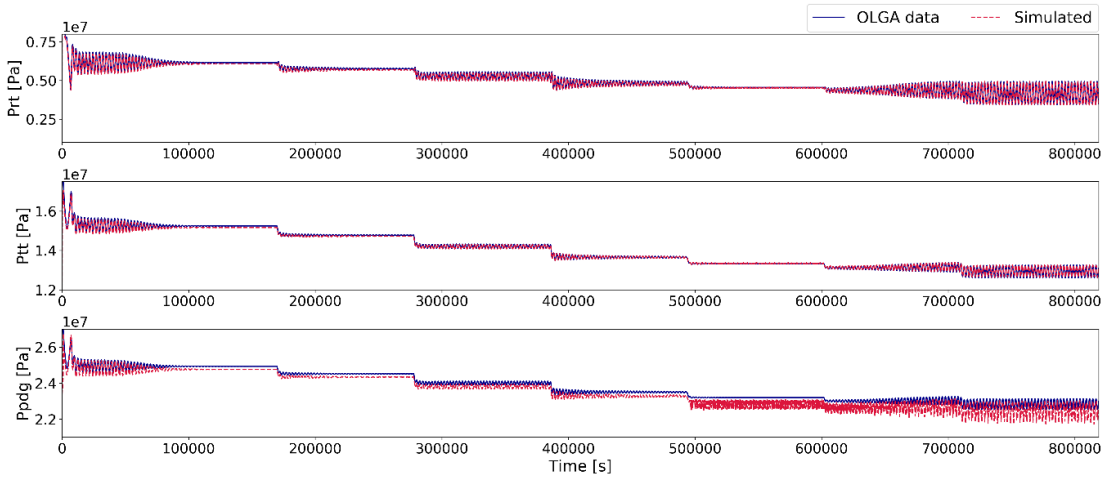
Figure 3.9: Derivative of the p_{pdg} estimated by the DEKF and the CKF for a) Scenario A and b) Scenario B.

Considering the shape of the violin plot in scenario A in Figure 3.8, the errors follow a normal distribution for the extended techniques, showing equally distributed errors along time (both in frequency and amplitude). However, the methods with no linearization show a bimodal distribution. This means that the data have two different groups of errors, either

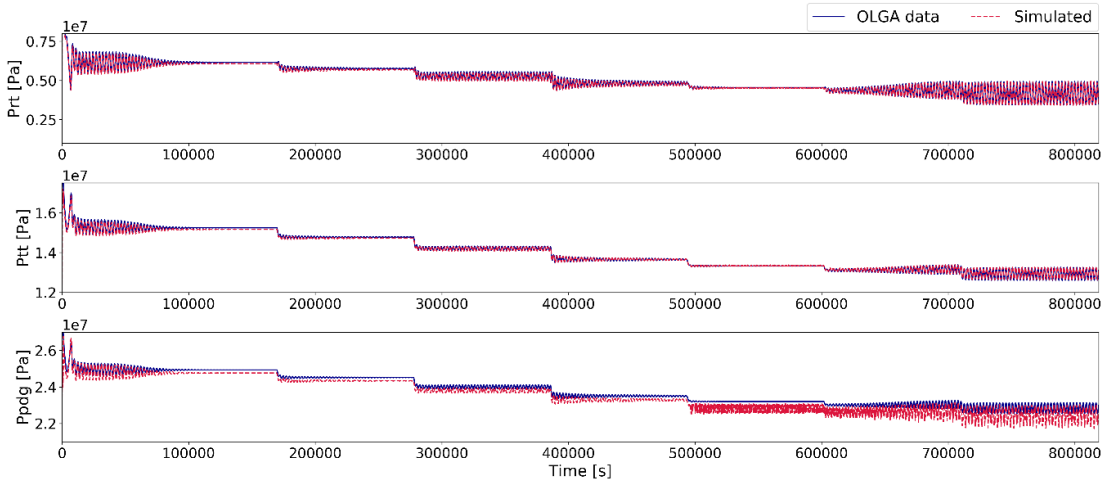
at the peaks or at the valleys of the oscillations, in which the errors are only distributed in their amplitude, as visualized in Figure 3.9. In scenario A, the errors are smaller at the beginning (lower half), whereas the upper quartile presents more visible discrepancies with a higher density distribution.

From scenario B, as shown in Figure 3.8, the p_{pdg} estimation using the DEKF follows the OLGA data behavior more appropriately than in scenario A. For all the state estimation techniques in scenario B, the violin plot presents a bimodal distribution. In this case, the errors are mainly distributed at the peaks and valleys of the oscillation (amplitude) and not distributed along their frequency, as shown in Figure 3.9. Furthermore, using only p_{tt} measurements for the p_{pdg} estimation (scenario B) returns similar results to using two measurements (scenario A). However, the decrease in computational time was not significantly lower to justify the use of a single variable.

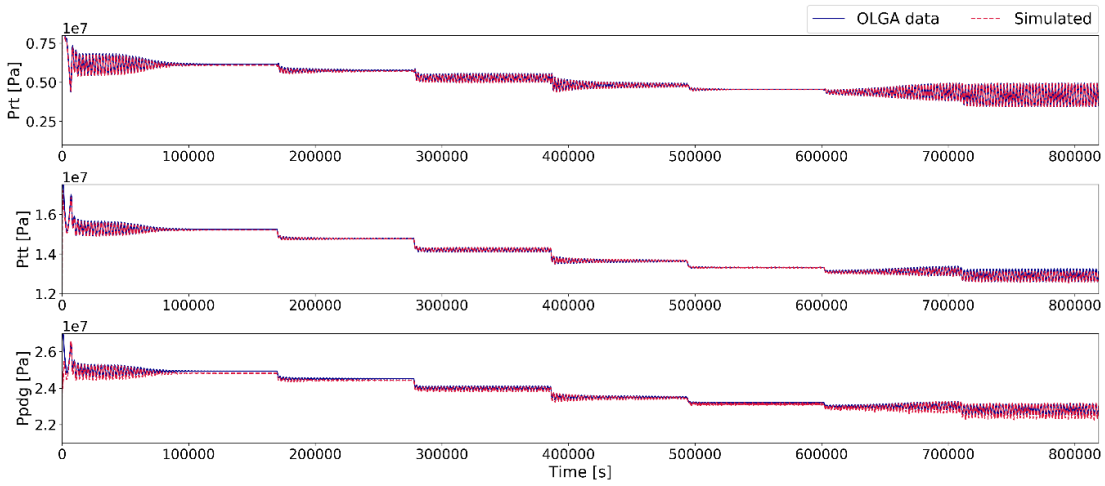
The results for scenario C are presented in Figure 3.10.



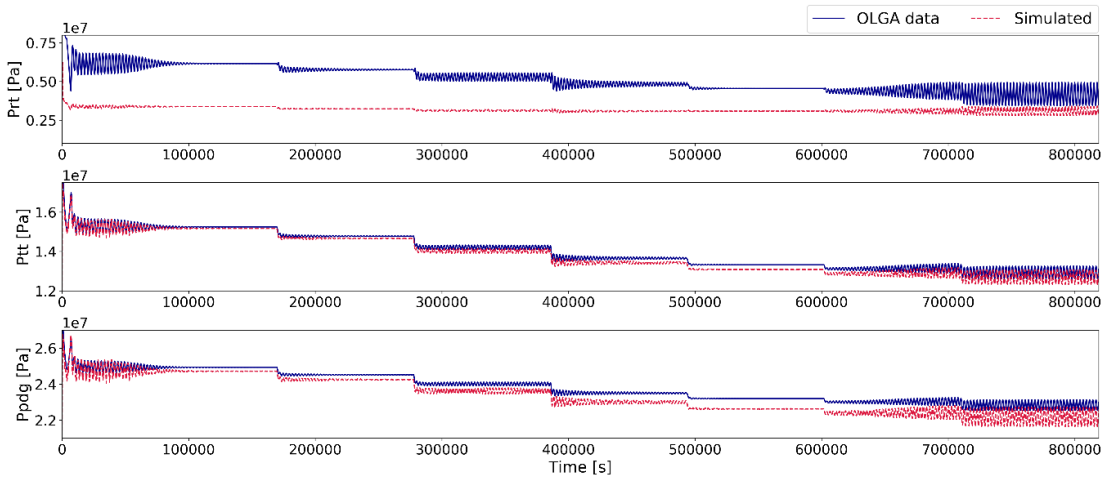
a) DEKF



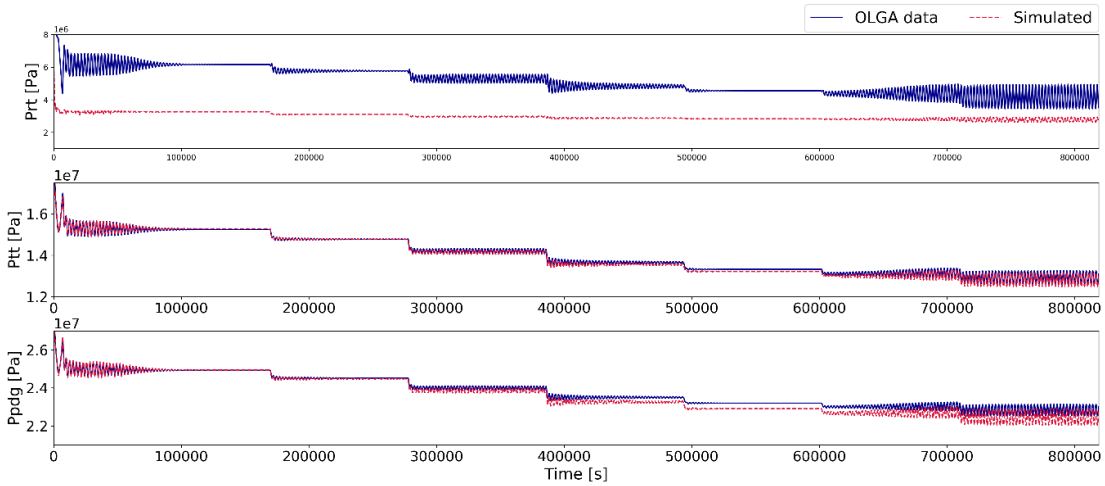
b) CEKF



c) CEKF&S



d) UKF



e) CKF

Figure 3.10: Scenario C: p_{pdg} estimation using p_{rt} and p_{tt} measurements by a) DEKF, b) CEKF, c) CEKF&S, d) UKF, and e) CKF.

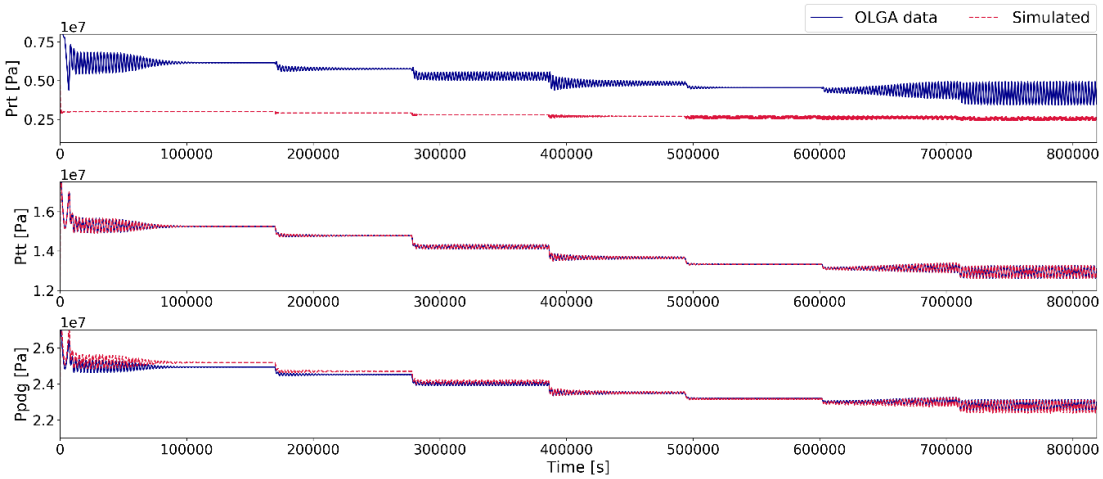
For scenario C, the MSE result for the CEKFS method is the smallest. Differently from scenarios A and B, the UKF methodology returns the largest error and the CKF the second smallest one. However, the UKF and CKF also present the largest computational times, as seen in Table 3.8.

Table 3.8: Computational time and MSE for scenario C.

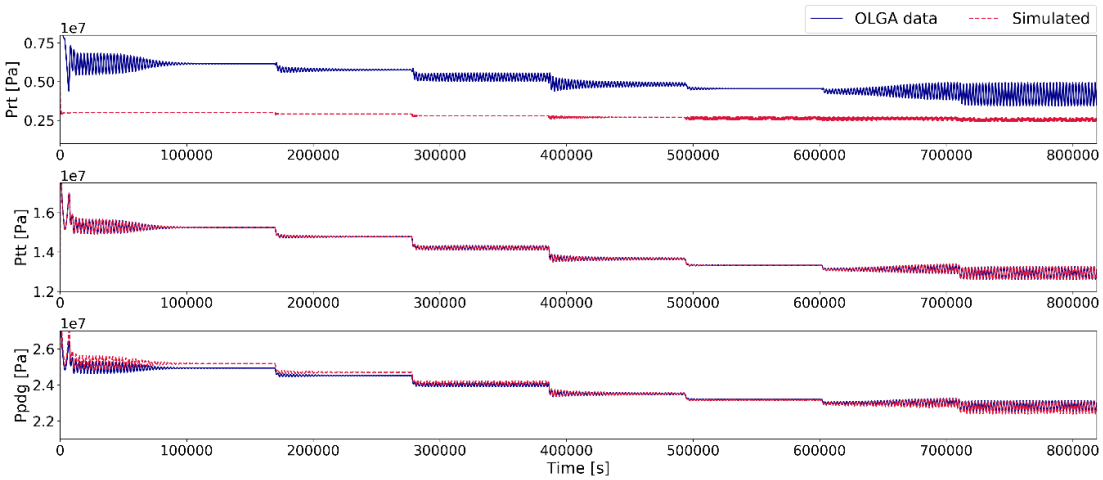
Filter	DEKF	CEKF	CEKFS	UKF	CKF	Ref. Value
Time (s)	1.00*	2.65*	16.24*	76.69*	76.34*	236.76
Error (Pa)	3.95*	3.85*	1.00*	8.80*	2.73*	1072.82

* multiplied by the reference value.

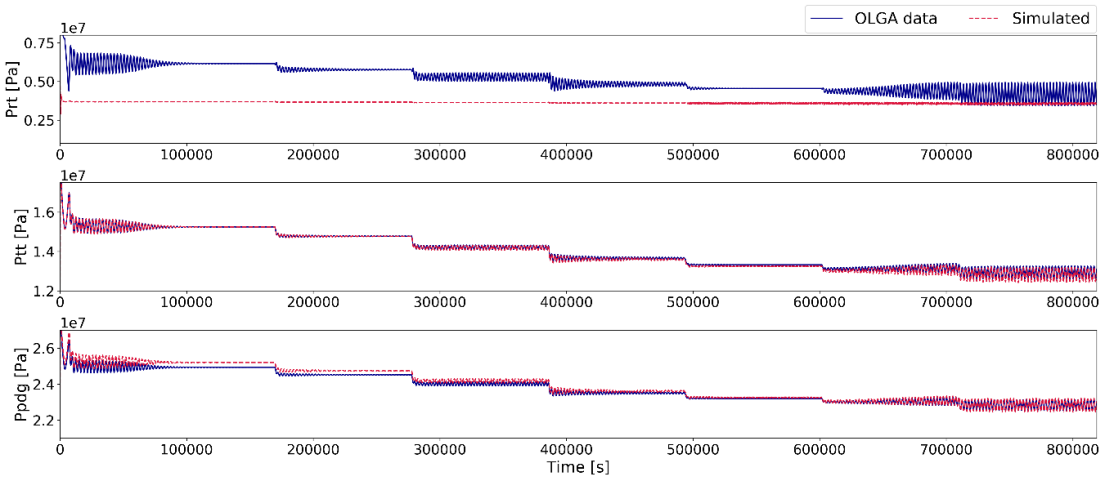
The results for scenario D are presented in Figure 3.11.



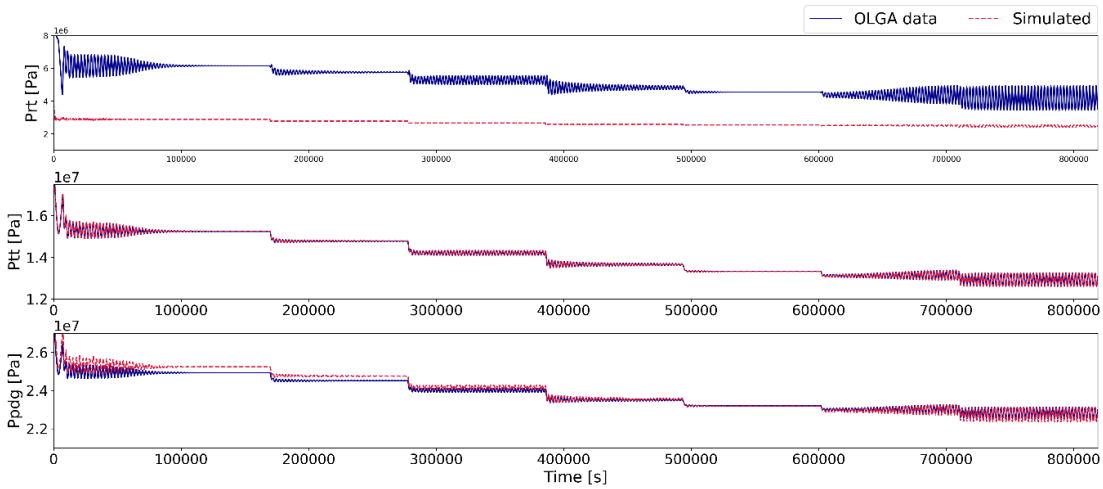
a) DEKF



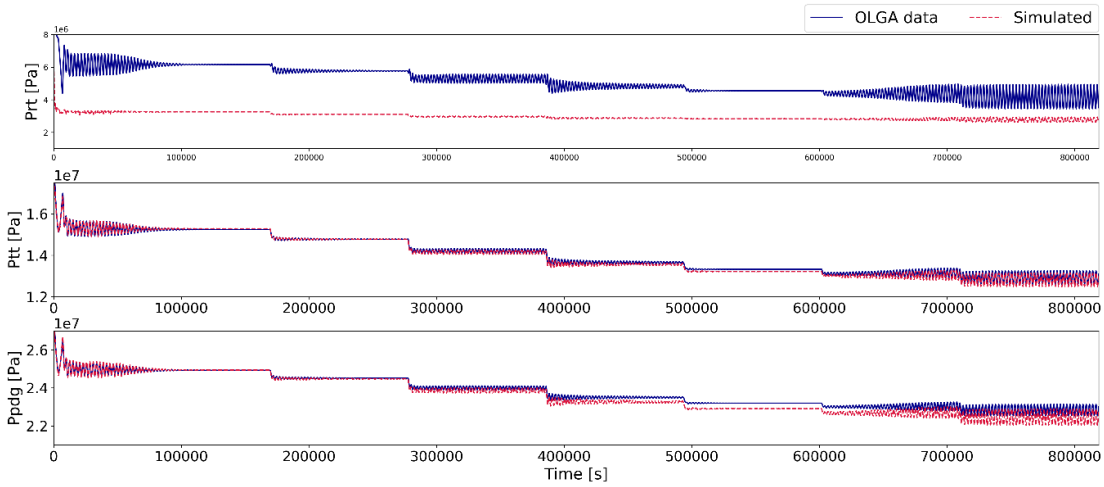
b) CEKF



c) CEKF&S



d) UKF



e) CKF

Figure 3.11: Scenario D: p_{pdg} estimation p_{tt} measurements by a) DEKF, b) CEKF, c) CEKF&S, d) UKF, and e) CKF.

In scenario D, the error for the p_{pdg} estimation is smaller for the DEKF methodology than for the others. The CKF method returns the third smallest error, but the second largest computational time, as seen in Table 3.9. Moreover, comparing the scenarios A and B, the MSE results from scenario D are very similar to those from scenario C, meaning that the use of p_{tt} measurement is enough to estimate the p_{pdg}.

Table 3.9: Computational time and MSE for scenario D.

Filter	DEKF	CEKF	CEKFS	UKF	CKF	Ref. value
Time (s)	1.00*	2.84*	11.26*	55.08*	66.82*	310.22
Error (Pa)	1.00*	1.00*	1.25*	1.79*	1.20*	1162.56

* multiplied by the reference value.

In scenarios C and D, a series of perturbations changed the PDG pressure behavior. It seems that the filters with no linearization suffer more from the model quality. Considering Figure 3.4, the p_{prt} is poorly simulated with the current set of parameters, resulting in a poor estimation of this variable by the UKF and the CKF. Thus, disregarding the p_{rt} measurement in the state estimation (scenario D), the errors from the filters with no linearization are smaller than in scenario C. Meanwhile, the extended filters do not suffer so much with the model fit since they are able to estimate satisfactorily the p_{rt}.

The box and violin plots of the p_{pdg} residuals are presented in Figure 3.12 and Figure 3.13.

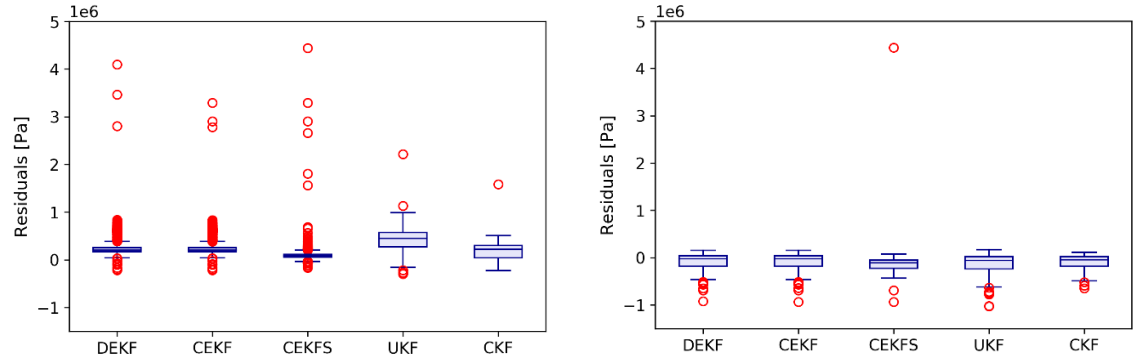
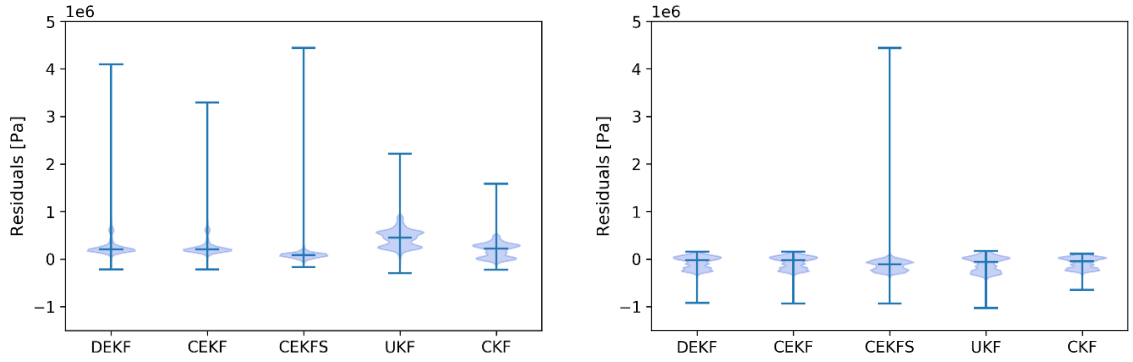


Figure 3.12: Residual box plot of the p_{pdg} for a) Scenario C and b) Scenario D.

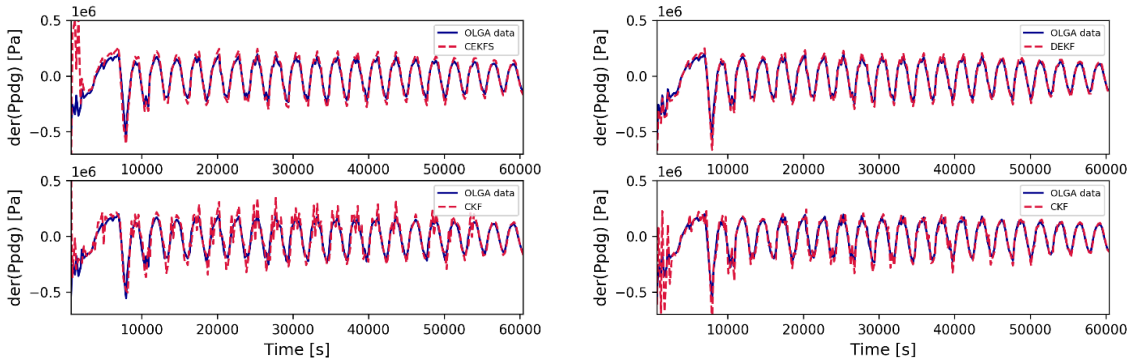


c) d)

Figure 3.13: Residual violin plot of the p_{pdg} for a) Scenario C and b) Scenario D.

For scenarios C and D, the box and violin plots show smaller vertical distribution and the median closer to zero for the extended methods. Comparing both scenarios, it is possible to conclude that using both measurements to estimate de PDG pressure is slightly better than using a single one. The mean error of the p_{pdg} estimated for scenario C using the CEKFS is $9.04.10^4$ Pa (0.38%), and for scenario D using the DEKF is $1.34.10^5$ Pa (0.56%), which are considered small in terms of practical purposes.

Figure 3.14 shows the derivative of p_{pdg} estimated by the DEKF and the CKF for the first 400 points in order to compare the errors, capturing the behavior of this variable and disregarding its bias.



a) b)

Figure 3.14: Derivative of the p_{pdg} estimated by the CEKFS and the CKF for a) Scenario C, and by the DEKF and the CKF for b) Scenario D.

In scenarios C and D, the violin plots from all the Kalman filter techniques show a bimodal distribution with more apparent errors in the amplitude of the oscillations, as seen in Figure 3.14. For both cases, the extended filters show smoother results for the p_{pdg} derivative compared to the CKF. However, for scenario D, the CKF estimation improved perceptibly compared to scenario C due to the absence of the p_{rt} measurement.

Considering the synthetic data simulated in OLGA, there is a model discrepancy. The model used in OLGA is much more complex in terms of modeling than the FOWM, which is

why the Kalman filter estimation is difficult. Therefore, in this section, in which simulated data are used, the results using extended Kalman filters are considered the most suitable in terms of cost-benefit between accuracy and computational time.

3.5.2 Real data

The results for the PDG pressure estimation using different methodologies of Kalman filters for real industrial data are presented in this section. The CEKFS methodology was not able to estimate the p_{pdg} for both real data scenarios. For this reason, its results are not reported in this section.

The results for scenario E are presented in Figure 3.15.

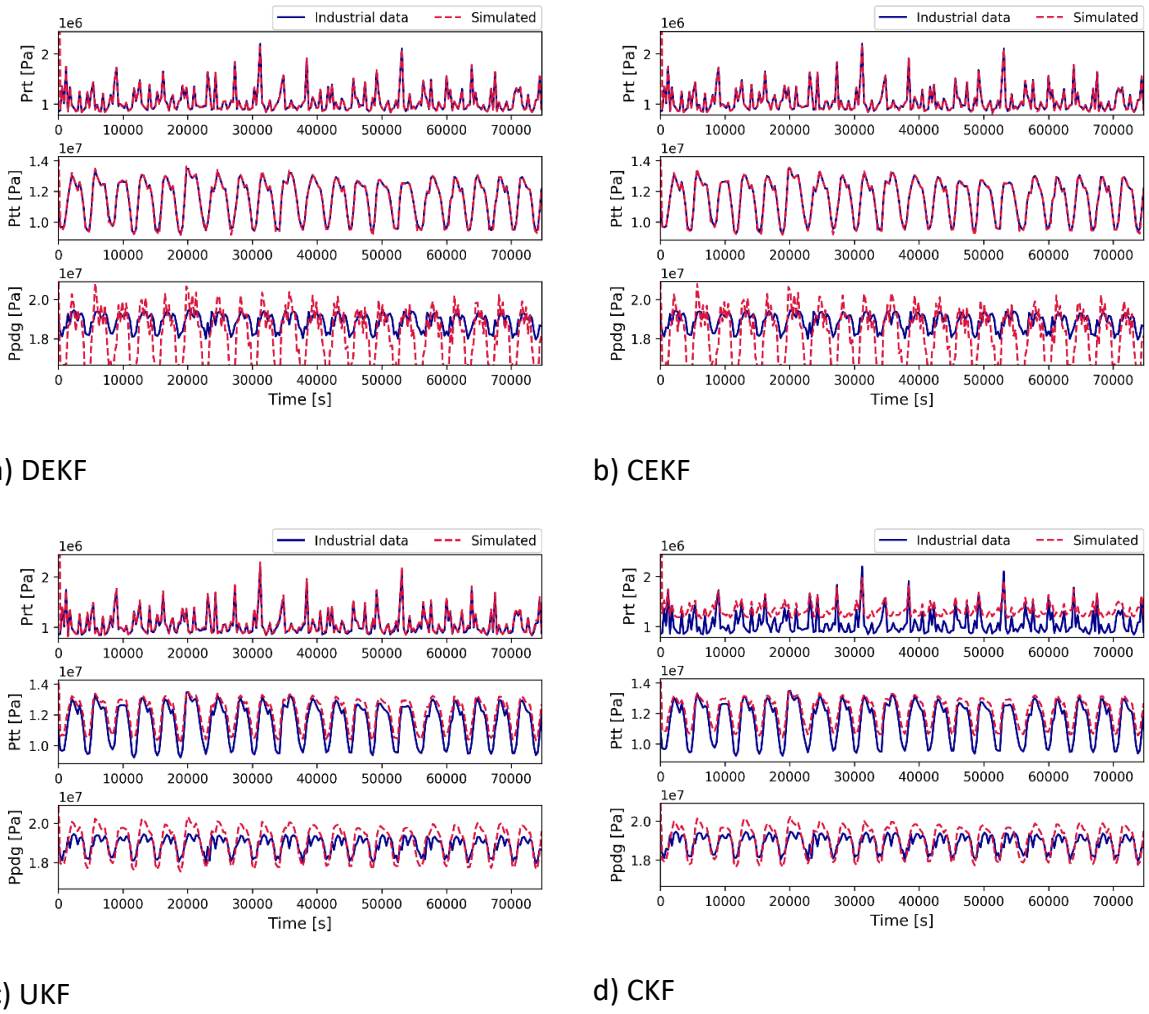


Figure 3.15: Scenario E: p_{pdg} estimation using p_{rt} and p_{tt} measurements of a real production system with a) DEKF, b) CEKF, c) UKF, and d) CKF.

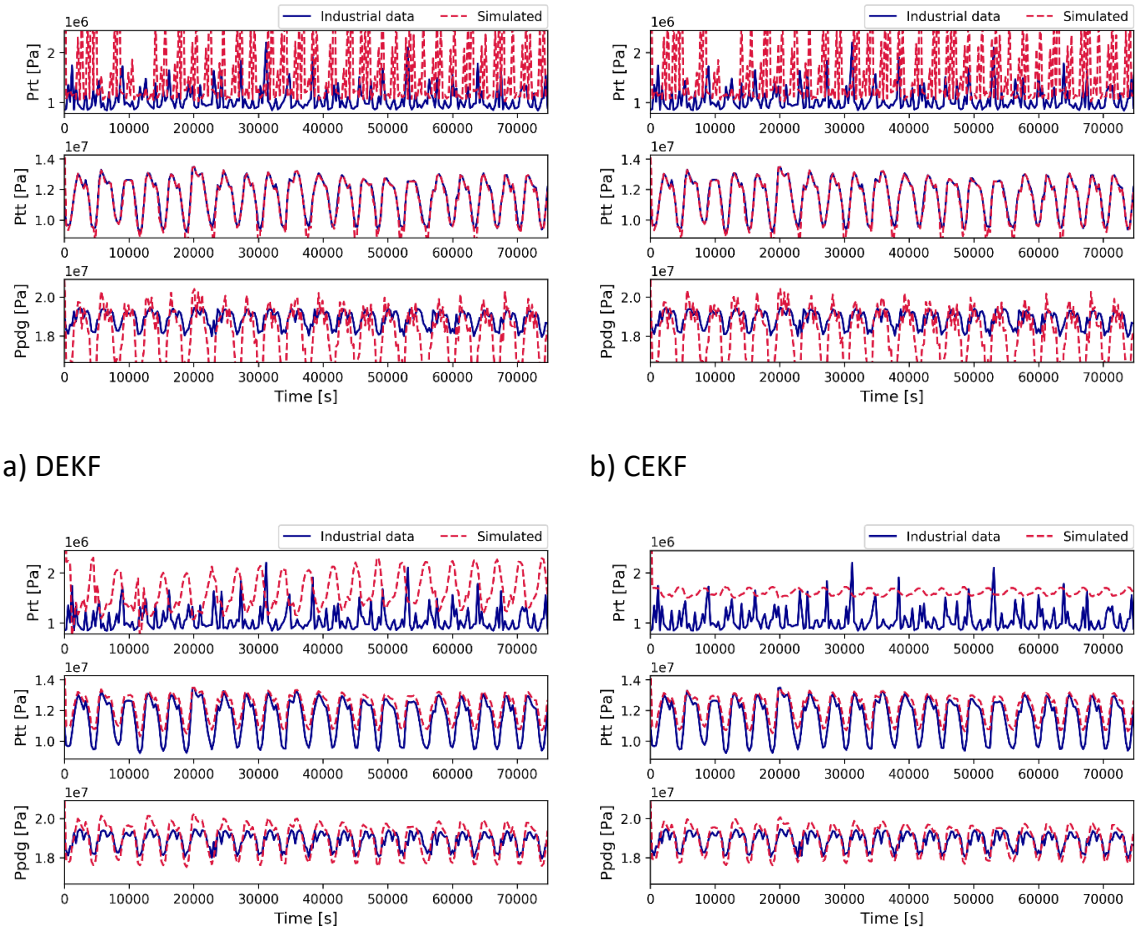
Table 3.10 shows the mean squared error and the computational time for scenario E, in which the CKF method presents the smallest MSE value with the second largest computation time. Once again, the PDG pressure estimation follows the same frequency as the experimental data for the filter with no linearization. In this case, it is even more apparent that the results with extended filters lose information when the model is linearized, since their amplitudes are much higher and their frequency does not follow properly the industrial data, when compared to the filters with no linearization.

Table 3.10: Computational time and MSE for scenario E.

Filter	DEKF	CEKF	UKF	CKF	Ref. Value
Time (s)	1.00*	3.58*	5.24*	4.57*	67.79
Error (Pa)	8.36*	8.35*	1.23*	1.00*	11468.26

* multiplied by the reference value.

Figure 3.16 shows the results for scenario F comparing the four state estimators.



a) DEKF b) CEKF

c) UKF d) CKF

Figure 3.16: Scenario F: p_{pdg} estimation using p_{tt} measurements of a real production system by a) DEKF, b) CEKF, c) UKF, and d) CKF.

By comparing the results from scenario F, it is seen that the CKF can estimate the p_{pdg} with the highest accuracy. The results using only the p_{tt} measurement are even more reliable than using both p_{rt} and p_{tt} measurements, as seen in Table 3.11.

Table 3.11: Computational time and MSE for scenario F.

Filter	DEKF	CEKF	UKF	CKF	Ref. Value
Time	1.00*	1.37*	3.38*	3.23*	93.90
Error	11.01*	11.00*	1.36*	1.00*	9579.84

* multiplied by the reference value.

By comparing the errors in scenarios E and F, the advantages of using nonlinear filters over extended filters for highly nonlinear systems, when the model is properly adjusted (see Figure 3.4), are very clear. In these cases, linearizing the process model, considering the strong noise presented in industrial data, is not the best option, since it results in higher errors and consequently in a poor estimation. When nonlinear filters are used, it is evident that the PDG pressure estimation is much smoother than in other cases This is because the model is not linearized and, therefore, no information is lost during the estimation. Nevertheless, due to the process complexity and unmeasured disturbances, the estimation is not perfect.

The box and violin plots of the p_{pdg} pressure residuals for the real data from industry are presented in Figure 3.17 and Figure 3.18, in which the first point is not considered due to the initialization error.

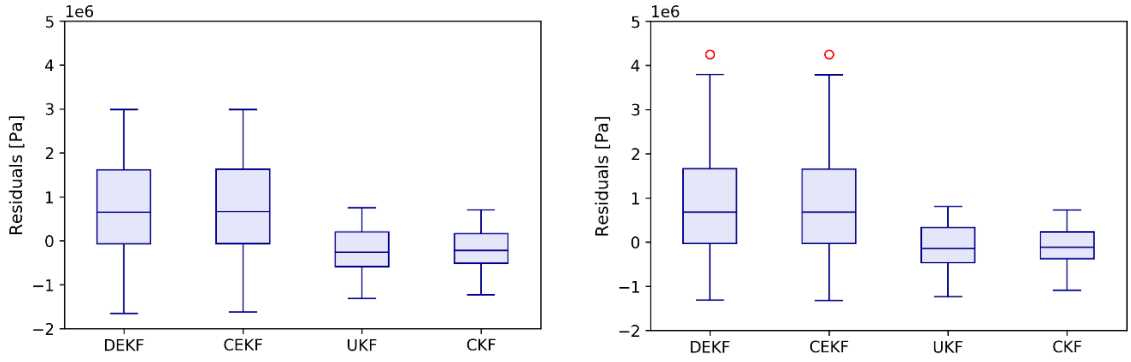


Figure 3.17: Residual box plot of the p_{pdg} for a) Scenario E and b) Scenario F.

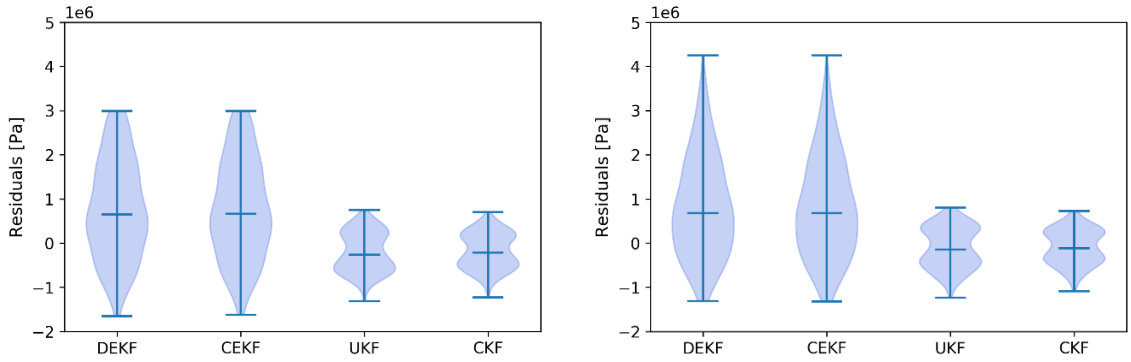


Figure 3.18: Residual violin plot of the p_{pdg} for a) Scenario E and b) Scenario F.

From the box and violin plots from scenario E and F, in a first glance, the CKF and the UKF show better performances, respectively, because they show a smaller vertical distribution and the median closer to zero. It means that they have less data discrepancy and more confidence in the p_{pdg} estimation. The mean error of the p_{pdg} estimated by the CKF for scenario E is $1.92.10^5$ Pa (1.02%) and $9.73.10^4$ Pa (0.52%) for scenario F, which are considered small in terms of practical purposes. In Figure 3.19, the behavior of the p_{pdg} estimated by the DEKF and the CKF is analyzed, considering its derivative evaluation.

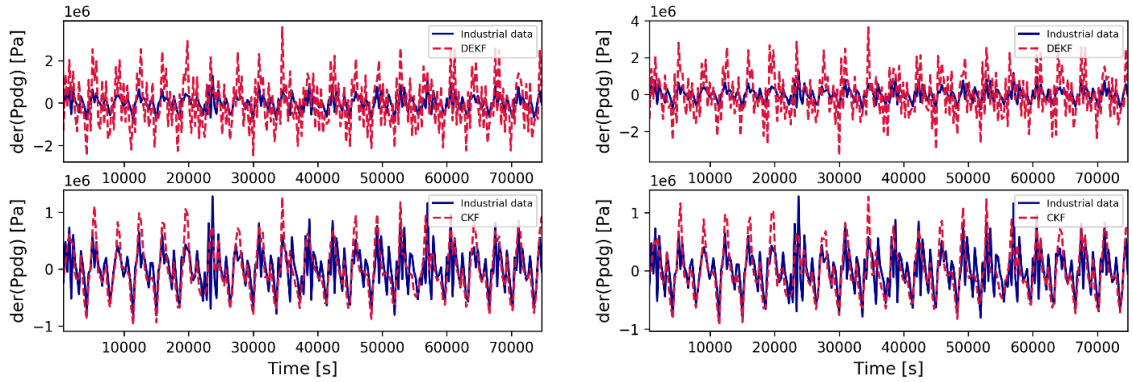


Figure 3.19: Derivative of the p_{pdg} estimated by the DEKF and the CKF for a) Scenario E and b) Scenario F.

The p_{pdg} estimation using the DEKF, in both scenarios, does not capture correctly the industrial data behavior. In this case, the information is lost during the linearization of the extended filter, leading to more significant discrepancies. Thus, there are errors of amplitude and frequency, which follow a normal distribution, all along with the dataset. Meanwhile, the p_{pdg} estimation using the CKF captures the industrial data behavior, except for its amplitude, as shown in Figure 3.19. Considering the violin plot of this case study, similar to the previous scenarios, the filters with no linearization show a bimodal distribution. Therefore, due to the oscillations, there are two different groups of errors: either at the peaks or at the valleys.

In our case study, in the simulated scenarios, the model is not properly adjusted as in the industrial ones. In scenarios A and B, the CKF slightly outperformed the extended filters, whereas for scenarios C and D, the DEKF performed better for the p_{pdg} estimation. As discussed before, the model simulation for these scenarios (Figure 3.4) showed a poor performance for the p_{rt} variable, which may have hindered the UKF and the CKF estimation. Meanwhile, for the industrial case (scenarios E and F), the model fit was not as problematic. In this case, the advantage of using a filter with no linearization for highly nonlinear models arose, in which the visible improvement of the p_{pdg} estimation obtained by the CKF over the DEKF can be worth the high computational cost (4 times larger than that demanded by the DEKF).

From the case studies, it was verified that using only the p_{tt} measurements, the results of the PDG pressure estimation were similar to or better than those using both the p_{rt} and p_{tt} measurements. As the Christmas tree pressure is close to the permanent downhole gauge, it may represent the p_{pdg} better than when using both measurements.

In oil well systems, some papers apply the UKF as a data-driven soft sensor to estimate online the downhole pressure based on available measurements (AGUIRRE *et al.*, 2017; REZENDE; TEIXEIRA; MENDES, 2015; TEIXEIRA *et al.*, 2014). In this case, an alternative to the UKF is to apply the CKF, which results in even more accuracy with less computational time with the advantage of having fewer tuning parameters than the UKF.

Considering that a simplified semi-empirical model and one dataset were used, the results presented here were surprisingly good. In this industrial case, the CKF presented the best cost-benefit between accuracy and computational time for the p_{pdg} estimation, differently from the state estimators previously used in the literature for the same purpose. It is indispensable to mention the greatest objective of the PDG pressure estimation again, which is its control to achieve the most productive oil production in an optimized way, injecting less amount of gas lift, saving electricity and money.

3.6 Conclusions

The PDG pressure estimation is of great importance to describe the dynamics of an oil well, mainly in terms of process control. In this paper, the p_{pdg} was estimated using state estimators, which provide an estimate of the desired variable based on three available data sets (two simulated and one real industrial data set from both top and Christmas tree pressures) using a simple semi-empirical model that predicts the slugging behavior using gas lift. Five different Kalman filter-based approaches were compared to conclude which one is the best for the PDG estimation: discrete extended Kalman filter (DEKF), constrained extended Kalman filter (CEKF), constrained extended Kalman filter and smoother (CEKF&S), unscented Kalman filter (UKF) and cubature Kalman filter (CKF).

For the scenarios considered in this work, the CKF works better if the model is adjusted correclty, as in the industrial case. In this case, using a filter with no linearization for highly nonlinear models may be worth it. On the other hand, the DEKF works fine when the model is not correctly adjusted, as in the simulated scenarios. In this case, the model simulated poorly the p_{rt} variable, hindering the p_{pdg} estimation with the Kalman filters with no linearization. The extended filters, however, estimated the p_{pdg} satisfactory. For all scenarios presented in this paper, the mean error of the estimated p_{pdg} was around 1%, which is considered small in terms of practical purposes. In this case, the authors consider a relative error up to 5% still acceptable in terms of field application and practical purposes.

Even when the CKF works better, the problem of using this filter is its high computational cost. Thus, the user must evaluate the cost-benefit for each case. For example, when simulated data is used, the errors of the DEKF estimation are not so significant (around 2 to 3 times the magnitude of the CKF), thus this state estimation with linearization fits well. On the other hand, when industrial data is used, the errors of the DEKF estimation are higher (8 to 11 times the magnitude of the CKF), which compensates the computational cost.

Also, it is possible to verify that using only p_{tt} measurements, the results of the PDG pressure estimation have, on average, similar precision to using both the p_{rt} and p_{tt} measurements. This happens once the Christmas tree is close to the Pressure Downhole Gauge (PDG). As mentioned before, the advantage of using both p_{rt} and p_{tt} (or only the p_{rt}) as inputs to estimate the p_{pdg} is that their gauges are easy to replace, in case of a fault, and they are reliable, considering the process noise. Moreover, some p_{pdg} values can be obtained by the well test, and their measurements can be used in the Kalman correction step to update the covariance matrix for the next simulations.

The results presented in this work are also interesting in terms of the oil production control, since the correct estimation of the PDG pressure can help to achieve the most

productive oil production in an optimized way, injecting less amount of gas lift, saving electricity and money.

3.7 Acknowledgement

The authors acknowledge Eng. Fabio C. Diehl for providing the simulation and industrial data and the financial support from the National Petroleum, Natural Gas and Biofuels Agency (ANP) and Petróleo Brasileiro S.A. (PETROBRAS).

Capítulo 4 – **Fouling and operational monitoring of heat exchanger network by a state estimator technique**

O presente capítulo e parte do manuscrito que foi submetido para a revista *Industrial & Engineering Chemistry Research*.

ABSTRACT: Heat exchanger network (HEN) is a fundamental mechanism to reduce external heating and cooling utility consumption in industrial processes, leading to lower operational costs and environmental impacts. HEN efficiency depends on the conditions of the heat exchangers, whose performance is reduced over time due to the constant deposit of impurities over the heat exchangers wall. This deposit, known as fouling, generates resistance to the heat transfer. The heat exchangers must be monitored and maintained according to their condition and fouling resistance to control the fouling impact. To estimate the fouling resistance, techniques have been proposed, which fail in the common industrial case where all the necessary physical properties are not available. In this work, a constrained Kalman filter and smoother is applied to estimate the unavailable measurements and the fouling resistance. The technique is applied to a real case study, which is a preheating train of crude distillation unit from a refinery industry. The results show that the technique is efficient in the estimation of the desired variables, increasing the monitoring capability and generating energy savings of millions of dollars.

4.1 Introduction

Heat exchangers (HEs) are common equipment in process industries, such as oil and gas, pulp and paper, and petrochemicals. They are used to transfer thermal energy between two or more fluids for heat recovery and energy management (SHAH; SEKULIC, 2003). Usually, a set of HEs is configurated in an optimized network aiming at the reduction of energy demand, operational cost, and carbon emission. This set forms a heat exchanger network.

Energy consumption is one of the major concerns of oil refineries. The preheat train (PHT) of crude distillation units is the most critical system in the refinery and plays an essential role in reducing energy consumption due to the process streams heat integration.

Thus, its operation and performance must be precisely tracked to detect and correct loss of heat transfer efficiency (SILVA; LIPORACE; QUEIROZ, 2005). In figures, the crude oil fractioning is an energy-intensive process, where 65% of the energy necessary can be recovered in the PHT, leaving only 35% to be supplied by a furnace (COLETTI, F *et al.*, 2015; SANTAMARIA; MACCHIETTO, 2019; YEAP *et al.*, 2004).

Fouling in the PHT for crude oil distillation has become one of the most challenging issues within the refinery industry (LOYOLA-FUENTES; SMITH; JOBSON, 2017). The efficiency of heat exchangers decreases over time because of the undesired progressive deposition and accumulation of material over the surfaces, increasing the thermal resistance and pressure drop (SANTAMARIA; MACCHIETTO, 2019). For a single refinery that processes 100 thousand barrels per day, Van Nostrand et al. (1981) estimated fouling related losses at US$ 25.7 million per year (2014 basis), with almost 50% of it attributed to fouling in the PHT. Refinery operators are constantly faced with problems caused by the buildup of fouling in the PHT, including operating difficulties, economic penalties, increased environmental impact, and health and safety hazards (COLETTI, F *et al.*, 2015). Lalot et al. (2007) stated that classical fouling detection methods are based on 1) examination of the heat transfer coefficient (or the effectiveness), 2) simultaneous observations of the pressure drops and mass flow rates, 3) temperature measurements, e.g., $(T_{h,in} - T_{h,out})/\left(T_{h,in} - T_{h,out}\right)_{design}$, 4) ultrasonic or electrical measurements, and 5) weighting of heat exchangers plates. To be very accurate, these methods require either that the system presents successive steady-states (1-3), i.e., the inlet temperatures ad flows must be stable for a period long enough to be able to compute or measure the values of interest, or are local (4), or require to stop the process (3), which is far too restrictive or costly. To estimate the fouling resistance techniques have been proposed (BOTT, 2000; CHEN, X. D. *et al.*, 2004; JERÓNIMO *et al.*, 1997; JONSSON, G. R. *et al.*, 2007a; M. M. PRIETO B. SIGALES, 1999; NEMA; DATTA, 2005; RIVEROL; NAPOLITANO, 2005; SILVA; LIPORACE; QUEIROZ, 2005) , which fail in the common industrial case where all the necessary physical properties are not available (e.g., data from the clean heat exchanger).

In industrial crude oil PHT, the unavailability of process measurements hinders the operational monitoring of the heat exchanger network. Sensors to measure some process variables are either faulty or not available. In this case, unknown process variables, including temperatures and the fouling coefficient, can be estimated by a state estimator, which is the aim of this work. In short, process data are combined with a representative model of the system and with a state estimator to estimate the unknown process variables.

The estimation of the fouling coefficient and the unknown temperatures promote better monitoring and control of the HEs operational conditions, which guarantees higher energy saving. As far as the authors know, this paper is the first to apply a state estimator for monitoring the fouling of a PHT.

Following this introduction, this works continues in Section 4.2 with a review of the heat exchanger network simulation. Section 3 introduces the industrial case study based on the preheat train of a distillation unit from a refinery. Section 4.4 presents the methodology based on the constrained extended Kalman filter and smoother. Section 4.5 shows the results, and the conclusions of the work are drawn in Section 4.6.

4.2 Review of heat exchanger network synthesis and Kalman filter applications

Several papers discuss the heat exchanger networks (HEN) synthesis (CIRIC; FLOUDAS, 1991; ESCOBAR; TRIERWEILER, 2013b; FLOUDAS; CIRIC; GROSSMANN, 1986; FURMAN; SAHINIDIS, 2002; LINNHOFF; FLOWER, 1978; YEE; GROSSMANN, 1990), but only a few present their simulation: Sanaye & Niroomand (2007) simulated a HEN by choosing an asymptotic fouling function for planning its optimum cleaning schedule; Ijaz, Ati, & Mahalec (2013) used a HEN for simulation, data reconciliation and optimization that is suitable for use in large scale site-wide energy models; Kayabasi & Kurt (2018) simulated a HEN using linear equation systems by using an economic simulation model.

The Kalman filter methodology is also studied in heat exchangers. G. Jonsson, Palsson, & Sejling (1992) estimated the parameters of counterflow and parallel flow heat exchangers models using a Kalman filter. G. Jonsson & Palsson (1994) applied the extended Kalman filter to the parameter estimation in continuous time heat exchanger models. Mutambara & Al-Haik (1999) estimated the model parameters and states of a lumped counter-flow one plate heat exchanger using the extended Kalman filter. Bagui, Abdelghani-Idrissi, & Chafouk (2004) used an adaptive fading Kalman filter to the design of an observer used to predict the state of a counter-current heat exchanger. Jonsson, Lalot, Palsson, & Desmet (2007) used the extended Kalman filter to detect fouling in a heat exchanger.; Lalot, Palsson, Jonssonb, & Desmet (2007) presented a comparison between a neural network model and a Kalman filter model applied for fouling detection. Zhang, Chen, Xiong, Zhang, & Hou (2014) described an unscented Kalman filter's application to the problem of fault detection and estimation of the sensor failures in the heat exchanger systems.

4.3 Case study

The case study aims at monitoring of a series of heat exchanger networks located at a distillation unit from a Brazilian oil refinery using a Kalman filter-based approach, in which unavailable measures are estimated and the fouling coefficient is monitored.

4.3.1 Plant description

The heat exchanger network is located in the distillation unit of an oil refinery, which transforms crude oil into various products, such as diesel, gasoline, fuel oil, aviation kerosene, solvents, asphalt, etc. The transformation of petroleum into derivatives begins with the physical separation of their fractions by the distillation process. According to their boiling temperature ranges, these are sent to storage tanks composing the final derivatives, where they may be mixed with other fractions or sent to intermediate tanks. From there, the derivatives are separated, transformed, or finished. For this process to happen, the oil is heated at high temperatures until it partially evaporates. Heat exchangers and furnaces provide the heat.

Crude oil enters the distillation unit with impurities such as water, salts, and sediments that must be removed to prevent corrosion and fouling in equipment. Such impurities are removed before the distillation through oil desalination in the equipment called desalters.

The gradual increase in the oil temperature is obtained by a series of heat exchangers called the preheat train (PHT), which promotes the temperature increase of the load using

the heat of products leaving the distillation tower. There are two preheating batteries (PHB): the first one is placed before the desalter, and the second, after it. Posteriorly, the oil receives even more heat load in the furnace to then be separated into derivatives in the distillation tower. Figure 4.1 shows the heating system in a simplified way.

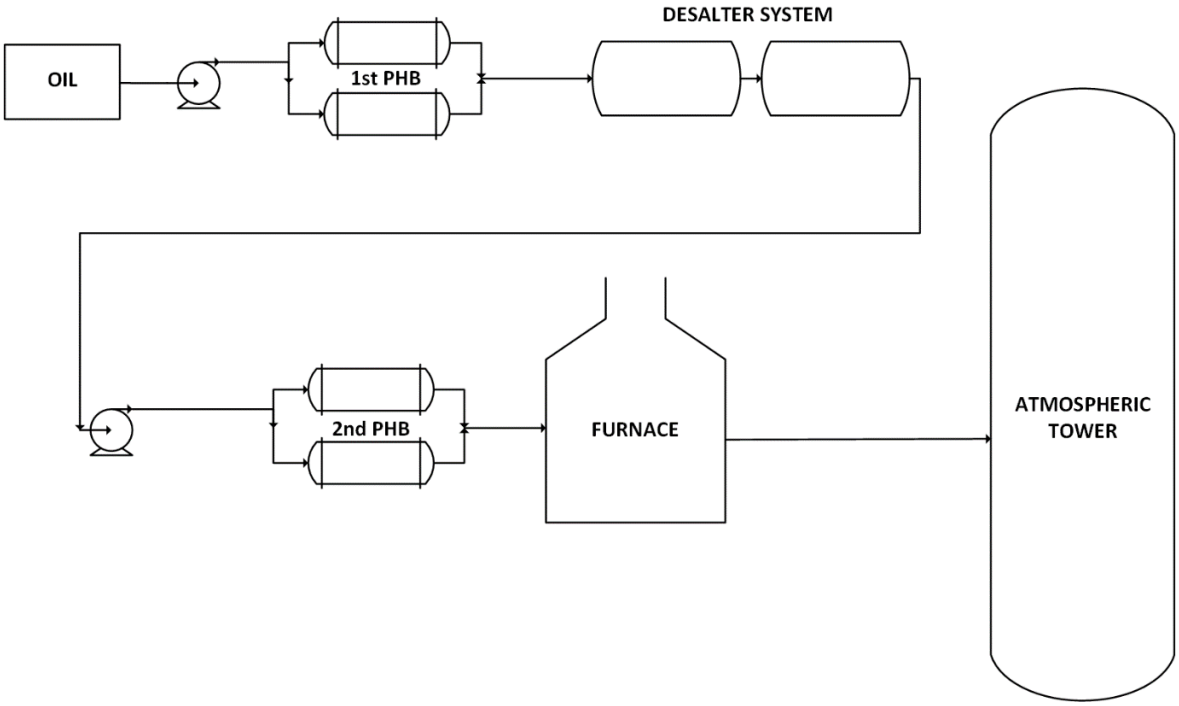


Figure 4.1: The heating system of the crude oil distillation unit.

PHT usage improves plant's utilities consumption efficiency, once it promotes furnace fuel consumption saving (reducing its size and operating cost) and lower consumption of cooling water to cool the products leaving the distillation towers.

4.3.2 Heat exchanger network configuration

As mentioned in the previous section, the distillation unit has two PHTs (one upstream and the other downstream of the desalter). This work analyzes the heat exchangers in the second PHT.

The second PHT is divided into two branches. One branch is the mirror of the other with the same number of heat exchangers and characteristics. For this study, only one branch of the second PHT is analyzed, which has five shell and tube heat exchangers in series with countercurrent exchange. Oil passes through the tubes absorbing heat. In the shell side, two products leaving the distillation tower, called distillate A and distillate B, are cooled down. This configuration aims at increasing the heat exchange efficiency of the battery. The design of the heat exchangers network from the analyzed branch of the second PHT is shown in Figure 4.2.

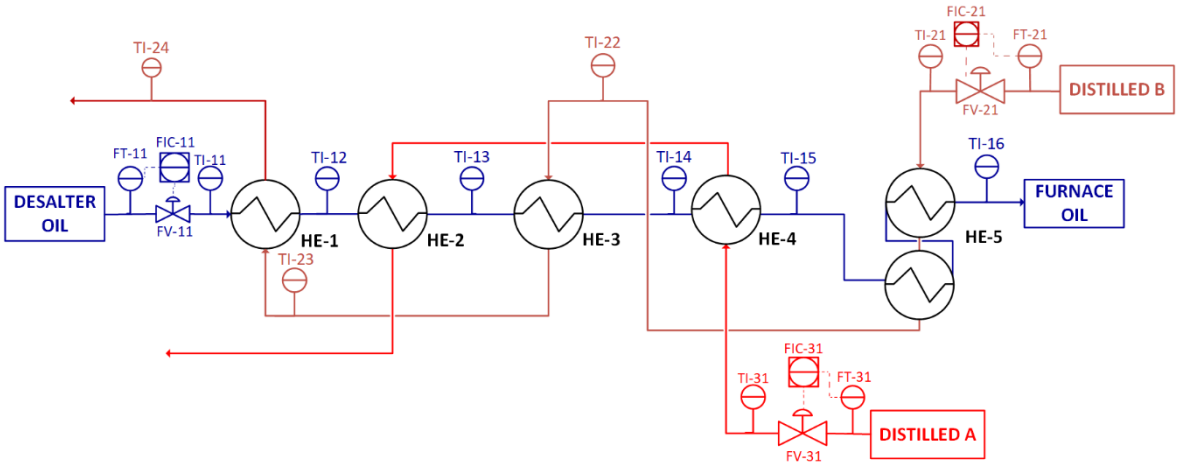


Figure 4.2: Heat exchanger network configuration of PHT of a distillation unit.

The first four heat exchangers (HE) are four-and-one pass designs in the tube and shell side, respectively while the last heat exchanger is two and eight pass designs in the tube and shell side. The PHT system has the flows and temperatures measured according to Figure 4.2.

4.3.3 Heat exchanger model

In this work, it is considered a simple but representative model for the heat exchangers, which is very important for the success of a state estimator approach. The energy balance, shown below, is the basis for the design of the mathematical model of the countercurrent heat exchanger:

$$\frac{dE_i}{dt} = \dot{H}_{i,in} - \dot{H}_{i,out} + UAFdT_{ln} \tag{4.1}$$

$$\frac{dE_o}{dt} = \dot{H}_{o,in} - \dot{H}_{o,out} - UAFdT_{ln} \tag{4.2}$$

where the subscript i represents the internal fluid (cold steam) in the tube side, o the external fluid (hot stream) in the shell side, and in and out are the inlet and outlet temperatures of the heat exchanger, respectively. The description of the model variables is shown in Table 4.1.

Table 4.1: Description of the model variables.

Symbol	Nomenclature	Unit
E	total energy	W
$\dot{H}$	fluid enthalpy	J
U	thermal coefficient of global exchange	W/m². ºC
dT_{ln}	logarithmic mean temperature	ºC
F	logarithmic mean correction factor that depends on the configuration of the heat exchanger	-
$\dot{m}$	mass flow	kg/s
C_p	specific heat	J/kg. ºC
T	fluid temperature	ºC
ρ	specific mass	kg/m³
μ	fluid viscosity	Pa.s
h	convective heat transfer coefficient	W/m². ºC

k	thermal conductivity of the inner pipe material	W/m². ºC
k_i	thermal conductivity of the inner fluid	W/m². ºC
k_o	thermal conductivity of the outer fluid	W/m². ºC
$R_{f,i}$	fouling resistance at the inner surface (tubes)	m². ºC /W
$R_{f,o}$	fouling resistance at the outer surface (shell)	m². ºC /W
R_f	fouling resistance at the inner and outer surfaces	m². ºC /W
A	area of thermal exchange	m²
V	volume through which the fluids flow	m³
d_i	internal diameter of the tube	m
d_e	external diameter of the tube	m
D_i	internal diameter of the shell	m
D_e	equivalent diameter of the shell	m
L	tubes length	m
F	logarithmic mean correction factor	-
n_t	number of tubes in the heat exchanger	-
n_b	number of baffles	-
n_{PT}	number of passes in the tubes of the heat exchanger	-
n_{PS}	number of passages in the tubes	-

The following simplifications were made to determine the inlet and outlet temperatures of the tube and shell sides fluids:

$$\dot{H} = \dot{m} C_p T \tag{4.3}$$

$$E = V \rho C_p T \tag{4.4}$$

Therefore, the following equations were obtained

$$\frac{dT_{i,out}}{dt} = \frac{\dot{m}_i Cp_i (T_{i,in} - T_{i,out}) + UA_i F dT_{ln}}{\rho_i V_i Cp_i} \tag{4.5}$$

$$\frac{dT_{o,out}}{dt} = \frac{\dot{m}_o Cp_o (T_{o,in} - T_{o,out}) - UA_o F dT_{ln}}{\rho_o V_o Cp_o} \tag{4.6}$$

Applying the logarithmic mean temperature difference (LMTD) equation for the countercurrent configuration gives the following expression:

$$dT_{ln} = \frac{\Delta T_1 - \Delta T_2}{ln\left(\frac{\Delta T_1}{\Delta T_2}\right)} \tag{4.7}$$

where ln is the natural logarithm in base e, and ΔT_1 and ΔT_2 are defined as:

$$\Delta T_1 = T_{o,in} - T_{i,out} \tag{4.8}$$

$$\Delta T_2 = T_{o,out} - T_{i,in} \tag{4.9}$$

To avoid convergence problems and mathematical singularities, it was used the modification proposed by Chen (1987) to evaluate the LMTD, given by:

$$dT_{ln} = \frac{\Delta T_1 + \Delta T_2}{2} - \frac{[\Delta T_1 - \Delta T_2]^2}{6\,[\Delta T_1 + \Delta T_2]} \tag{4.10}$$

To evaluate the global coefficient of thermal exchange, the following expression was used (ÇENGEL, 2002):

$$\frac{1}{UA} = \frac{1}{h_i A_{is}} + \frac{R_{f,i}}{A_{is}} + \frac{ln\left(\frac{d_e}{d_i}\right)}{2\pi k l} + \frac{1}{h_o A_{os}} + \frac{R_{f,o}}{A_{os}} \tag{4.11}$$

Rearranging Equation 4.11 and grouping the parameters of the fouling in the inner and outer surfaces gives:

$$\frac{1}{UA} = \frac{1}{h_i A_{is}} + \frac{ln\left(\frac{d_e}{d_i}\right)}{2\pi k L} + \frac{1}{h_o A_{os}} + \frac{1}{A} R_f \tag{4.12}$$

$$R_f = R_{f,i} + R_{f,o} \tag{4.13}$$

The fouling resistance is also considered as a state variable for the reasons explained in section 4.4.2.

$$\frac{dR_f}{dt} = 0 \tag{4.14}$$

From the Nusselt dimensionless number, it is possible to evaluate the convective exchange coefficient h.

$$h_i = \frac{Nu_i k_i}{d_i} \tag{4.15}$$

$$h_o = \frac{Nu_o k_o}{D_e} \tag{4.16}$$

The Reynolds and Prandtl dimensionless numbers for the internal and external fluids, respectively, are given by the following expressions:

$$Re_i = \frac{\dot{m}_i d_i}{A_i \mu_i} \tag{4.17}$$

$$Re_o = \frac{\dot{m}_o D_e}{A_o \mu_o} \tag{4.18}$$

$$Pr_i = \frac{\mu_i C_{pi}}{k_i} \tag{4.19}$$

$$Pr_o = \frac{\mu_o C_{po}}{k_o} \tag{4.20}$$

The internal flow Nusselt number was calculated using the Petukhov's equation (modified by Gnielinski) (VDI HEAT ATLAS, 2010) for turbulent flow through pipes, which holds in the range $10^4 < \mathrm{Re} < 10^6$ and $0.6 < \mathrm{Pr} < 1000$.

$$Nu_i = \frac{Re_i Pr_i \zeta/8}{1 + 12.7\sqrt{\zeta/8}\left(Pr_i^{\frac{2}{3}} - 1\right)}\left[1 + \left(\frac{d_i}{L}\right)^{\frac{2}{3}}\right] \tag{4.21}$$

$$\zeta = (0.78\ ln\ (Re_i) - 1.5)^{-2} \tag{4.22}$$

For the external flow Nusselt number, it is assumed fully developed turbulent flow,

$$Nu_o = 0.024 Re_o^{0.8} Pr_o^{0.3} \tag{4.23}$$

which holds in the range $10^4 < \mathrm{Re} < 10^6$ and $0.6 < \mathrm{Pr} < 1000$.

The flow and superficial areas from the tubes inner and outer surfaces of the heat exchanger are described by:

$$A_i = \frac{\pi d_i^2}{4 n_{PT}} n_t \tag{4.24}$$

$$A_o = \frac{Di(pl - d_e)\frac{L}{(n_b+1)}}{pl} \tag{4.25}$$

$$A_{is} = \pi d_i n_t L \tag{4.26}$$

$$A_{os} = \pi d_e n_t L \tag{4.27}$$

and the equivalent diameter of the shell is evaluated as:

$$D_e = \frac{\left(4pl^2 - \pi d_e^2\right)}{\pi d_e} \tag{4.28}$$

The volumes in the inner and outer surfaces of the tubes are:

$$V_i = A_i L \tag{4.29}$$

$$V_o = A_o L \tag{4.30}$$

Considering the HEN configuration, it is possible to identify the connections of the variables between each heat exchanger model, shown in Table 4.2.

Table 4.2: Variables connections for the heat exchanger network model.

HE	Connections
HE-1 and HE-3	$HE1.T_{o,in} = HE3.T_{o,out}$
HE-2 and HE-4	$HE2.T_{o,in} = HE4.T_{o,out}$
HE-3 and HE-5	$HE3.T_{o,in} = HE5.T_{o,out}$

In this case, only the connection between HE-2 and HE-4 is used, due to the lack of measurements from the $T_{o,in}$ in the HE-2.

4.3.4 Process data

To estimate the HEN model parameters, the process data were collected from the software PI ProcessBook from OSIsoft and the heat exchangers parameters from the equipment datasheets. The process data have the input and output temperatures and the flow rate from the hot and cold fluids. Data from 255 days (approximately 8.5 months) were

saved in a sampling time equal to 10 minutes, which is sufficient to capture the dynamic behavior of the plant.

Considering **Erro! Fonte de referência não encontrada.**, the output and input temperatures (or output temperature in the shell from HE-4) in the shell side from HE-2 are not available. The flow rates were obtained by the flow sensors installed at the entrance of the tube and shell.

The heat exchanger parameters, from the equipment datasheets, are shown in Table 4.3.

Table 4.3: Physical properties of the heat exchanger network.

	HE-1	HE-2	HE-3	HE-4	HE-5
A	658.15	897.48	658.15	897.48	1762.85
d_i	0.0148	0.0148	0.0148	0.0148	0.0148
d_e	0.01905	0.01905	0.01905	0.01905	0.01905
D_i	1.3	1.528	1.3	1.528	1.522
L	6.096	6.096	6.096	6.096	12.192
F	0.99	0.99	0.99	0.99	0.93
n_t	1804	2460	1804	2460	2416
pl	0.0254	0.0254	0.0254	0.0254	0.0254
n_b	17	13	17	13	29
n_{PT}	4	4	4	4	8
n_{PS}	1	1	1	1	2
k	67.4	67.4	67.4	67.4	67.4

The physical properties of the oil, distillate A, and distillate B were obtained from the heat exchangers network datasheet. The properties are considered constant for simplification purposes and also to consider the worst-case possible, in which they do not change with the temperature and the API gravity, shown in Table 4.4.

Table 4.4: Physical properties of the heat exchanger fluids.

	HE-1	HE-2	HE-3	HE-4	HE-5
ρ_i	755	755	755	755	755
ρ_o	980	980	980	980	980
$\dot{\mu}_i$	0.00126	0.00126	0.00126	0.00126	0.00126
$\dot{\mu}_o$	0.0101	0.0101	0.0101	0.0101	0.0101
k_i	0.1219	0.1219	0.1219	0.1219	0.1219
k_o	0.1103	0.1103	0.1103	0.1103	0.1103
Cp_i	2133.84	2133.84	2133.84	2133.84	2133.84
Cp_o	920.48	920.48	920.48	920.48	920.48

4.4 Methodology

This section presents a review of the constrained extended Kalman filter and smoother approach applied to this work. The techniques and tests were entirely coded in Python 2.7 and the model implemented in JModelica (ÅKESSON *et al.*, 2010). The tests were run in a

PC with an Intel® Core™ i7-3632QM CPU @ 2.20GHz 2.20 GHz processor and with 16 GB RAM.

4.4.1 Kalman filter approach

The Kalman filter (KF) (KALMAN, 1960) methodology requires a dynamic model of the system, input measurements, and other available measurements either to predict unknown variables or to filter known ones. This data may present noise and other discrepancies (e.g., from the sensors) that are corrected by the filter (APIO, Andressa *et al.*, 2019b).

The Kalman filter equations provide a recursive estimation of the states and their covariance error. The quality of this estimation depends on the system parameters and the noise statistics given as inputs to the estimator. In this context, the Kalman filter blends new information introduced by the measurements with old information embodied in the prior state with the Kalman gain matrix, which balances uncertainty in the measurements with the uncertainty in the dynamic model (ALFRIEND *et al.*, 2010). Thus, the error propagation in the covariance matrix *P*, which estimates the uncertainties from the state prediction, is what brings accuracy to the Kalman filter (SIMON, 2006).

For this case study, the constrained extended Kalman filter and smoother was applied to soften the noisy real data. In this section, this methodology is described.

3.3.1.1. Constrained Kalman filter and smoother

The constrained extended Kalman filter (GESTHUISEN; KLATT; ENGELL, 2001) comes from the moving horizon estimation (MHE), which is an optimization approach to estimate measured and unmeasured states of dynamical systems considering a moving window when the horizon length is equal to zero. This simplifies the complexity of solving the MHE dynamic nonlinear optimization problem (FRANKE *et al.*, 2001), resulting exactly in the formulation of the CEKF, as follows:

$$\min_{\omega_{k-1|k},v_{k|k}} J = \omega_{k-1|k}^{T}\left(P_{k-1|k-1}\right)^{-1}\omega_{k-1|k} + v_{k|k}^{T}(R_k)^{-1}v_{k|k} \tag{4.31}$$

with the following constraints:

$$H_k\omega_{k-1|k} + v_{k|k} = y_k - h\left(\hat{x}_{k|k}\right) \tag{4.32}$$

$$x_{min} - \hat{x}_{k|k} \leq \omega_{k-1|k} \leq x_{max} - \hat{x}_{k|k} \tag{4.33}$$

$$y_{min} - h\left(\hat{x}_{k|k}\right) \leq H_k\omega_{k|k-1} + v_{k|k} \leq y_{max} - h\left(\hat{x}_{k|k}\right) \tag{4.34}$$

in which the prediction matrix is given by the Riccati matrix in discrete time:

$$P_{k|k} = \phi_{k-1}P_{k-1|k-1}\phi_{k-1}^{T} - \left(\phi_{k-1}P_{k-1|k-1}H_k^{T}\right)\left(H_kP_{k-1|k-1}H_k^{T} + R_k\right)^{-1}\left(H_kP_{k-1|k-1}\phi_{k-1}^{T}\right) + Q_{k-1} \tag{4.35}$$

and the final correction by:

$$\hat{x}_{k|k} = \hat{x}_{k|k-1} + \omega_{k-1|k} \tag{4.36}$$

$$y_k = \hat{y}_{k|k} + v_{k|k} \tag{4.37}$$

where *k* represents the step considered in discrete time, *x* is the vector of states, *f* is a model function, *ω* is the process noise vector, *y* is the output vector, *h* is a function that relates the states to the outputs, *v* is the measurement noise vector, *F* is the Jacobian of *f* in relation to the states, *φ* is the transition matrix from one state to another, *H* is the Jacobian of *h* in relation to the outputs, *P* is the covariance matrix of the states, *Q* is the process noise covariance matrix and *R* is the measurement noise covariance,

The constrained extended Kalman filter and smoother (CEKFS) (SALAU; TRIERWEILER; SECCHI, 2012b) includes the EKF smoother counterpart in the CEKF. Its main difference is that the recursion in the filter moves forward and the smoother backward (HAYKIN, 2001). This smoothing is significant once the CEKF and DEKF fail to converge swiftly to the actual states when the system is subject to poor guesses at the initial state (RAUCH; STRIEBEL; TUNG, 1965). In this context, smoothing means providing an estimate of the system state at some time step, given that all the measurements, including the ones encountered after that particular time step, are available. In short, the CEKFS gives a smoothed estimate of the system history for all the measurements obtained so far.

Firstly, from the CEKF evaluation results, the following variables are set:

$$\hat{x}^S_{N|k} = \hat{x}_{k|k} \text{ and } P^S_{N|k} = P_{k|k} \tag{4.38}$$

Considering $k = N-1, N-2, \ldots, 0$, the Rauch-Tugh-Striebel (RTS) smoother, which is detailed in Rauch et al. (1965) and Haykin (2001), is evaluated as:

$$\hat{x}_{k+1|k} = \hat{x}_{k|k} + \int_k^{k+1} f(x,u,t)\, dt \tag{4.39}$$

$$P_{k+1|k} = \phi_k P_{k|k} \phi_k^T + Q_k \tag{4.40}$$

$$C_k = P_{k|k} \phi_k^T P_{k+1|k}^{-1} \tag{4.41}$$

$$\hat{x}^S_{k|k} = \hat{x}_{k|k} + C_k(\hat{x}^S_{k+1|k} - \hat{x}_{k+1|k}) \tag{4.42}$$

$$P^S_{k|k} = P_{k|k} + C_k(P^S_{k+1|k} - P_{k+1|k})C_k^T \tag{4.43}$$

where *N* is the horizon size and C_k is the RTS smoother of the Kalman gain. In this work, the horizon size is *N* = 4. The new smoothed values (P_0^S and $\hat{x}_0^S$) are the initial guess for the CEKF algorithm, which is re-evaluated until the current step:

$$P_k = P_0^S \quad \text{and} \quad \hat{x}_{k|k} = \hat{x}_0^S \tag{4.44}$$

4.4.2 Simulation settings

In this work, the Kalman filter used the model of the heat exchanger presented in section 4.3.3 as the dynamic model of the system, the input measurements $\dot{m}_i$, $\dot{m}_o$, $T_{i,in}$ and $T_{o,in}$, and the available output measurements $T_{i,in}$ and $T_{o,in}$ to estimate and filter the states $R_f, T_{i,out}$ and $T_{o,out}$. The system has 15 equations, 15 states, 8 output measurements, and 19 input measurements, resulting in an observable system according to the Popov-Belevitch-Hautus criterion (HAUTUS, 1969).

The filter parameters for all heat exchangers composing the HEN are shown in Table 4.5. The values of P0 and Q0 were chosen according to the state order of magnitude, and R0 based on the measurement order of magnitude.

Table 4.5: Filter parameters for the heat exchanger network.

	P0	R0	Q0
HE-1	$I^3 10^2$	$I^2 10^2$	diag(10^{-6}, 10^4, 10^4)
HE-2	$I^3 10^1$	$I^1 10^2$	diag(10^{-6}, 10^4, 10^4)
HE-3	$I^3 10^2$	$I^2 10^2$	diag(10^{-6}, 10^4, 10^4)
HE-4	$I^3 10^1$	$I^1 10^2$	diag(10^{-6}, 10^4, 10^4)
HE-5	$I^3 10^2$	$I^2 10^2$	diag(10^{-6}, 10^4, 10^4)

In this case, for the Kalman filter process noise covariance matrix Q_0, it is considered more confidence in the model for the R_f variable, and more confidence in the measurements for the $T_{i,in}$ and $T_{o,in}$ variables.

The Kalman filter available input and output measurements used for each heat exchanger are shown in Table 4.6.

Table 4.6: Data used in the Kalman filter for heat exchanger network.

HE	States	Inputs	Outputs
HE-1	$R_f, T_{i,out}$ and $T_{o,out}$	$\dot{m}_i$, $\dot{m}_o$, $T_{i,in}$, and $T_{o,in}$	$T_{i,out}$ and $T_{o,out}$
HE-2	$R_f, T_{i,out}$ and $T_{o,out}$	$\dot{m}_i$, $\dot{m}_o$, and $T_{i,in}$	$T_{i,out}$
HE-3	$R_f, T_{i,out}$ and $T_{o,out}$	$\dot{m}_i$, $\dot{m}_o$, $T_{i,in}$, and $T_{o,in}$	$T_{i,out}$ and $T_{o,out}$
HE-4	$R_f, T_{i,out}$ and $T_{o,out}$	$\dot{m}_i$, $\dot{m}_o$, $T_{i,in}$, and $T_{o,in}$	$T_{i,out}$
HE-5	$R_f, T_{i,out}$ and $T_{o,out}$	$\dot{m}_i$, $\dot{m}_o$, $T_{i,in}$, and $T_{o,in}$	$T_{i,out}$ and $T_{o,out}$

As the heat exchangers model considers its physical variables constant, it is necessary to distribute the model's error in an estimated variable. In this case, the fouling resistance coefficient was chosen R_f to receive these errors.

The initial conditions of the HEN states are presented in Table 4.7. For simplification purposes, it was considered the same values for all the five heat exchangers.

Table 4.7: Initial conditions for the heat exchanger network.

	R_f	$T_{i,out}$	$T_{o,out}$
HE	0.0011	140	180

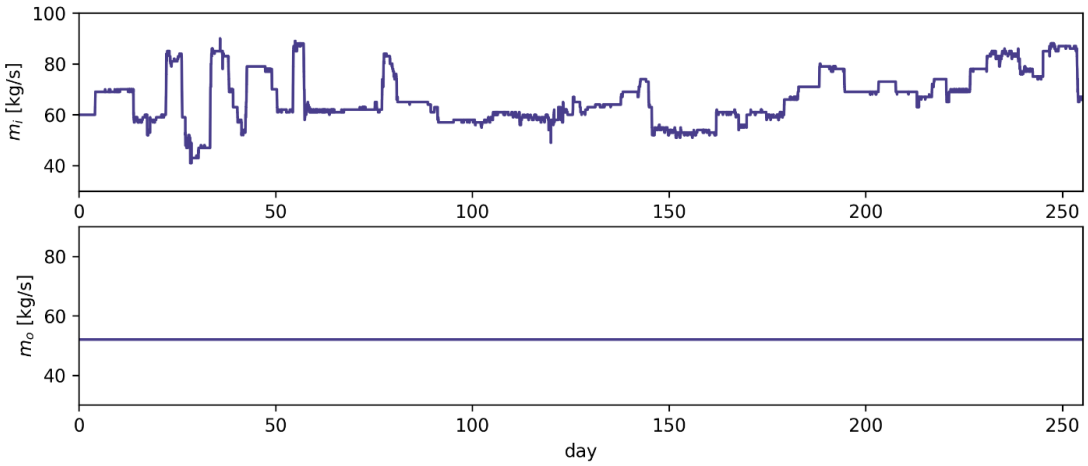
In this case study, the state and parameters from the dynamic model are simultaneously estimated using Kalman filter. The approach, commonly known as state augmentation (JAZWINSKI, A. H., 1970), consists of defining an augmented dynamical system that allocates, along with the system's state, the model parameters to be estimated. As the parameters are constant, the right side of the corresponding differential equations is equal to zero.

4.5 Results and discussion

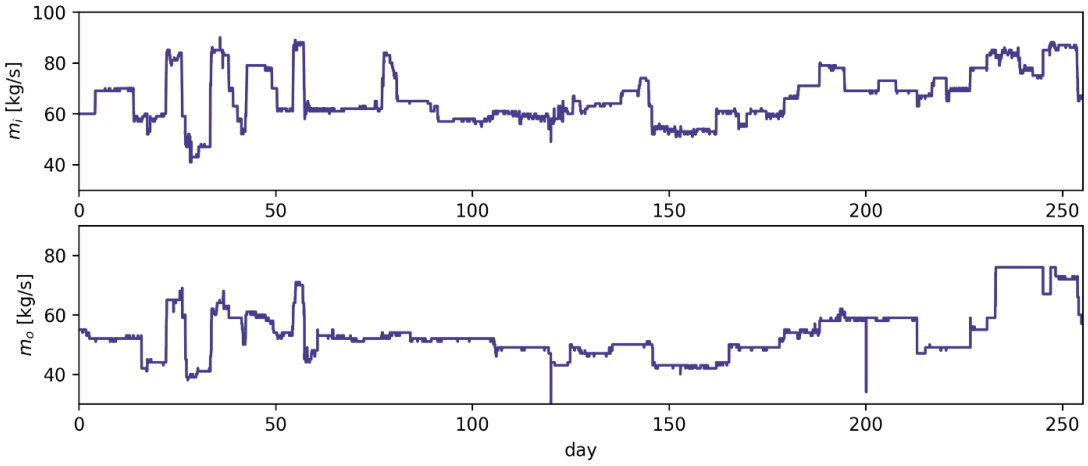
In this section, the Kalman filter reviewed in Section 4.4 is applied to the PHT case study presented in Section 4.3. Firstly, the results for the model simulation are presented, followed by the results for the Kalman filter application, including the fouling monitoring for each heat exchanger.

4.5.1 Model simulation results

In this section, the simulation of the PHT is presented. The mass flow input for all the heat exchangers and the results of the simulation are shown, respectively, in Figure 4.3 and Figure 4.4.

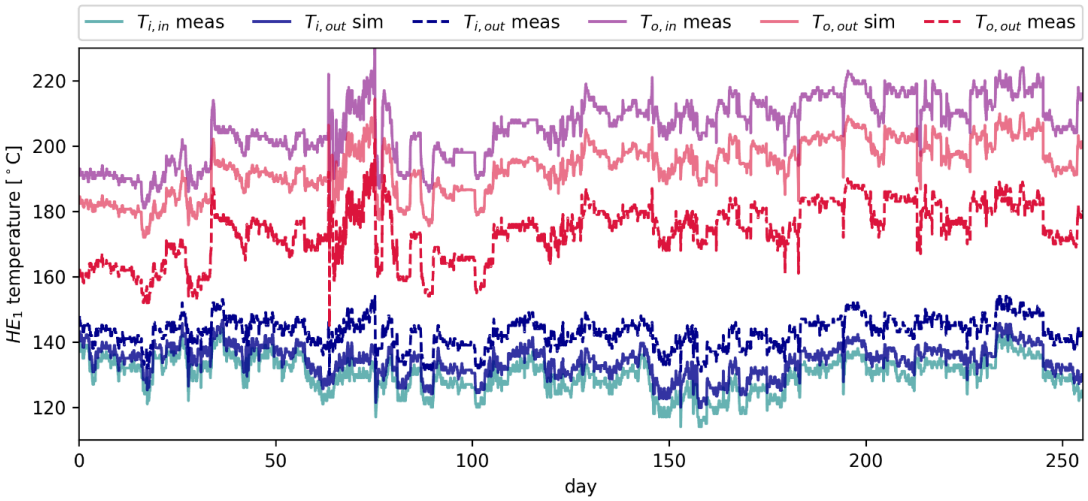


a) HE-1, HE-3, and HE-5

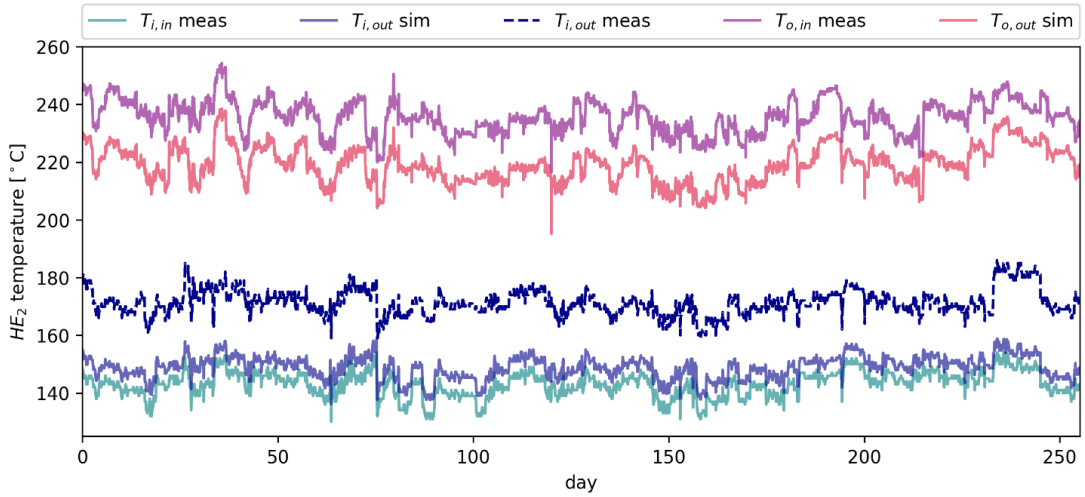


b) HE-2 and HE-4

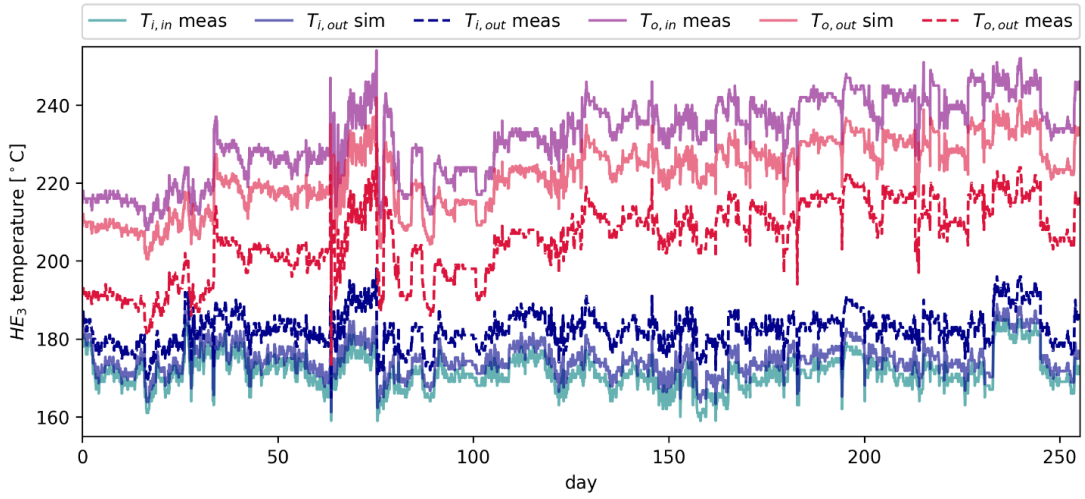
Figure 4.3: Mass flow input measurements for the heat exchanger network.



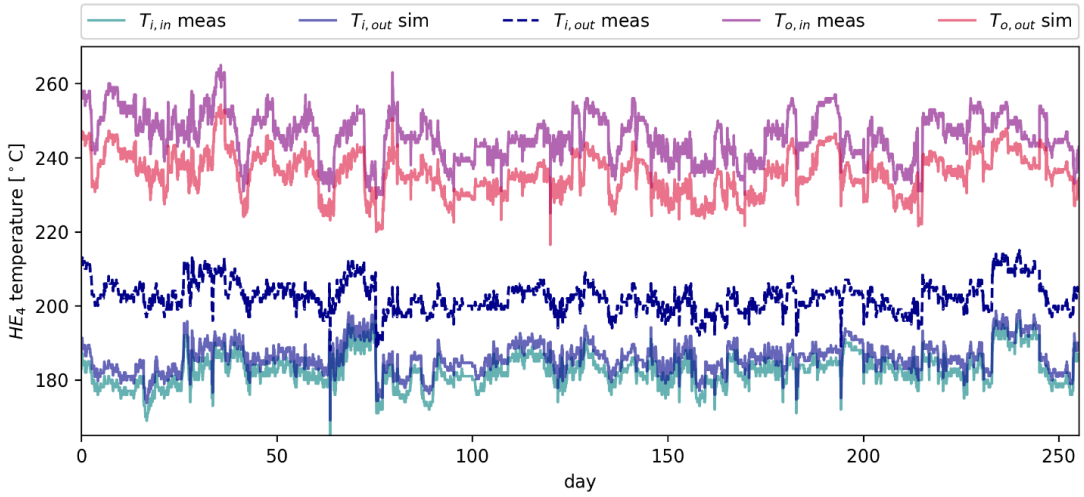
a) HE-1



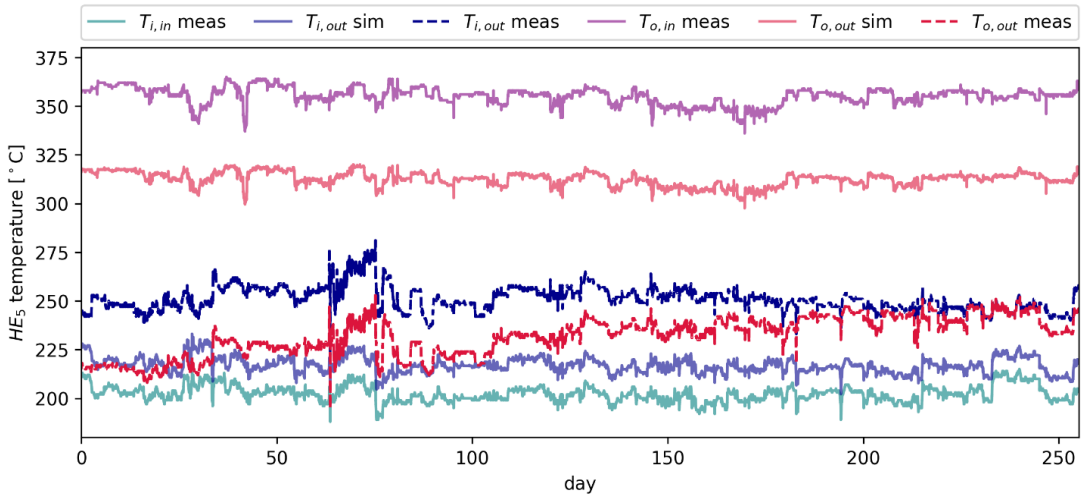
b) HE-2



c) HE-3



d) HE-4



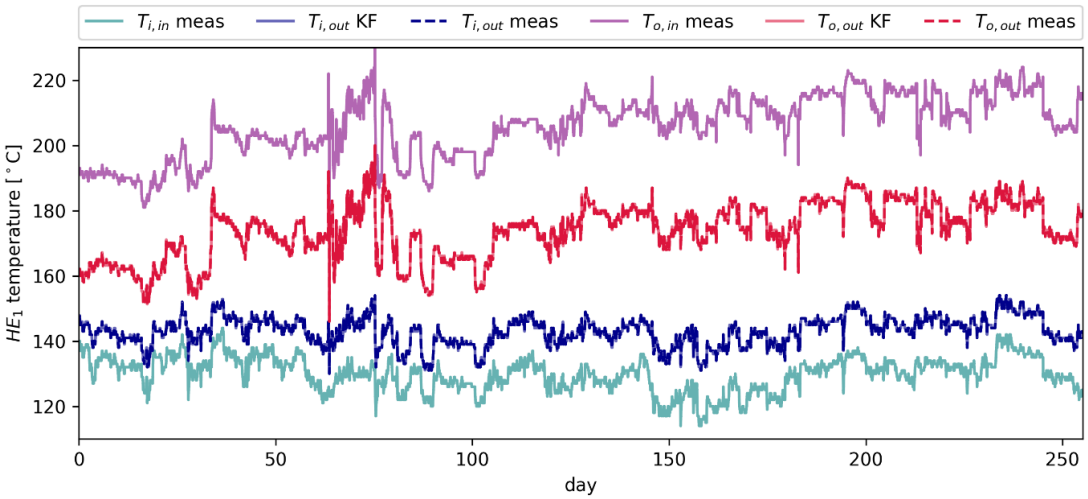
e) HE-5

Figure 4.4: Simulation results of the PHT system, where *meas* refers to measurements and *sim* to simulation data.

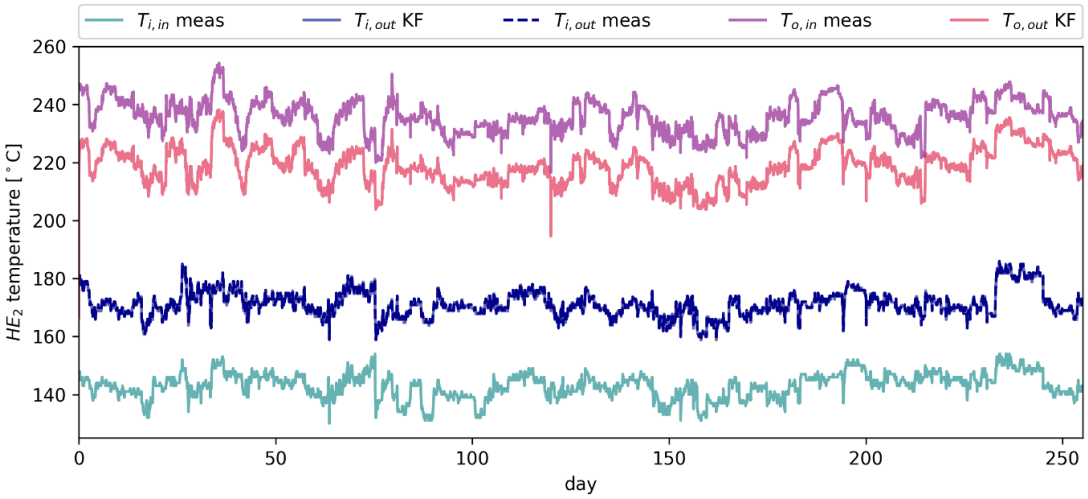
In Figure 4.4, the outer temperatures for both cold and hot streams are simulated and compared with the real data. The simulated results' behavior is very similar to the real data, presenting only a bias between each other. Considering all the heat exchangers, the simulated cold stream outer temperature is more distant than its real values compared to the hot stream. In this case, the most critical feature to apply the Kalman filter is that the model may describe dynamics of the real data well, as the state estimator may quickly correct the bias.

4.5.2 Kalman filter results

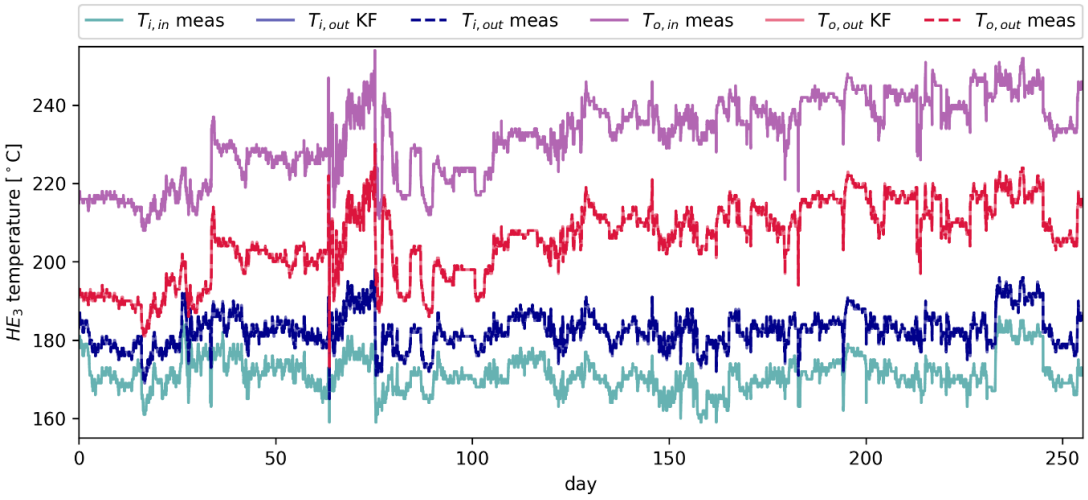
As discussed in Section 4.3.4, all the physical properties of the heat exchanger fluids are considered fixed. Although some properties such as viscosity, conductivity, and specific heat may change with the fluid's temperature and API gravity, this last value is not known. Different types of oil pass through the HEN with different API gravity, which would modify all these fluids properties. To correct this lack of information, the Kalman filter is applied to the simplified HEN model, in which the results are shown in Figure 4.5.



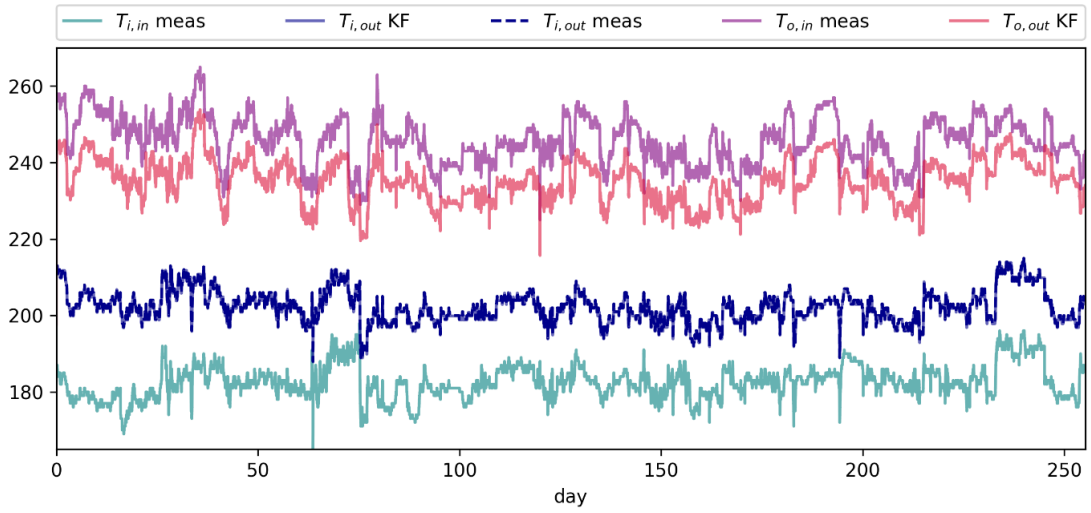
a) HE-1



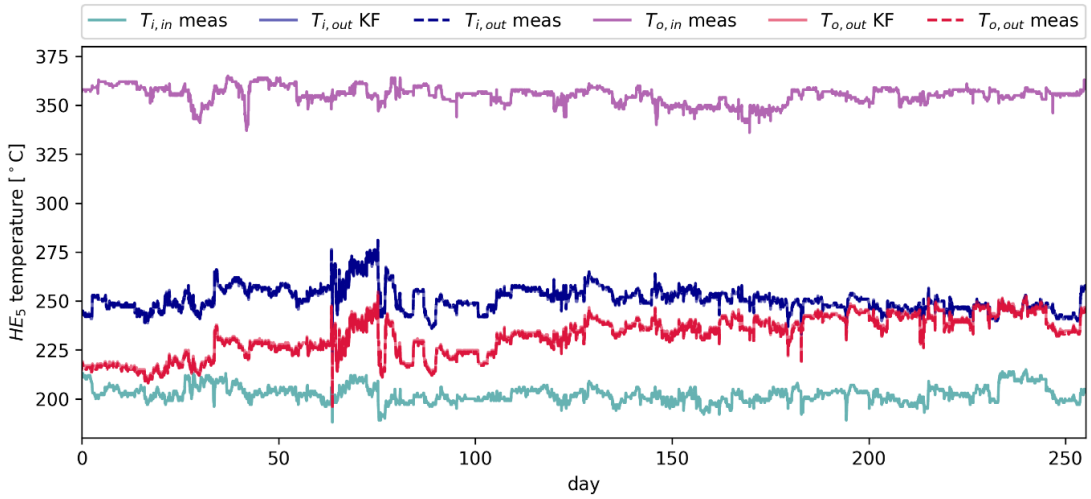
b) HE-2



c) HE-3



d) HE-4

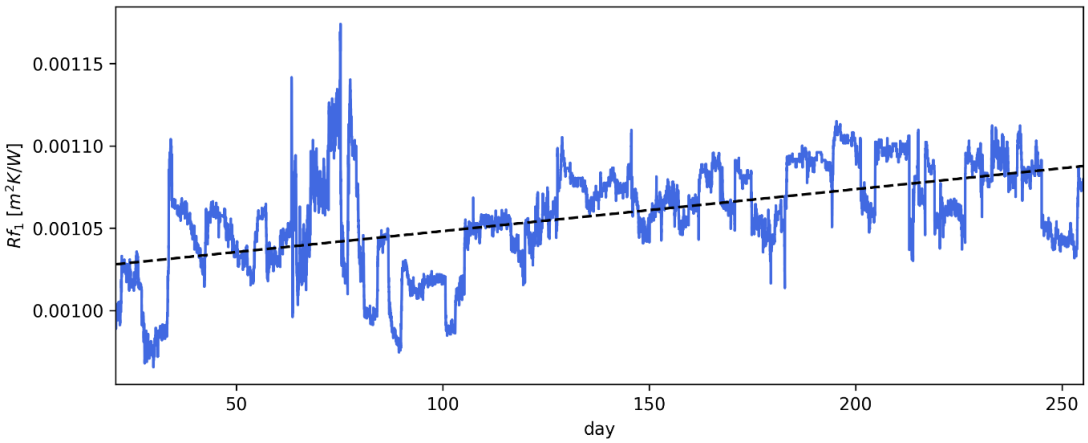


e) HE-5

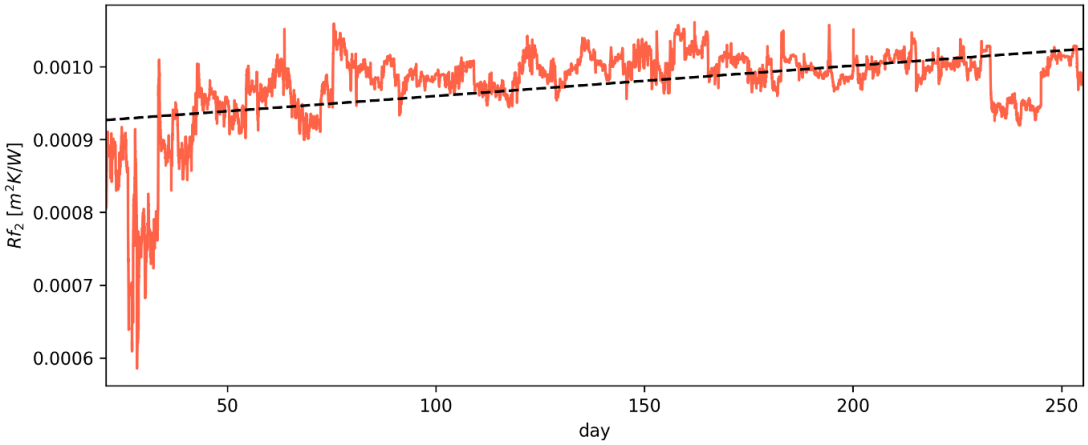
Figure 4.5: Kalman filter application results of the PHT system.

The results of the Kalman filter application in the HEN model (Figure 4.5) show the Kalman filter simulation and real data fit. As expected, the bias presented in the model simulation (Section 4.5.1) was corrected by adapting the Rf value. The unkown inlet temperatures of the HE-2 and HE-4 were simulated knowing that $HE2.T_{o,in} = HE4.T_{o,out}$. On the other hand, the unknown outer temperatures of the HE-2 and HE-4, which were unknown also unavailable, were estimated by the Kalman filter. In this case, the lines from the real data and Kalman filter simulation were stacked together.

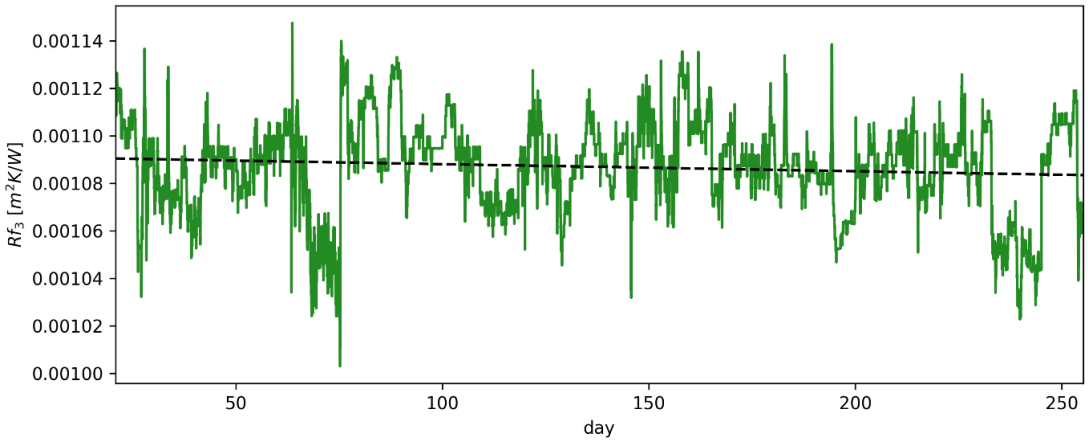
Figure 4.6 shows the fouling monitoring for each HE starting in the 20th day since the state estimator takes time to reach the steady-state.



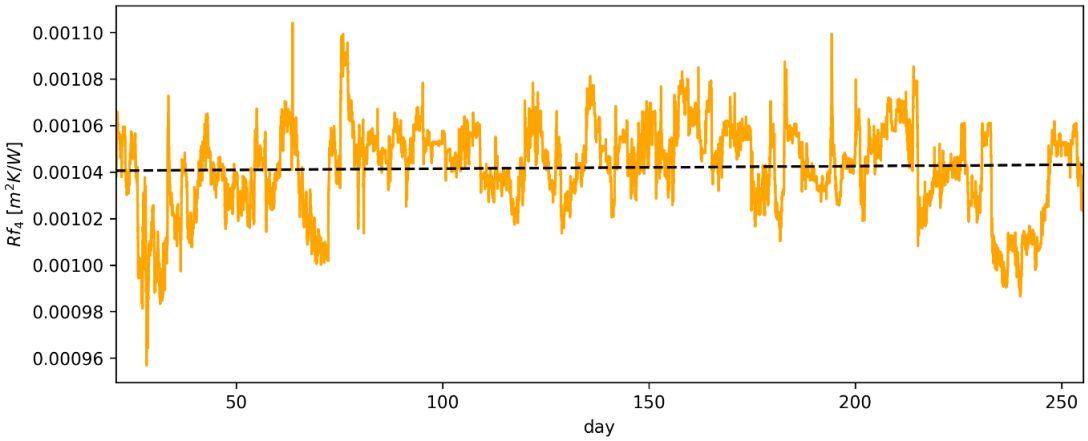
a) HE-1



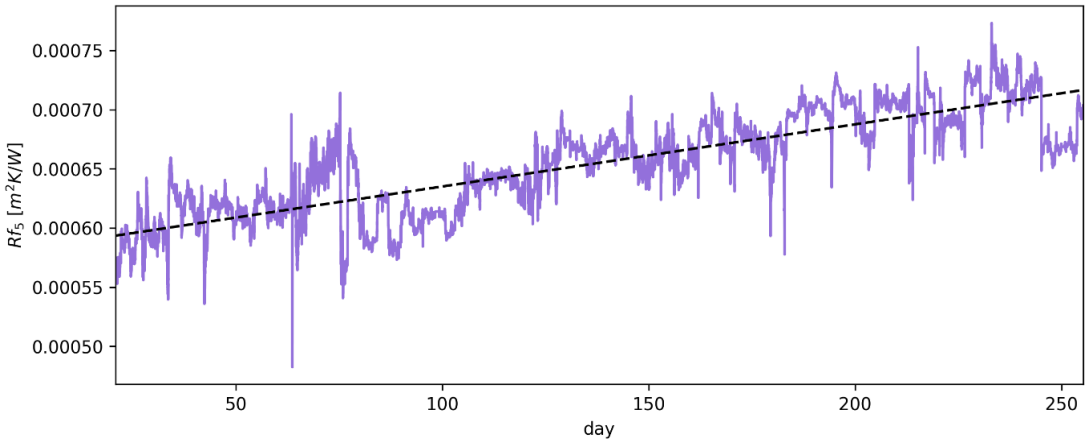
b) HE-2



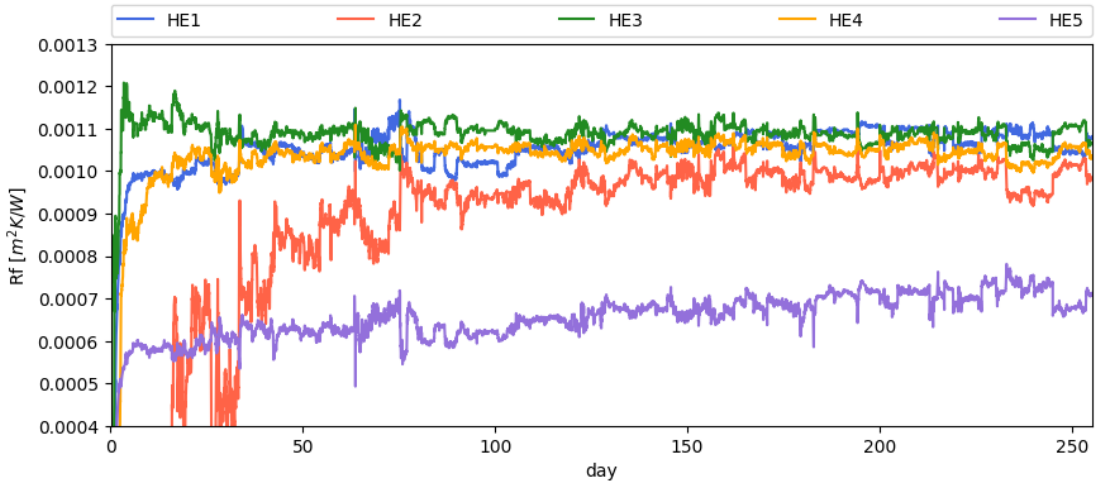
c) HE-3



d) HE-4



e) HE-5



f) All

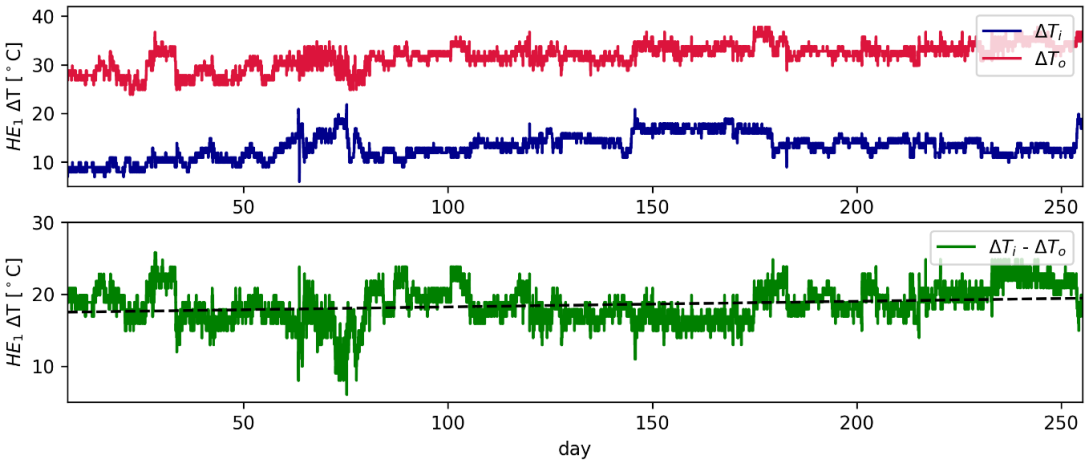
Figure 4.6: Kalman filter application results of the PHT system – fouling monitoring.

Figure 4.6 shows the fouling monitoring for each heat exchanger of the PHT system. Analyzing their behavior, it is possible to identify several random variations, which are not standard on fouling profiles. As discussed before, the R_f is influenced by the dynamical variation from other variables of the system, such as the fluid properties. Due to this fact,

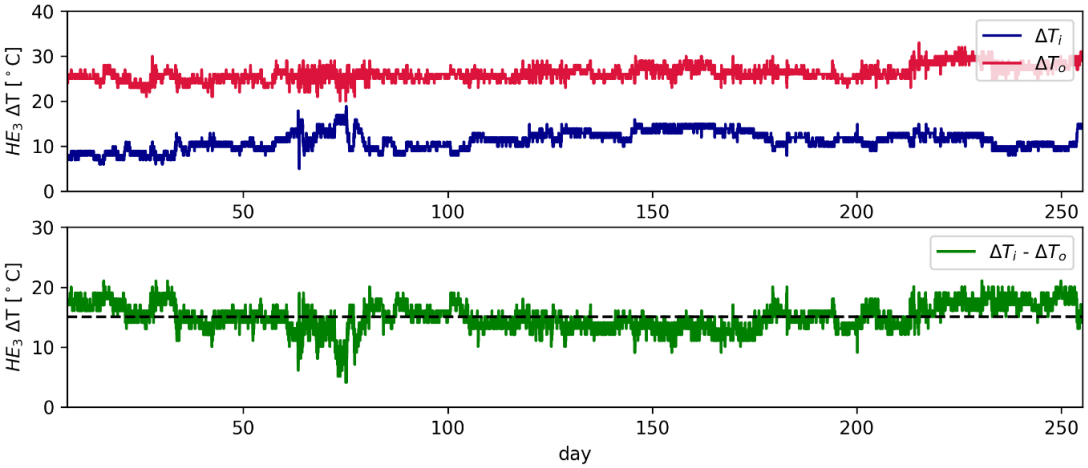
it is applied a robust regression to these results to evaluate the heat exchanger's fouling slope. Thus, it is possible to infer the five HE fouling states.

For the heat exchangers 3 and 4, the slope is almost zero, meaning the possible absence of fouling increases. Due to the lack of the $T_{i,in}$ measurements, the heat exchanger 2 presents a delay to reach the steady-state. Heat exchanger 1 shows a slightly positive slope, while the positive slope from heat exchanger 5 suggests the fouling increase.

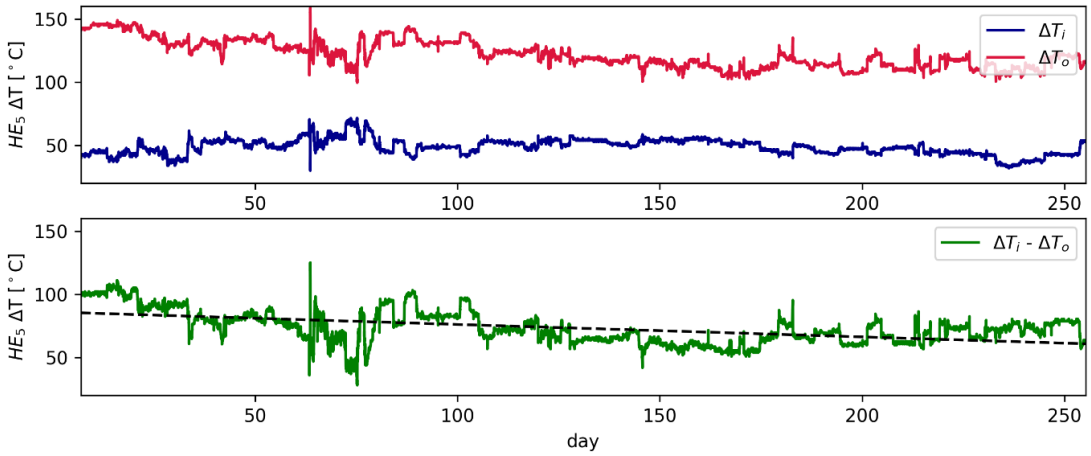
Figure 4.7 shows the temperature exchange for HE-1, HE-3, and HE-5, which present all the input temperatures. The black dashed line represents the robust regression using the difference between the temperature exchange of the hot and cold stream. In this case, the least-squares method was used to fit a simple linear function $y = ax + b$ to the data with the Huber (HUBER, 1964) loss function. For HE-1, the hot stream provides at about 18 ºC to the cold stream along 255 days. Meanwhile, for HE-3, it is provided at about 15 ºC from the hot to the cold stream along this period. These regressions show that the temperatures remain practically the same, maintaining the fouling almost constant. For HE-5, the loss of heat exchange capacity is more evident, as the temperature exchange starts at 80 ºC and is reduced to 60 °C in 255 days, which shows the presence of fouling.



a) HE-1



b) HE-3



c) HE-5

Figure 4.7: Kalman filter application results of the PHT system – temperature exchange.

The fouling monitoring may be improved if the model receives more data about the fluid properties. In this case study, the worst case possible was considered, in which these fluid properties do not change with the temperature and API gravity. Nevertheless, the results presented in this section were enough to show the Kalman filter capacity to estimate the desired variables, considering that a simplified model and limited data were used.

4.6 Conclusions

Heat exchanger networks are essential to reduce energy consumption due to the process stream heat integrations. In the petroleum refining industry, the PHT of crude distillation unit is the most critical system in the refinery, in which it is fundamental to detect loss of heat transfer efficiency. Fouling in these systems represent high costs and operational difficulties, which makes its prediction necessary.

In this paper, a constrained Kalman filter with smoothing was applied to a HEN simple model, with the addition of real data, in order to estimate unavailable measurements and the fouling resistance. It was considered the worst case possible, where the physical properties from the fluids were considered constant. Besides that, these fluid properties could be costinually changing, regarding the oil API gravity passing though the PHT.

The results for the fouling monitoring of the five heat exchangers from the HEN showed several variations in their profiles. Possibly the fouling resistance was influenced by the dynamical variation from other variables of the system. Applying a robust regression to these results, it was obtained the fouling slope of each heat exchanger. In short, for HE-3 and HE-4, the slope is almost zero, indicating the absence of fouling. HE-2 presents in reaching the steady-state due to its lack of measurements. HE-1 shows a slightly positive slope, but does not show an apparent loss of heat capacity. HE-5 suggests the fouling presence, once it was a positive slope. In this last case, the loss of heat capacity is demonstrated as the temperature exchanged is reduced by approximately 20 ºC in 255 days.

For the first time, the operation and fouling by a constrained extended Kalman Filter and smoother of an oil PHT was monitored. From this case study, the state estimator was

able to estimate the desirable variable using a simple model and limited data. The operational monitoring of the PHT may be improved if the model receives more data about the fluid properties, e.g., physical properties changing with temperature and API gravity from the oil.

4.7 Acknowledgments

The authors acknowledge the financial support from the National Petroleum, Natural Gas, and Biofuels Agency (ANP) and Petróleo Brasileiro S.A. (PETROBRAS).

Capítulo 5 – Bias estimation: a simple solution for the main drawback of the nonlinear state estimators

O presente capítulo é a reprodução da primeira versão do manuscrito que será submetido a revista a ser definida.

ABSTRACT: Since its proposal in 1960, Kalman filters have been widely applied in industry for virtual sensing and data reconciliation. Its vast use motivated researchers to work in improvements, which led to new approaches such as the extended Kalman filter, unscented Kalman filter, and cubature Kalman filter. Each of these approaches has its advantages and disadvantages, which makes them more suitable for a particular application than another. In general, the nonlinear state estimators, such as the unscented and cubature-based filters, have better performance on state estimation compared to the extended Kalman Filter versions. However, when the process model is poorly fit, the estimated variable may be biased, which causes problems in terms of process monitoring. To solve this problem, this work proposes a new improvement based on bias estimation as a variable in a simple state augmentation technique. The new approach was tested on a real industrial application on offshore oil production and was successful in terms of bias removal. To illustrate the success of the proposed approach, the discrete extended Kalman filter (DEKF) and the UKF and CKF with and without bias estimation were compared. The improvement turns the unscented and cubature-based filters more accurate, even in a poor model fitting scenario.

5.1 Introduction

Kalman filters (KFs) are gray box approaches that combine a phenomenological model of the process and a set of known measurements aiming at filtering these measurements or to estimate unknown ones. This feature guarantees a broad range of applications in industry, which include virtual sensing, fault detection (KANO; FUJIWARA, 2013), control systems (AUGER *et al.*, 2013), digital twin (TAO; ZHANG; NEE, 2019), among others.

The most common KF application to nonlinear systems is by extended Kalman filter (EKFs) (JAZWINSKI, A. H., 1970). The EKF linearizes all nonlinear transformations and substitutes the Jacobian matrices for linear transformations in the KF equations by expanding it into a Taylor series. Different from the EKF, the unscented Kalman filter (UKF) does not require the linearization of nonlinear functions. The states' distribution is specified using a minimum set of carefully selected sample points that capture the posterior mean and covariance with a second-order precision when propagated through the actual nonlinear system (WAN; VAN DER MERWE, 2002). Similar to the UKF, the cubature Kalman filter (CKF) (ARASARATNAM; HAYKIN, 2009) uses a set of cubature points with equal weights to calculate the mean and the covariance of state variables that, after a nonlinear transformation, improves the performance of the nonlinear optimal approximation, filtering accuracy, and numerical stability.

Although the EKF maintains the elegant and computationally efficient recursive update form of the KF, it is limited by the linear transformations, which are only reliable if the error propagation can be adequately fit by a linear function (JULIER, S. J.; UHLMANN, 2004). If this condition does not hold, the linearized approximation can be extremely poor. Recent works are comparing among the EKF, UKF, and CKF performances: Astroza et al. (2019) and Garcia et al. (2019) stated the outperformance of the UKF and CKF over the EKF. St-Pierre and Gingras (2004), Pardal et al. (2013), D'Alfonso et al. (2015), and Yang et al. (2017) concluded that the differences in accuracy between the EKF and the UKF were not significant. LaViola (2003) inferred that the UKF performed equivalently with EKF. Besides that, Chowdhary and Jategaonkar (2010) concluded that even though the UKF algorithm is a theoretically superior alternative to the EKF, it may not add much to the recursive system identification process if the identification model and the identification data are poor representations of the system. The UKF is indeed superior in terms of time to convergence and relative reliability of the estimates, however, it is computationally more expensive.

Apio et al. (2019) have shown that the CKF and UKF return the best estimation in cases where the model is appropriately fit, while extended filters have the best performance for poor-fitting models. When a variable is not well fitted with the current set of parameters, it results in a poor estimation (bias) of this variable by both UKF and CKF. Extended filters, in the opposite, are weakly affected by model fit since the model is linearized. By applying the Jacobian, the bias is eliminated since it is a constant value. The bias problem may hinder some important applications of the Kalman filter, such as virtual sensing, fault detection, among others. In these cases, it is vital to ensure the correct estimation of the desired variables for process monitoring.

Knowing that the CKF and UKF approaches perform better, but suffer from bias problem when the model is poorly fit, this work aims to refine UKF and CKF methodologies towards eliminating the bias by estimating it as an additional variable. For that, the original model is just augmented in the number of states through including null additional differential equations. To evaluate the proposed approach, the same case study from Apio et al. (2019) is considered, in which the permanent downhole gauge (PDG) pressure from an offshore oil well is estimated. The analysis and comparisons are handled by using a simulated dataset generated in OLGA (OiL and GAs dynamic multiphase flow simulator) (BENDIKSEN *et al.*, 1989).

5.2 Kalman filters, case study model and data

This section introduces all the necessary conception to implement and test the proposed technique, including the description of the unscented and cubature Kalman filters and the case study model with the data.

5.2.1 Kalman filters

The Kalman filter (KALMAN, 1960) requires a dynamic model of the system, input measurements, and other available measurements either to estimate unknown variables or to filter known ones, removing noise and other discrepancies caused by sensor fault or lack of precision, for example.

5.2.1.1. Unscented Kalman Filter

Different from the extended Kalman filters, the unscented Kalman filter does not require the linearization of any nonlinear functions: the states' distribution is specified using a minimum set of carefully selected sample points. These points capture entirely the true mean and the covariance of the Gaussian variable, and, when propagated through the nonlinear system, they also capture the posterior mean and covariance with a second-order precision (expansion of Taylor series) for any non-linearity (Wan and van der Merwe, 2002).

The UKF is calculated as follows. Firstly, the sigma points (χ) are evaluated:

$$\mu = \sqrt{ns + \lambda} \tag{5.1}$$

$$\lambda = \alpha^2(ns + \kappa) - ns \tag{5.2}$$

$$\chi_{i,k|k-1} = \begin{bmatrix} \hat{x}_{k-1} \\ \hat{x}_{k-1} + \mu\sqrt{P_{k-1}} \\ \hat{x}_{k-1} - \mu\sqrt{P_{k-1}} \end{bmatrix} \tag{5.3}$$

$$\hat{\chi}_{i,k|k-1} = f\left(\chi_{i,k|k-1}, u_{i,k|k-1}, \Delta t\right) \tag{5.4}$$

$$\hat{x}_{k|k-1} = \sum_{i=0}^{2ns} W_i^{(m)} \hat{\chi}_{i,k|k-1} \tag{5.5}$$

and the weights:

$$W_0^{(m)} = \frac{\lambda}{ns+\lambda} \tag{5.6}$$

$$W_0^{(c)} = \frac{\lambda}{ns+\lambda} + 1 - \alpha^2 + \beta \tag{5.7}$$

$$W_i^{(m)} = W_i^{(c)} = \frac{1}{2(ns+\lambda)}, \quad i = 1, \dots, 2ns \tag{5.8}$$

The covariance matrices are evaluated using the unscented transform:

$$P_{k|k-1} = \sum_{i=0}^{2ns} W_i^{(c)} \left(\hat{\chi}_{i,k|k-1} - \hat{x}_{k|k-1}\right)\left(\hat{\chi}_{i,k|k-1} - \hat{x}_{k|k-1}\right)^T + Q_{k-1} \tag{5.9}$$

$$\gamma_{i,k|k-1} = h\left(\hat{\chi}_{i,k|k-1}, u_{i,k|k-1}, \Delta t\right) \tag{5.10}$$

$$\hat{y}_{k|k-1} = \sum_{i=0}^{2ns} W_i^{(m)} \gamma_{i,k|k-1} \tag{5.11}$$

$$P_{y_k y_k} = \sum_{i=0}^{2ns} W_i^{(c)} \left(\gamma_{i,k|k-1} - \hat{y}_{k|k-1}\right)\left(\gamma_{i,k|k-1} - \hat{y}_{k|k-1}\right)^T + R_k \tag{5.12}$$

$$P_{x_k y_k} = \sum_{i=0}^{2ns} W_i^{(c)} \left(\hat{\chi}_{i,k|k-1} - \hat{x}_{k|k-1}\right)\left(\gamma_{i,k|k-1} - \hat{y}_{k|k-1}\right)^T \tag{5.13}$$

where the Kalman filter gain can be calculated

$$K_k = P_{x_k y_k} P_{y_k y_k}^{-1} \tag{5.14}$$

and the states and covariance of the filter are updated

$$\hat{x}_k = \hat{x}_{k|k-1} + K_k\left(y_k - \hat{y}_{k|k-1}\right) \tag{5.15}$$

$$P_k = P_{k|k-1} - K_k P_{y_k y_k} K_k^T \tag{5.16}$$

where *k* represents the step considered in discrete time, *x* is the vector of states, *y* is the output vector, *f* is a model function, *ns* is the number of states *x*, *nm* is the number of measurements y, *P* is the covariance matrix of the states, *Q* is the process noise covariance matrix, *R* is the measurement noise covariance, and *K* is the Kalman gain, α is the distribution of points around the mean ($0 \leq \alpha \leq 1$), β incorporates prior knowledge of the mean distribution (for Gaussian variables, $\beta = 2$) and κ is a secondary scaling parameter (usually set as 0 or 3-ns), χ and γ are the state and measurements sigma points, and $W_i^{(m)}$ and $W_i^{(c)}$ are the mean and covariance weights.

5.2.1.2. Cubature Kalman filter

Similarly to the UKF technique, which does not linearize the system, Arasaratnam and Haykin (2009) developed a spherical-radial cubature rule to compute multivariate moment integrals encountered in the nonlinear Kalman filter. Specifically, a third-degree spherical-radial cubature rule is derived to provide a set of cubature points that scale linearly with the state-vector dimension. The cubature Kalman filter uses a set of cubature points with equal weights to calculate the mean and the covariance of state variables that, after a nonlinear transformation, improve the performance of the nonlinear optimal approximation, filtering accuracy, and numerical stability.

In contrast to the UKF, the CKF has a different set of deterministic weighting points. For the sigma-point set (UKF), the stem at the center is highly significant since it carries more weight, whereas the cubature-point set does not have a stem at the center and presents equally distributed weights. Besides, Arasaratnam and Haykin (2009) mention some limitations of the sigma-point set built into the UKF, which are not present in the cubature-point built in the CKF, such as numerical inaccuracy, unavailability of a square-root solution, and filter instability. The CKF also chooses fewer sample/simulation points to evaluate the method, i.e., *2n* rather than *2n+1* as in the UKF where *n* is the number of states, thus being somewhat less costly in computations.

The following equations define the CKF algorithm. Firstly, generate the cubature points χ $(i = 1,2, \ldots ,2n)$:

$$\chi_{i,k|,k-1} = \sqrt{P_{k-1}}\xi^i + \hat{x}_{k-1} \tag{5.17}$$

where the unit cubature points are defined as $\xi^i = \sqrt{ns}$.

In the sequence, the cubature points are propagated:

$$\hat{\chi}_{i,k|k-1} = f\left(\chi_{i,k|,k-1}, u_{i,k|k-1}, \Delta t\right) \tag{5.18}$$

The propagated state and covariance matrix for instant *k* are estimated:

$$\hat{x}_{k|k-1} = \frac{1}{2ns}\sum_{i=0}^{2ns}\hat{\chi}_{i,k|k-1} \tag{5.19}$$

$$P_{k|k-1} = \frac{1}{2ns}\sum_{i=0}^{2ns}\hat{\chi}_{i,k|k-1}\hat{\chi}_{i,k|k-1}{}^T - \hat{x}_{k|k-1}\hat{x}_{k|k-1}{}^T + Q_{k-1} \tag{5.20}$$

$$\gamma_{i,k|k-1} = h\left(\hat{\chi}_{i,k|k-1}, u_{i,k|k-1}, \Delta t\right) \tag{5.21}$$

then, the measurement, the innovation, and the covariance and cross-covariance matrixes are predicted:

$$\hat{y}_{k|k-1} = \frac{1}{2ns}\sum_{i=0}^{2ns}\gamma_{i,k|k-1} \tag{5.22}$$

$$P_{y_k y_k} = \frac{1}{2ns}\sum_{i=0}^{2ns}\gamma_{i,k|k-1}\gamma_{i,k|k-1}{}^T - \hat{y}_{k|k-1}\hat{y}_{k|k-1}{}^T + R_k \tag{5.23}$$

$$P_{x_k y_k} = \frac{1}{2ns}\sum_{i=0}^{2ns}\hat{\chi}_{i,k|k-1}\gamma_{i,k|k-1}{}^T - \hat{x}_{k|k-1}\hat{y}_{k|k-1}{}^T \tag{5.24}$$

where the Kalman filter gain can be calculated by

$$K_k = P_{x_k y_k}P_{y_k y_k}^{-1} \tag{5.25}$$

and the states and covariance of the filter are updated as

$$\hat{x}_k = \hat{x}_{k|k-1} + K_k\left(y_k - \hat{y}_{k|k-1}\right) \tag{5.26}$$

$$P_k = P_{k|k-1} - K_k P_{y_k y_k}K_k^T \tag{5.27}$$

This section presented a review of the unscented and cubature Kalman filter-based approaches. For the comparison between these techniques and extended Kalman filters, see Apio et al. (2019), and the comparison between extended Kalman filters and artificial neural networks see Apio et al. (2019a).

5.2.2 Case study

The case study aims to estimate the PDG pressure of an offshore oil production system in a deepwater scenario using Kalman filter-based approaches. PDG pressure is an essencial variable for oil production control. However, this measurement is often unavailable due to

premature sensor failure and the considerable price for its replacement, which raises the importance of its estimation.

5.2.2.1. Plant Model

The fast offshore well model (FOWM), proposed by Diehl et al. (2017), is a phenomenological model based only on mass conservation equations. It includes the mass balance of the riser, flowline, production column, gas lift annular, and reservoir as follows:

$$\frac{dm_{ga}}{dt} = w_{gc} - w_{iv} \tag{5.28}$$

$$\frac{dm_{gt}}{dt} = w_r \alpha_{gw} + w_{iv} - w_{whg} \tag{5.29}$$

$$\frac{dm_{lt}}{dt} = w_r (1 - \alpha_{gw}) - w_{whl} \tag{5.30}$$

$$\frac{dm_{gb}}{dt} = (1 - \epsilon) w_{whg} - w_g \tag{5.31}$$

$$\frac{dm_{gr}}{dt} = \epsilon w_{whg} + w_g - w_{gout} \tag{5.32}$$

$$\frac{dm_{lr}}{dt} = w_{whl} - w_{lout} \tag{5.33}$$

The fluid flows used in the model are obtained by the following equations:

$$w_{iv} = K_a \sqrt{\rho_{ai} \frac{(p_{ai} - p_{tb}) + \sqrt{(p_{ai} - p_{tb})^2 + \varepsilon}}{2}} \tag{5.34}$$

$$w_r = K_r \left(1 - 0.2 \left(\frac{P_{bh}}{P_r}\right) - 0.8 \left(\frac{P_{bh}}{P_r}\right)^2\right) \tag{5.35}$$

$$w_{whg} = \alpha_{gt} K_w \sqrt{\rho_l \frac{(p_{tt} - p_{rb}) + \sqrt{(p_{tt} - p_{rb})^2 + \varepsilon}}{2}} \tag{5.36}$$

$$w_{whl} = (1 - \alpha_{gt}) K_w \sqrt{\rho_l \frac{(p_{tt} - p_{rb}) + \sqrt{(p_{tt} - p_{rb})^2 + \varepsilon}}{2}} \tag{5.37}$$

$$w_g = C_g \frac{(p_{eb} - p_{rb}) + \sqrt{(p_{eb} - p_{rb})^2 + \varepsilon}}{2} \tag{5.38}$$

$$w_{gout} = \alpha_g C_{out} z \sqrt{\rho_l \frac{(p_{rt} - p_s) + \sqrt{(p_{rt} - p_s)^2 + \varepsilon}}{2}} \tag{5.39}$$

$$w_{lout} = \alpha_l C_{out} z \sqrt{\rho_l \frac{(p_{rt} - p_s) + \sqrt{(p_{rt} - p_s)^2 + \varepsilon}}{2}} \tag{5.40}$$

and the equations related to the model pressures are presented below:

$$\rho_{ai} = \frac{M p_{ai}}{RT} \tag{5.41}$$

$$\alpha_{gt} = \frac{m_{gt}}{m_{gt} + m_{lt}} \tag{5.42}$$

$$\alpha_{gr} = \frac{m_{gr}}{m_{gr} + m_{lr}} \tag{5.43}$$

$$\alpha_{lr} = 1 - \alpha_{gr} \tag{5.44}$$

$$p_{ai} = \left(\frac{RT}{V_a M} + g\frac{L_a}{V_a}\right) m_{ga} \tag{5.45}$$

$$p_{tb} = p_{tt} + \rho_{mt} g H_{vgl} \tag{5.46}$$

$$p_{bh} = p_{pdg} + \rho_{mres} g (H_t - H_{pdg}) \tag{5.47}$$

$$p_{pdg} = p_{tb} + \rho_{mres} g (H_{pdg} - H_{vgl}) \tag{5.48}$$

$$p_{tt} = \frac{\rho_{gt} RT}{M} \tag{5.49}$$

$$p_{rb} = p_{rt} + \frac{g sin\theta}{A} (m_{lr} + m_{lstill}) \tag{5.50}$$

$$p_{eb} = \frac{RT}{M V_{eb}} m_{gb} \tag{5.51}$$

$$p_{rt} = \frac{RT}{M\left(V_r - \frac{m_{lr} + m_{lstill}}{\rho_l}\right)} m_{gr} \tag{5.52}$$

The other equations regarding the physical properties of the model are:

$$\rho_{mt} = \frac{m_{gt} + m_{lt}}{V_t} \tag{5.53}$$

$$\rho_{gt} = \frac{m_{gt}}{V_{gt}} \tag{5.54}$$

$$V_{gt} = V_t - \frac{m_{lt}}{\rho_l} \tag{5.55}$$

$$V_a = \frac{L_a \pi D_a^2}{4} \tag{5.56}$$

$$V_t = \frac{L_t \pi D_t^2}{4} \tag{5.57}$$

The set of parameters, their nomenclature, and respective values are presented in Table 5.1 At these process conditions, the system presents oscillatory behavior, i.e., a limit cycle.

Table 5.1: Parameters and variables of the Fast Offshore Well Model (FOWM).

Parameter	Nomenclature	Value	Unit
α_{gw}	gas fraction of mass at the reservoir pressure and temperature conditions	0.026	-
D_a	diameter of the annular section	0.1016	m
D_t	diameter of the tubing section	0.1242	m
H_{pdg}	vertical length between the Christmas Tree and the PDG transmitter	1392.2	m
H_t	vertical length between the Christmas Tree and the bottom hole	1593.1	m
H_{vgl}	vertical length between the Christmas Tree and the gas lift valve	927.4	m
L_a	annular length	937.4	m
L_t	tubing length	1622	m
M	gas molecular weight	18	kg/kmol

Parameter	Nomenclature	Value	Unit
p_r	pressure surrounding the production column bottom hole	3.52e7	Pa
p_s	pressure surrounding the production column gravitational separator	1013250	Pa
ρ_l	liquid density	965.5	kg/m3
ρ_{mres}	mixture density at the reservoir	902.5	kg/m3
T	average temperature in the production system	298	K
θ	average riser inclination	π/1.54	rad
R	universal gas constant	8314	J/kg.K
g	gravity acceleration	9.81	m2/s
m_{lstill}	minimum mass of liquid in the subsea pipeline	adjust parameter	kg
C_g	virtual valve constant	adjust parameter	m-1
C_{out}	choke valve constant	adjust parameter	m-1
V_{eb}	bubble volume	adjust parameter	m3
ϵ	gas fraction of mass that bypasses the bubble in the subsea pipeline	adjust parameter	-
K_w	flow coefficient between the annular and the tubing	adjust parameter	m-1
K_a	flow coefficient between the annular and the tubing	adjust parameter	m-1
V_r	riser volume	adjust parameter	m3
K_r	flow coefficient between the annular and the tubing	adjust parameter	m-1
w_{gc}	gas lift mass flow entering the annular	1.5205	kg/s
z	choke valve opening fraction	input variable	-
w_{gc}	gas lift flow	input variable	kg/s
V_a	annular volume	calculated	m3
V_{gt}	gas volume in the tubing	calculated	m3
V_t	tubing volume	calculated	m3
ρ_{mt}	mixture density in the tubing	calculated	kg/m3
ρ_{gt}	gas density in the tubing	calculated	kg/m3
α_{gt}	gas mass fraction in the tubing	calculated	-
α_{gr}	liquid mass fractions in the subsea pipeline	calculated	-
α_{lr}	liquid mass fractions in the subsea pipeline	calculated	-
w_r	reservoir to the bottom hole flow	calculated	kg/s
w_{whg}	gas mass that flows at the Christmas Tree	calculated	kg/s
w_{whl}	liquid mass that flows at the Christmas Tree	calculated	kg/s
w_g	flow at the virtual valve	calculated	kg/s
w_{gout}	gas flow through the topside choke valve	calculated	kg/s
w_{lout}	liquid flow through the topside choke valve.	calculated	kg/s
p_{ai}	pressure in the annular gas injection point to the tubing	calculated	Pa

Parameter	Nomenclature	Value	Unit
p_{tb}	pressure in the gas injection point on the tubing side	calculated	Pa
p_{bh}	pressure in the bottom hole	calculated	Pa
p_{rb}	pressure at the flowline before the bubble position	calculated	Pa
p_{eb}	bubble pressure	calculated	Pa
p_{pdg}	pressure at the PDG position	estimated	Pa
p_{tt}	pressure at the top of the tubing	filtered	Pa
p_{rt}	pressure at the top of the riser	filtered	Pa
m_{ga}	gas mass in the annular	estimated	kg
m_{gt}	gas mass in the production column or tubing	estimated	kg
m_{lt}	liquid mass in the tubing	estimated	kg
m_{gb}	gas mass in the bubble at the subsea production line	estimated	kg
m_{gr}	gas mass in the set flowline/riser	estimated	kg
m_{lr}	liquid mass in the set flowline/riser	estimated	kg

For more details about the Fast Offshore Well Model, see Diehl et al. (2017).

5.2.2.2. Experimental data

In this work, the Kalman filters used the FOWM, the input measurements z and w_{gc} (a constant value of 1.5205 kg/s), and the available output measurements p_{rt}, and p_{tt} to estimate the states ($m_{ga}, m_{gt}, m_{lt}, m_{gb}. m_{gr}, m_{lr}$). Then, from the state estimation, the variable p_{pdg} is calculated. The data used in this work was generated through the simulation of a real offshore oil production plant via gas-lift in OLGA (OiL and GAs – dynamic multiphase flow simulator) (BENDIKSEN *et al.*, 1989). The dataset presents perturbations in the choke valve opening in open-loop mode and oscillatory behavior in the output measurements. The variables have sampling time equal to 60 seconds and a total of 3411 measured points, as shown in Figure 5.1.

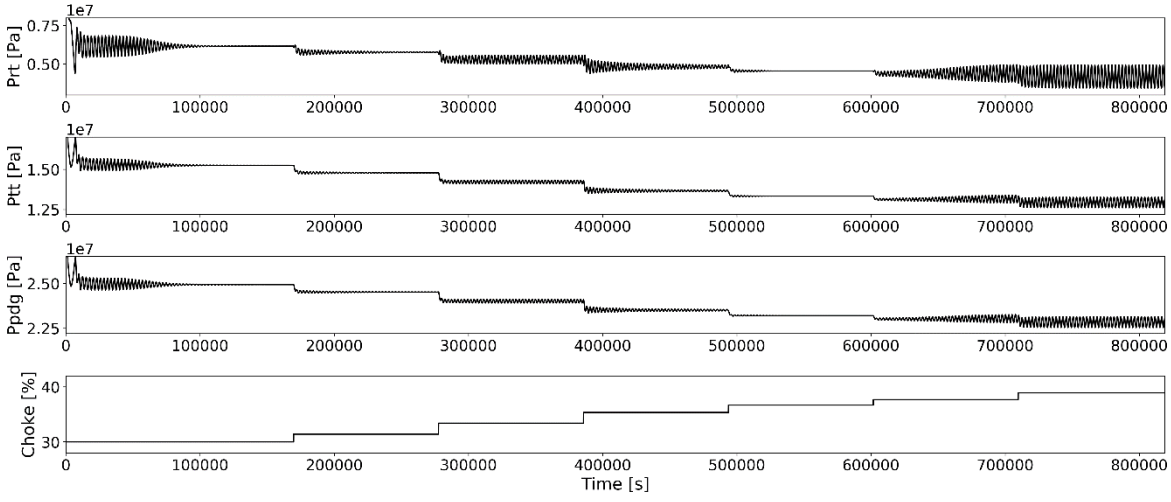


Figure 5.1: Data simulated in OLGA for a real oil production system with perturbations in the choke valve opening.

The comparison of the OLGA dataset with the FOWM simulation results with the parameters in Table 1 is presented in Figure 5.2.

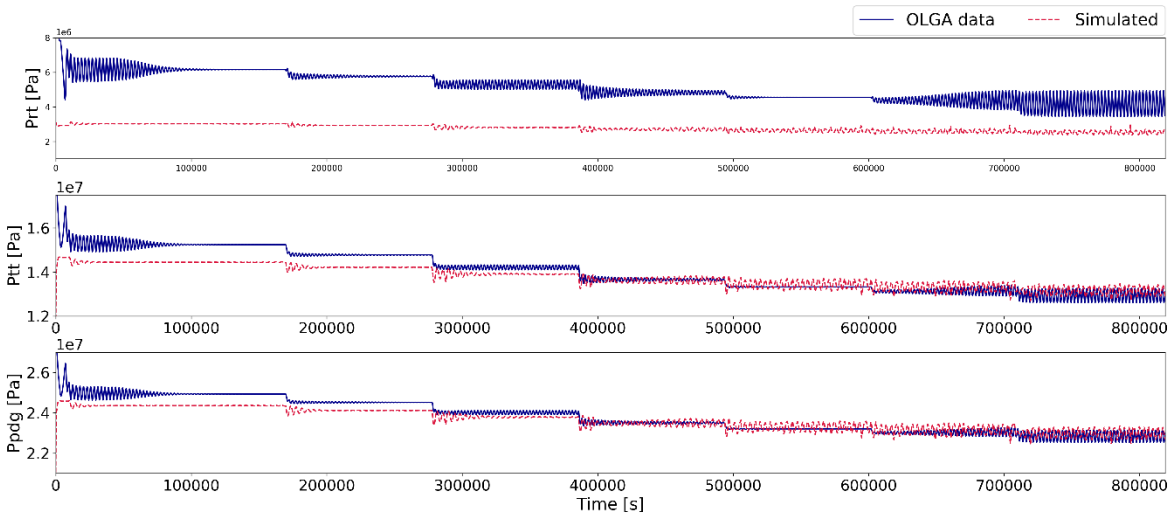


Figure 5.2: Comparison of the OLGA dataset and the FOWM simulation results.

Figure 5.2 shows that the model simulation returns biased estimations for the three variables compared to the experimental data, mainly for the p_{rt} simulation. Differently from the results of p_{tt} and p_{pdg}, the p_{rt} does not follow the disturbances of the real data and presents different magnitude and frequency of oscillations. This justifies the application of Kalman filter techniques to converge the simulated into the OLGA data and assure better estimates of the p_{rt}, p_{tt}, and p_{pdg} variables.

5.3 Methodology

This section describes the proposed methodology for removing the bias in UKF and CKF-based estimations.

5.3.1 Bias estimation

To eliminate the bias, a parameter is added to the variable presenting bias. This parameter refers to the bias value, which will be estimated by the Kalman filter. In this case study, a bias parameter is added to the measured variable, in this case, the p_{rt} variable, so that its correspondent equation (Equation 5.52) is rewritten as

$$p_{rt} = \frac{RT}{M\left(V_r - \frac{m_{lr}+m_{lstill}}{\rho_l}\right)} m_{gr} + p_{rtb} \tag{5.58}$$

where p_{rtb} is the bias from the p_{rt} to be estimated.

In other words, the states and parameter (bias) from the dynamic model will be simultaneously estimated using a Kalman filter, in an approach commonly known as state augmentation (JAZWINSKI, A. H., 1970). This methodology consists of defining an augmented dynamical system that allocates, along with the system's state, the model parameters to be estimated. As the parameters are constant, the right side of the corresponding differential equations is equal to zero, as shown in Equation 5.59.

$$\frac{dp_{rtb}}{dt} = 0 \tag{5.59}$$

As a state is added to the set of parameters that will be estimated, it is necessary to verify if the system is observable. The decision flowchart for the use of bias variables in the UKF or CKF estimation is shown in Figure 5.3.

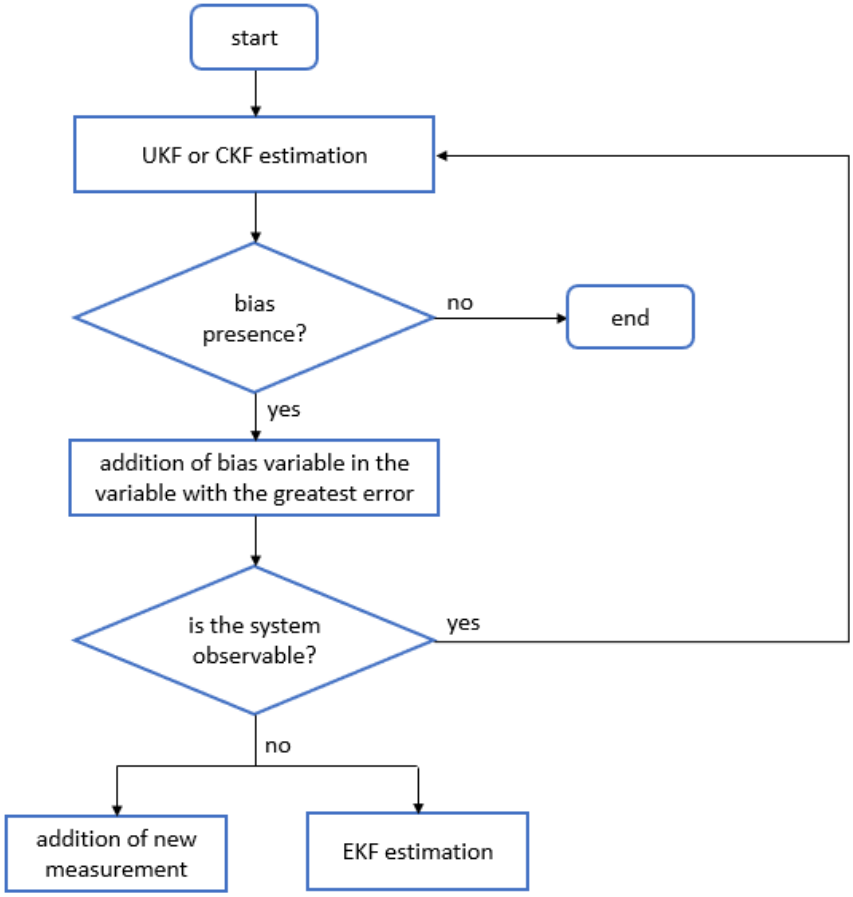


Figure 5.3: Decision flowchart for the use of bias variables for the UKF and CKF estimation

5.3.2 Observability analysis

A system is observable if its state at a specific time instant can be uniquely determined, given a finite sequence of its outputs (BEYENS, 1988). Intuitively, this means that the measurements of an observable system provide sufficient information for estimating its states (MIRZAEI; ROUMELIOTIS, 2008). Due to its better numeric robustness, we recommend the Popov-Belevitch-Hautus's observability test (HAUTUS, 1969) to verify if the state vector $x(t)$ can be observed from the output measurement $y(t)$. The Popov-Belevitch-Hautus's observability test can be formulated considering the linear invariant system, where F is a $ns \times ns$ and H is a $nm \times n$.

$$\frac{dx}{dt} = Fx \tag{5.60}$$

$$y = Hx \tag{5.61}$$

The system is observable if, and only if

$$rank\begin{bmatrix} F-\lambda I \\ H \end{bmatrix} = ns \tag{5.62}$$

where λ is an eigenvalue of the matrix F.

5.3.3 Simulation settings

The Kalman filter available input and output measurements used for testing the proposed technique are shown in Table 5.2.

Table 5.2: Data used in the Kalman filter for the FOWM model.

Kalman filter	States	Inputs	Measured variables	Estimated outputs
DEKF	$m_{ga}, m_{gt}, m_{lt}, m_{gb}. m_{gr}, m_{lr}$	z	p_{rt} and p_{tt}	p_{pdg}
UKF	$m_{ga}, m_{gt}, m_{lt}, m_{gb}. m_{gr}, m_{lr}$	z	p_{rt} and p_{tt}	p_{pdg}
CKF	$m_{ga}, m_{gt}, m_{lt}, m_{gb}. m_{gr}, m_{lr}$	z	p_{rt} and p_{tt}	p_{pdg}
UKF with bias estimation in p_{rt}	$m_{ga}, m_{gt}, m_{lt}, m_{gb}. m_{gr}, m_{lr}, p_{rtb}$	z	p_{rt} and p_{tt}	p_{pdg}
CKF with bias estimation in p_{rt}	$m_{ga}, m_{gt}, m_{lt}, m_{gb}. m_{gr}, m_{lr}, p_{rtb}$	z	p_{rt} and p_{tt}	p_{pdg}
UKF with bias estimation in p_{rt} and p_{tt}	$m_{ga}, m_{gt}, m_{lt}, m_{gb}. m_{gr}, m_{lr}, p_{rtb}, , p_{ttb}$	z	p_{rt} and p_{tt}	p_{pdg}
CKF with bias estimation in p_{rt} and p_{tt}	$m_{ga}, m_{gt}, m_{lt}, m_{gb}. m_{gr}, m_{lr}, p_{rtb}, , p_{ttb}$	z	p_{rt} and p_{tt}	p_{pdg}

The filter parameters values of P_0 ($I_3 10^2$) and Q_0 ($I_3 10^2$) were chosen according to the state order of magnitude and R_0 ($I_3 10^{10}$) based on the measurement order of magnitude. The UKF parameters α, β, and κ are, respectively, 1, 2, and 0.

The initial conditions for the FOWM model is given in Table 5.3, including the bias variables p_{rtb} and p_{ttb}.

Table 5.3: Initial conditions for FOWM model.

State	Initial condition
m_{ga}	7888.98
m_{gt}	1985.23
m_{lt}	24683.12
m_{gb}	982.21
m_{gr}	690.58
m_{lr}	11015.39
p_{rtb}	2961003.77
p_{ttb}	860752.75

The initial conditions of p_{rtb} and p_{ttb} are evaluated by

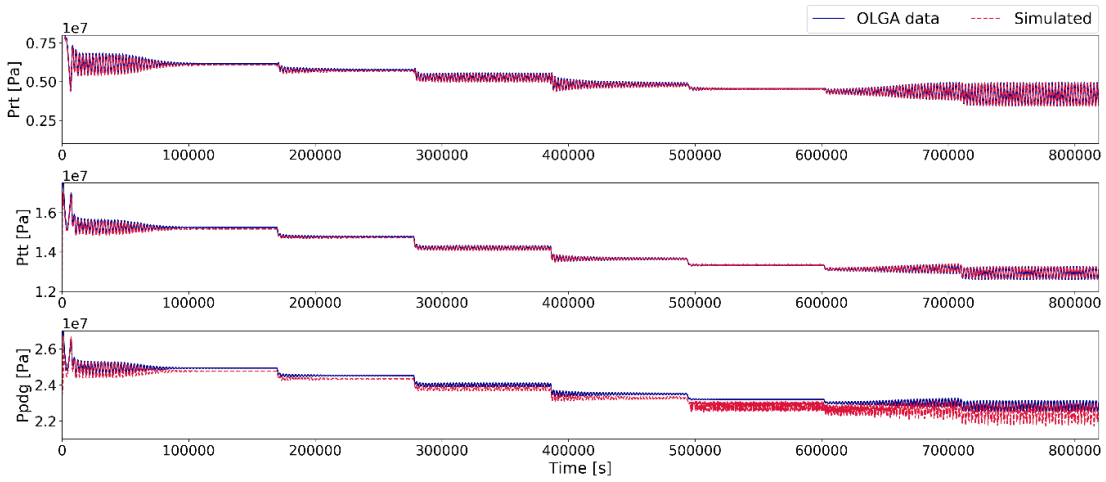
$$p_{rtb}[0] = mean(p_{rtb,sim} - p_{rtb,mes}) \tag{5.63}$$

$$p_{ttb}[0] = mean(p_{ttb,sim} - p_{ttb,mes}) \tag{5.64}$$

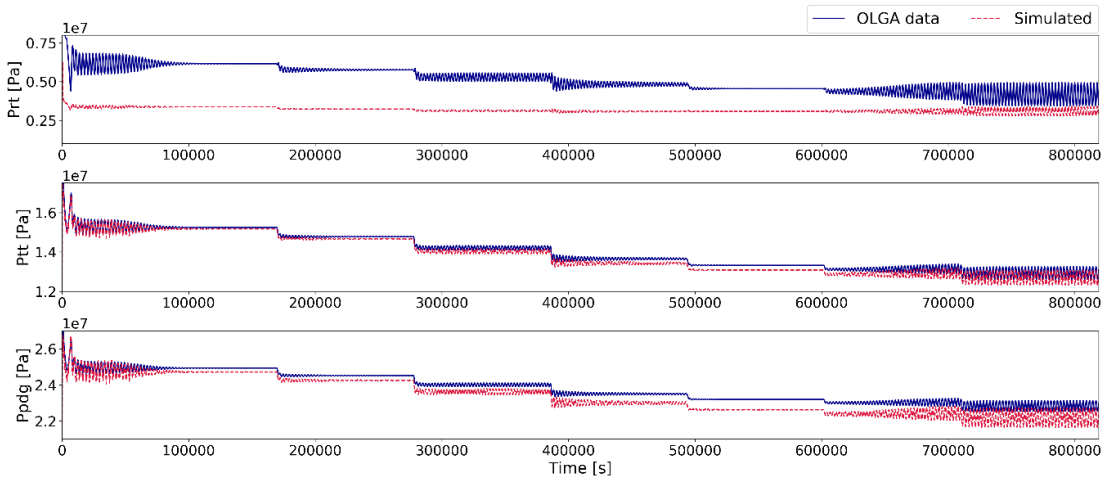
The performance of the filters is measured through the mean squared error (MSE). The Kalman filters, the FOWM model, and the proposed techniques were entirely coded in Python 2.7 with the aid of JModelica (ÅKESSON *et al.*, 2010) modeling platform.

5.4 Results and discussion

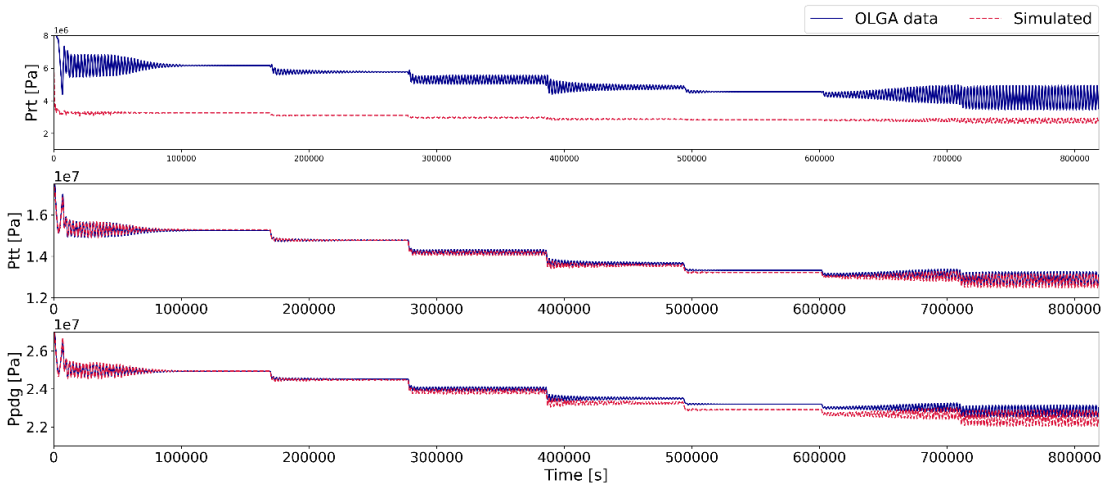
In this section, the results for the Kalman filter estimation using the FOWM model and the OLGA data are presented. The compared state estimation approaches were the discrete extended Kalman filter (DEKF) and the UKF and CKF with and without bias estimation, as shown in Figure 5.4.



a) DEKF



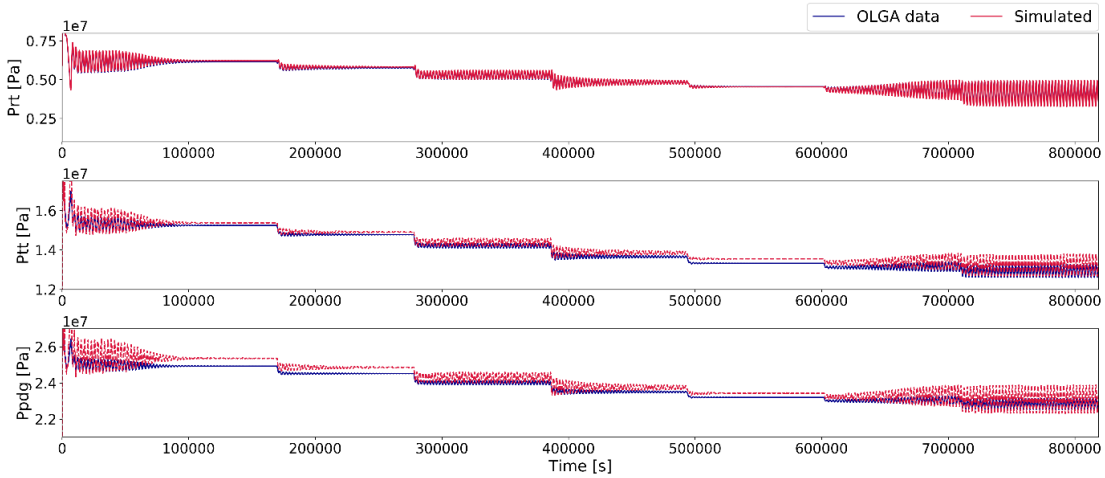
b) UKF



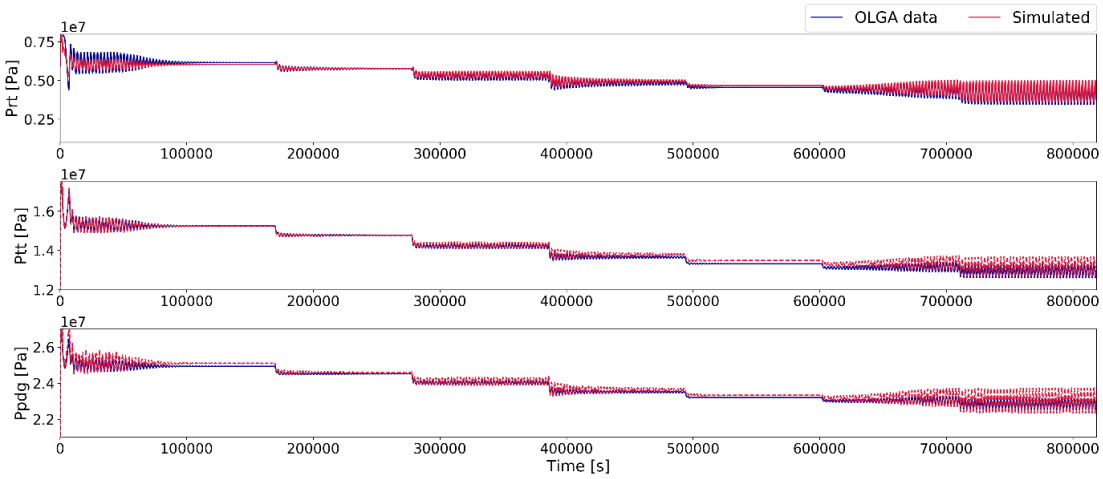
c) CKF

Figure 5.4: p_{pdg} estimation by a) DEKF, b) UKF, and c) CKF without bias estimation.

Figure 4.a and Figure 4.b show that the traditional UKF and CKF poorly estimate the p_{prt}. For both methodologies, the bias presented in the simulation (Figure 2) was not removed when Kalman filters were applied, compared to the DEKF methodology. For this reason, the bias from the p_{prt} variable was estimated using the state augmentation technique, as seen in Figure 5.a and Figure 5.b.



a) UKF with bias estimation in p_{rt}



b) CKF with bias estimation in p_{rt}

Figure 5.5: p_{pdg} estimation by a) UKF with bias estimation, and e) CKF with bias estimation.

The proposed technique to estimate the bias from the measured variable p_{rt}, shown in Figure 5.5 was enough to overcome the poor estimation from this variable. Besides that, the p_{rt} bias estimation followed the series of perturbations in the choke valve variable, which changed the behavior of this variable as well as the p_{tt} and p_{pdg} variables. Table 5.4 shows the mean squared error of these three variables comparing the experimental data (from OLGA simulator) with the results from the model without Kalman filter (Sim), with UKF and CKF, and their versions with bias estimation (UKF bias and CKF bias).

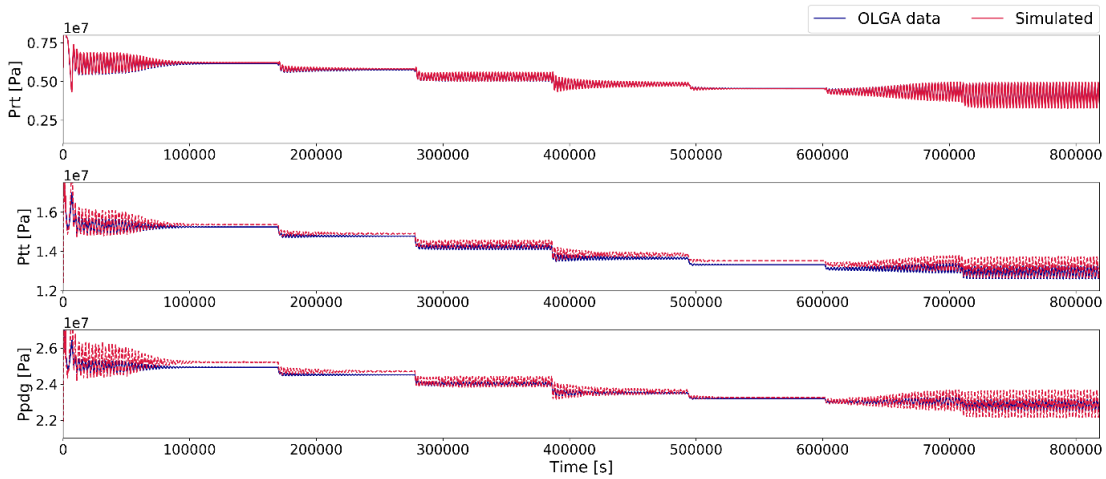
Table 5.4: Mean squared error for the p_{rt}, p_{tt} and p_{pdg} variables.

Filter	Sim	DEKF	UKF	CKF	UKF bias	CKF bias	Ref. Value
p_{rt} error	294.04	1.85	209.58	247.20	1.00	2.12	3989.36
p_{tt} error	11.98	0.90	2.35	1.00	3.01	1.82	1670.50
p_{pdg}error	2.76	1.81	3.92	1.12	2.61	1.00	2606.12

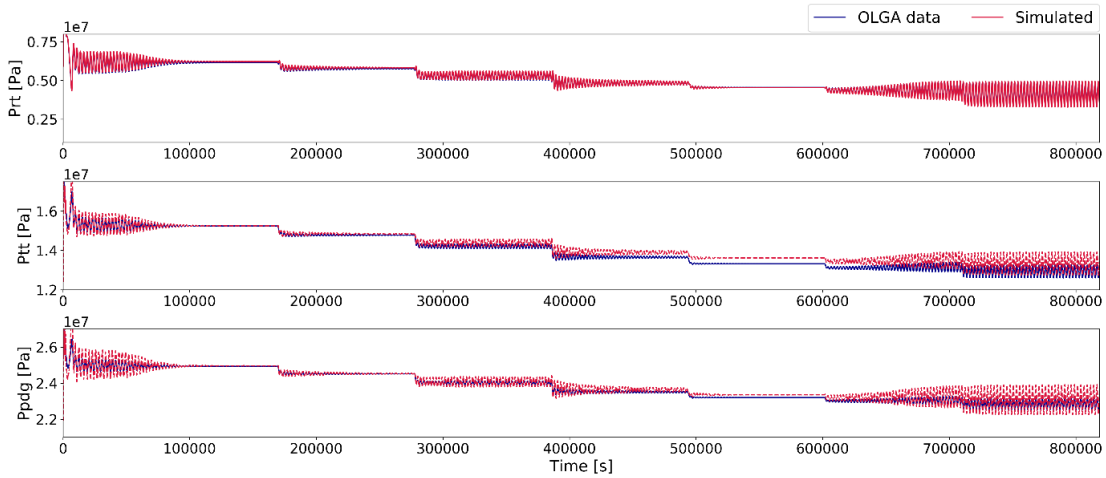
* multiplied by the reference value.

From the MSE evaluation, the model simulation (Sim) error for the variable p_{rt} is much larger than for the variables p_{tt} and p_{pdg} . This error remains of the same magnitude even using UKF and CKF, which means that these methodologies do not eliminate the bias present in this variable. On the other hand, estimating the bias using the proposed state augmentation-based technique reduced the p_{rt} error around 210 and 247 times for UKF and CKF, respectively. This technique also improved the results for the p_{pdg} estimation for both filters. As expected, the CKF method returned a smaller error compared to the UKF.

As a second test, Figure 5.6 shows bias estimation in both p_{rt} and p_{tt}. In this case, it is assumed that both variables are measured, whereas p_{pdg} is the estimated variable.



a) UKF with bias estimation in p_{rt} and p_{tt}



b) CKF with bias estimation in p_{rt} and p_{tt}

Figure 5.6: . p_{pdg} estimation by a) UKF and e) CKF with bias estimation in both p_{rt} and p_{tt}.

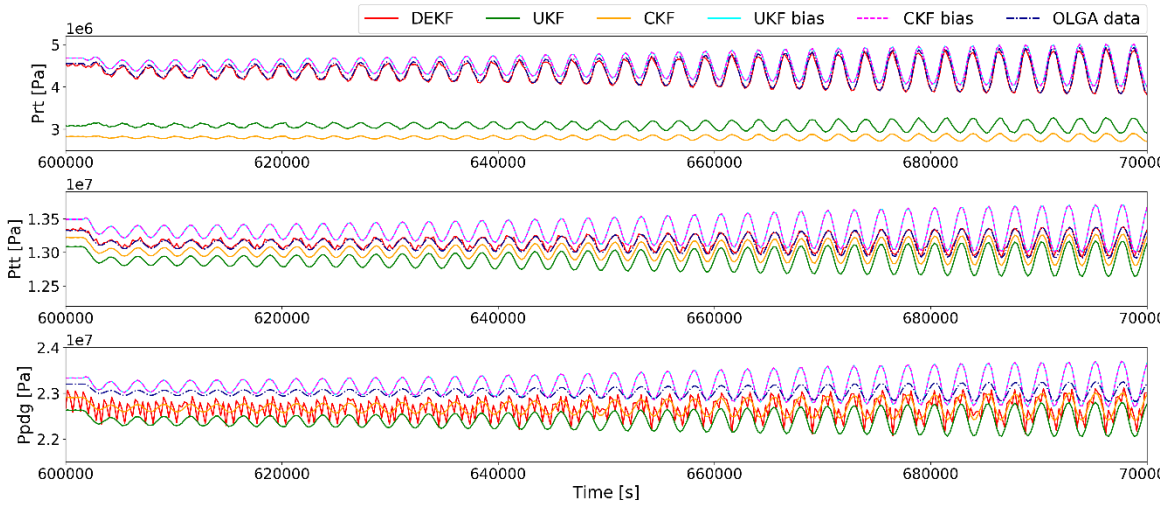
For both UKF and CKF methodologies with bias estimation in p_{rt} and p_{tt}, the bias present in p_{rt} has vanished. In this case, the addition of the deviation variable p_{ttb} did not result in significant improvements over the use of only the p_{rtb}, as shown by the mean squared errors in Table 5.5.

Table 5.5: Mean squared error for the p_{rt}, p_{tt} and p_{pdg} variables.

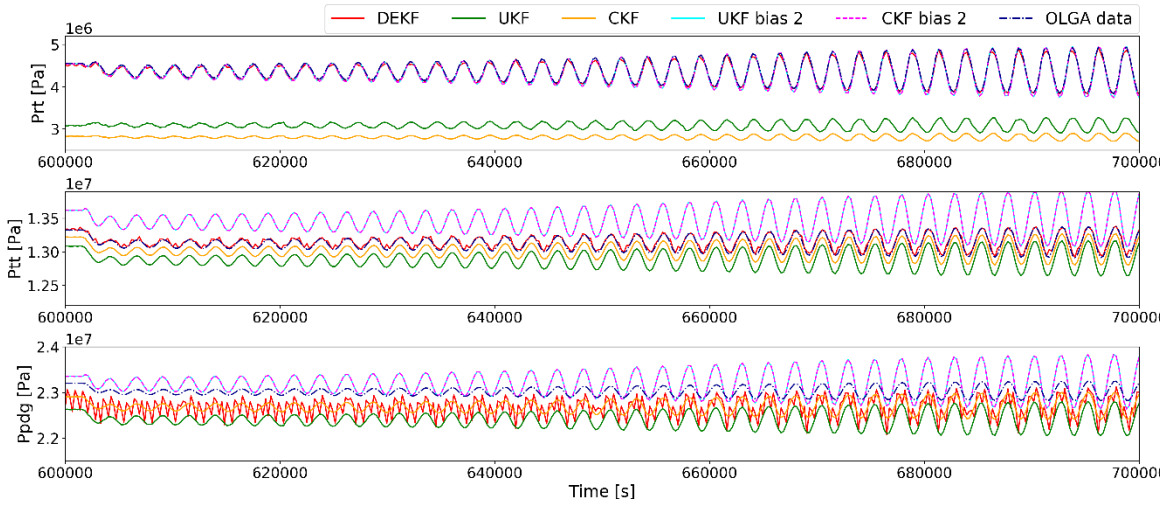
Filter	Sim	UKF	CKF	UKF bias	CKF bias	UKF bias 2	CKF bias 2	Ref. Value
p_{rt} error	297.25	211.88	249.90	1.01	2.14	1.00	1.01	3946.17
p_{tt} error	11.98	2.35	1.00	3.01	1.82	2.48	3.51	1670.50
p_{pdg} error	2.76	3.92	1.12	2.61	1.00	1.33	1.14	2606.12

* multiplied by the reference value.

As seen in Table 5.5, the use of the CKF with bias estimation in p_{rt} (CKF bias 2) returned better results than the other methodologies. This methodology showed significant from the traditional DEKF especially for the p_{pdg} estimation, which is the variable of interest in terms of control. Figure 5.7 shows a fragment zoom of the p_{pdg} estimation with bias estimation in both variables from Figure 5.5 and Figure 5.6.



a)



b)

Figura 5.7: Fragment zoom of p_{pdg} estimation with bias estimation in a) both p_{rt}, and b) both p_{rt} and p_{tt}.

In this case study it was considered the addition of bias in the measured variables p_{rt} and p_{tt}. However, the bias could be added to any system variable, as for example in the input variable z instead of p_{rt} or p_{tt}. Care must be taken in choosing the states to be estimated, as the system must remain observable. In this case, the estimation of bias in p_{rt} and z did not return relevant results, so they are not shown in this work.

5.5 Conclusions

Kalman filters approach with no linearization may generate biased variables when the model is poorly fit to the process. For instance, for the offshore oil production case study, the UKF and CKF approaches can not overcome the bias problem of the variable p_{rt}.

For this reason, we proposed a state augmentation technique using the UKF and CKF to estimate and remove the bias. The results showed that the aim was achieved, reducing the

mean squared error on the p_{rt} estimation around 210 times for the UKF and 247 times for the CKF compared with the application without bias estimation. This technique also improved the results for the p_{pdg} estimation for both methodologies. As expected, the CKF method returned a smaller error compared to the UKF.

5.6 Acknowledgments

The authors acknowledge Eng. Fabio C. Diehl for providing the simulation and industrial data and the financial support from the National Petroleum, Natural Gas and Biofuels Agency (ANP) and Petróleo Brasileiro S.A. (PETROBRAS).

Capítulo 6 – **Robust extended Kalman filter estimation with moving window through a quadratic programming formulation**

O presente capítulo é a reprodução da primeira versão do manuscrito que será submetido a revista *Journal of Process Control*.

ABSTRACT: The state estimation of dynamic systems using data from the recent past, known as moving window or receding horizon estimation, improves estimation accuracy for highly nonlinear systems. In this work, two new formulations for the extended (MW-EKF) and robust extended Kalman filter with moving window estimation (MW-REKF) are proposed, which are based on the receding (RNK) and robust receding (RRNK) horizon nonlinear Kalman filter, respectively. The MW-EKF and MW-REKF are formulated using an elegant quadratic programming problem that facilitates its implementation and decreases its computational cost. Besides that, the constrained extended Kalman filter (CEKF), constrained extended Kalman filter and smoother (CEKFS), moving horizon estimation (MHE), and the proposed MW-EKF and MW-REKF are compared in terms of computational cost and fit to the real data. The comparison is performed over a spherical-quadruple-tank model with eight different settings aiming to raise each approach's advantages and disadvantages to different scenarios. Finally, the estimation of deviation variables instead of directly estimating the desired parameters was also proposed, which enabled their estimation while the system's observability was maintained. The results show that the moving windows are the best approach to simultaneous state and parameter estimation, once they reduce modeling errors and return unbiased and smoother estimations. The computational cost of the proposed techniques rewritten as a QP problem is only four times higher than CEKF and nine times smaller than the MHE. For both state and parameter estimation the MW-REKF has shown the smoothest and most robust behavior among all methodologies. This technique minimized the effect of the outliers, physical limitations, structural discrepancies, among others.

6.1 Introduction

The problem of estimating a dynamic system's state using the information over the last time window can be handle by approaches such as finite-memory, receding-horizon, sliding-window (ALESSANDRI; BAGLIETTO; BATTISTELLI, 2003), and moving horizon estimation. Jazwinski (1970) was the first to propose a moving window technique when the extended Kalman filter performed poorly or diverged due to modeling or computational errors. Since then, the importance of these estimation methods has grown in many application areas where model uncertainties limit the use of Kalman filter techniques.

The idea behind the receding horizon state estimation is to estimate the state vector based on a finite number of past measured samples, where the oldest sample is discarded as a new sample becomes available. Thus, the state estimator's memory is fixed (LING; LIM, 1999), which means that the estimation is computed based on data from the recent past. The filter's memory length should coincide with the time length over which the approximate dynamical system represents a satisfactory approximation of reality (JAZWINSKI, A. H., 1970). It reduces the effects of old samples on filtering and improving the estimation accuracy (HUANG *et al.*, 2019).

In many engineering applications, besides estimating the internal states online, it is necessary to estimate the system parameters. Many of these parameters and state variables are often not measurable or are too costly to measure online. Simultaneous parameter and state estimations use the measurements of other available variables at a much faster rate and a mathematical model relating them with the quality variables or even a key performance index (KPI) to generate their estimates in real-time (PATWARDHAN *et al.*, 2012). In this work, an online parameter estimation via state estimation is applied, where a model is fitted optimally to the past and present process measurements while the process is in operation. This method requires a dynamic model for each of the unknown parameters to be estimated (SOROUSH, 1998). Several papers have applied a combination of state and parameter estimation using several Kalman filter formulations, such as extended Kalman filter (DE VALLIÈRE, P.; BONVIN, 1989; DE VALLIÈRE, Ph; BONVIN, 1990; GUDI; SHAH; GRAY, 1994; PLETT, 2004; SEMINO; MORRETTA; SCALI, 1996), ensemble Kalman filter (EVENSEN, 2009), and unscented Kalman filter (MERWE; WAN, 2001).

Considering state estimators with the receding horizon, Kühl et al. (2011) applied an MHE approach to simultaneously estimate states and parameters. Salau et al. (2012a) included the EKF smoother counterpart in the CEKF using the Rauch-Tugh-Striebel (RTS) smoother, denominated constrained extended Kalman filter and smoother. Rangegowda et al. (2018) and Rangegowda et al. (2019) proposed simultaneous state and parameter estimation using RNK and robust RNK, denominated RRNK, where the parameters are modeled as a random walk process. These methodologies prove to be better suited for parameter estimation, once they reduce modeling errors and return unbiased and smoother estimates due to their receding window approach.

Some of these moving window methodologies, as the RNK and RRNK, are solved by a computationally expensive nonlinear programming (NLP) optimization problem. In this paper, this problem is rewritten as a quadratic programming (QP), which is easy to be implemented, computationally efficient and accurate, and more likely to be convex. The quadratic optimization approach was not explicitly formulated when the RNK and RRNK were presented. Therefore, we propose a robust and elegant state estimator rewritten as

a QP based on the RNK and RRNK, named extended (MW-EKF) and robust extended Kalman filter with moving window estimation (MW-REKF). Besides that, we choose to write these problems with the states as decision variables, instead of their process and measurement noise variables, which is the Kalman filter's traditional formulation when it is implemented as an optimization problem. Thus, it is possible to directly formulate the constraints and bounds of the problem taking the states directly into account. Therefore, the number of variables to be minimized is half compared to the implementation using the process and measurement noise variables, reducing the optimization's complexity.

Also, assuming the parameter estimation is solved with the state augmentation technique in this work, we propose to estimate the deviation variables to improve the system's observability.

Briefly, the main contributions of this work are:

a) propose an extended and robust extended Kalman filter with moving window considering an elegant and practical implementation using the quadratic programming approach,

b) show the importance of the moving window state estimators for state and parameter estimation by comparing different approaches to different scenarios, and

c) estimate the deviation parameters instead of the parameter itself to increase the observability of the system.

Here, we systematically compare the use of the following four state estimators-based approaches for estimation of the states and parameters of a spherical-quadruple-tank system (ESCOBAR; TRIERWEILER, 2013a):

- constrained extended Kalman filter (CEKF) (GESTHUISEN; KLATT; ENGELL, 2001),
- constrained extended Kalman filter and smoother (CEKFS) (SALAU; TRIERWEILER; SECCHI, 2012b),
- moving horizon estimation (MHE) (RAO, C. V; RAWLINGS; LEE, 2001),
- extended Kalman filter with moving window estimation (MW-EKF) based on the receding horizon nonlinear Kalman filter (RNK) (RENGASWAMY, R; NARASIMHAN; KUPPURAJ, 2013), and
- robust extended Kalman filter with moving window estimation (MW-REKF), based on the robust receding horizon nonlinear Kalman filter (RRNK) (RANGEGOWDA *et al.*, 2019).

Following the introduction, this work continues in Section 6.2 with a brief literature review. The description of the proposed methodology, where the state estimator-based approaches are explained and formulated, is presented in Section 6.3. In Section 6.4, the spherical-quadruple-tank case study and the performance evaluation criteria are presented. Section 6.5 shows the state and parameter estimation results for each proposed methodology considering different scenarios, such as the presence of noise, gross errors, and structural discrepancy. The summary of contributions of this work are presented in Section 6, and the conclusions in Section 6.6.

6.2 Literature review

Until 1968, some methodologies (e.g., continuous filtering) used all the available data, so that the estimated variable was based on all the available information. If, for example, the dynamics were imprecisely known, then the filter might have learned the state "too well": because of imprecise dynamics used in the filter, the "good estimate" could be wrong (JAZWINSKI, A. H., 1970). Jazwinski (1968) proposed a limited memory optimal filtering, which computes an estimate based on recent past data forgetting the long distant past. The filter memory length should be in the order of the time length over which the approximate dynamical system represents a satisfactory approximation to reality.

Since then, among the main receding horizon Kalman filter approaches, Muske et al. (1993) proposed constraints to the receding horizon recursive state estimation method (JAZWINSKI, A. H., 1970). This methodology later would result in the moving horizon estimation (MHE) (MUSKE, Kenneth R.; RAWLINGS, 1995; RAO, C. V.; RAWLINGS; MAYNE, 2003; RAO, C. V.; RAWLINGS, 2000; RAO, C. V; RAWLINGS, 2002; RAO, C. V; RAWLINGS; LEE, 2001; RAWLINGS; BAKSHI, 2006; ROBERTSON; LEE; RAWLINGS, 1996), which prevents physically unrealistic state estimates due to spurious output measurements and, therefore, improving the state estimator robustness.

Ling and Lim (1999) described a receding horizon state observer using the deterministic least squares framework, exploring an appropriate state weighting on the estimator cost function. Kwon et al. (1999) presented a receding horizon Kalman finite impulse response (FIR), which combines the Kalman filter and the receding horizon strategy when the horizon initial state is assumed to be unknown. In this case, the FIR filter uses finite measurements over the most recent time interval. However, Ling and Lim (1999) and Kwon et al. (1999) do not consider any predictive term, unlike the moving horizon approach proposed by Rao et al. (2001) and the receding horizon estimation proposed by Alessandri et al. (2003). The receding horizon objective function included a weighted penalty term related to the states' prediction by Alessandri et al. (2003). Although the Rao et al. (2001) methodology turns out to be more general than Alessandri et al. (2003), it requires heavy online computations (an optimization problem must be solved at every sample time).

Rengaswamy et al. (2011) presented a promising receding horizon approach, which, instead of the MHE approach, follows the Kalman filter predictor-corrector framework. This methodology demonstrates computational advantages, since it avoids repeated integration within an optimization loop required in the MHE approach. Rangegowda et al. (2019) presented a robust version of this methodology to minimize the effect of gross errors on state estimates. The robust receding horizon Kalman filter was developed by integrating Huber's objective function M-estimator with the RNK to incorporate robustness to the filter. The proposed robust RNK formulation has achieved estimation performances comparable to the robust moving horizon estimation (MHE) scheme.

6.3 Methodology

This section presents a brief review of the state estimation-based approaches with moving windows. State estimation is a widely adopted soft sensing technique that incorporates predictions from an accurate process model and measurements to provide reliable estimates of unmeasured variables (DAS *et al.*, 2018). Among the state estimators are the particle filter (METROPOLIS; ULAM, 1949), Kalman filter (KALMAN, 1960), H∞ filter

(BANAVAR, 1992), moving horizon estimation (RAO, C. V; RAWLINGS; LEE, 2001), and others. Measurement related challenges and model inaccuracies threaten the reliability of such estimators.

Moving window estimation techniques use a sliding time window, which at each sampling time, the window moves one step forward, as shown in Figure 6.1. They estimate the states in the window by analyzing the measured output sequence, while the last estimated state out of the window is used as the prior knowledge.

In this work, we focus on the moving horizon estimation, receding horizon nonlinear Kalman filter, and the robust receding horizon nonlinear Kalman filter. The constrained extended Kalman filter and the corresponding short implementation form are also explained, once they are the basis of the receding horizon Kalman filter methodologies applied here. For more information about Kalman filters, including nonlinear implementations, see Apio *et al.* (2019).

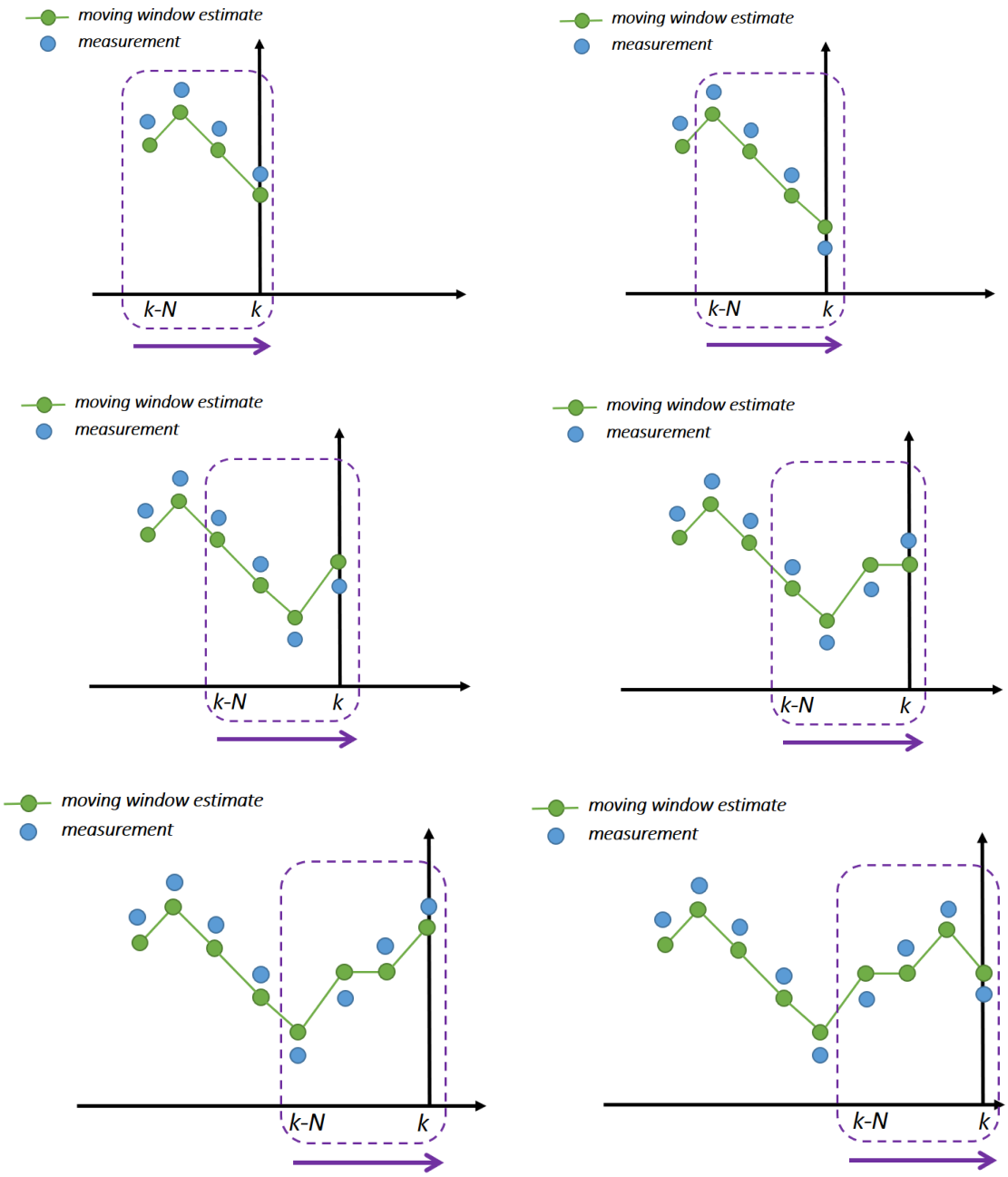


Figure 6.1: Illustration of a moving window sequence scheme.

6.3.1 Moving Horizon Estimation

The moving horizon estimation (MHE) is an optimization-based method that works on a horizon or "window" covering a limited number of past values (KÜHL *et al.*, 2011), minimizing the deviation of the model from the last *N* measurements subject to equality and inequality constraints. When the state at the next time index is estimated, a new measurement is added to the data window, and the oldest measurement is removed (RAO, C. V.; RAWLINGS, 2000). For unconstrained linear systems with Gaussian noise, the MHE reduces precisely to the Kalman filter. One option is to use a linearization approximation in the nonlinear case as in the extended Kalman filter (EKF). With a large value of N (i.e., $N \geq 5$), the corresponding computation time of the MHE is considerably higher than the EKF. On the other side, some studies show that MHE's can better fit the data in the moving window and, since it is based on the full nonlinear model, it can increase the robustness and quality of the estimations in comparison to the EKF (HASELTINE; RAWLINGS, 2005; RAWLINGS; BAKSHI, 2006).

The following equations define the discrete-time MHE algorithm.

$$\min_{\substack{\omega_{k-N-1|k},\cdots,\omega_{k-N-1|k} \\ v_{k-N|k},\ldots,v_{k|k}}} J = \omega_{k-N-1|k}^{T}\left(P_{k-1|k-1}\right)^{-1}\omega_{k-N-1|k} + \sum_{j=k-N}^{k=1}\omega_{j|k}^{T}(Q_k)^{-1}\omega_{j|k} + \sum_{j=k-N}^{k} v_{j|k}^{T}(R_k)^{-1}v_{k|k} \tag{6.1}$$

with the following equality constraints:

$$\hat{x}_{k-N|k} = \hat{x}_{k-N|k-1} + \hat{\omega}_{k-N-1|k} \tag{6.2}$$

$$\hat{x}_{j+1|k} = f\left(\hat{x}_{j|k}, u_j\right) + \hat{\omega}_{j|k}, \qquad j = k-N, \ldots, k-1 \tag{6.3}$$

$$\mathrm{y_j} = h\left(\hat{x}_{j|k}\right) + \hat{v}_{j|k}, \qquad j = k-N, \ldots, k \tag{6.4}$$

and the following inequality constraints:

$$x_{min} \leq \hat{x}_{j|k} \leq x_{max} \tag{6.5}$$

$$\hat{\omega}_{min} \leq \hat{\omega}_{j-1|k} \leq \hat{\omega}_{max}, \qquad j = k-N, \ldots, k \tag{6.6}$$

$$\hat{v}_{min} \leq \hat{v}_{j|k} \leq \hat{v}_{max}, \qquad j = k-N, \ldots, k \tag{6.7}$$

The state update is given by

$$\hat{x}_{k-N|k} = \hat{x}_{k-N|k-1} + \hat{\omega}_{k-N-1|k} \tag{6.8}$$

$$\hat{x}_{j+1|k} = f(\hat{x}_{j|k}, u_j) + \hat{\omega}_{j|k}, \qquad j = k-N, \ldots, k-1 \tag{6.9}$$

$$y_j = h\left(\hat{x}_{j|k}\right) + \hat{v}_{j|k}, \qquad j = k-N, \ldots, k-1 \tag{6.10}$$

where *k* is the step considered in discrete time, *x* is the vector of states, *f* is a model function, *ω* is the process noise vector, *y* is the output vector, *h* is a function that relates

the states to the outputs, *v* is the measurement noise vector, *P* is the covariance matrix of the states, *Q* is the process noise covariance matrix, and *R* is the measurement noise covariance.

To solve the optimal control problem given by Equation 6.1, it can be applied the multiple shooting approach (BOCK; PLITT, 1984), which leads to a large, but specially structured nonlinear programming (NLP) problem, which is solved very efficiently by a tailored sequential quadratic programming (SQP) technique (BOCK *et al.*, 2000). Another common alternative is to formulate the problem using the simultaneous approach (ZAVALA; LAIRD; BIEGLER, 2007).

In a typical MHE formulation, the decision variables in the optimization problem are the states at the beginning of the window and process noise variables relevant to that window. The constraints include the model equations and other possible bounds on the state variables and process noise variables. In many cases, the nonlinear state equations do not have an analytical solution, and hence the calculation of the states and noise variables will involve numerical integration (RAO, C. V; RAWLINGS, 2002). The integration needs to be performed repeatedly in an optimization loop resulting in a significant computational load, which hinders the MHE approach from being applied online (RENGASWAMY, R; NARASIMHAN; KUPPURAJ, 2013).

Regarding the arrival cost, GEKKO's package implementation of the Moving Horizon Estimation has a weighting factor to penalize the deviation of current model predictions from prior model predictions. The penalty from a prior model prediction is a "forgetting factor" that approximates an infinite estimation horizon or favor prior predictions. The infinite estimation horizon approximation is handy for systems that have weakly observable or unobservable states. Choosing the forgetting factor can also reduce the estimator's aggressiveness in aligning with the measurements by balancing with a penalty against shifting too far from the prior predictions (BEAL *et al.*, 2018).

6.3.2 Constrained Extended Kalman Filter

The Kalman filter (KF) is a methodology that requires a dynamic model of the system, input measurements, and other available measurements to estimate unknown variables or filter known ones. These data are usually distorted by noise and other discrepancies (e.g., from the sensors) that are corrected by the filter.

The Kalman filter equations provide a recursive estimate of the states and their covariance error. The quality of this estimation depends on the system parameters and the noise statistics given as inputs to the estimator. In this context, the Kalman filter blends new information introduced by the measurements with old information embodied in the prior state with the Kalman gain matrix, which balances uncertainty related to the measurements and the dynamic model (ALFRIEND *et al.*, 2010). Thus, the error propagation in the covariance matrix *P*, which quantifies the state estimation uncertainties, brings accuracy to the Kalman filter (SIMON, 2006).

The constrained extended Kalman filter (GESTHUISEN; KLATT; ENGELL, 2001) corresponds to the case of MHE with a moving window equal to zero, which considerably simplifies the complexity of solving the MHE dynamic nonlinear optimization problem (FRANKE *et al.*, 2001), resulting in the following formulation for the CEKF:

$$\min_{\omega_{k|k},v_{k|k}} J = \omega_{k|k}^T \left(P_{k|k-1}\right)^{-1} \omega_{k|k} + v_{k|k}^T (R_k)^{-1} v_{k|k} \tag{6.11}$$

with the following constraints:

$$v_{k|k} = y_k - h\left(\hat{x}_{k|k}\right) \tag{6.12}$$

$$x_{min} \leq \hat{x}_{k|k} \leq x_{max} \tag{6.13}$$

$$y_{min} \leq y_k \leq y_{max} \tag{6.14}$$

Considering that $\hat{x}_{k|k}$ has not been evaluated yet,

$$y_k = h\left(\hat{x}_{k|k}\right) + v_{k|k} \tag{6.15}$$

y_k is approximated by

$$y_k \approx h\left(\hat{x}_{k|k-1}\right) + \left.\frac{\partial h}{\partial x}\right|_{\hat{x}_{k|k-1},u_k} \omega_{k|k} + v_{k|k} \tag{6.16}$$

So, Equation 6.12 is rewritten as

$$H_k \omega_{k|k} + v_{k|k} = y_k - h\left(\hat{x}_{k|k-1}\right) \tag{6.17}$$

and Equation 6.13 and 6.14 as follows:

$$x_{min} \leq \hat{x}_{k|k-1} + \omega_{k|k} \leq x_{max} \tag{6.18}$$

$$y_{min} \leq h\left(\hat{x}_{k|k}\right) + v_{k|k} \leq y_{max} \tag{6.19}$$

Replacing Equation 6.19 by the approximation given by 6.16, results:

$$y_{min} \leq h\left(\hat{x}_{k|k-1}\right) + H_k \omega_{k|k} + v_{k|k} \leq y_{max} \tag{6.20}$$

In short, the new constraints are given by Equation 6.18, Equation 6.19, and Equation 6.21:

$$H_k \omega_{k|k} + v_{k|k} = y_k - h\left(\hat{x}_{k|k-1}\right) \tag{6.17}$$

$$x_{min} \leq \hat{x}_{k|k-1} + \omega_{k|k} \leq x_{max} \tag{6.18}$$

$$y_{min} - h\left(\hat{x}_{k|k-1}\right) \leq H_k \omega_{k|k} + v_{k|k} \leq y_{max} - h\left(\hat{x}_{k|k-1}\right) \tag{6.21}$$

where the system of non-linear equations is given as follows:

$$\dot{x}_k = f(x, u, t) + \omega_k \tag{6.22}$$

$$y_k = h(x_k, t_k) + v_k \tag{6.23}$$

and the linearized system

$$F(t) = \left(\frac{\partial f}{\partial x}\right)_{x,u,t} \tag{6.24}$$

$$\phi_{k-1} = e^{F(t_k - t_{k-1})} \tag{6.25}$$

$$H = \left(\frac{\partial h}{\partial x}\right)_{x,u,t} \tag{6.26}$$

The prediction matrix *a priori* in discrete time is:

$$P_{k|k-1} = \phi_{k-1} P_{k-1|k-1} \phi_{k-1}^T + Q_k \tag{6.27}$$

and the prediction matrix a *posteriori* is given by:

$$P_{k|k} = [I_n - K_k H_k] P_{k|k-1} \tag{6.28}$$

where the Kalman gain is evaluated by:

$$K_k = P_{k|k-1} H_k^T \left[H_k P_{k|k-1} H_k^T + R_k\right]^{-1} \tag{6.29}$$

Then, the final correction is:

$$\hat{x}_{k|k} = \hat{x}_{k|k-1} + \omega_{k|k} \tag{6.30}$$

$$\hat{y}_{k|k} = y_k - v_{k|k} \tag{6.31}$$

where *F* is the Jacobian of *f* concerning the states, ϕ is the transition matrix from one state to another, and H is the Jacobian of h in relation to the outputs.

The CEKF is usually implemented as a quadratic programming problem given by

$$\min_{\omega_{k|k}, v_{k|k}} J = \frac{1}{2} \begin{bmatrix} \omega_{k|k} \\ v_{k|k} \end{bmatrix}^T \alpha \begin{bmatrix} \omega_{k|k} \\ v_{k|k} \end{bmatrix} + \beta^T \begin{bmatrix} \omega_{k|k} \\ v_{k|k} \end{bmatrix} \tag{6.32}$$

subject to

$$A \begin{bmatrix} \omega_{k-1|k} \\ v_{k|k} \end{bmatrix} \leq b \tag{6.33}$$

$$A_{eq} \begin{bmatrix} \omega_{k-1|k} \\ v_{k|k} \end{bmatrix} = b_{eq} \tag{6.34}$$

where

$$\alpha = \begin{bmatrix} P_{k|k-1}^{-1} & 0 \\ 0 & R_k^{-1} \end{bmatrix} \tag{6.35}$$

$$\beta = \begin{bmatrix} 0 \\ 0 \end{bmatrix} \tag{6.36}$$

$$A = \begin{bmatrix} -I_{ns} & 0 \\ I_{ns} & 0 \\ -H_k & -I_{ns} \\ H_k & I_{ns} \end{bmatrix} \tag{6.37}$$

$$b = \begin{bmatrix} \hat{x}_{k|k-1} - x_{min} \\ x_{max} - \hat{x}_{k|k-1} \\ h(\hat{x}_{k|k-1}) - y_{min} \\ y_{max} - h(\hat{x}_{k|k-1}) \end{bmatrix} \tag{6.38}$$

$$A_{eq} = [H_k \quad I_{ns}] \tag{6.39}$$

$$b_{eq} = [y_k - \hat{y}_{k|k-1}] \tag{6.40}$$

where $ns = len(\hat{x}_{k|k})$.

6.3.3 Constrained Extended Kalman Filter– rewritten in the short formulation

The constrained extended Kalman filter presented by Equation 6.11 can be rewritten as an optimization problem with the states $\hat{x}_{k|k}$ as the decision variables (RANGEGOWDA *et al.*, 2018, 2019; VALLURU; PATWARDHAN; BIEGLER, 2018). In this form, the constraint from the CEKF represented by Equation 6.12 is replaced in Equation 6.11 (see the approximation that resulted in that expression in Section 3.2), resulting in Equation 6.41.

$$\min_{\hat{x}_{k|k}} J = (\hat{x}_{k|k} - \hat{x}_{k|k-1})^T (P_{k|k-1})^{-1} (\hat{x}_{k|k} - \hat{x}_{k|k-1}) + (y_k - H_k \hat{x}_{k|k})^T (R_k)^{-1} (y_k - H_k \hat{x}_{k|k}) \tag{6.41}$$

Considering that $\hat{x}_{k|k}$ should be represented by a deviation variable, the term $(y_k - H_k \hat{x}_{k|k})$ is rewritten as

$$\min_{\hat{x}_{k|k}} J = (\hat{x}_{k|k} - \hat{x}_{k|k-1})^T (P_{k|k-1})^{-1} (\hat{x}_{k|k} - \hat{x}_{k|k-1}) + (\Delta y_k - H_k \Delta \hat{x}_{k|k})^T (R_k)^{-1} (\Delta y_k - H_k \Delta \hat{x}_{k|k}) \tag{6.42}$$

where the deviation variables $\Delta y_k = y_k - \hat{y}_{k|k-1}$ and $\Delta \hat{x}_{k|k} = \hat{x}_{k|k} - \hat{x}_{k|k-1}$ were replaced in Equation 6.42, resulting in Equation 6.43.

$$\min_{\hat{x}_{k|k}} J = (\hat{x}_{k|k} - \hat{x}_{k|k-1})^T (P_{k|k-1})^{-1} (\hat{x}_{k|k} - \hat{x}_{k|k-1}) + (y_k - \hat{y}_{k|k-1} + H_k \hat{x}_{k|k-1} - H_k \hat{x}_{k|k})^T (R_k)^{-1} (y_k - \hat{y}_{k|k-1} + H_k \hat{x}_{k|k-1} - H_k \hat{x}_{k|k}) \tag{6.43}$$

The QP of this problem is written as

$$\min_{\hat{x}_{k|k}} J = \frac{1}{2} {\hat{x}_{k|k}}^T \alpha \hat{x}_{k|k} + \beta^T \hat{x}_{k|k} \tag{6.44}$$

subject to

$$\hat{x}_{min} \leq \hat{x}_{k|k} \leq \hat{x}_{max} \tag{6.45}$$

where

$$\alpha = [P_{k|k-1}^{-1} + H_k^T R_k^{-1} H_k] \tag{6.46}$$

$$\beta = [-\hat{x}_{k|k-1}^T P_{k|k-1}^{-1} - (y_k - \hat{y}_{k|k-1} + H_k \hat{x}_{k|k-1})^T R_k^{-1} H_k] \tag{6.47}$$

The quadratic programming form of the constrained extended Kalman filter rewritten in its short implementation is also a contribution of this work (see Appendix 6.A1 for a complete derivation). Unlike the CEKF, its short implementation establishes the states directly as constraints and lower and upper bounds of the problem. This form will also be useful for the robust extended Kalman filter, where the likelihood term ($\left(y_k - H_k\hat{x}_{k|k}\right)^T (R_k)^{-1}(y_k - H_k\hat{x}_{k|k})$) of Equation 6.41 will be replaced with an M-estimator.

6.3.4 Extended Kalman Filter with Moving Window Estimation

The extended Kalman filter with moving window estimation is based on the receding horizon nonlinear Kalman (RNK) filter, proposed by Rengaswamy et al. (2013), which is a moving window-based recursive formulation that involves prediction and update steps similar to the conventional Kalman filter. It is assumed that N measurements are available over a window $[k-N+1, k]$. Also, the states $\hat{x}_{k-N|k-N}$ and the covariance $P_{k-N|k-N}$ at $(k-N)^{th}$ instant are assumed to be known. The prediction and update steps for RNK are as follows:

In the prediction step, the filtered estimate $\hat{x}_{k-N|k-N}$ at the $(k-N)^{th}$ instant is used to find all the predicted estimates in the interval $[k-N+1, k]$, by using the state evolution model described as

$$\hat{x}_{l|k-N} = f(\hat{x}_{l-1|k-N}, u_{l-1}, \theta) \tag{6.48}$$

where l varies from $k-N+1$ to k, i.e., the predicted states are obtained by performing an open-loop simulation of Equation 6.48. The predicted states are denoted as $\hat{x}_{k-N+1|k-N}, \hat{x}_{k-N+2|k-N}, \ldots, \hat{x}_{k|k-N}$. At time k, the stacked state vector is defined as

$$X_k^a = [x_{k-N+1}^T \quad x_{k-N+2}^T \quad \ldots \quad x_k^T]^T \tag{6.49}$$

then the stacked predicted state estimates can be represented as follows, considering $\hat{X}_{k|k-N}^a = f(X_k^a)$

$$\hat{X}_{k|k-N}^a = [\hat{x}_{k-N+1|k-N}^T \quad \hat{x}_{k-N+2|k-N}^T \quad \ldots \quad \hat{x}_{k|k-N}^T]^T \tag{6.50}$$

At kth time instant, the error covariance matrix of the stacked predicted states is a matrix consisting of $N \cdot ns \times N \cdot ns$ elements, with $ns \times ns$ block elements P. The error covariance matrix is calculated using the linearized state transition matrices defined as Equations 6.24 and 6.25.

The diagonal matrices of the predicted error covariance matrix represent the auto-covariance matrices of the estimation errors in the open-loop state estimates at the same time instants and the off-diagonal matrices of the predicted error covariance matrix represent the cross-covariance matrix between the open-loop estimation errors at different time instants. The first block of the error covariance matrix $P_{k|k-N}^a$ is initialized as

$$P_{k|k-N}^a(1,1) = \phi_{k-N} P_{k-N|k-N} \phi_{k-N}^T + Q \tag{6.51}$$

The remaining blocks of $P_{k|k-N}^a$ are computed as follows:

when $i = j$ (i.e., diagonal blocks)

$$P^a_{k|k-N}(i,i) = \phi_{k-N+i-1} P^a_{k|k-N}(i-1,i-1)\phi^T_{k-N+i-1} + Q \tag{6.52}$$

when $i \neq j$ and $i < j$ (i.e., upper triangular blocks)

$$P^a_{k|k-N}(i,j) = P^a_{k|k-N}(i,j-1)\phi^T_{k-N+j-1} \tag{6.53}$$

where i and j vary from 1 to *N*, where *ns* is the number of states, and *N* is the window size. Since $P^a_{k|k-N}$ is a symmetric matrix, the lower triangular blocks can be calculated by taking the transpose of the upper triangular blocks. An example of $P^a_{k|k-N}$ for *N*=3 is shown in Equation 6.54.

$$P^a_{k|k-3} = \begin{bmatrix} \phi_{k-3}P_{k-3|k-3}\phi^T_{k-3} + Q & P^a_{k|k-3}(1,1)\phi^T_{k-2} & P^a_{k|k-3}(1,2)\phi^T_{k-1} \\ \left(P^a_{k|k-3}(1,1)\phi^T_{k-2}\right)^T & \phi_{k-2}P^a_{k|k-3}(1,1)\phi^T_{k-2} + Q & P^a_{k|k-3}(2,2)\phi^T_{k-1} \\ \left(P^a_{k|k-3}(1,2)\phi^T_{k-1}\right)^T & (P^a_{k|k-3}(2,2)\phi^T_{k-1})^T & \phi_{k-1}P^a_{k|k-3}(2,2)\phi^T_{k-1} + Q \end{bmatrix} \tag{6.54}$$

The update step involves merging of the predicted state estimates $\hat{X}^a_{k|k-N}$ with the stacked measurements

$$Y^a_k = [y^T_{k-N+1} \quad y^T_{k-N+2} \quad \dots \quad y^T_k]^T \tag{6.55}$$

in the time window $[k-N+1, k]$. The updated state estimates

$$\hat{X}^a_{k|k} = [\hat{x}^T_{k-N+1|k} \quad \hat{x}^T_{k-N+2|k} \quad \dots \quad \hat{x}^T_{k|k}]^T \tag{6.56}$$

for a linear measurement model and unconstrained case are obtained as follows

$$K^a = P^a_{k|k-N}H^{aT}(H^a P^a_{k|k-N}H^{aT} + R^a)^{-1} \tag{6.57}$$

$$\hat{X}^a_{k|k} = \hat{X}^a_{k|k-N} + K^a[Y^a_k - \hat{Y}^a_k] \tag{6.58}$$

$$P^a_{k|k} = (I - K^a H^a)P^a_{k|k-N} \tag{6.59}$$

where K is the Kalman gain, and

$$H^a = block\ diag(H, H, \dots, H) \tag{6.60}$$

$$R^a = block\ diag(R, R, \dots, R) \tag{6.61}$$

The solutions obtained at the kth instant are the filtered state estimates $\hat{x}_{k|k}$, and for the other time instants $k-N-j$ $(1 \leq j \leq N)$ corresponds to the smoothed estimates $\hat{x}_{k|k-N+j|k}$. Also, the updated augmented error covariance $P^a_{k|k}$ gives the filtered estimates for the error covariance matrix at time k and smoothed estimates for the error covariance matrix in the interval $k-N+1$ to $k-1$.

Equation 6.58 can also be formulated as an optimization problem, as Equation 6.41. The MW-EKF proposed by this work reformulates Equations 6.46 and 6.47 as Equations 6.62 and 6.63.

The QP of this problem is written as Equations 6.44 and 6.45, where

$$\alpha = \left[{P^a_{k|k-N}}^{-1} + H^{aT} R^{a^{-1}} H^a\right] \tag{6.62}$$

$$\beta = \left[-{\hat{X}^a_{k|k-N}}^T {P^a_{k|k-N}}^{-1} - \left(Y^a_k - \hat{Y}^a_k + H^a \hat{X}^a_{k|k-N}\right)^T R^{a^{-1}} H^a\right] \tag{6.63}$$

Rengaswamy et al. (2013) emphasize that since MHE explicitly estimates the noise variables, ω_k, it is possible to include constraints on ω_k, which is also possible in the RNK. However, ω_k in the standard MHE formulation has to be calculated through numerical integration at each iteration of the optimization algorithm. In contrast, the states themselves are used as the optimization variables in the proposed approach. This results in optimization being decoupled from the numerical integration. The RNK requires only a single integration at every estimation step, which leads to significant computational gains. Further, if the measurement model is linear, irrespective of whether the state-space model is linear or nonlinear, the optimization problem for the correction step reduces to a quadratic problem. This will be true in the standard MHE formulation if both the measurements and state-space models are linear.

The linearization in the receding window for the calculation of the covariance matrix could also be a concern. However, in Rengaswamy et al. (2013) implementation, the linearized measurement model is obtained by linearizing around the updated state estimates and not the predicted state estimates. The updated estimates are used because they represent the 'best' estimates of the states in the interval $[k-N+1, k]$. For the unconstrained linear case, the RNK filter solution for a fixed window length N results in RTS-smoothed estimates for all prior states in the window and a Kalman filter solution for the current states. The calculation scheme of the receding horizon nonlinear Kalman filter can be seen in Figure 6.2.

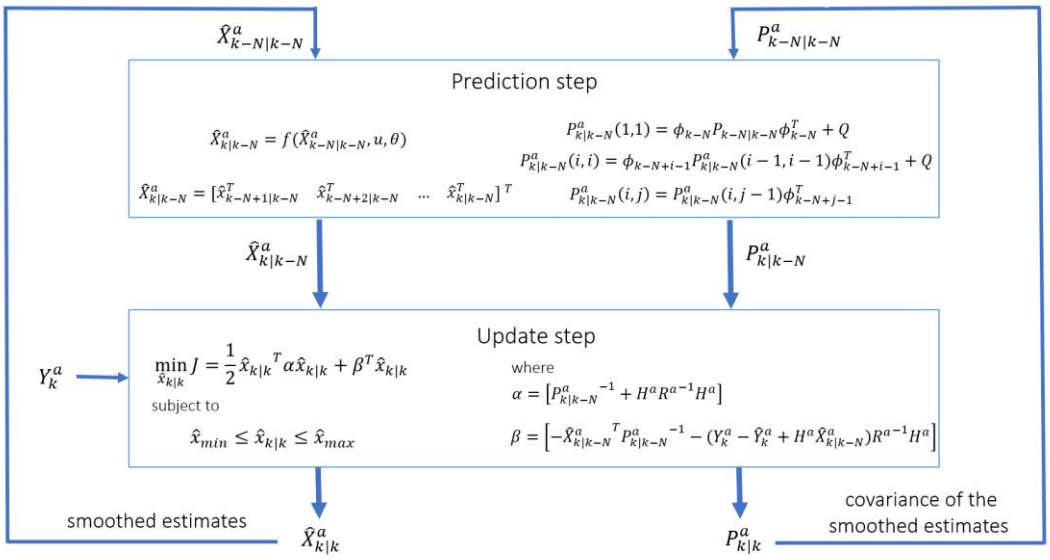


Figure 6.2: Calculation scheme of the extended Kalman filter with moving window estimation.

In short, the main contribution of the RNK methodology is the covariance matrix evaluation. In order to $P^{a}_{k|k-N}$ be consistent, the model predictions need to be re-simulated over the window using the filtered estimate $\hat{x}_{k-N|k-N}$.

6.3.5 Robust Extended Kalman Filter with Moving Window Estimation

The Kalman filter considers the measurement noise as following a zero-mean Gaussian distribution. Therefore, in the presence of gross errors, the measurement noise is no longer zero-mean, and determining the exact noise distribution is a difficult task. So, performing state estimation using Equation 6.11 in the presence of measurement biases may result in biased estimates. The MW-REKF is based on Valluru et al. (2018), which employed robust M-estimators to reduce the effect of gross errors on estimated states and parameters. The likelihood term in the Kalman update step given by the Equation 6.41 is replaced with an M-estimator, which is independent of noise distribution and insensitive to outliers, given by Equation 6.64. To make easier the comparison, the Equation 6.41 is repeated here close to the definition of Equation 6.64.

$$\min_{\hat{x}_{k|k}} J = \left(\hat{x}_{k|k} - \hat{x}_{k|k-1}\right)^{T}\left(P_{k|k-1}\right)^{-1}\left(\hat{x}_{k|k} - \hat{x}_{k|k-1}\right) + \rho_k(y_k^* - H_k\hat{x}_{k|k}\,, \delta \tag{6.64}$$

where

$$y_k^* = y_k - \hat{y}_{k|k} + H_k\hat{x}_{k|k-1} \tag{6.65}$$

It is possible to rewrite the second part of Equation 6.41 as the Huber penalty function (HUBER, 2011). The Huber function, also known as the fair function, is given by:

$$\rho_k(\zeta_k, \delta) = \delta^2\left[\frac{|\zeta_k|}{\delta} - log\left(1 + \frac{|\zeta_k|}{\delta}\right)\right] \tag{6.66}$$

From this function, for a small normalized error ζ, the Huber function is a good approximation of the least-squares estimator. As the value of ζ increases, the behavior of the Huber function changes from quadratic to linear. This function is robust to large measurement errors, placing less weight on them. Thus, depending on the magnitude of the normalized residuals, the expression of the Huber function can be approximated as follows:

$$\min_{\hat{x},\zeta,\varepsilon} \rho_k(y_k^* - H_k\hat{x}_{k|k}) \tag{6.67}$$

$$subject\ to\ \rho_k(\zeta, \delta) = \begin{Bmatrix} \zeta^2 & |\zeta| \le \delta \\ \delta(2|\zeta| - \delta) & |\zeta| > \delta \end{Bmatrix} \tag{6.68}$$

The Huber function can be rewritten as a QP problem (BOYD; VANDENBERGHE, 2004):

$$\min_{\hat{x},\zeta,\varepsilon}(\zeta^2 + 2\delta\varepsilon) \tag{6.69}$$

$$subject\ to \begin{Bmatrix} -\zeta - \varepsilon \le y_k^* - H_k\hat{x}_{k|k} \le \zeta + \varepsilon \\ 0 \le \zeta \le \delta \\ \varepsilon \ge 0 \end{Bmatrix} \tag{6.70}$$

Therefore, the robust problem from Equation 6.64 is rewritten as

$$\min_{\hat{x}_{k|k},\zeta,\varepsilon} J = \left(\hat{x}_{k|k} - \hat{x}_{k|k-1}\right)^T \left(P_{k|k-1}\right)^{-1} \left(\hat{x}_{k|k} - \hat{x}_{k|k-1}\right) + \zeta^T R^{-1} \zeta + 2\delta\varepsilon \tag{6.71}$$

$$subject\ to \begin{Bmatrix} -\zeta - \varepsilon \le y_k^* - H_k \hat{x}_{k|k} \le \zeta + \varepsilon \\ 0 \le \zeta \le \delta \\ \varepsilon \ge 0 \end{Bmatrix} \tag{6.72}$$

which is reformulated as QP problem as (see Appendix 6.A2 for its complete derivation):

$$\begin{gathered} \min_{\hat{x}_{k|k},\zeta,\varepsilon} J = \frac{1}{2} \begin{bmatrix} \hat{x}_{k|k} \\ \zeta \\ \varepsilon \end{bmatrix}^T \alpha \begin{bmatrix} \hat{x}_{k|k} \\ \zeta \\ \varepsilon \end{bmatrix} + \beta^T \begin{bmatrix} \hat{x}_{k|k} \\ \zeta \\ \varepsilon \end{bmatrix} \\ subject\ to \qquad A \begin{bmatrix} \hat{x}_{k|k} \\ \zeta \\ \varepsilon \end{bmatrix} \le b \end{gathered} \tag{6.73}$$

where

$$\alpha = \begin{bmatrix} P_{k|k-1}^{-1} & 0 & 0 \\ 0 & R^{-1} & 0 \\ 0 & 0 & 0 \end{bmatrix} \tag{6.74}$$

$$\beta = \begin{bmatrix} -\hat{x}_{k|k-1}^T P_{k|k-1}^{-1} \\ 0 \\ \delta \end{bmatrix} \tag{6.75}$$

$$A = \begin{bmatrix} -H_k & -1 & -1 \\ H_k & -1 & -1 \\ 0 & -1 & 0 \\ 0 & 1 & 0 \\ 0 & 0 & -1 \end{bmatrix} \tag{6.76}$$

$$b = \begin{bmatrix} -y_k^* \\ y_k^* \\ 0 \\ \delta \\ 0 \end{bmatrix} \tag{6.77}$$

For a moving window problem, the following equations are considered:

$$\begin{gathered} \min_{\hat{X}_{k|k}^a,\zeta,\varepsilon} J = \frac{1}{2} \begin{bmatrix} \hat{X}_{k|k}^a \\ \zeta \cdot I_{(1,nm)} \\ \varepsilon \cdot I_{(1,nm)} \end{bmatrix}^T \alpha \begin{bmatrix} \hat{X}_{k|k}^a \\ \zeta \cdot I_{(1,nm)} \\ \varepsilon \cdot I_{(1,nm)} \end{bmatrix} + \beta^T \begin{bmatrix} \hat{X}_{k|k}^a \\ \zeta \cdot I_{(1,nm)} \\ \varepsilon \cdot I_{(1,nm)} \end{bmatrix} \\ subject\ to \qquad A \begin{bmatrix} \hat{X}_{k|k}^a \\ \zeta \cdot I_{(1,nm)} \\ \varepsilon \cdot I_{(1,nm)} \end{bmatrix} \le b \end{gathered} \tag{6.78}$$

where

$$\alpha = \begin{bmatrix} {P_{k|k-N}^a}^{-1} & 0 & 0 \\ 0 & {R^a}^{-1} & 0 \\ 0 & 0 & 0 \end{bmatrix}_{(N(ns+2nm),N(ns+2nm))} \tag{6.79}$$

$$\beta = \begin{bmatrix} -\hat{X}^a_{k|k-N}{}^T P^a_{k|k-N}{}^{-1} \\ 0 \\ \delta \cdot I_{nm} \end{bmatrix}_{(1,N(ns+2nm))} \tag{6.80}$$

$$A = \begin{bmatrix} -H^a & -I_{nm} & -I_{nm} \\ H^a & -I_{nm} & -I_{nm} \\ 0 & -I_{nm} & 0 \\ 0 & I_{nm} & 0 \\ 0 & 0 & -I_{nm} \end{bmatrix} \tag{6.81}$$

$$b = \begin{bmatrix} -Y^{a*}_k \\ Y^{a*}_k \\ 0 \\ \delta \cdot I_{(1,nm)} \\ 0 \end{bmatrix} \tag{6.82}$$

Where

$$Y^{a*}_k = Y^a_k - \hat{Y}^a_k + H^a \hat{X}^a_{k|k-N} \tag{6.83}$$

where $nm = len(y_k)$

The calculation scheme of the robust receding horizon nonlinear Kalman filter can be seen in Figure 6.3.

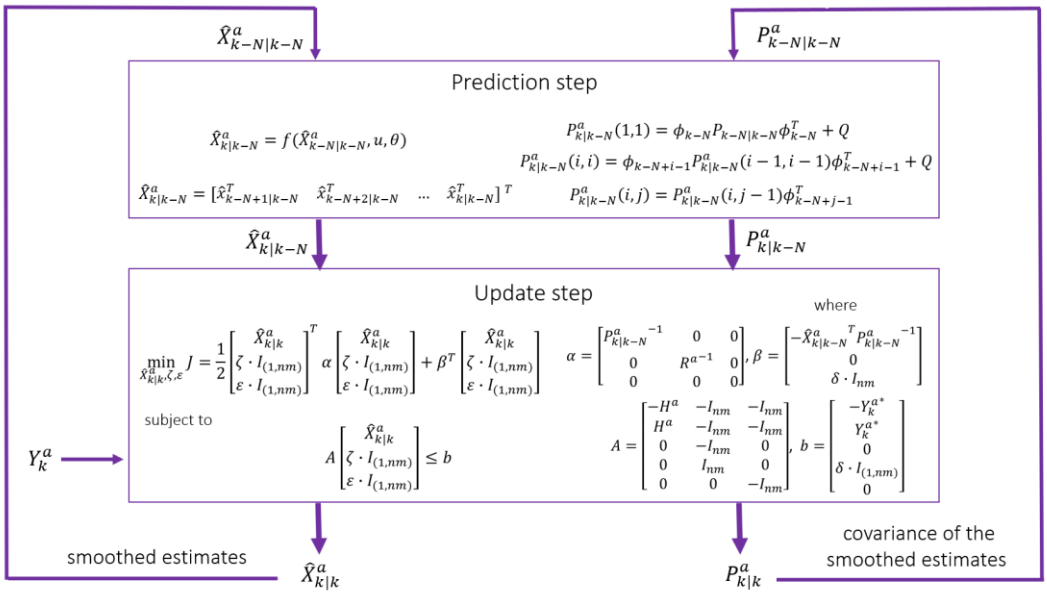


Figure 6.3: Calculation scheme of the robust extended Kalman filter with moving window estimation.

Valluru et al. (2018) and Rangegowda et al. (2018) formulated the covariance of the estimation error $P_{k|k}$ related to the Huber's influence function. According to Valluru et al.

(2018), one of the most popular tools for accessing the robustness of any M-estimator is the influence function, which is proportional to the first derivative of the estimator. An estimator is said to be robust if its influence function is bounded as the measurement errors tend to infinity. For a least-squares estimator, the influence function is linear and unbounded as measurements go to infinity. Thus, the use of the least-squares estimator in the presence of gross errors in the measurements can result in biased estimations. The influence function of Huber's fair function estimator is given as follows

$$\Psi(\zeta_k) = \frac{\partial \rho_k}{\partial \zeta_k} = \frac{\zeta_k}{\left(1+\frac{|\zeta_k|}{\delta}\right)} \tag{6.84}$$

When the normalized residuals ζ_k approach to infinity, the influence function will attain a constant value, indicating that the fair function is robust to large measurement errors. It places less weight on the larger residuals rather than nullifying them. The performance of the fair function depends on the tuning parameter δ. Equation 6.82 can be approximated as

$$\Psi(\zeta_k) = \begin{Bmatrix} \zeta_k & |\zeta| \leq \delta \\ \pm\delta & |\zeta| > \delta \end{Bmatrix} \tag{6.85}$$

$$\frac{\partial \Psi(\zeta_k)}{\partial \zeta_k} = \begin{Bmatrix} 1 & |\zeta| \leq \delta \\ 0 & |\zeta| > \delta \end{Bmatrix} \tag{6.86}$$

Valluru et al. (2018) have derived an approximate recursive formula for updating the covariance of the estimation error for the fair function based robust EKF, showing that the use of M-estimator in the update step amounts to removing the effect of measurements corrupted with the gross errors while computing the update covariance. Rangegowda et al. (2018) proposed an approximate update of the covariance matrix, which is based on removing the measurements affected by gross errors. To achieve this, the stacked measurement matrix $H^a_{m,k}$ and the associated stacked noise covariance matrix $R^a_{m,k}$ are modified as follows:

$$H^a_{m,k} = P^a_{m,} H^a_k \tag{6.87}$$

$$R^a_{m,k} = P^a_m R^a_k P^{aT}_m \tag{6.88}$$

where P^a_m is the stacked projection matrix given by

$$[P^a_m]_{Nv \times Nv} = \text{non zero rows of } [\nabla \Psi(\zeta_k(X^a_k))] \tag{6.89}$$

The stacked matrix $[\nabla \Psi(\zeta_k(X^a_k))]$ consists of

$$\nabla \Psi\left(\zeta_k(X^a_k)\right) = diag\left[\frac{\partial \Psi(\zeta_{k,1}(x_{k-N+1}))}{\partial \zeta_{k,1}} \ldots \frac{\partial \Psi(\zeta_{k,N}(x_{k-N+1}))}{\partial \zeta_{k,N}}\right]_{N \times N} \tag{6.90}$$

and $Nv \leq N$ represents the number of measurements over the window $[k-N+1, k]$ without gross errors. Thus, the modified update Kalman gain and covariance matrix for the robust horizon Kalman filter is given as follows:

$$K^a = P^a_{k|k-N} {H^a_{m,k}}^T (H^a_{m,k} P^a_{k|k-N} {H^a_{m,k}}^T + R^a_{m,k})^{-1} \tag{6.91}$$

$$P^a_{k|k} = (I - K^a H^a_{m,k}) P^a_{k|k-N} \tag{6.92}$$

In the absence of gross error measurements, $\nabla\Psi\left(\zeta_k(X_k^a)\right) = I_{N\times N}$ and $P_m^a = I_{N\times N}$. This results in reducing the modified update Kalman gain and covariance matrix given by Equations 6.91 and 6.92 into the conventional update Equation 6.57 and Equation 6.59.

6.3.6 Constrained Extended Kalman Filter and Smoother

The constrained extended Kalman filter and smoother (CEKFS) (SALAU; TRIERWEILER; SECCHI, 2012b) includes the EKF smoother counterpart in the CEKF. Its main difference is that the recursion in the filter moves forward and the smoother backward (HAYKIN, 2001). This smoothing is significant once the CEKF and the DEKF (discrete EKF) fail to converge swiftly to the actual states when the system is subject to poor guesses at the initial state (RAUCH; STRIEBEL; TUNG, 1965). In this context, smoothing means providing an estimate of the system state at some time step, given that all the measurements, including the ones encountered after that particular time step, are available. In short, the CEKFS gives a smoothed estimate of the system history for all the measurements obtained so far.

Firstly, from the CEKF evaluation results, the following variables are set:

$$\hat{x}_{N|k}^S = \hat{x}_{k|k} \text{ and } P_{N|k}^S = P_{k|k} \tag{6.93}$$

Considering $i = N-1, N-2, \dots, 0$, the Rauch-Tugh-Striebel (RTS) smoother, which is detailed in Rauch et al. (1965) and Haykin (2001), is evaluated as:

$$\hat{x}_{k+1|k} = \hat{x}_{k|k} + \int_k^{k+1} f(x,u,t)\, dt \tag{6.94}$$

$$P_{k+1|k} = \phi_k P_{k|k} \phi_k^T + Q_k \tag{6.95}$$

$$C_k = P_{k|k}\phi_k^T P_{k+1|k}^{-1} \tag{6.96}$$

$$\hat{x}_{k|k}^S = \hat{x}_{k|k} + C_k(\hat{x}_{k+1|k}^S - \hat{x}_{k+1|k} \tag{6.97}$$

$$P_{k|k}^S = P_{k|k} + C_k(P_{k+1|k}^S - P_{k+1|k})C_k^T \tag{6.98}$$

where *N* is the horizon size and C_k is the RTS smoother of the Kalman gain. In this work, the horizon size is *N* = 4. The new smoothed values (P_0^S and $\hat{x}_0^S$) are the initial guess for the CEKF algorithm, which is re-evaluated until the current step:

$$P_k = P_0^S \quad \text{and} \quad \hat{x}_{k|k} = \hat{x}_0^S \tag{6.99}$$

6.4 Case study

The case study aims to evaluate the performance of the moving window Kalman filter approaches by estimating the states and parameters of the spherical-quadruple-tank process.

6.4.1 Plant model

The spherical-quadruple-tank process is adapted from the six spherical tanks process proposed by Escobar and Trierweiler (2013) and the cylindrical quadruple tank process proposed by Johansson (2000). This process comprises four spherical tanks (two columns

of two stacked tanks) that interact with each other, two control valves, two split manual valves, one recycling tank, and pumps. Figure 6.4 provides a sketch of the unit.

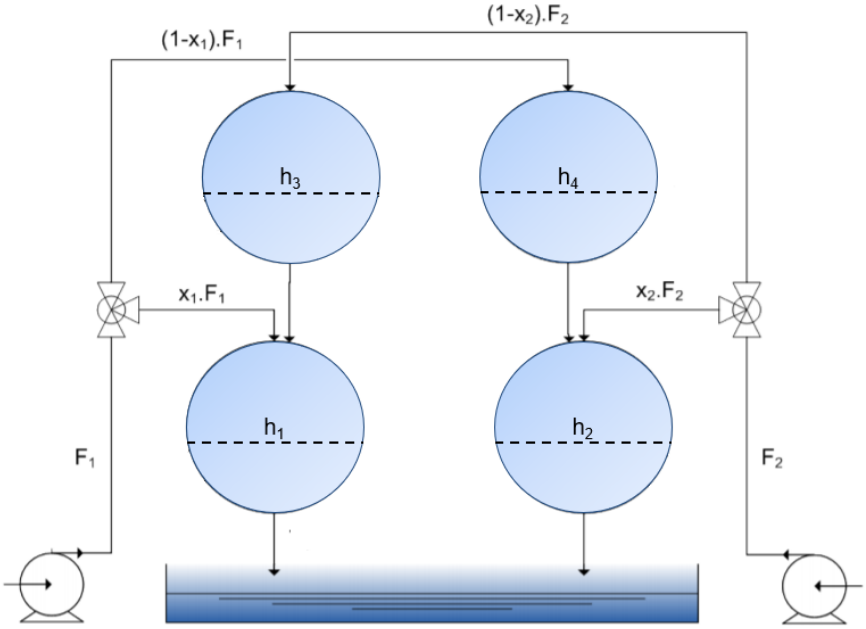


Figure 6.4: The spherical-quadruple-tank process.

The phenomenological model is described by the simplified mass balance given by:

$$\frac{dh_1}{dt} = \frac{x_1 F_1 + R_3\sqrt{h_3} - R_1\sqrt{h_1}}{A_1(h_1)} \tag{6.100}$$

$$\frac{dh_2}{dt} = \frac{x_2 F_2 + R_4\sqrt{h_4} - R_2\sqrt{h_2}}{A_2(h_2)} \tag{6.101}$$

$$\frac{dh_3}{dt} = \frac{(1-x_2) F_2 - R_3\sqrt{h_3}}{A_3(h_3)} \tag{6.102}$$

$$\frac{dh_4}{dt} = \frac{(1-x_1) F_1 - R_4\sqrt{h_4}}{A_4(h_4)} \tag{6.103}$$

where the area of the cylindrical tanks is given by:

$$A_i(h_i) = \pi h_i (D_i - h_i) \tag{6.104}$$

The description of the model variables and their units is presented in Table 6.1.

Table 6.1: Description of the spherical-quadruple-tank process.

Symbol	Description	Unit	Variable
D_i	tank *i* diameter	cm	Parameter
A_i	tank *i* area	cm^2	Parameter
R_i	tank *i* discharge coefficient	$cm^{2.5}/s$	Parameter
x_i	valve opening from tank *i*	-	input
F_i	flow rate from tank *i*	cm^3/s	Input

h_i	height level of the tank i	cm	Output

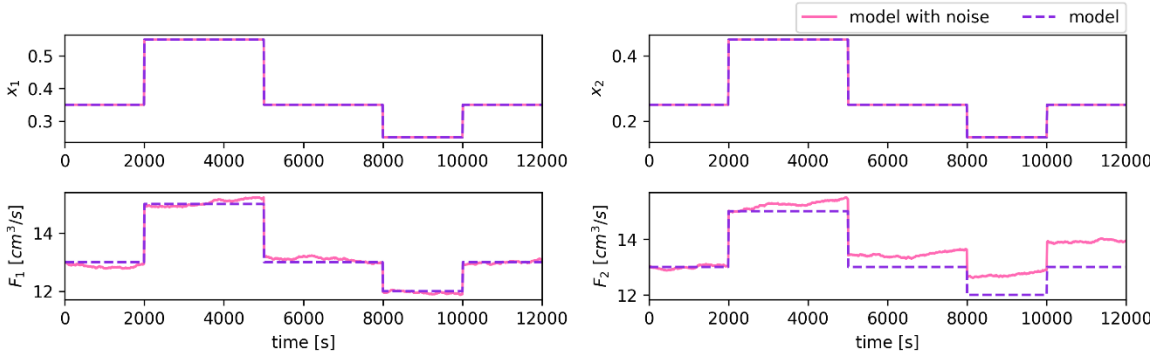
For all case studies of this paper, $D_i = 25$ and $R_i = 3.75$.

The case study evaluates seven scenarios. Each one has its characteristic problem that hinders the state and parameter estimation. Table 6.2 shows the characteristics problem, variables estimated, measured states, plant model, and state estimator model of each scenario.

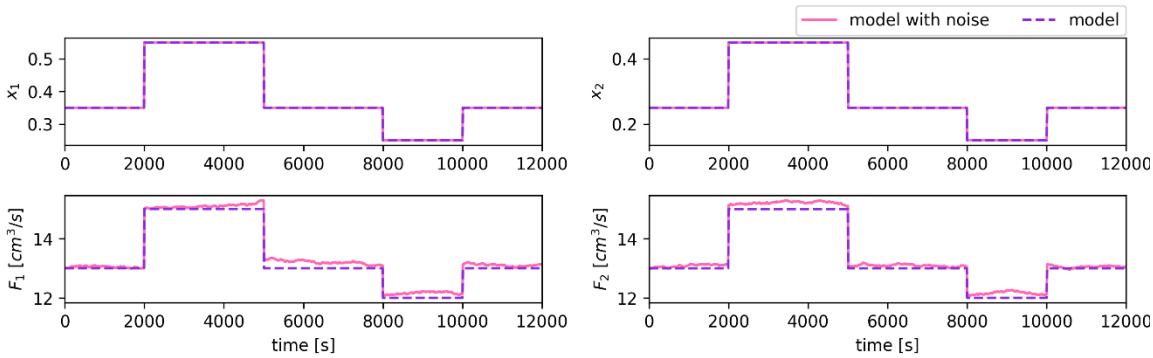
Table 6.2: Scenarios of the spherical-quadruple-tank plant.

Scenarios	Characteristic problem	States estimated	Input variables	Measured states	Plant model	State estimator model
A	None	h_1, h_2, h_3, h_4, and R_1	x_1, x_2, F_1 and F_2	h_1 and h_2	Spherical	Spherical
B	Outliers	h_1, h_2, h_3, h_4, and R_1	x_1, x_2, F_1 and F_2	h_1 and h_2	Spherical	Spherical
C	Structural discrepancy	h_1, h_2, h_3, h_4, and R_1	x_1, x_2, F_1 and F_2	h_1 and h_2	Spherical	Cylindrical
D	Physical limitation	h_1, h_2, h_3, h_4, and R_1	x_1, x_2, F_1 and F_2	h_1 and h_2	Cylindrical	Cylindrical
E	Physical limitation	h_1, h_2, h_3, h_4, and R_1	x_1, x_2, F_1 and F_2	h_1 and h_2	Cylindrical	Cylindrical
F	Outliers	h_1, h_2, h_3, h_4, and x_1	x_1, x_2, F_1 and F_2	h_1 and h_2	Spherical	Spherical
G	Outliers	$h_1, h_2, h_3, h_4, x_{1d}$ and x_{2d}	x_1, x_2, F_1 and F_2	h_1 and h_2	Spherical	Spherical
H	Structural discrepancy	$h_1, h_2, h_3, h_4, A_{3d}$ and A_{4d}	x_1, x_2, F_1 and F_2	h_1 and h_2	Cylindrical	Cylindrical

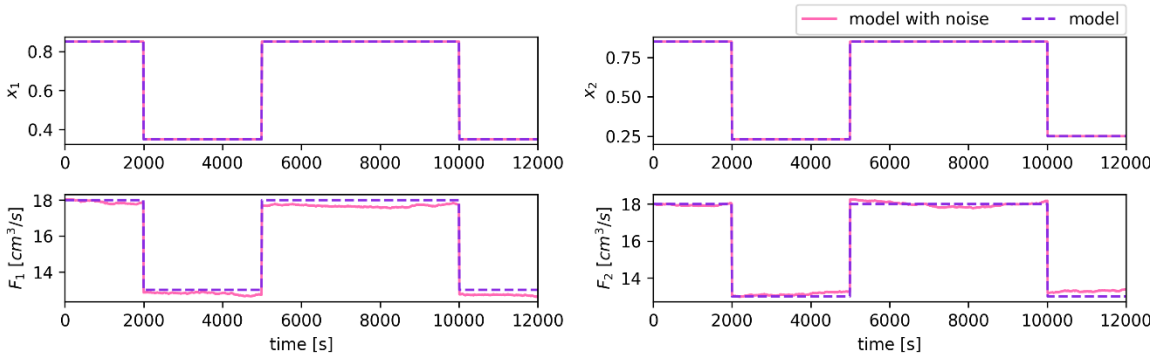
The dataset, shown in Figure 6.5, has perturbations in the input variables x_1, x_2, F_1, and F_2 for the seven scenarios. The simulated data have a sampling time of 10 seconds and a total of 1201 measured points.



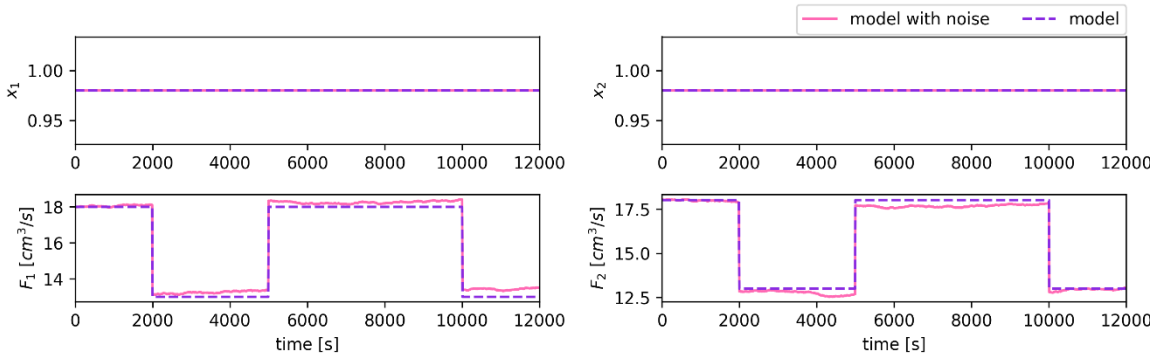
a) Scenario A



b) Scenarios B, C, F and G



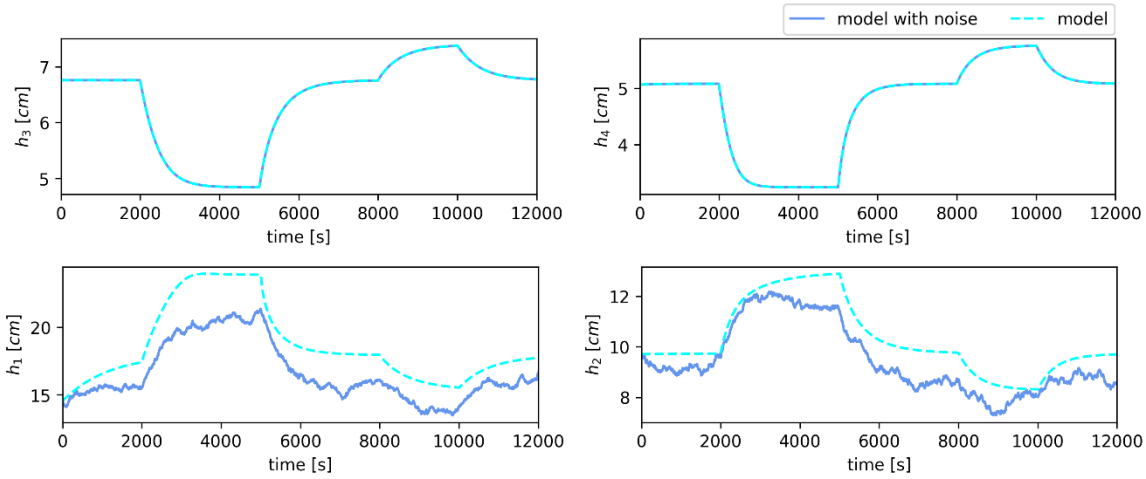
c) Scenario D and H



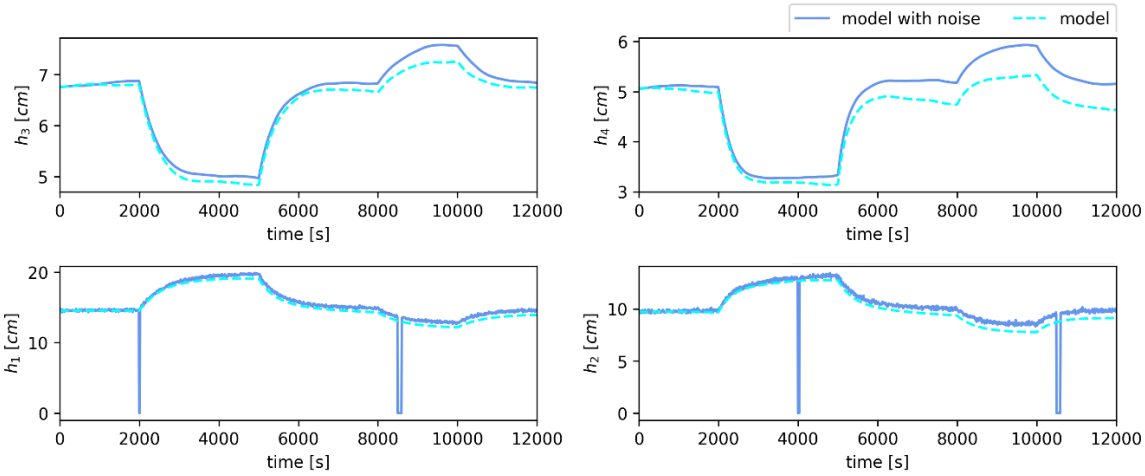
d) Scenario E

Figure 6.5: Inputs variables x_1, x_2, F_1 and F_2 of the spherical-quadruple-tank plant.

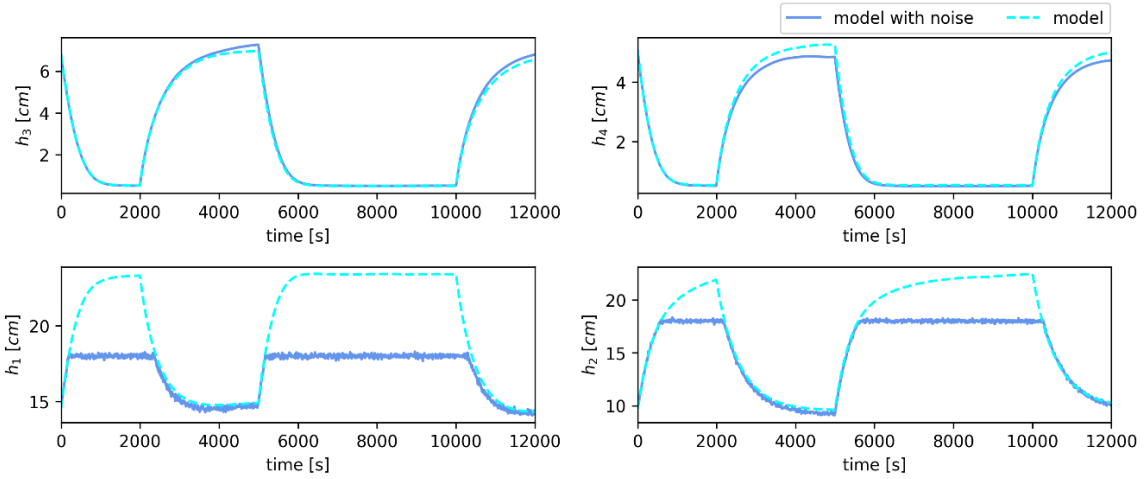
The outputs variables h_1, h_2, h_3 and h_4 corresponding to each scenario are shown in Figure 6.6. In order to bring more truthfulness to the simulated data, colored (cumulative) noise was added to the input variables (F_1 and F_2) of Scenarios A, B, C, F, and G (Figure 6.5a and Figure 6.5b) and white noise to the input variables of Scenarios D, H, and E (Figure 6.5c and 6.5d). White noise was also added to the original model simulation results of h_1 and h_2, resulting in Figure 6.6.



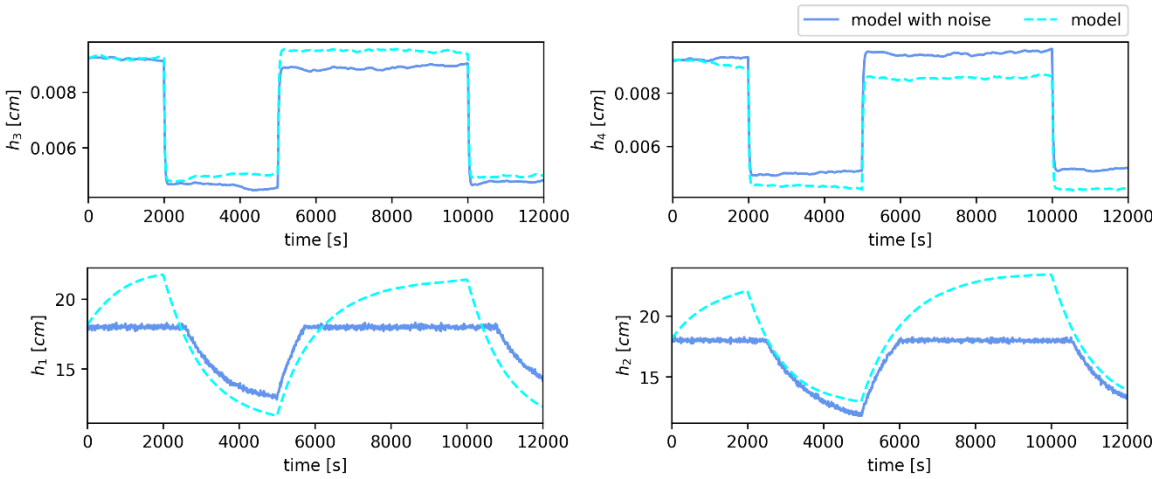
a) Scenario A



b) Scenarios B, C, F and G



c) Scenario D and H



d) Scenario E

Figure 6.6: Outputs h_1, h_2, h_3 and h_4 of the spherical-quadruple-tank plant.

Scenario A presents a colored noise in its input perturbations and white noise in the measured variables. Scenario B, in addition to the colored noise in the input variables, also exhibits the presence of outliers. This simulates the loss of measurements due to errors in the sensor reading. Scenario C still considers the presence of outliers in the simulated data, but in this case, the model used by the state estimators has a structural discrepancy: i.e., the plant consisted of the spherical-quadruple-tank model, while the state estimators used a cylindrical-quadruple-tank model for the state and parameter estimation.

In Scenario D, the cylindrical tanks of the plant, which generate the simulated data, are 18 cm height. The state estimators do not consider this physical limitation in the model, resulting in a structural discrepancy. It was chosen not to add constraints to the optimization problems to observe their adaptability to the physical limitations. In Scenario E, it is still considered the physical limitation in the model as Scenario D. However, both valve opening, and both flow rates are considered high, emptying the tanks 3 and 4. If a lower bound would not be added to the optimization problem, it would not be possible to estimate the model states.

In Scenario F, the input variable x_1 is estimated instead of the parameter R_1, using the simulated data with the presence of outliers. Scenario G estimates deviations in x_1 and x_2 to reduce the effect of these variables' sensitivity and also to make the system observable by estimating two variables ($x_{1\mathrm{b}}$ and $x_{2\mathrm{b}}$). In Scenario H, the simulated data were generated by a spherical-quadruple-tank model, while the state estimator considered a cylindrical-quadruple-tank model. The idea is to estimate the areas from cylindrical tanks 3 and 4 given by the deviation parameters $A_{3\mathrm{b}}$ and $A_{4\mathrm{b}}$.

All the simulated data were generated considering spherical tanks (Equation 6.104). For case study C, the state estimators consider the model has cylindrical tanks (Equation 6.105). The difference consists that the area from the spherical tanks varies with height, while the cylindrical tank area is constant.

$$A_i = \frac{\pi {D_i}^2}{4} \tag{6.105}$$

For the case study G, the deviation variables x_{1d} and x_{2d} are estimated. They are considered as uncertainties in the valve opening, as they are added to the input values of x_1 and x_2. The system is observable when x_{1d} and x_{2d} are estimated as state variables, which is not true when x_1 and x_2 are estimated directly. To apply the state augmentation technique, the system of differential equations, for this case, is given by

$$\frac{dh_1}{dt} = \frac{(x_1+x_{1d})F_1+R_3\sqrt{h_3}-R_1\sqrt{h_1}}{A_1(h_1)} \tag{6.106}$$

$$\frac{dh_2}{dt} = \frac{(x_2+x_{2d})F_2+R_4\sqrt{h_4}-R_2\sqrt{h_2}}{A_2(h_2)} \tag{6.107}$$

$$\frac{dh_3}{dt} = \frac{(1-(x_2+x_{2d}))F_2-R_3\sqrt{h_3}}{A_3(h_3)} \tag{6.108}$$

$$\frac{dh_4}{dt} = \frac{(1-(x_1+x_{1d}))F_1-R_4\sqrt{h_4}}{A_4(h_4)} \tag{6.109}$$

$$\frac{dx_{1d}}{dt} = 0 \tag{6.110}$$

$$\frac{dx_{2d}}{dt} = 0 \tag{6.111}$$

where the area from the spherical tank is given by Equation 6.104.

As discussed before, for the case study H, the deviation variables A_{3d} and A_{4d} are estimated. As the simulated data resulted from a spherical-quadruple-tank plant and a cylindrical-quadruple-tank model is used by the state estimators, the areas are estimated as deviations to the constant area. The system is observable when A_{3d} and A_{4d} are estimated as state variables. Otherwise when A_3 and A_4 are estimated directly, the corresponding system is not observable. To apply the state augmentation technique, the system of differential equations, for this case, is given by:

$$\frac{dh_1}{dt} = \frac{x_1F_1+R_3\sqrt{h_3}-R_1\sqrt{h_1}}{A_1} \tag{6.112}$$

$$\frac{dh_2}{dt} = \frac{x_2F_2+R_4\sqrt{h_4}-R_2\sqrt{h_2}}{A_2} \tag{6.113}$$

$$\frac{dh_3}{dt} = \frac{(1-x_2)F_2-R_3\sqrt{h_3}}{A_3+A_{3d}} \tag{6.114}$$

$$\frac{dh_4}{dt} = \frac{(1-x_1)F_1-R_4\sqrt{h_4}}{A_4+A_{4d}} \tag{6.115}$$

$$\frac{dA_{3d}}{dt} = 0 \tag{6.116}$$

$$\frac{dA_{4d}}{dt} = 0 \tag{6.117}$$

where the area from the cylindrical tank is given by Equation 6.105.

6.4.2 Simulation Settings

In this work, the state estimator techniques used the spherical/cylindrical-quadruple-tank (section 6.4.1) as the dynamical model of the system, the input measurements x_1, x_2, F_1, and F_2 and the available output measurements h_1 and h_2 are used to estimate the states h_1, h_2, h_3, and h_4. The system has 4 equations, 4 states, 2 output measurements, and 2 input measurements, resulting in an observable system according to the Popov-Belevitch-Hautus criterion (HAUTUS, 1969).

The filter parameters for all study cases are shown in Table 6.3, in which the values of P_0 and Q_0 were chosen according to the state order of magnitude, and R_0 based on the measurement order of magnitude.

Table 6.3: Filter parameters for spherical/cylindrical-quadruple-tank model.

Scenario	P_0	R_0	Q_0	δ
A	I_5	I_2	I_5	0.01
B	I_5	I_2	I_5	0.01
C	I_5	I_2	I_5	0.01
D	I_5	I_2	I_5	0.01
E	I_5	I_2	I_5	0.01
F	I_5	I_2	*diag*(1, 1,1,1,0.1)	0.1
G	I_6	I_2	*diag*(1, 1,1,1,0.01,0.01)	0.1
H	I_6	I_2	*diag*(1, 1,1,1,100,100)	0.1

All the receding horizon methodologies apply the window size of $N = 4$, which was representative in terms of the system dynamics. For larger window sizes, no significant changes were obtained.

The Kalman filter available input and output measurements used for each scenario are shown in Table 6.2. The initial conditions of the spherical/cylindrical-quadruple-tank model states are presented in Table 6.4.

Table 6.4: Initial conditions for the states of the spherical/cylindrical-quadruple-tank model.

Scenario	h_1	h_2	h_3	h_4	R_1	x_1	x_{1d}	x_{2d}	A_{3d}	A_{4d}
A	14.54	9.71	6.76	5.06	3.75	-	-	-	-	-
B	14.54	9.71	6.76	5.06	3.75*0.9	-	-	-	-	-
C	14.54	9.71	6.76	5.06	3.75*0.7	-	-	-	-	-
D	14.54	9.71	6.76	5.06	3.75*0.8	-	-	-	-	-
E	14.54	9.71	6.76	5.06	3.75*0.8	-	-	-	-	-
F	14.54	9.71	6.76	5.06	-	0.3	-	-	-	-
G	14.54	9.71	6.76	5.06	-	-	0.05	0.05	-	-
H	14.54	9.71	6.76	5.06	-	-	-	-	0.00	0.00

6.4.3 Simultaneous State and Parameter Estimation

In this case study, the dynamic model's state and parameters are simultaneously estimated using different Kalman filter techniques. The approach, commonly known as state augmentation (JAZWINSKI, A. H., 1970), consists of defining an augmented dynamical system that allocates the model parameters to be estimated along with the system's state. As the parameters are constant, the corresponding differential equations' right-hand sides are equal to zero.

The implementation from the GEKKO's package (BEAL *et al.*, 2018) was used for the moving horizon estimation methodology. In this case study, it was used an l_1-norm objective form for the optimization problem. Regarding the arrival cost, GEKKO's package implementation of the MHE has a weighting factor to penalize the deviation of current model predictions from prior model predictions. The penalty from a prior model prediction is a "forgetting factor" that approximates an infinite estimation horizon or favor prior predictions. In this case, a high forgetting factor was chosen to ignore measured values in favor of matching prior model predictions.

The other methodologies presented below were entirely coded in Python 2.7 with the dynamic model implemented in JModelica (ÅKESSON *et al.*, 2010). The tests were run on a PC with an Intel® Core™ i7-3632QM CPU @ 2.20GHz processor and 16 GB RAM.

6.4.4 Performance Evaluation Criteria

The quantification of the computational time consumed by the state estimation-based approaches and the mean squared error (MSE) between the expected and estimated results are the criteria for the performance evaluation, in which the MSE is given by:

$$MSE = \frac{1}{n}\sum_{i=1}^{n}(Y_i - \hat{Y}_i)^2 \tag{6.118}$$

where Y is the expected vector, $\hat{Y}$is the estimated vector, and n is the length of Y.

6.5 Results and Discussion

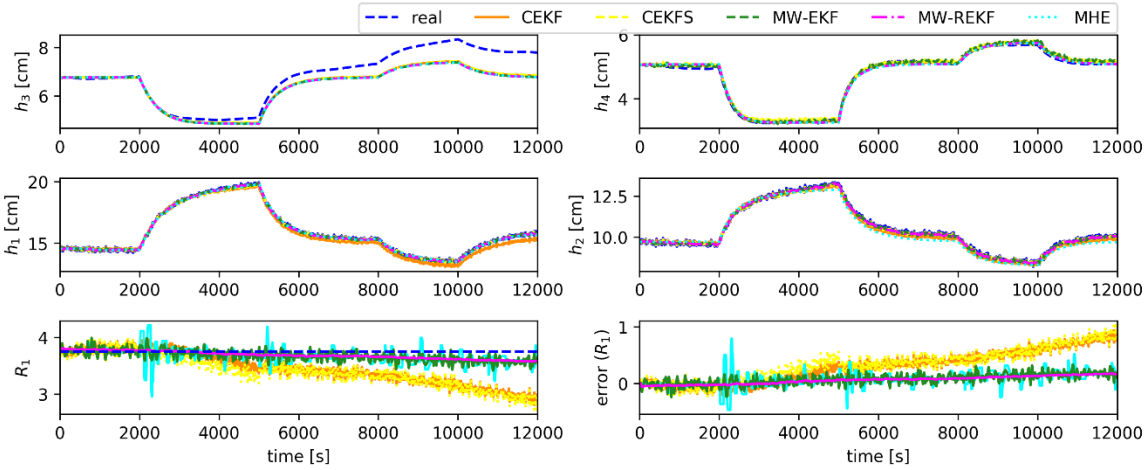
Firstly, in order to show that the CEKF optimization approximation in a QP problem (approximation of y_k given by Equation 6.16) is possible, their performance was compared applied to scenario A, shown in Table 6.5.

Table 6.5: Mean squared error for scenario A of the spherical-quadruple-tank case study using the CEKF-OPT and CEKF-QP methodologies.

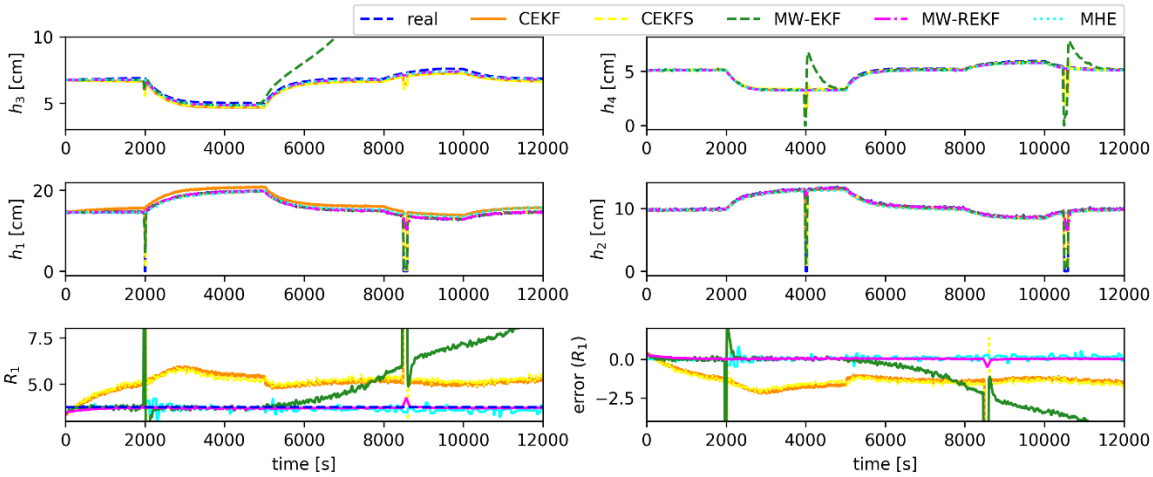
Scenario A			
Filter	CEKF-OPT	CEKF-QP	Ref. Value
time [s]	1.0000	0.8595	18.1650
h_1 error	1.0000	1.0003	0.0595
h_2 error	1.0000	0.9986	0.0096
h_3 error	1.0000	1.0010	0.2796
h_4 error	1.0000	0.9956	0.0043
R_1 error	1.0000	1.0020	0.1670

For Table 6.5, the CEKF-OPT results were chosen as reference values. The CEKF-OPT and CEKF-QP results are multiplied by the column “Ref. Value” to make comparison easier.

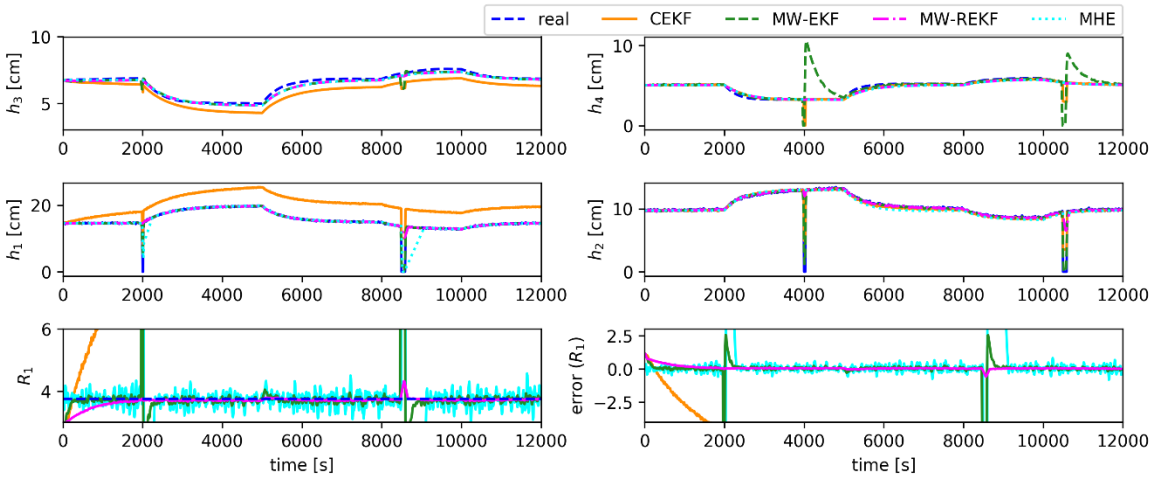
Table 6.5 showed that the results of the CEKF-OPT (CEKF solved by optimization problem) and CEKF-QP (CEKF solved by quadratic programming) methodologies are very similar, though the computational effort of CEKF-QP is 14% smaller than the CEKF-OPT. Therefore, it was chosen to keep the approximation using QP for the CEKF evaluation. Considering that, the four state estimation methodologies reviewed in Section 6.3 are applied to the spherical-quadruple-tank model specified in Section 6.4 to estimate the states and parameters. The results for all the scenarios detailed in Table 6.2 are shown in Figure 6.7.



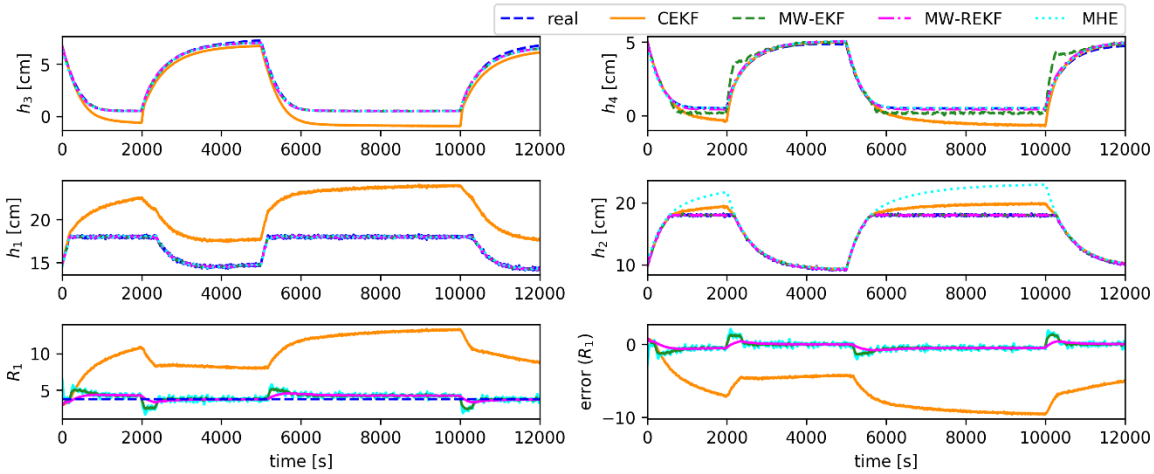
a) Scenario A – with colored noise and R_1 parameter estimation



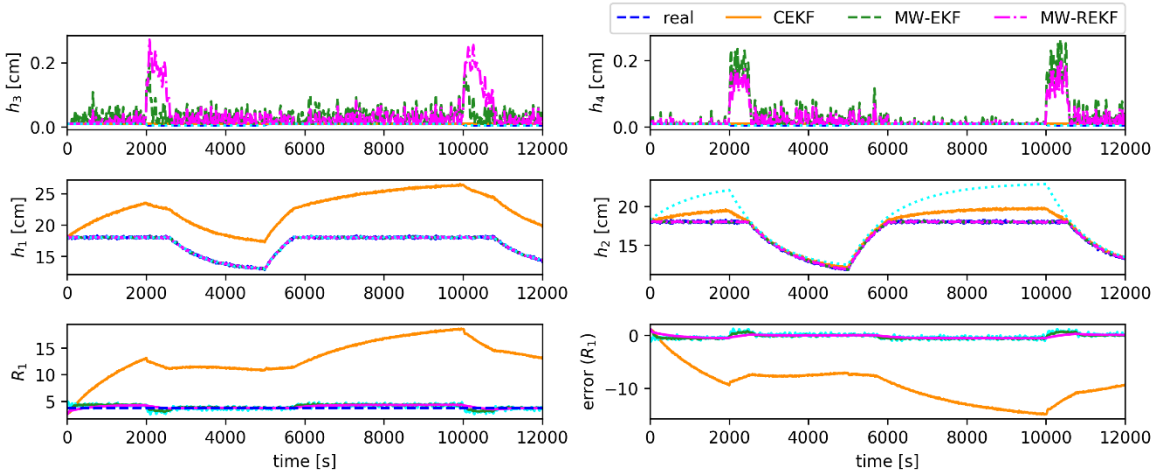
b) Scenario B – with outliers and R_1 parameter estimation



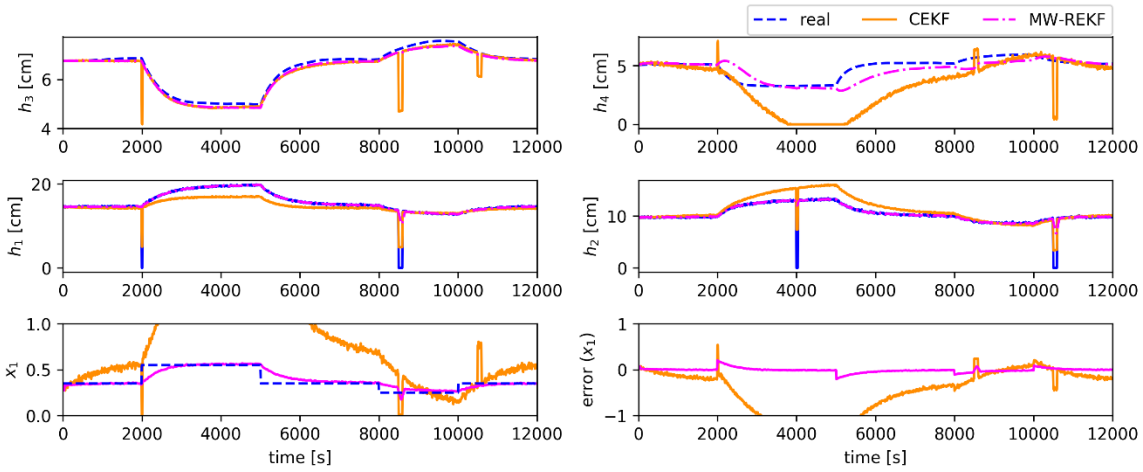
c) Scenario C – with outliers, model with cylindrical tanks, and R_1 parameter estimation



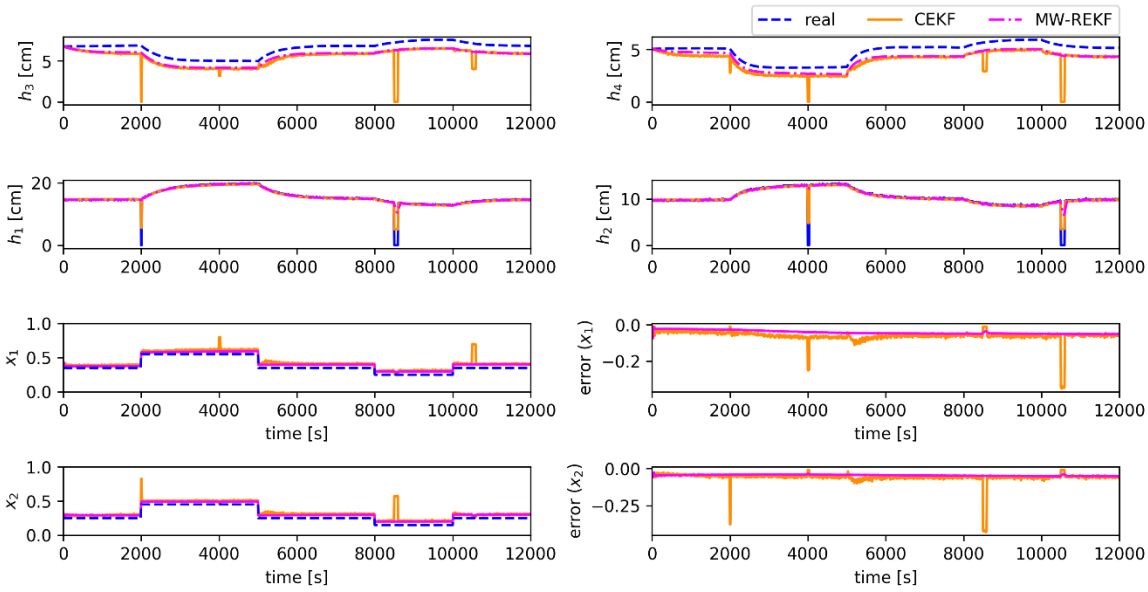
d) Scenario D - with limited tank height on plant model and R_1 parameter estimation – no constraints



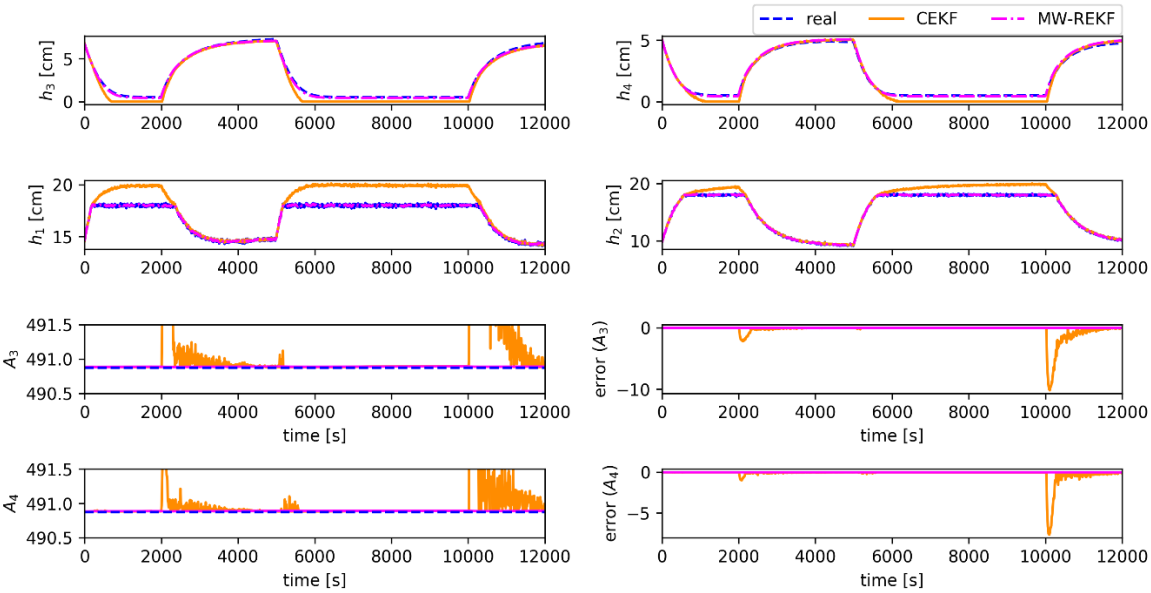
e) Scenario E - with limited tank height on plant model and R_1 parameter estimation – with constraints



f) Scenario F – with outliers and x_1 parameter estimation



g) Scenario G – with outliers and x_{1d} and x_{2d} parameter estimation



h) Scenario H - with limited tank height on plant model and A_{3d} and A_{4d} parameter estimation

Figure 6.7: Results for the seven scenarios of the spherical-quadruple-tank case study.

Figure 6.7a shows the parameter and state estimation of Scenario A. The CEKF and CEKFS returned the worst results for the parameter estimation of R_1 with noisy behavior due to the colored noise discrepancies. As expected, the addition of a moving window technique brought the R_1 closer to its real value. The MW-REKF had the smoothest result, as seen by the mean squared error evaluation in Table 6.6.

In Scenario B (Figure 6.7b), the CEKF for both state and parameter estimation could not eliminate the effect of the outliers. Meanwhile, the MHE resulted in values closer to the real, but with a significant computational cost. The MW-EKF estimates diverged from the simulated one for this scenario due to the outliers. Besides that, the inclusion of robustness in the MW-EKF, denominated MW-REKF, was able to minimize the effect of the gross errors on the state estimations in this scenario, resulting in even more smoothed results for R_1 parameter. As the CEKFS did not return significant improvements over the CEKF for scenarios A and B, it was disregarded for the next scenarios.

In Scenario C (Figure 6.7c), similar to scenario B, the MW-REKF was able to minimize the outliers' effect, returning the smoothest results. Meanwhile, the MW-EKF and MHE resulted in parameter and state estimations closer to the real values. It was not able to disregard the effect of the outliers. Even so, the MW-EKF obtained less errors than the MHE. The CEKF, which does not consider a moving window, had the worst results for the simultaneous state and parameter estimation.

In Scenario D (Figure 6.7d), the results from the CEKF did not consider the height limitation of the cylindrical tanks, where these discrepancies are easily detected in the R_1 parameter estimation. The MHE also suffered from this structural discrepancy, although the R_1 values were closer to the real. The MW-EKF and MW-REKF managed to overcome the spherical tank physical limitations, returning results closer to the real values. According to the MSE, the MW-REKF achieved slightly better results than the MW-EKF.

In Scenario E (Figure 6.7e), as scenario D, MW-EKF and MW-REKF managed to overcome the spherical tank physical limitations, returning results closer to the real values. The results from the MHE also suffered from this structural discrepancy, although the R_1 values were closer to the real. Meanwhile, the results from the CEKF did not consider the height limitation of the cylindrical tanks. For the next scenarios, it was chosen to compare only the CEKF and MW-REKF approaches.

Scenario F (Figure 6.7f) shows how the valve opening is sensitive during the parameter estimation. As in previous scenarios, the CEKF returned the worst results. MW-REKF brought the smoothest results. For Scenario G (Figure 6.7g), the results show less sensitivity in these parameters, and, as stated before, the best results were obtained by the MW-REKF and CEKF, respectively. Meanwhile, Figure 6.7h shows the results for the $A_{3\mathrm{b}}$ and $A_{4\mathrm{b}}$ deviation parameters are given by Scenario H. The results obtained by the MW-REKF show that the areas from the cylindrical tank would practically remain the same as from the spherical tank.

For all scenarios, both the MW-EKF and MW-REKF methodologies solved by QP had just four times higher computational cost than the CEKF. From this case study, it is possible to assure the significant improvement of using moving window state estimators to simultaneously estimate state and parameters, especially when the data present specific problems as outliers, colored noise, physical limits, etc. The moving window methodologies proved to reduce modeling errors, returning unbiased and smoother estimates for parameter estimation.

Table 6.6: Mean squared error for the eight scenarios of the spherical/cylindrical-quadruple-tank case study.

Mean squared error for the eight scenarios of the quadruple-tank case study						
Scenario A						
Filter	CEKF	CEKFS	RNK	RRNK	MHE	Ref. Value
time [s]	1.0000*	4.6489*	4.4028*	4.1927*	35.9889*	18.4180
h_1 error	27.3428*	1.0000*	1.4068*	3.4335*	6.2052*	0.0022
h_2 error	3.7134*	1.0000*	1.3043*	3.2402*	24.9079*	0.0025
h_3 error	1.0214*	1.0000*	1.1391*	1.1355*	1.1429*	0.2740
h_4 error	1.0000*	1.4269*	1.3787*	1.1540*	1.2800*	0.0042
R_1 error	20.5825*	23.3827*	1.7555*	1.0000*	2.9626*	0.0081
Scenario B						
Filter	CEKF	CEKFS	RNK	RRNK	MHE	Ref. Value
time [s]	1.0000*	4.8613*	4.3393*	3.7963*	36.1068*	17.9749
h_1 error	16.0447*	1.0000*	1.3558*	17.8499*	25.9294*	0.0818
h_2 error	3.0006*	1.0000*	1.0839*	15.1253*	20.4795*	0.0642
h_3 error	4.4961*	4.9582*	4849.03*	1.0141*	1.0000*	0.0153
h_4 error	4.1688*	8.0963*	39.2973*	1.0000*	1.0742*	0.0117
R_1 error	543.03*	646.46*	1436.70*	1.0000*	2992.02*	0.0052
Scenario C						
Filter	CEKF	CEKFS	RNK	RRNK	MHE	Ref. Value
time [s]	1.0000*	-	3.2037*	3.3379*	35.7437*	18.6910
h_1 error	213.86*	-	1.0000*	13.2561*	25.7266*	0.1096
h_2 error	2.8967*	-	1.0000*	14.1659*	19.8692*	0.0685
h_3 error	15.0865*	-	1.3905*	1.0322*	1.0000*	0.0252
h_4 error	2.5893*	-	31.7014*	1.0000*	1.0950*	0.0417
R_1 error	1943.10*	-	97.10*	1.0000*	2372.87*	0.0266
Scenario D						
Filter	CEKF	CEKFS	RNK	RRNK	MHE	Ref. Value
time [s]	1.0000*	-	3.5973*	3.8638*	33.5453*	17.9690
h_1 error	5553.74*	-	1.0000*	1.3510*	3.1816*	0.0035
h_2 error	300.31*	-	1.0000*	1.3517*	2.1421*	0.0032
h_3 error	77.2963*	-	1.1528*	1.0000*	2.1420*	0.0132
h_4 error	34.7057*	-	17.1618*	1.2560*	1.0000*	0.0139
R_1 error	262.70*	-	1.8294*	1.0000*	2.3868*	0.1782
Scenario E						
Filter	CEKF	CEKFS	RNK	RRNK	MHE	Ref. Value
time [s]	1.0000*	-	4.2167*	4.7600*	34.4241*	17.9649

Mean squared error for the eight scenarios of the quadruple-tank case study						
h_1 error	1064.12*	-	1.0000*	1.4201*	3.1918*	0.0032
h_2 error	276.49*	-	1.0000*	1.3669*	2200.65*	0.0033
h_3 error	1993.23*	-	19918.35*	54944.49*	1.0000*	6.18e-8
h_4 error	174.13*	-	5095.26*	27539.32*	1.0000*	6.02e-8
R_1 error	806.23*	-	1.6307*	1.0000*	1.8447*	0.1234
Scenario F						
Filter	CEKF	CEKFS	RNK	RRNK	MHE	Ref. Value
time [s]	1.0000*	-	-	2.9198*	-	26.4560
h_1 error	1.3290*	-	-	1.0000*	-	1.4728
h_2 error	1.7902*	-	-	1.0000*	-	0.9772
h_3 error	5.6901*	-	-	1.0000*	-	0.0157
h_4 error	10.6571*	-	-	1.0000*	-	0.3683
x_1 error	211.25*	-	-	1.0000*	-	0.0022
Scenario G						
Filter	CEKF	CEKFS	RNK	RRNK	MHE	Ref. Value
time [s]	1.0000*	-	-	3.3371*	-	17.5150
h_1 error	1.0000*	-	-	5.2547*	-	0.2801
h_2 error	1.0000*	-	-	5.1392*	-	0.1890
h_3 error	2.0060*	-	-	1.0000*	-	0.7531
h_4 error	2.0940*	-	-	1.0000*	-	0.5080
x_{1b} error	2.5745*	-	-	1.0000*	-	0.0018
x_{2b} error	2.3722*	-	-	1.0000*	-	0.0021
Scenario H						
Filter	CEKF	RNK	RNK	RRNK	MHE	Ref. Value
time [s]	1.0000*	-	-	3.3148*	-	19.2660
h_1 error	396.52*	-	-	1.0000*	-	0.0048
h_2 error	225.88*	-	-	1.0000*	-	0.0044
h_3 error	16.9863*	-	-	1.0000*	-	0.0150
h_4 error	8.6231*	-	-	1.0000*	-	0.0139
A_{3b} error	6671.62*	-	-	1.0000*	-	0.0002
A_{4b} error	2426.22*	-	-	1.0000*	-	0.0002

* multiplied by the reference value

In Table 6.6, the smallest row value was chosen for each variable and scenario as the reference value. To make comparison easier, for each state estimator result, the current value is multiplied by the "Ref. Value".

Figure 6.8 shows the window size versus the R_1 MSE for Scenario C, which is one of the most representative cases. The window size for the moving window approaches in this case study was the smallest possible. For window sizes larger than four, no significant change is seen in the estimation. If the system is oscillatory, for example, the dynamics and the sampling time of the system may be considered during window size selection so that the window must cover at least one complete cycle. If the window size is wrongly selected, the estimation performance may be unsatisfactory. Furthermore, the computational time increases linearly with the window size, as seen in Figure 6.8.

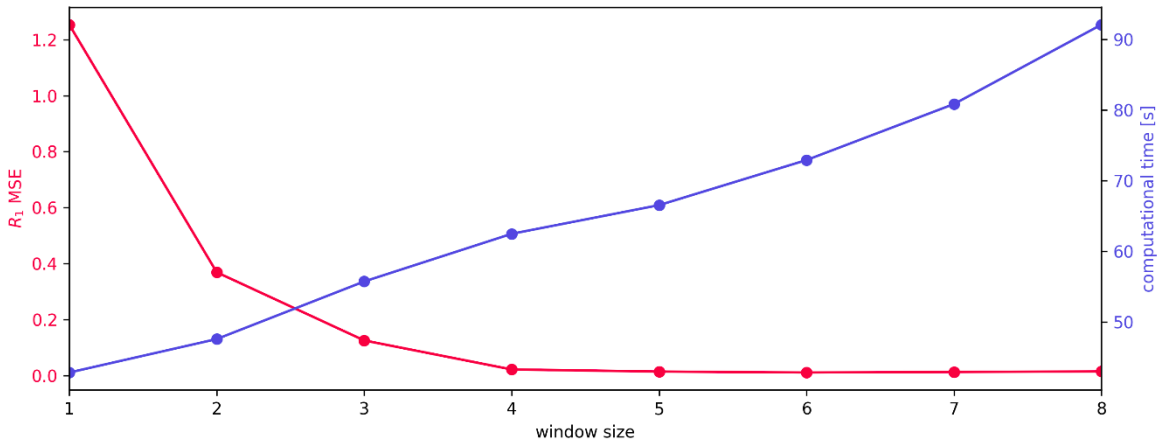


Figure 6.8: Window size versus the R_1 MSE for Scenario C.

The methodologies presented in this paper were also applied to an industrial case study with a large-scale model, The Fast Offshore Well Model (DIEHL, Fabio César *et al.*, 2017), which is a dynamic model for multiphase oil production systems in deepwater and ultra-deepwater scenarios, returned similar results to the spherical-quadruple-tank case study. Some of the state estimator results can be seen in Apio et al. (2019b).

6.6 Summary of Contributions

Contribution #1: CEKF (short formulation) Quadratic Programming. The CEKF was rewritten in its short implementation, which establishes the states directly as constraints. The CEKF quadratic programming, given by Equations 6.44-6.47, constitutes a simple and quick implementation of the problem.

Contribution #2: MW-EKF Quadratic Programming. Rengaswamy et al. (RENGASWAMY, R; NARASIMHAN; KUPPURAJ, 2013) proposed the RNK, in which Equation 6.11 was presented as an optimization problem. One of our contributions was to rewrite this problem as quadratic programming, resulting in Equations 6.44, 6.45, 6.62, and 6.63. The idea was to expand the CEKF (short formulation) implementation from only one sample to a finite number of past measured samples (moving window).

Contribution #3: MW-REKF Quadratic Programming. Based on Rangegowda et al. (RANGEGOWDA et al., 2018) RRNK, the MW-REKF replaces the likelihood term from Equation 6.41 with an M-estimator, the fair function. The major contribution of the present manuscript is the reformulation of this optimization problem in the robust and elegant QP given by Equations 6.73-6.77. For the moving window problem, the QP is written as Equations 6.78-6.82.

Contribution #4: Moving window state estimators for state and parameter estimation. In this paper, the importance of using moving windows to estimate states and parameters is clearly shown, mainly in Scenario C.

Contribution #5: Estimating the deviation variables to increase the observability of the system. In Scenarios F, G, H, the deviation variables were estimated instead of the variables themselves, increasing the observability of the system. For example, for Scenario F, instead of estimating x_1, the x_d was estimated, considering that $x_1 = x_1 + x_d$ (Equations 6.106-6.111).

6.7 Conclusions

State estimation of dynamic systems using the information over a moving window interval has grown in application since its first proposed by Jazwinski (1968). As the filter memory is limited, the estimates are computed based on data from the recent past, representing a satisfactory approximation of reality by reducing the effects of old samples on filtering and improving the estimation accuracy. In this paper, we proposed the extended (MW-EKF) and robust extended Kalman filter with moving window estimation (MW-REKF), which are based on the receding (RNK) and robust receding horizon nonlinear Kalman filter (RRNK). The MW-EKF and MW-REKF were presented using an elegant quadratic programming formulation that facilitates its implementation and decreases its computational cost. In this paper, states and parameters from the spherical-quadruple-tank case study were estimated using different moving window state estimator approaches. Four different methodologies were compared to conclude which one is the most suitable for this case study: constrained extended Kalman filter (CEKF), constrained extended Kalman filter and smoother (CEKFS), moving horizon estimation (MHE), and the proposed extended Kalman filter with moving window estimation (MW-EKF), and robust extended Kalman filter with moving window estimation (MW-REKF).

The CEKF showed unsatisfactory results for the simultaneous state and parameter estimation for most methodologies, highlighting the need for moving windows mainly for the parameter estimation. This methodology was hindered by the colored noise, outliers, structural discrepancies, among others. The CEKFS showed similar results to the CEKF, but with more computational effort. Although the RNK brought smoother results than CEKF, it suffered from mathematical errors caused by outliers. The MW-REKF returned the smoothest results for both state and parameter estimation. This technique minimized the effect of outliers, physical limitations, structural discrepancies, among others. The MHE methodology presented better results, with values closer to the real, but it could not overcome the effect of gross errors.

Meanwhile, although the MW-EKF brought smoother results than CEKF and MHE, it suffered from mathematical errors caused by outliers. The robust version of the MW-REKF emphasizes the main contribution of the MW-EKF methodology, which is the state covariance matrix evaluation, with the addition of an M-estimator. In short, including moving horizon in these Kalman filter-based methodologies prove to reduce modeling errors, resulting in unbiased and smoother estimates for the parameter estimation.

Considering that one of the main contributions of this paper is reformulating the RNK and RRNK with a robust and elegant QP formulation, it was verified that this approximation returns very similar results as the original optimization problem. These techniques' computational cost was only about four times higher than the CEKF, and nine times smaller than the MHE.

The addition of deviation variables enabled their estimation while the observability of the system was maintained. The estimation of the deviations in x_1 and x_2 was less sensitive than estimating the x_1 and x_2 directly.

6.8 Acknowledgments

The authors acknowledge Dr. Jayaram Valluru for his help in understanding the RNK methodology. Also, the financial support from the National Petroleum, Natural Gas, and Biofuels Agency (ANP) and Petróleo Brasileiro S.A. (PETROBRAS).

6.9 Appendix A

A.1. QP derivation for the constrained extended Kalman filter – short implementation

In this form, the constraint from the CEKF represented by Equation 6.12 is directly replaced in Equation 6.11, resulting in Equation 6.41:

$$\min_{\omega_{k|k},v_{k|k}} J = \omega_{k|k}^T \left(P_{k|k-1}\right)^{-1} \omega_{k|k} + v_{k|k}^T (R_k)^{-1} v_{k|k} \tag{6.11}$$

$$v_{k|k} = y_k - h\left(\hat{x}_{k|k}\right) \tag{6.17}$$

$$\min_{\hat{x}_{k|k}} J = \left(\hat{x}_{k|k} - \hat{x}_{k|k-1}\right)^T \left(P_{k|k-1}\right)^{-1} \left(\hat{x}_{k|k} - \hat{x}_{k|k-1}\right) + \left(y_k - H_k \hat{x}_{k|k}\right)^T (R_k)^{-1} (y_k - H_k \hat{x}_{k|k}) \tag{6.119}$$

Considering that $\hat{x}_{k|k}$ should be represented by a deviation variable, the term $\left(y_k - H_k \hat{x}_{k|k}\right)$ is rewritten as

$$\min_{\hat{x}_{k|k}} J = \left(\hat{x}_{k|k} - \hat{x}_{k|k-1}\right)^T \left(P_{k|k-1}\right)^{-1} \left(\hat{x}_{k|k} - \hat{x}_{k|k-1}\right) + \left(\Delta y_k - H_k \Delta \hat{x}_{k|k}\right)^T (R_k)^{-1} (\Delta y_k - H_k \Delta \hat{x}_{k|k}) \tag{6.120}$$

$$\min_{\hat{x}_{k|k}} J = \left(\hat{x}_{k|k} - \hat{x}_{k|k-1}\right)^T \left(P_{k|k-1}\right)^{-1} \left(\hat{x}_{k|k} - \hat{x}_{k|k-1}\right) + \left(y_k - \hat{y}_{k|k-1} + H_k \hat{x}_{k|k-1} - H_k \hat{x}_{k|k}\right)^T (R_k)^{-1} (y_k - \hat{y}_{k|k-1} + H_k \hat{x}_{k|k-1} - H_k \hat{x}_{k|k}) \tag{6.121}$$

Equation 6.43 is rewritten as

$$\min_{\hat{x}_{k|k}} J = \left(\hat{x}_{k|k} - \hat{x}_{k|k-1}\right)^T \left(P_{k|k-1}\right)^{-1} \left(\hat{x}_{k|k} - \hat{x}_{k|k-1}\right) + \left(y_k^* - H_k \hat{x}_{k|k}\right)^T (R_k)^{-1} (y_k^* - H_k \hat{x}_{k|k}) \tag{6.A1}$$

where

$$y_k^* = y_k - \hat{y}_{k|k} + H_k \hat{x}_{k|k-1} \tag{6.122}$$

Applying the following property of transpose of a matrix

$$(A + B)^T = A^T + B^T \tag{6.A2}$$

$$(AB)^T = B^T A^T \tag{6.A3}$$

results in

$$\min_{\hat{x}_{k|k}} J = (\hat{x}_{k|k}^T - \hat{x}_{k|k-1}^T)\left(P_{k|k-1}\right)^{-1}\left(\hat{x}_{k|k} - \hat{x}_{k|k-1}\right) + (y_k^{*,T} - \hat{x}_{k|k}^T H_k^T)(R_k)^{-1}(y_k^* - H_k\hat{x}_{k|k}) \tag{6.A4}$$

Solving the first two parenthesis multiplication

$$\min_{\hat{x}_{k|k}} J = (\hat{x}_{k|k}^T P_{k|k-1}^{-1} - \hat{x}_{k|k-1}^T P_{k|k-1}^{-1})\left(\hat{x}_{k|k} - \hat{x}_{k|k-1}\right) + (y_k^{*,T} R_k^{-1} - \hat{x}_{k|k}^T H_k^T R_k^{-1})(y_k^* - H_k\hat{x}_{k|k}) \tag{6.A5}$$

and now the remaining two parenthesis multiplication

$$\min_{\hat{x}_{k|k}} J = \hat{x}_{k|k}^T P_{k|k-1}^{-1}\hat{x}_{k|k} - \hat{x}_{k|k}^T P_{k|k-1}^{-1}\hat{x}_{k|k-1} - \hat{x}_{k|k-1}^T P_{k|k-1}^{-1}\hat{x}_{k|k} + \hat{x}_{k|k-1}^T P_{k|k-1}^{-1}\hat{x}_{k|k-1} + y_k^{*,T} R_k^{-1} y_k^* - y_k^{*,T} R_k^{-1} H_k\hat{x}_{k|k} - \hat{x}_{k|k}^T H_k^T R_k^{-1} y_k^* + \hat{x}_{k|k}^T H_k^T R_k^{-1} H_k\hat{x}_{k|k} \tag{6.A6}$$

Disregarding the constant variables $\hat{x}_{k|k-1}^T P_{k|k-1}^{-1}\hat{x}_{k|k-1}$ and $y_k^{*,T} R_k^{-1} y_k^*$:

$$\min_{\hat{x}_{k|k}} J = \hat{x}_{k|k}^T (P_{k|k-1}^{-1} + H_k^T R_k^{-1} H_k)\hat{x}_{k|k} - \hat{x}_{k|k}^T P_{k|k-1}^{-1}\hat{x}_{k|k-1} - \hat{x}_{k|k-1}^T P_{k|k-1}^{-1}\hat{x}_{k|k} - y_k^{*,T} R_k^{-1} H_k\hat{x}_{k|k} - \hat{x}_{k|k}^T H_k^T R_k^{-1} y_k^* \tag{6.A7}$$

As $P_{k|k-1}^{-1}$ and R_k^{-1} are symmetric, results in $\hat{x}_{k|k}^T P_{k|k-1}^{-1}\hat{x}_{k|k-1} = \hat{x}_{k|k-1}^T P_{k|k-1}^{-1}\hat{x}_{k|k}$ and $y_k^{*,T} R_k^{-1} H_k\hat{x}_{k|k} = \hat{x}_{k|k}^T H_k^T R_k^{-1} y_k^*$, so it is possible to join the common terms from Equation 6.A7:

$$\min_{\hat{x}_{k|k}} J = \hat{x}_{k|k}^T (P_{k|k-1}^{-1} + H_k^T R_k^{-1} H_k)\hat{x}_{k|k} - 2\hat{x}_{k|k-1}^T P_{k|k-1}^{-1}\hat{x}_{k|k} - 2y_k^{*,T} R_k^{-1} H_k\hat{x}_{k|k} \tag{6.A8}$$

simplifying

$$\min_{\hat{x}_{k|k}} J = \hat{x}_{k|k}^T (P_{k|k-1}^{-1} + H_k^T R_k^{-1} H_k)\hat{x}_{k|k} - 2(\hat{x}_{k|k-1}^T P_{k|k-1}^{-1} + y_k^{*,T} R_k^{-1} H_k)\hat{x}_{k|k} \tag{6.A9}$$

Lastly, the QP of this problem is written as

$$\min_{\hat{x}_{k|k}} J = \frac{1}{2}\hat{x}_{k|k}{}^T \alpha \hat{x}_{k|k} + \beta^T \hat{x}_{k|k} \tag{6.123}$$

subject to

$$\hat{x}_{min} \leq \hat{x}_{k|k} \leq \hat{x}_{max} \tag{6.124}$$

where

$$\alpha = \left[P_{k|k-1}^{-1} + H_k^T R_k^{-1} H_k\right] \tag{6.125}$$

$$\beta = \left[-\hat{x}_{k|k-1}^T P_{k|k-1}^{-1} - (y_k - \hat{y}_{k|k-1} + H_k\hat{x}_{k|k-1})^T R_k^{-1} H_k\right] \tag{6.126}$$

Considering the first term of Equation 6.44 $\left(\frac{1}{2}\hat{x}_{k|k}{}^T \alpha \hat{x}_{k|k}\right)$, α is multiplied by 2. As the β term of Equation 6.A9 is originally multiplied by 2, both α and β are simplified, resulting in Equations 6.46 and 6.47.

A.2. QP derivation for the robust extended extended Kalman filter

$$\min_{\hat{x}_{k|k},\zeta,\varepsilon} J = \left(\hat{x}_{k|k} - \hat{x}_{k|k-1}\right)^T \left(P_{k|k-1}\right)^{-1} \left(\hat{x}_{k|k} - \hat{x}_{k|k-1}\right) + \zeta^T R^{-1} \zeta + 2\delta\varepsilon \tag{6.127}$$

$$subject\ to \begin{Bmatrix} -\zeta - \varepsilon \le y_k^* - H_k \hat{x}_{k|k} \le \zeta + \varepsilon \\ 0 \le \zeta \le \delta \\ \varepsilon \ge 0 \end{Bmatrix} \tag{6.128}$$

Solving Equation 6.71:

$$\min_{\hat{x}_{k|k},\zeta,\varepsilon} J = \hat{x}_{k|k}^T P_{k|k-1}^{-1} \hat{x}_{k|k} + \zeta^T R^{-1} \zeta - 2\hat{x}_{k|k-1}^T P_{k|k-1}^{-1} \hat{x}_{k|k} + 2\delta\varepsilon + \hat{x}_{k|k-1}^T P_{k|k-1}^{-1} \hat{x}_{k|k-1} \tag{6.A10}$$

$$ssubject\ to \begin{Bmatrix} y_k^* - H_k \hat{x}_{k|k} \le \zeta + \varepsilon \\ -\zeta - \varepsilon \le y_k^* - H_k \hat{x}_{k|k} \\ -\zeta \le 0 \\ \zeta \le \delta \\ -\varepsilon \le 0 \end{Bmatrix} \tag{6.A11}$$

Disregarding $\hat{x}_{k|k-1}^T P_{k|k-1}^{-1} \hat{x}_{k|k-1}$ for its constant value and solving Equations 6.A10 and 6.A11 for $\hat{x}_{k|k}$, ζ, and ε:

$$\min_{\hat{x}_{k|k},\zeta,\varepsilon} J = \hat{x}_{k|k}^T P_{k|k-1}^{-1} \hat{x}_{k|k} + \zeta^T R^{-1} \zeta - 2\hat{x}_{k|k-1}^T P_{k|k-1}^{-1} \hat{x}_{k|k} + 2\delta\varepsilon \tag{6.A12}$$

$$subject\ to \begin{Bmatrix} -H_k \hat{x}_{k|k} - \zeta - \varepsilon \ge -y_k^* \\ H_k \hat{x}_{k|k} - \zeta - \varepsilon \le y_k^* \\ -\zeta \le 0 \\ \zeta \le \delta \\ -\varepsilon \le 0 \end{Bmatrix} \tag{6.A13}$$

which is reformulated as QP problem as

$$\begin{gathered} \min_{\hat{x}_{k|k},\zeta,\varepsilon} J = \frac{1}{2} \begin{bmatrix} \hat{x}_{k|k} \\ \zeta \\ \varepsilon \end{bmatrix}^T \alpha \begin{bmatrix} \hat{x}_{k|k} \\ \zeta \\ \varepsilon \end{bmatrix} + \beta^T \begin{bmatrix} \hat{x}_{k|k} \\ \zeta \\ \varepsilon \end{bmatrix} \\ subject\ to \qquad A \begin{bmatrix} \hat{x}_{k|k} \\ \zeta \\ \varepsilon \end{bmatrix} \le b \end{gathered} \tag{6.129}$$

where

$$\alpha = \begin{bmatrix} P_{k|k-1}^{-1} & 0 & 0 \\ 0 & R^{-1} & 0 \\ 0 & 0 & 0 \end{bmatrix} \tag{6.130}$$

$$\beta = \begin{bmatrix} -\hat{x}_{k|k-1}^T P_{k|k-1}^{-1} \\ 0 \\ \delta \end{bmatrix} \tag{6.131}$$

$$A = \begin{bmatrix} -H_k & -1 & -1 \\ H_k & -1 & -1 \\ 0 & -1 & 0 \\ 0 & 1 & 0 \\ 0 & 0 & -1 \end{bmatrix} \tag{6.132}$$

$$b = \begin{bmatrix} -y_k^* \\ y_k^* \\ 0 \\ \delta \\ 0 \end{bmatrix} \tag{6.133}$$

Capítulo 7 – **Considerações finais**

Este capítulo apresenta as principais conclusões do trabalho e sugere futuras pesquisas em estimadores de estado não-lineares e com janela móvel.

7.1 Conclusões

Os estimadores de estado, ou observadores, são técnicas que reconstroem os estados de um modelo dinâmico a partir das medidas de entrada e saída do sistema. Eles podem ser baseados na teoria probabilística (proposto por Kalman), que considera ruídos no modelo ou na teoria determinística (introduzida por Luenberger) sem a presença de ruídos. Embora, na sua gênese, o controle "moderno" tenha motivado o surgimento dessas técnicas em 1960, os estimadores de estado são hoje em dia aplicados também em reconciliação de dados, analisadores virtuais, estimação de parâmetros, gêmeos digitais e detecção de falhas.

Considerando que o número de metodologias para a estimação de estados é elevado, uma breve revisão das técnicas foi apresentada no Capítulo 2 de modo a facilitar o entendimento. Além da revisão histórica, foram discutidas características de interesse, tais como linearidade, custo computacional, e vantagens e desvantagens do uso de diferentes estimadores de estado.

Através de uma aplicação em caso real, estimadores de estado estendidos e não lineares foram utilizados na estimação da PDG como analisador virtual no Capítulo 3. Os resultados mostraram que os filtros não lineares retornam os melhores resultados quando o modelo estava bem ajustado, que era o caso real. Os filtros estendidos, no entanto, mostraram uma melhor performance para os cenários simulados, considerando que o modelo não estava tão bem ajustado.

Por isso, no Capítulo 5, foi proposta uma metodologia para compensação do "bias" para os filtros não lineares para casos em que o modelo não estava tão bem ajustado. Essa técnica simples estima o "bias" como uma variável através de técnica de estado aumentado, deixando o filtro de Kalman sem rastro e de cubatura mais precisos, mesmo em um cenário de ajuste inadequado do modelo.

No Capítulo 4 foi abordada a estimação do parâmetro do coeficiente de incrustação em tempo real de uma bateria de trocadores industrial através de técnica de estado aumentado. Embora outras técnicas para cálculo da resistência à incrustação tenham sido

propostas, elas falham no caso industrial comum, onde todas as propriedades físicas necessárias não estão disponíveis. Os resultados se mostraram promissores para estimação de variáveis desconhecidas em paralelo com a estimação do parâmetro desejado, aumentando a capacidade de monitoramento do sistema.

O Capítulo 6 complementa a tese, mostrando a importância da utilização de estimadores de estado com janelas móveis para a estimação simultânea de estados e parâmetros em tempo real para o estudo que motivou a tese, a planta de quatro tanques esféricos. Nesse caso, metodologias com janelas móveis se mostram mais adequadas, uma vez que elas são capazes de reduzir erros de modelagem e também retornar estimados mais suavizados e sem *bias*. Além disso, no estudo, são apresentadas formas simples e robustas para reescrever o filtro de Kalman "não linear" retrocedido e retrocedido robusto como programação quadrática. Além disso, essa última técnica mostrou os resultados mais suavizados para todas as metodologias, tanto para a estimação de estados e parâmetros, sendo, portanto, a mais recomendada para uma aplicação industrial.

7.2 Sugestões para trabalhos futuros

Assim como os filtros estudos neste trabalho, o mesmo faz parte de uma janela de desenvolvimentos, os quais permitem que se sugira os próximos passos a serem realizados. Tendo em vista os desenvololvimentos realizados nesta tese, as seguintes sugestões são algumas das mais promissoras:

- **Técnica de auditoria e diagnóstico de controle baseada em filtro de Kalman com janela móvel** – Os parâmetros relacionados ao funcionamento da malha de controle podem ser estimados em tempo real utilizando técnica de horizonte móvel suavizada e robusta.

- **Combinação de janela móvel com estimação do bias em estimadores não lineares –** Nesse caso, seriam combinadas as técnicas de estimação de bias e janela móvel na estimação simultânea de estados e parâmetros. Dessa forma, a janela móvel pode suavizar a estimação do bias.

- **Técnica para ajuste do tamanho da janela –** Considerando que o tamanho da janela quando se utiliza estimadores com horizonte móvel é dependente da dinâmica do sistema, amostragem, dentre outros, seria interessante desenvolver uma metodologia que determinasse o seu tamanho. Assim não seria necessário ajustá-la por testes em simulação.

- **Utilização de outras técnicas matemáticas para pré-tratamento de janela móvel –** A utilização de dados dos últimos pontos (ao invés de apenas o último) nos estimadores de estado, abre a possibilidade de utilizar técnicas de suavização, remoção de outliers, dentre outros, diretamente na janela móvel.

Referências

AAMO, O.M. *et al.* Observer design for multiphase flow in vertical pipes with gas-lift—theory and experiments. **Journal of Process Control**, [*s. l.*], v. 15, n. 3, p. 247–257, 2005. Disponível em: https://doi.org/10.1016/j.jprocont.2004.07.002

AFSHARI, H.H.; GADSDEN, S.A.; HABIBI, S. Gaussian filters for parameter and state estimation: A general review of theory and recent trends. **Signal Processing**, [*s. l.*], v. 135, p. 218–238, 2017. Disponível em: https://doi.org/10.1016/j.sigpro.2017.01.001

AGUIRRE, Luis A *et al.* Development of soft sensors for permanent downhole Gauges in deepwater oil wells. **Control Engineering Practice**, [*s. l.*], v. 65, p. 83–99, 2017. Disponível em: https://doi.org/10.1016/j.conengprac.2017.06.002

ÅKESSON, J. *et al.* Modeling and optimization with Optimica and JModelica.org—Languages and tools for solving large-scale dynamic optimization problems. **Computers & Chemical Engineering**, [*s. l.*], v. 34, n. 11, p. 1737–1749, 2010. Disponível em: https://doi.org/10.1016/j.compchemeng.2009.11.011

ALESSANDRI, A; BAGLIETTO, M; BATTISTELLI, G. Receding-horizon estimation for discrete-time linear systems. **IEEE Transactions on Automatic Control**, [*s. l.*], v. 48, n. 3, p. 473–478, 2003. Disponível em: https://doi.org/10.1109/TAC.2003.809155

ALFRIEND, Kyle T *et al.* The Basics of Analytical Mechanics, Optimization, Control and Estimation. *In*: ALFRIEND, Kyle T *et al.* (org.). **Spacecraft Formation Flying**. Oxford: Elsevier, 2010. p. 39–57. Disponível em: https://doi.org/10.1016/B978-0-7506-8533-7.00208-6

ALGEROY, John *et al.* Permanent Monitoring: Taking It to the Reservoir. **Oilfield Review**, [*s. l.*], v. 22, n. 1, p. 34–41, 2010. Disponível em: http://www.slb.com/resources/publications/industry_articles/oilfield_review/2010/or2010spr03_perm_monitoring.aspx

ANTONELO, Eric A; CAMPONOGARA, Eduardo; FOSS, Bjarne. Echo State Networks for data-driven downhole pressure estimation in gas-lift oil wells. **Neural Networks**, [*s. l.*], v. 85, p. 106–117, 2017. Disponível em: https://doi.org/10.1016/j.neunet.2016.09.009

APIO, A. *et al.* PDG pressure estimation in offshore oil well: Extended Kalman filter vs. artificial neural networks. *In*: , 2019a. **IFAC-PapersOnLine**. [*S. l.: s. n.*], 2019. Disponível em: https://doi.org/10.1016/j.ifacol.2019.06.113

APIO, Andressa *et al.* Comparison of Kalman filter-based approaches for permanent downhole gauge pressure estimation in offshore oil production. **Journal of Petroleum Science and Engineering**, [*s. l.*], v. 182, p. 106254, 2019b. Disponível em: https://doi.org/10.1016/j.petrol.2019.106254

APIO, Andressa *et al.* PDG Pressure Estimation in Offshore Oil Well: Extended Kalman Filter vs. Artificial Neural Networks. *In*: , 2019c, Florianópolis, Brazil. **12th IFAC Symposium on Dynamics and Control of Process Systems, including Biosystems**. Florianópolis, Brazil: IFAC Papers Online, 2019.

ARASARATNAM, I; HAYKIN, S. Cubature Kalman Filters. **IEEE Transactions on Automatic Control**, [*s. l.*], v. 54, n. 6, p. 1254–1269, 2009. Disponível em: https://doi.org/10.1109/TAC.2009.2019800

ASTROZA, Rodrigo; EBRAHIMIAN, Hamed; CONTE, Joel P. Performance comparison of Kalman−based filters for nonlinear structural finite element model updating. **Journal of Sound and Vibration**, [*s. l.*], v. 438, p. 520–542, 2019. Disponível em: https://doi.org/10.1016/j.jsv.2018.09.023

AUGER, F *et al.* Industrial Applications of the Kalman Filter: A Review. **IEEE Transactions on Industrial Electronics**, [*s. l.*], v. 60, n. 12, p. 5458–5471, 2013. Disponível em: https://doi.org/10.1109/TIE.2012.2236994

BAGUI, F; ABDELGHANI-IDRISSI, M A; CHAFOUK, H. Heat exchanger Kalman filtering with process dynamic acknowledgement. **Computers & Chemical Engineering**, [*s. l.*], v. 28, n. 8, p. 1465–1473, 2004. Disponível em: https://doi.org/10.1016/j.compchemeng.2003.11.005

BANAVAR, R. **A game theoretic approach to linear dynamic estimation**. 1992. - University of Texas, [*s. l.*], 1992.

BARBOSA, Bruno H.G. *et al.* Downhole Pressure Estimation Using Committee Machines and Neural Networks. *In*: , 2015, Florianópolis, Brazil. **2nd IFAC Workshop on Automatic Control in Offshore Oil and Gas Production OOGP 2015**. Florianópolis, Brazil: IFAC Papers Online, 2015. p. 286–291. Disponível em: https://doi.org/10.1016/j.ifacol.2015.08.045

BEAL, Logan D.R. *et al.* GEKKO optimization suite. **Processes**, [*s. l.*], 2018. Disponível em: https://doi.org/10.3390/pr6080106

BENDIKSEN, K. H. *et al.* Dynamic two-fluid model OLGA. Theory and application. **Society of Petroleum Engineers of AIME, (Paper) SPE**, [*s. l.*], 1989.

BESTLE, D; ZEITZ, M. Canonical form observer design for non-linear time-variable systems. **International Journal of Control**, [*s. l.*], v. 38, n. 2, p. 419–431, 1983. Disponível em: https://doi.org/10.1080/00207178308933084

BEYENS, J. **Modern control theory (second edition). William L. Brogan**. [*S. l.: s. n.*], 1988. Disponível em: https://doi.org/10.1016/0005-1098(88)90019-2

BOCK, H. G. *et al.* A Direct Multiple Shooting Method for Real-Time Optimization of Nonlinear DAE Processes. *In*: NONLINEAR MODEL PREDICTIVE CONTROL. Basel: Birkhäuser Basel, 2000. p. 245–267. Disponível em: https://doi.org/10.1007/978-3-0348-8407-5_14

BOCK, H.G.; PLITT, K.J. A Multiple Shooting Algorithm for Direct Solution of Optimal Control Problems *. **IFAC Proceedings Volumes**, [*s. l.*], v. 17, n. 2, p. 1603–1608, 1984. Disponível em: https://doi.org/10.1016/S1474-6670(17)61205-9

BOGDANSKI, Karol; BEST, Matthew C. A new structure for non-linear black-box system identification using the extended Kalman filter. **Proceedings of the Institution of Mechanical Engineers, Part D: Journal of Automobile Engineering**, [*s. l.*], v. 231, n. 14, p. 2005–2015, 2017. Disponível em: https://doi.org/10.1177/0954407017692219

BORNARD, G; HAMMOURI, H. A high gain observer for a class of uniformly observable systems. *In*: , 1991. **[1991] Proceedings of the 30th IEEE Conference on Decision and Control**. [*S. l.: s. n.*], 1991. p. 1494–1496 v.2. Disponível em: https://doi.org/10.1109/CDC.1991.261650

BOTT, T. R. Biofouling control with ultrasound. **Heat Transfer Engineering**, [*s. l.*], 2000. Disponível em: https://doi.org/10.1080/014576300270898

BOYD, Stephen; VANDENBERGHE, Lieven. **Convex Optimization**. [*S. l.: s. n.*], 2004. Disponível em: https://doi.org/10.1017/cbo9780511804441

CAMPOS, M *et al.* **Anti-Slug Advanced Control for Offshore Production Platforms**. Rio de Janeiro, Brazil: Offshore Technology Conference, 2015. Disponível em: https://doi.org/10.4043/26243-MS

ÇENGEL, Yunus A. **Heat Transfer: A Practical Approach**. 2nd editioed. [*S. l.*]: Mcgraw-Hill, 2002.

CHEN, J.J.J. Comments on improvements on a replacement for the logarithmic mean. **Chemical Engineering Science**, [*s. l.*], v. 42, n. 10, p. 2488–2489, 1987. Disponível em: https://doi.org/10.1016/0009-2509(87)80128-8

CHEN, Xiao Dong *et al.* On-line fouling/cleaning detection by measuring electric resistance-equipment development and application to milk fouling detection and chemical cleaning monitoring. **Journal of Food Engineering**, [*s. l.*], 2004. Disponível em: https://doi.org/10.1016/S0260-8774(03)00085-2

CHOWDHARY, Girish; JATEGAONKAR, Ravindra. Aerodynamic parameter estimation from flight data applying extended and unscented Kalman filter. **Aerospace Science and Technology**, [*s. l.*], v. 14, n. 2, p. 106–117, 2010. Disponível em: https://doi.org/10.1016/j.ast.2009.10.003

CIRIC, A.R.; FLOUDAS, C.A. Heat exchanger network synthesis without decomposition. **Computers & Chemical Engineering**, [*s. l.*], v. 15, n. 6, p. 385–396, 1991. Disponível em: https://doi.org/10.1016/0098-1354(91)87017-4

COLETTI, F *et al.* Introduction. *In*: COLETTI, Francesco; HEWITT, Geoffrey F B T - Crude Oil Fouling (org.). **Crude Oil Fouling**. Boston: Elsevier, 2015. p. 1–22. Disponível em: https://doi.org/10.1016/B978-0-12-801256-7.00001-4

D'ALFONSO, Luigi *et al.* Mobile robot localization via EKF and UKF: A comparison based on real data. **Robotics and Autonomous Systems**, [*s. l.*], v. 74, p. 122–127, 2015. Disponível em: https://doi.org/10.1016/j.robot.2015.07.007

DAS, Laya *et al.* A novel approach for benchmarking and assessing the performance of state estimators. **ISA Transactions**, [*s. l.*], v. 80, p. 137–145, 2018. Disponível em: https://doi.org/10.1016/j.isatra.2018.06.005

DE VALLIÈRE, P.; BONVIN, D. Application of estimation techniques to batch reactors-II. Experimental studies in state and parameter estimation. **Computers and Chemical Engineering**, [*s. l.*], 1989. Disponível em: https://doi.org/10.1016/0098-1354(89)89003-9

DE VALLIÈRE, Ph; BONVIN, D. Application of estimation techniques to batch reactors-III. Modelling refinements which improve the quality of state and parameter estimation. **Computers and Chemical Engineering**, [*s. l.*], 1990. Disponível em: https://doi.org/10.1016/0098-1354(90)87087-6

DI MEGLIO, F *et al.* Model-based control of slugging: advances and challenges. *In*: , 2012, Trondheim, Norway. **1st IFAC Workshop on Automatic Control in Offshore Oil and Gas Production**. Trondheim, Norway: IFAC Proceedings Volumes, 2012. p. 109–115. Disponível em: https://doi.org/10.3182/20120531-2-NO-4020.00029

DI MEGLIO, F; KAASA, G O; PETIT, N. A first principle model for multiphase slugging flow in vertical risers. *In*: , 2009, Shanghai, China. **Proceedings of the 48h IEEE Conference on Decision and Control (CDC) held jointly with 28th Chinese Control Conference**. Shanghai, China: IEEE, 2009. p. 8244–8251. Disponível em: https://doi.org/10.1109/CDC.2009.5400680

DI MEGLIO, Florent *et al.* Stabilization of slugging in oil production facilities with or without upstream pressure sensors. **Journal of Process Control**, [*s. l.*], v. 22, n. 4, p. 809–822, 2012. Disponível em: https://doi.org/10.1016/j.jprocont.2012.02.014

DIEHL, Fabio C *et al.* Oil production increase in unstable gas lift systems through nonlinear model predictive control. **Journal of Process Control**, [*s. l.*], v. 69, p. 58–69, 2018. Disponível em: https://doi.org/10.1016/j.jprocont.2018.07.009

DIEHL, Fabio César *et al.* Fast Offshore Wells Model (FOWM): A practical dynamic model for multiphase oil production systems in deepwater and ultra-deepwater scenarios. **Computers & Chemical Engineering**, [*s. l.*], v. 99, n. 6, p. 304–313, 2017. Disponível em: https://doi.org/10.1016/j.compchemeng.2017.01.036

EIKREM, Gisle Otto; IMSLAND, Lars; FOSS, Bjarne. Stabilization of Gas Lifted Wells Based on State Estimation. *In*: , 2004, Hong Kong, China. **7th International Symposium on Advanced Control of Chemical Processes (ADCHEM 2003)**. Hong Kong, China: IFAC Proceedings Volumes, 2004. p. 323–328. Disponível em: https://doi.org/10.1016/S1474-6670(17)38752-9

ESCOBAR, Marcelo; TRIERWEILER, Jorge O. Multivariable PID controller design for chemical processes by frequency response approximation. **Chemical Engineering Science**, [*s. l.*], v. 88, p. 1–15, 2013a. Disponível em: https://doi.org/10.1016/j.ces.2012.11.011

ESCOBAR, Marcelo; TRIERWEILER, Jorge O. Optimal heat exchanger network synthesis: A case study comparison. **Applied Thermal Engineering**, [*s. l.*], v. 51, n. 1–2, p. 801–826, 2013b. Disponível em: https://doi.org/10.1016/j.applthermaleng.2012.10.022

EVENSEN, G. The ensemble Kalman filter for combined state and parameter estimation.

IEEE Control Systems Magazine, [*s. l.*], v. 29, n. 3, p. 83–104, 2009. Disponível em: https://doi.org/10.1109/MCS.2009.932223

FENG, Shuqiang. **Global Offshore Gas Production Grows**. [*S. l.*], 2017. Disponível em: https://www.hartenergy.com/exclusives/global-offshore-gas-production-grows-176763. Acesso em: 5 maio 2019.

FLOUDAS, C A; CIRIC, A R; GROSSMANN, I E. Automatic synthesis of optimum heat exchanger network configurations. **AIChE Journal**, [*s. l.*], v. 32, n. 2, p. 276–290, 1986. Disponível em: https://doi.org/10.1002/aic.690320215

FRANKE, Meik *et al.* Online monitoring of semi-continuous emulsion copolymerization: Comparing constrained extended Kalman filtering to feed-forward calorimetry. *In*: , 2001, Jejudo Island, Korea. **6th IFAC Symposium on Dynamics and Control of Process Systems**. Jejudo Island, Korea: IFAC Proceedings Volumes, 2001. p. 227–232. Disponível em: https://doi.org/10.1016/S1474-6670(17)33828-4

FRIEDLAND, Bernard. Observers. *In*: THE CONTROL SYSTEMS HANDBOOK: CONTROL SYSTEM ADVANCED METHODS, SECOND EDITION. [*S. l.: s. n.*], 2010. Disponível em: https://doi.org/10.1201/b10384

FURMAN, Kevin C; SAHINIDIS, Nikolaos V. A Critical Review and Annotated Bibliography for Heat Exchanger Network Synthesis in the 20th Century. **Industrial & Engineering Chemistry Research**, [*s. l.*], v. 41, n. 10, p. 2335–2370, 2002. Disponível em: https://doi.org/10.1021/ie010389e

GAO, Fei *et al.* Parameter identification for Van Der Pol–Duffing oscillator by a novel artificial bee colony algorithm with differential evolution operators. **Applied Mathematics and Computation**, [*s. l.*], v. 222, n. Supplement C, p. 132–144, 2013. Disponível em: https://doi.org/10.1016/j.amc.2013.07.053

GARCIA, R.V. *et al.* Nonlinear filtering for sequential spacecraft attitude estimation with real data: Cubature Kalman Filter, Unscented Kalman Filter and Extended Kalman Filter. **Advances in Space Research**, [*s. l.*], v. 63, n. 2, p. 1038–1050, 2019. Disponível em: https://doi.org/10.1016/j.asr.2018.10.003

GEREVINI, Giovani G; FARENZENA, Marcelo; TRIERWEILER, Jorge O. Slugging attenuation using Nonlinear Model Predictive Control in offshore oil production. **Journal of Petroleum Science and Engineering**, [*s. l.*], v. 165, p. 187–198, 2018. Disponível em: https://doi.org/10.1016/j.petrol.2018.01.054

GESTHUISEN, R; KLATT, K.-U.; ENGELL, S. Optimization-based state estimation — A comparative study for the batch polycondensation of polyethyleneterephthalate. *In*: , 2001, Porto, Portugal. **2001 European Control Conference (ECC)**. Porto, Portugal: IEEE, 2001. p. 1062–1067. Disponível em: https://doi.org/10.23919/ECC.2001.7076055

GRYZLOV, A; SCHIFERLI, W; MUDDE, R.F. Soft-sensors: Model-based estimation of inflow in horizontal wells using the extended Kalman filter. **Flow Measurement and Instrumentation**, [*s. l.*], v. 34, p. 91–104, 2013. Disponível em: https://doi.org/10.1016/j.flowmeasinst.2013.09.002

GUDI, R. D.; SHAH, S. L.; GRAY, M. R. Multirate state and parameter estimation in an

antibiotic fermentation with delayed measurements. **Biotechnology and Bioengineering**, [*s. l.*], 1994. Disponível em: https://doi.org/10.1002/bit.260441102

HASELTINE, Eric L; RAWLINGS, James B. Critical Evaluation of Extended Kalman Filtering and Moving-Horizon Estimation. **Industrial & Engineering Chemistry Research**, [*s. l.*], v. 44, n. 8, p. 2451–2460, 2005. Disponível em: https://doi.org/10.1021/ie034308l

HAUTUS, M. L. J. Controllability and observability conditions of linear autonomous systems. **Ned. Akad. Wetenschappen**, [*s. l.*], v. 72, p. 443–448, 1969.

HAYKIN, Simon. **Kalman Filtering and Neural Networks**. [*S. l.: s. n.*], 2001. v. 5 Disponível em: https://doi.org/10.1002/0471221546

HU, Bin. **Characterizing gas-lift instabilities**. 2004. - Norwegian University of Science and Technology, [*s. l.*], 2004. Disponível em: https://brage.bibsys.no/xmlui/bitstream/handle/11250/239283/123385_FULLTEXT01.pdf?sequence=1

HUANG, Bin *et al.* Calculation Algorithm of Tire-Road Friction Coefficient Based on Limited-Memory Adaptive Extended Kalman Filter. **Mathematical Problems in Engineering**, [*s. l.*], v. 2019, p. 1056269, 2019. Disponível em: https://doi.org/10.1155/2019/1056269

HUBER, Peter J. Robust Estimation of a Location Parameter. **Ann. Math. Statist.**, [*s. l.*], v. 35, n. 1, p. 73–101, 1964. Disponível em: https://doi.org/10.1214/aoms/1177703732

HUBER, Peter J. Robust Statistics BT - International Encyclopedia of Statistical Science. *In*: LOVRIC, Miodrag (org.). Berlin, Heidelberg: Springer Berlin Heidelberg, 2011. p. 1248–1251. Disponível em: https://doi.org/10.1007/978-3-642-04898-2_594

HÜFFNER, Leonardo Nardi; TRIERWEILER, Jorge Otávio; FARENZENA, Marcelo. Are complex black-box models for Permanent Downhole Gauge pressure estimation necessary? **Journal of Petroleum Science and Engineering**, [*s. l.*], v. 173, p. 715–732, 2019. Disponível em: https://doi.org/10.1016/j.petrol.2018.10.047

IJAZ, Humaad; ATI, Uma M K; MAHALEC, Vladimir. Heat exchanger network simulation, data reconciliation & optimization. **Applied Thermal Engineering**, [*s. l.*], v. 52, n. 2, p. 328–335, 2013. Disponível em: https://doi.org/10.1016/j.applthermaleng.2012.11.033

JAHANSHAHI, Esmaeil; SKOGESTAD, Sigurd; HANSEN, Henrik. Control structure design for stabilizing unstable gas-lift oil wells. **IFAC Proceedings Volumes**, Singapore, v. 45, n. 15, p. 93–100, 2012. Disponível em: https://doi.org/10.3182/20120710-4-SG-2026.00110. Acesso em: 25 jan. 2017.

JANSEN, Bård *et al.* Automatic Control of Unstable Gas Lifted Wells. *In*: , 1999, Houson, USA. **SPE Annual Technical Conference and Exhibition**. Houson, USA: Society of Petroleum Engineers, 1999. Disponível em: https://doi.org/10.2118/56832-MS

JAZWINSKI, A. Limited memory optimal filtering. **IEEE Transactions on Automatic Control**, [*s. l.*], v. 13, n. 5, p. 558–563, 1968. Disponível em: https://doi.org/10.1109/TAC.1968.1098981

JAZWINSKI, A. H. **Stochastic Process and Filtering Theory**. San Diego, CA: Academic, 1970.

JERÓNIMO, M. A.S. *et al.* Monitoring the thermal efficiency of fouled heat exchangers: A simplified method. **Experimental Thermal and Fluid Science**, [*s. l.*], 1997. Disponível em: https://doi.org/10.1016/S0894-1777(96)00146-X

JOHANSSON, K H. The quadruple-tank process: a multivariable laboratory process with an adjustable zero. **IEEE Transactions on Control Systems Technology**, [*s. l.*], v. 8, n. 3, p. 456–465, 2000. Disponível em: https://doi.org/10.1109/87.845876

JONSSON, G; PALSSON, O P. An Application of Extended Kalman Filtering to Heat Exchanger Models. **Journal of Dynamic Systems, Measurement, and Control**, [*s. l.*], v. 116, n. 2, p. 257–264, 1994. Disponível em: http://dx.doi.org/10.1115/1.2899218

JONSSON, G; PALSSON, O P; SEJLING, K. Modeling and Parameter Estimation of Heat Exchangers—A Statistical Approach. **Journal of Dynamic Systems, Measurement, and Control**, [*s. l.*], v. 114, n. 4, p. 673–679, 1992. Disponível em: http://dx.doi.org/10.1115/1.2897740

JONSSON, Gudmundur R *et al.* Use of extended Kalman filtering in detecting fouling in heat exchangers. **International Journal of Heat and Mass Transfer**, [*s. l.*], v. 50, n. 13–14, p. 2643–2655, 2007a. Disponível em: https://doi.org/10.1016/j.ijheatmasstransfer.2006.11.025

JONSSON, Gudmundur R *et al.* Use of extended Kalman filtering in detecting fouling in heat exchangers. **International Journal of Heat and Mass Transfer**, [*s. l.*], v. 50, n. 13–14, p. 2643–2655, 2007b. Disponível em: https://doi.org/10.1016/j.ijheatmasstransfer.2006.11.025

JULIER, S.J.; UHLMANN, J.K. Unscented Filtering and Nonlinear Estimation. **Proceedings of the IEEE**, [*s. l.*], v. 92, n. 3, p. 401–422, 2004. Disponível em: https://doi.org/10.1109/JPROC.2003.823141

JULIER, S; UHLMANN, J; DURRANT-WHYTE, H F. A new method for the nonlinear transformation of means and covariances in filters and estimators. **IEEE Transactions on Automatic Control**, [*s. l.*], v. 45, n. 3, p. 477–482, 2000. Disponível em: https://doi.org/10.1109/9.847726

KAASA, Glenn Ole *et al.* Nonlinear model-based control of unstable wells. **Modeling, Identification and Control**, [*s. l.*], v. 28, n. 3, p. 69–79, 2007. Disponível em: https://doi.org/10.4173/mic.2007.3.2

KALMAN, Rudolph Emil. A New Aproach to Linear Filtering and Prediction Problems. **Transactions of the ASME - Journal of Basic Engineering**, [*s. l.*], v. 82, n. Series D, p. 35–45, 1960.

KANO, Manabu; FUJIWARA, Koichi. **Virtual sensing technology in process industries: Trends and challenges revealed by recent industrial applications**. [*S. l.: s. n.*], 2013. Disponível em: https://doi.org/10.1252/jcej.12we167

KAYABASI, E; KURT, H. Simulation of heat exchangers and heat exchanger networks with an economic aspect. **Engineering Science and Technology, an International Journal**, [*s. l.*], v. 21, n. 1, p. 70–76, 2018. Disponível em: https://doi.org/10.1016/j.jestch.2018.02.006

KÜHL, Peter *et al.* A real-time algorithm for moving horizon state and parameter estimation. **Computers & Chemical Engineering**, [*s. l.*], v. 35, n. 1, p. 71–83, 2011. Disponível em: https://doi.org/10.1016/j.compchemeng.2010.07.012

KWON, Wook Hyun; KIM, Pyung Soo; PARK, PooGyeon. A receding horizon Kalman FIR filter for discrete time-invariant systems. **IEEE Transactions on Automatic Control**, [*s. l.*], v. 44, n. 9, p. 1787–1791, 1999. Disponível em: https://doi.org/10.1109/9.788554

LALOT, S. *et al.* Comparison of Neural Networks and Kalman Filters Performances for Fouling Detection in a Heat Exchanger. **International Journal of Heat Exchangers**, [*s. l.*], v. VII, p. 69–96, 2007.

LAVIOLA, J J. A comparison of unscented and extended Kalman filtering for estimating quaternion motion. *In*: , 2003. **Proceedings of the 2003 American Control Conference, 2003.** [*S. l.: s. n.*], 2003. p. 2435–2440 v.3. Disponível em: https://doi.org/10.1109/ACC.2003.1243440

LEVINE, William S. **The Control Systems Handbook, Second Edition: Control System Advanced Methods, Second Edition**. 2nd. ed. USA: CRC Press, Inc., 2009.

LI, Wenling; JIA, Yingmin. H-infinity filtering for a class of nonlinear discrete-time systems based on unscented transform. **Signal Processing**, [*s. l.*], v. 90, n. 12, p. 3301–3307, 2010. Disponível em: https://doi.org/10.1016/j.sigpro.2010.05.023

LING, K V; LIM, K W. Receding horizon recursive state estimation. **IEEE Transactions on Automatic Control**, [*s. l.*], v. 44, n. 9, p. 1750–1753, 1999. Disponível em: https://doi.org/10.1109/9.788546

LINNHOFF, Bodo; FLOWER, John R. Synthesis of heat exchanger networks: I. Systematic generation of energy optimal networks. **AIChE Journal**, [*s. l.*], 1978. Disponível em: https://doi.org/10.1002/aic.690240411

LOYOLA-FUENTES, José; SMITH, Robin; JOBSON, Megan. Fouling Modelling in Crude Oil Preheat Systems. *In*: ESPUÑA, Antonio; GRAELLS, Moisès; PUIGJANER, Luis B T - Computer Aided Chemical Engineering (org.). **27 European Symposium on Computer Aided Process Engineering**. [*S. l.*]: Elsevier, 2017. v. 40, p. 409–414. Disponível em: https://doi.org/10.1016/B978-0-444-63965-3.50070-2

LUENBERGER, D G. Observing the State of a Linear System. **IEEE Transactions on Military Electronics**, [*s. l.*], v. 8, n. 2, p. 74–80, 1964. Disponível em: https://doi.org/10.1109/TME.1964.4323124

M. M. PRIETO B. SIGALES, J Miranda. Application of a Stepwise Method for Analyzing Fouling in Shell-and-Tube Exchangers. **Heat Transfer Engineering**, [*s. l.*], v. 20, n. 4, p. 19–26, 1999. Disponível em: https://doi.org/10.1080/014576399271259

MANNING, Mathew. **Offshore production nearly 30% of global crude oil output in 2015**. [*S. l.*], 2016. Disponível em: https://www.eia.gov/todayinenergy/detail.php?id=28492. Acesso em: 6 mar. 2019.

MERWE, R Van der; WAN, E A. The square-root unscented Kalman filter for state and parameter-estimation. *In*: , 2001. **2001 IEEE International Conference on Acoustics,**

Speech, and Signal Processing. Proceedings (Cat. No.01CH37221). [*S. l.: s. n.*], 2001. p. 3461–3464 v.6. Disponível em: https://doi.org/10.1109/ICASSP.2001.940586

METROPOLIS, Nicholas; ULAM, S. The Monte Carlo Method. **Journal of the American Statistical Association**, [*s. l.*], 1949. Disponível em: https://doi.org/10.1080/01621459.1949.10483310

MIRZAEI, F M; ROUMELIOTIS, S I. A Kalman Filter-Based Algorithm for IMU-Camera Calibration: Observability Analysis and Performance Evaluation. **IEEE Transactions on Robotics**, [*s. l.*], v. 24, n. 5, p. 1143–1156, 2008. Disponível em: https://doi.org/10.1109/TRO.2008.2004486

MOHD ALI, Jarinah *et al.* Review and classification of recent observers applied in chemical process systems. **Computers & Chemical Engineering**, [*s. l.*], v. 76, p. 27–41, 2015. Disponível em: https://doi.org/10.1016/j.compchemeng.2015.01.019

MUSKE, K R; RAWLINGS, J B; LEE, J H. Receding Horizon Recursive State Estimation. *In*: , 1993. **1993 American Control Conference**. [*S. l.: s. n.*], 1993. p. 900–904. Disponível em: https://doi.org/10.23919/ACC.1993.4792993

MUSKE, Kenneth R.; RAWLINGS, James B. Nonlinear Moving Horizon State Estimation. *In*: METHODS OF MODEL BASED PROCESS CONTROL. [*S. l.: s. n.*], 1995. Disponível em: https://doi.org/10.1007/978-94-011-0135-6_14

MUTAMBARA, A G O; AL-HAIK, M S Y. EKF based parameter estimation for a heat exchanger. *In*: , 1999. **Proceedings of the 1999 American Control Conference (Cat. No. 99CH36251)**. [*S. l.: s. n.*], 1999. p. 3918–3922 v.6. Disponível em: https://doi.org/10.1109/ACC.1999.786251

NEMA, P. K.; DATTA, A. K. A computer based solution to check the drop in milk outlet temperature due to fouling in a tubular heat exchanger. **Journal of Food Engineering**, [*s. l.*], 2005. Disponível em: https://doi.org/10.1016/j.jfoodeng.2004.10.025

NYGAARD, G; NAEDAL, G; MYLVAGANAM, S. Evaluating nonlinear Kalman filters for parameter estimation in reservoirs during petroleum well drilling. *In*: , 2006, Munich, Germany. **2006 IEEE Conference on Computer Aided Control System Design, 2006 IEEE International Conference on Control Applications, 2006 IEEE International Symposium on Intelligent Control**. Munich, Germany: IEEE, 2006. p. 1777–1782. Disponível em: https://doi.org/10.1109/CACSD-CCA-ISIC.2006.4776910

OGATA, Katsuhiko. **Modern Control Engineering Fifth Edition**. [*S. l.: s. n.*], 2009. ISSN 0018-9286. Disponível em: https://doi.org/10.1109/TAC.1972.1100013

PARDAL, Paula Cristiane Pinto Mesquita; KUGA, HÃ\copyrightlio Koiti; MORAES, Rodolpho Vilhena de. Analyzing the Unscented Kalman Filter Robustness for Orbit Determination Through Global Positioning System Signals. **Journal of Aerospace Technology and Management**, [*s. l.*], v. 5, p. 395–408, 2013. Disponível em: http://www.scielo.br/scielo.php?script=sci_arttext&pid=S2175-91462013000400395&nrm=iso

PATWARDHAN, Sachin C *et al.* Nonlinear Bayesian state estimation: A review of recent developments. **Control Engineering Practice**, [*s. l.*], v. 20, n. 10, p. 933–953, 2012.

Disponível em: https://doi.org/10.1016/j.conengprac.2012.04.003

PLETT, Gregory L. Extended Kalman filtering for battery management systems of LiPB-based HEV battery packs: Part 3. State and parameter estimation. **Journal of Power Sources**, [*s. l.*], v. 134, n. 2, p. 277–292, 2004. Disponível em: https://doi.org/10.1016/j.jpowsour.2004.02.033

QI, Junjian; TAHA, Ahmad; WANG, Jianhui. Comparing Kalman Filters and Observers for Power System Dynamic State Estimation With Model Uncertainty and Malicious Cyber Attacks. **IEEE Access**, [*s. l.*], v. 6, p. 77155–77168, 2018.

RANGEGOWDA, Pavanraj H *et al.* Simultaneous State and Parameter Estimation using Receding-horizon Nonlinear Kalman Filter. **IFAC-PapersOnLine**, [*s. l.*], v. 51, n. 18, p. 411–416, 2018. Disponível em: https://doi.org/10.1016/j.ifacol.2018.09.335

RANGEGOWDA, Pavanraj H *et al.* Simultaneous State and Parameter Estimation using Robust Receding-horizon Nonlinear Kalman Filter. **IFAC-PapersOnLine**, [*s. l.*], v. 52, n. 1, p. 10–15, 2019. Disponível em: https://doi.org/10.1016/j.ifacol.2019.06.030

RAO, C.V.; RAWLINGS, J.B.; MAYNE, D.Q. Constrained state estimation for nonlinear discrete-time systems: stability and moving horizon approximations. **IEEE Transactions on Automatic Control**, [*s. l.*], v. 48, n. 2, p. 246–258, 2003. Disponível em: https://doi.org/10.1109/TAC.2002.808470

RAO, Christopher V.; RAWLINGS, James B. Nonlinear Moving Horizon State Estimation. *In*: NONLINEAR MODEL PREDICTIVE CONTROL. [*S. l.: s. n.*], 2000. Disponível em: https://doi.org/10.1007/978-3-0348-8407-5_3

RAO, Christopher V; RAWLINGS, James B. Constrained process monitoring: Moving-horizon approach. **AIChE Journal**, [*s. l.*], v. 48, n. 1, p. 97–109, 2002. Disponível em: https://doi.org/10.1002/aic.690480111

RAO, Christopher V; RAWLINGS, James B; LEE, Jay H. Constrained linear state estimation—a moving horizon approach. **Automatica**, [*s. l.*], v. 37, n. 10, p. 1619–1628, 2001. Disponível em: https://doi.org/10.1016/S0005-1098(01)00115-7

RAUCH, H. E.; STRIEBEL, C. T.; TUNG, F. Maximum likelihood estimates of linear dynamic systems. **AIAA Journal**, [*s. l.*], v. 3, n. 8, p. 1445–1450, 1965. Disponível em: https://doi.org/10.2514/3.3166

RAWLINGS, James B; BAKSHI, Bhavik R. Particle filtering and moving horizon estimation. **Computers & Chemical Engineering**, [*s. l.*], v. 30, n. 10–12, p. 1529–1541, 2006. Disponível em: https://doi.org/10.1016/j.compchemeng.2006.05.031

RENGASWAMY, R; NARASIMHAN, S; KUPPURAJ, V. Receding-Horizon Nonlinear Kalman (RNK) Filter for State Estimation. **IEEE Transactions on Automatic Control**, [*s. l.*], v. 58, n. 8, p. 2054–2059, 2013. Disponível em: https://doi.org/10.1109/TAC.2013.2253271

RENGASWAMY, Raghunathan; NARASIMHAN, Shankar; KUPPURAJ, Vidyashankar. Receding Nonlinear Kalman (RNK) Filter for Nonlinear Constrained State Estimation. *In*: PISTIKOPOULOS, E N; GEORGIADIS, M C; KOKOSSIS, A C B T - Computer Aided Chemical Engineering (org.). **21 European Symposium on Computer Aided Process Engineering**. [*S.*

l.]: Elsevier, 2011. v. 29, p. 844–848. Disponível em: https://doi.org/10.1016/B978-0-444-53711-9.50169-3

REZENDE, Edson F.A.; TEIXEIRA, Alex F; MENDES, Eduardo M.A.M. BR-Sensor: An On-line Data-driven Soft Sensor of Downhole Pressure. **IFAC-PapersOnLine**, Florianópolis, Brazil, v. 48, n. 6, p. 311–316, 2015. Disponível em: https://doi.org/10.1016/j.ifacol.2015.08.049

RIVEROL, C.; NAPOLITANO, V. Estimation of fouling in a plate heat exchanger through the application on neural networks. **Journal of Chemical Technology and Biotechnology**, [*s. l.*], 2005. Disponível em: https://doi.org/10.1002/jctb.1198

ROBERTSON, Douglas G.; LEE, Jay H.; RAWLINGS, James B. A moving horizon-based approach for least-squares estimation. **AIChE Journal**, [*s. l.*], 1996. Disponível em: https://doi.org/10.1002/aic.690420811

SALAU, Nina P G. **Abordagem Sistemática para Construção e Sintonia de Estimadores de Estados Não-Lineares**. 2009. - Universidade Federal do Rio Grande do Sul, [*s. l.*], 2009.

SALAU, Nina P.G.; TRIERWEILER, Jorge O; SECCHI, Argimiro R. Practical aspects on nonlinear state estimation. *In*: 22ND EUROPEAN SYMPOSIUM ON COMPUTER AIDED PROCESS ENGINEERING. [*S. l.*]: Elsevier, 2012a. v. 30, p. 1272–1276. Disponível em: https://doi.org/10.1016/B978-0-444-59520-1.50113-5

SALAU, Nina P G; TRIERWEILER, Jorge O; SECCHI, Argimiro R. State estimators for better bioprocesses operation. *In*: BOGLE, Ian David Lockhart; FAIRWEATHER, Michael B T - Computer Aided Chemical Engineering (org.). **22 European Symposium on Computer Aided Process Engineering**. [*S. l.*]: Elsevier, 2012b. v. 30, p. 1267–1271. Disponível em: https://doi.org/10.1016/B978-0-444-59520-1.50112-3

SANAYE, Sepehr; NIROOMAND, Behzad. Simulation of heat exchanger network (HEN) and planning the optimum cleaning schedule. **Energy Conversion and Management**, [*s. l.*], v. 48, n. 5, p. 1450–1461, 2007. Disponível em: https://doi.org/10.1016/j.enconman.2006.12.006

SANTAMARIA, Federico Lozano; MACCHIETTO, Sandro. Integration of optimal cleaning scheduling and control of heat exchanger networks under fouling: MPCC solution. **Computers & Chemical Engineering**, [*s. l.*], v. 126, p. 128–146, 2019. Disponível em: https://doi.org/10.1016/j.compchemeng.2019.04.012

SANTOS, José Eduardo Weber. **Método de ajuste para MPC baseado em multi-cenários para sistemas não quadrados**. 2016. - Universidade Federal do Rio Grande do Sul, [*s. l.*], 2016. Disponível em: https://lume.ufrgs.br/handle/10183/141217

SEMINO, D.; MORRETTA, M.; SCALI, C. Parameter estimation in extended Kalman filters for quality control in polymerization reactors. **Computers and Chemical Engineering**, [*s. l.*], 1996. Disponível em: https://doi.org/10.1016/0098-1354(96)00160-3

SHAH, R. K.; SEKULIC, D. P. **Fundamentals of Heat Exchanger Design**. 1st editioed. [*S. l.*]: John Wiley & Sons, 2003.

SILVA, C.D.S.; LIPORACE, F. S.; QUEIROZ, E. M. Fouling models for real time exchanger fouling detection. *In*: , 2005, Rio de Janeiro, Brazil. **2nd Mercosur Congress on Chemical**

Engineering. Rio de Janeiro, Brazil: Proceedings of the 2nd Mercosur Congress on Chemical Engineering – ENPROMER and 4th Mercosur Congress on Process Systems Engineering, 2005.

SIMON, Dan. **Optimal State Estimation: Kalman, H Infinity, and Nonlinear Approaches**. [*S. l.*]: Wiley-Interscience, 2006.

SINEGRE, L; PETIT, N; MENEGATTI, P. Predicting instabilities in gas-lifted wells simulation. *In*: , 2006, Minneapolis, USA. **2006 American Control Conference**. Minneapolis, USA: IEEE, 2006. p. 8 pp. Disponível em: https://doi.org/10.1109/ACC.2006.1657604

SOROUSH, Masoud. State and parameter estimations and their applications in process control. **Computers & Chemical Engineering**, [*s. l.*], v. 23, n. 2, p. 229–245, 1998. Disponível em: https://doi.org/10.1016/S0098-1354(98)00263-4

SPESIVTSEV, Pavel *et al.* Predictive model for bottomhole pressure based on machine learning. **Journal of Petroleum Science and Engineering**, [*s. l.*], v. 166, p. 825–841, 2018. Disponível em: https://doi.org/10.1016/j.petrol.2018.03.046

ST-PIERRE, M; GINGRAS, D. Comparison between the unscented Kalman filter and the extended Kalman filter for the position estimation module of an integrated navigation information system. *In*: , 2004. **IEEE Intelligent Vehicles Symposium, 2004**. [*S. l.: s. n.*], 2004. p. 831–835. Disponível em: https://doi.org/10.1109/IVS.2004.1336492

TAO, Fei; ZHANG, Meng; NEE, A. Y. C. **Digital Twin Driven Smart Manufacturing**. [*S. l.*]: Academic Press, 2019.

TEIXEIRA, Bruno O.S. *et al.* Data-driven soft sensor of downhole pressure for a gas-lift oil well. **Control Engineering Practice**, [*s. l.*], v. 22, p. 34–43, 2014. Disponível em: https://doi.org/10.1016/j.conengprac.2013.09.005

TORRE, A J *et al.* Casing Heading in Flowing Oil Wells. **SPE Production Engineering**, [*s. l.*], v. 2, n. 04, 1987. Disponível em: https://doi.org/10.2118/13801-PA

UILHOORN, F E. Comparison of Bayesian estimation methods for modeling flow transients in gas pipelines. **Journal of Natural Gas Science and Engineering**, [*s. l.*], v. 38, p. 159–170, 2017. Disponível em: https://doi.org/10.1016/j.jngse.2016.12.007

VALLURU, Jayaram; PATWARDHAN, Sachin C; BIEGLER, Lorenz T. Development of robust extended Kalman filter and moving window estimator for simultaneous state and parameter/disturbance estimation. **Journal of Process Control**, [*s. l.*], v. 69, p. 158–178, 2018. Disponível em: https://doi.org/10.1016/j.jprocont.2018.05.008

VAN NOSTRAND, W. L. L.; LEACH, S. H.; HALUSKA, J. L. **Economic penalties associated with the fouling of refinery heat transfer equipment**. New York. Hemisphere, Washington: [*s. n.*], 1981.

VDI HEAT ATLAS. [*S. l.: s. n.*], 2010. Disponível em: https://doi.org/10.1007/978-3-540-77877-6

WALCOTT, B L; CORLESS, M J; ŻAK, S H. Comparative study of non-linear state-observation techniques. **International Journal of Control**, [*s. l.*], v. 45, n. 6, p. 2109–2132, 1987.

Disponível em: https://doi.org/10.1080/00207178708933870

WAN, Eric A; VAN DER MERWE, Rudolph. The Unscented Kalman Filter. *In*: KALMAN FILTERING AND NEURAL NETWORKS. New York, USA: John Wiley & Sons, Inc., 2002. (Wiley Online Books).p. 221–280. Disponível em: https://doi.org/10.1002/0471221546.ch7

YANG, Cheng; SHI, Wenzhong; CHEN, Wu. Comparison of Unscented and Extended Kalman Filters with Application in Vehicle Navigation. **Journal of Navigation**, [*s. l.*], v. 70, n. 2, p. 411–431, 2017. Disponível em: https://doi.org/DOI: 10.1017/S0373463316000655

YEAP, B.L. *et al.* Mitigation of Crude Oil Refinery Heat Exchanger Fouling Through Retrofits Based on Thermo-Hydraulic Fouling Models. **Chemical Engineering Research and Design**, [*s. l.*], v. 82, n. 1, p. 53–71, 2004. Disponível em: https://doi.org/10.1205/026387604772803070

YEE, T F; GROSSMANN, I E. Simultaneous optimization models for heat integration—II. Heat exchanger network synthesis. **Computers & Chemical Engineering**, [*s. l.*], v. 14, n. 10, p. 1165–1184, 1990. Disponível em: https://doi.org/10.1016/0098-1354(90)85010-8

YUAN, Bin. **Formation Damage during Improved Oil Recovery: Fundamentals and Applications**. 2018. ed. [*S. l.*]: Elsevier, 2018.

ZAVALA, Victor M; LAIRD, Carl D; BIEGLER, Lorenz T. A FAST COMPUTATIONAL FRAMEWORK FOR LARGE-SCALE MOVING HORIZON ESTIMATION. **IFAC Proceedings Volumes**, [*s. l.*], v. 40, n. 5, p. 19–28, 2007. Disponível em: https://doi.org/10.3182/20070606-3-MX-2915.00122

ZEITZ, M. The extended Luenberger observer for nonlinear systems. **Systems & Control Letters**, [*s. l.*], v. 9, n. 2, p. 149–156, 1987. Disponível em: https://doi.org/10.1016/0167-6911(87)90021-1

ZHANG, J *et al.* Sensor fault detection and estimation for heat exchanger using Unscented Kalman Filter. *In*: , 2014. **2014 9th IEEE Conference on Industrial Electronics and Applications**. [*S. l.: s. n.*], 2014. p. 540–545. Disponível em: https://doi.org/10.1109/ICIEA.2014.6931223